TECHNICAL REPORT

JANAIR Report 680610

JANAIR
JOINT ARMY-NAVY AIRCRAFT INSTRUMENTATION RESEARCH

Effects of Varying Levels of Autopilot Assistance and Workload on Pilot Performance in the Helicopter Formation Flight Mode

ONR Contract
N 00014-66-C-0362
NR213-054

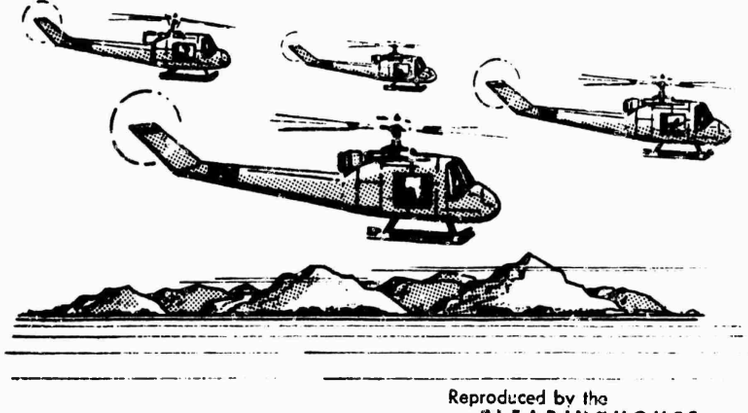

HONEYWELL INC.

March 1970

BLANK PAGES
IN THIS
DOCUMENT
WERE NOT
FILMED

JANAIR

Joint Army-Navy Aircraft Instrumentation Research

JANAIR Report 680610

EFFECTS OF VARYING LEVELS OF AUTOPILOT ASSISTANCE AND WORKLOAD ON PILOT PERFORMANCE IN THE HELICOPTER FORMATION FLIGHT MODE

P. A. Anderson and M. L. Toivanen
Honeywell Inc.

March 1970

(HoneywellDocument No. 12543-FR4)

This work was conducted for the JANAIR Program under
Office of Naval Research Contract N00014-66-C-0362
NR 213-054

Sponsored by

OFFICE OF NAVAL RESEARCH
NAVAL AIR SYSTEMS COMMAND
ARMY ELECTRONICS COMMAND

NOTICE

Change of Address

Organizations receiving JANAIR Reports on the initial distribution list should confirm correct address. This list is located at the end of the report just prior to the DDC Form 1473. Any change in address or distribution list should be conveyed to the Office of Naval Research, Code 461, Washington, D. C. 20360, ATTN: JANAIR Chairman.

Disposition

When this report is no longer needed it may be transmitted to other organizations. Do not return it to the originator or the monitoring office.

Disclaimer

The findings in this report are not to be construed as an official Department of Defense or Military Department position unless so designated by other official documents.

FOREWORD

This report presents work which was performed under the Joint Army-Navy Aircraft Instrumentation Research (JANAIR) Program, a research and exploratory development program directed by the United States Navy, Office of Naval Research. Special guidance is provided to the program for the Army Electronics Command, the Naval Air Systems Command, and the Office of Naval Research through an organization known as the JANAIR Working Group. The Working Group is currently composed of representatives from the following offices:

- U. S. Navy, Office of Naval Research, Aeronautics, Code 461, Washington, D. C.
  - Aircraft Instrumentation and Control Program Area
- U. S. Navy, Naval Air Systems Command, Washington, D. C
  - Avionics Division; Navigation Instrumentation and Display Branch (NAVAIR 5337)
  - Crew Systems Division; Cockpit/Cabin Requirements and Standards Branch (NAVAIR 5313)
- U. S Army, Army Electronics Command, Avionics Laboratory, Fort Monmouth, New Jersey
  - Instrument Technology Area (AMSEL-VL-I)

The Joint Army-Navy Aircraft Instrumentation Research Program objective is: To conduct applied research using analytical and experimental investigations for identifying, defining, and validating advanced concepts which may be applied to future, improved Naval and Army aircraft instrumentation systems. This includes sensing elements, data processors, displays, controls, and man/machine interfaces for fixed-and rotary-wing aircraft for all flight regimes.

ACKNOWLEDGEMENT

The study reported herein was performed by the Manned Systems Technology Group of the Systems and Research Center, Honeywell Inc. Mr. R. M. Nicholson was Program Manager of the study, and Mr. P. A. Anderson served as Program Technical Director. In addition to the listed authors, the following Honeywell personnel had significant participation in the program.

J. E. Dietz	W. R. Jost
M. E. Ebsen	B. A. Olson
R. B. Hoppe	J. A. Timmons

Special acknowledgement is paid LCDR F. L. Cundari, ONR, Washington, D. C , who served as the Scientific Officer and Mr. B. S. Gurman, Avionics Laboratory, USAE Command, Ft. Monmouth, New Jersey, who served as the Army's Technical representative.

Special acknowledgement is also paid Major Troy Reeves, Jr., Chief Warrant Officer Jose Anorga, and Major Donald Ingham of the 50th Artillery Group (AD), Snelling AADS, St. Paul, Minnesota, who served as test subjects during the study.

ABSTRACT

The objective of this study was to evaluate pilot performance in manual IFR formation flight with varying levels of autopilot assistance and pilot workload. The study was conducted for a conventional helicopter, i. e., the UH-1 Iroquois, and an advanced vehicle, the AH-56 Cheyenne. Man-in-the-loop simulations of these vehicles were conducted to evaluate pilot performance under six levels of autopilot assistance, ranging in sophistication from the free vehicle to outer loop hold modes in heading and altitude, and under three levels of pilot workload, consisting of a forced-pace, secondary concomitant task. Results of the study, within the constraints imposed by the simulation, indicated that increasing the level of autopilot assistance resulted in a less demanding task for the pilot and provided greater system stability. This was borne out in terms of both quantitative performance data and pilot opinion. However, position errors were not consistently reduced beyond the levels obtained during manual flight control modes where the highly quickened display was used. Only at the highest workload level tested did autopilot assistance serve to reduce the position errors from what was experienced under the manual control conditions.

CONTENTS

ILLUSTRATIONS

TABLES

LIST OF ABBREVIATIONS AND SYMBOLS

ABBREVIATIONS

A/C	Aircraft
AFCS	Automatic Flight Control System
BDHI	Bearing distance heading indicator
CSS	Control stick steering
IAD	Indicated airspeed dial
IAS	Indicated airspeed
IFR	Instrument flight rules
JANAIR	Joint Army/Navy Aircraft Instrumentation Research (Committee)
PAI	Pitch activity index
PPI	Plan position indicator (display format)
RAI	Roll activity index
RMS	Root-mean-square (i.e., $\sqrt{\frac{\Sigma X_E^2}{N}}$, where X_E is longitudinal position error)
SAS	Stability augmentation system
SK/FF	Station keeping/formation flight
SD	Standard deviation ($\sqrt{\frac{\Sigma(x-\bar{X})^2}{N}}$, where $\bar{X}$ is the mean and X the raw measurement of a sample distribution)
VFR	Visual Flight rules

SYMBOLS

B	Bearing from follower to leader
D	Drag of vehicle
E	Elevation angle from follower to leader

g	Gravity
K_X, K_Y	Scale factors for quickening symbol movement
$K_{\dot{X}}, K_{\dot{Y}}$	Gains for velocity terms in quickening equations
K_e, K_ϕ	Gains for pitch and roll attitude terms in quickening equations
$K_{\dot{\theta}}, K_{\dot{\phi}}$	Gains for attitude rate terms in quickening equations
K_ψ	Gain for heading term in quickening equations
M	Vehicle mass
N_B	Noise introduced into bearing measurement
N_E	Noise introduced into elevation measurement
N_R	Noise introduced into range measurement
R	Range from follower to leader
T	Sampling period
t	Time
X, Y, Z	Longitudinal, lateral, and vertical position coordinates, respectively
X_E, Y_E, Z_E	Position error - difference between actual and commanded positions
X_I, Y_I, Z_I	Inertial position coordinates
X_L, Y_L, Z_L	Inertial position coordinates referenced to leader's heading
X_Q, Y_Q	Distance from represented command position to quickening symbol position on PPI display format
$\dot{X}, \dot{Y}, \dot{Z}$	X. Y, and Z velocities
$\ddot{X}$	Longitudinal accelerations
$\delta_{\theta c}$	Pitch cyclic control movement
$\Delta X, \Delta Y, \Delta Z$	Follower position errors
$\Delta\dot{X}, \Delta\dot{Y}$	Velocity difference between follower and leader

θ	Pitch attitude of follower
$\dot{\theta}$	Follower's pitch attitude rate
ϕ	Follower's Roll attitude
$\dot{\phi}$	Follower's roll attitude rate
ψ_L	Heading of leader
ψ_S	Heading of follower
ψ_E	$\psi_S - \psi_L$ (heading difference)
$(\bar{\ })$	Denotes the nominal or command value of a given parameter

SECTION I
INTRODUCTION

The development of an effective helicopter IFR formation flight capability to increase the helicopter's effectiveness in future military operations is one of the objectives of the Joint Army-Navy Aircraft Instrumentation Research (JANAIR) Committee. As part of this program, Honeywell has performed a series of studies to define the display/control requirements for the manual IFR helicopter formation flight problem. The first study (Reference 1) was conducted to investigate basic information requirements and to develop and evaluate display concepts customized for the helicopter formation flight task. The results of this study indicated that IFR formation flight may be a realizable goal with the aid of digital computer-generated display formats. A second study (Reference 2), conducted to evaluate an existing formation flight system, demonstrated the important effects on system performance of filter lags, system update rates, and display quickening. The third study (Reference 3) investigated the effectiveness of conventional flight instrumentation in the manual formation flight situation. Two state-of-the-art electro-mechanical displays (i.e., a flight director and a horizontal situation indicator) were used to display the required information and were evaluated under alternative display formats. The results indicated that it was possible for the pilot to maintain precise position control with the electro-mechanical displays under the simulated conditions. The primary objective of the fourth study (Reference 4) was to relate total system performance to variations in the data rate and accuracy of the displayed information for the manual IFR helicopter formation flight mode. This study demonstrated the significant effects on system performance of the interactions between the rate quickening gains, display update rate, and data accuracy.

The objective of the present study was to relate pilot performance during manual IFR formation flight in two different classes of helicopters to various levels of autopilot assistance. All of the simulations conducted in the previous studies were performed using a UH-1 helicopter equipped with a three-axis stability augmentation system (SAS). The decision to include the three-axis SAS was based on the results of earlier analytical work performed in support of a station-keeping autopilot coupler study. This study suggested that an SAS would be required to provide the precision necessary for formation flight with the UH-1 helicopter in manual flight modes. Simulation results indicated that the UH-1 helicopter can be flown in the station-keeping flight mode with considerable precision with the simulated three-axis SAS. However, it represents additional cost to the basic UH-1 helicopter. As such, this cost must be justified in terms of improved system performance. The basic question to be answered by this study was the extent to which autopilot assistance could be expected to improve pilot performance, reduce pilot workload, increase pilot acceptance, and improve the operational capabilities of a helicopter in the manual formation flight mode.

Six levels of automatic flight control were investigated in this study, ranging in complexity from the free vehicle (no flight control assist) to outer loop hold modes in altitude and heading. To broaden the applicability of the results, two helicopters were simulated -- a current conventional vehicle, the UH-1 Iroquois, and a high-performance compound vehicle, the AH-56 Cheyenne.

A description of the autopilot modes used for each vehicle, the testing procedures followed, and the final evaluation based on the test results are described in this report.

SECTION II
BACKGROUND

This section provides a general description of the philosophy used in this study to relate pilot performance during manual helicopter IFR formation flight to various levels of flight control assistance to the pilot.

SELECTION OF VEHICLES FOR EVALUATION

Since the extent to which the results of this study could be generalized was dependent on the number of different classes of helicopters represented in this study, it was decided to examine both a current conventional vehicle and an advanced class of vehicle envisioned to be operational in the 1970s. It is obvious that any autopilot requirements derived solely for one class of vehicle cannot be generalized to all other helicopters because of differences in basic vehicle stability and response characteristics. The UH-1 Iroquois helicopter was selected to represent the conventional class of helicopters, and the AH-56 Cheyenne helicopter was selected to represent the advanced class of high-speed, high-performance helicopters.

The display concept for the UH-1 in the station keeping/formation flight (SK/FF) mission has been thoroughly analyzed in previous Honeywell studies and is an optimal configuration for that helicopter. Although a comparable analysis has not been done for the AH-56, for the purposes of this study the UH-1 display format and form of the quickening law were also used for this compound vehicle.

The AH-56 differs from conventional helicopters in that it incorporates short, fixed wings, a rigid rotor, and a pusher-propeller in its design. For control purposes, the most important difference is the pusher-propeller. Optimum control of fore-and-aft (X-axis) position in the AH-56 is accomplished by maintaining zero pitch attitude and varying the twist-grip pusher-propeller control. The situation is somewhat complicated by vehicle cross-coupling, which results in the variations in pusher-propeller power causing variations in pitch and roll attitude. The importance of these cross-coupling effects is a function of the autopilot mode and workload at any given time.

AUTOMATIC FLIGHT CONTROL SYSTEM (AFCS)

Six levels of automatic flight control were selected for each vehicle, ranging in sophistication from a free vehicle to outer loop hold modes in heading and altitude. Ideally, as the level of flight control augmentation is increased, the pilot's task would become easier. Finally, with both altitude and heading hold engaged, the pilot's task is reduced to manual control of only a single axis

(i.e., airspeed) and monitoring of the other axes. The autopilot modes selected for evaluation were

- Free vehicle
- Yaw stability augmentation
- Three-axis stability augmentation
- Heading hold
- Altitude hold
- Heading and altitude hold

As mentioned previously, a basic difference between the UH-1 and the AH-56 was the addition of a pusher-prop control on the AH-56 which permitted a separate control input for airspeed, while airspeed is controlled by pitch attitude and collective power on the UH-1. This difference between vehicles required that separate piloting techniques be developed for each vehicle. The mechanization of the autopilot modes was also influenced by this control difference between vehicles. The mode of operation for each level of autopilot and each vehicle is discussed below.

Free Vehicle

UH-1 -- In this mode of operation the pilot flies the vehicle without the aid of either ineer-loop stabilization or automatic outer-loop control. Airspeed is controlled with pitch attitude and collective power.

AH-56 -- Same as the UH-1 except that zero pitch attitude is maintained and airspeed is controlled with the pusher-prop.

Yaw Stability Augmentation

UH-1 and AH-56 -- Inner-loop yaw axis stability is provided whenever this mode is engaged. As with the free vehicle, the pilot must manually control attitude, airspeed, heading, and altitude.

Three-Axis Stability Augmentation

UH-1 -- This mode of operation is identical to the yaw stability augmentation except that the two remaining inner loops (i.e., pitch and roll) are stability augmented in addition to the yaw axis. This level of augmentation is the same as that simulated in the previous station-keeping studies.

AH-56 -- This mode of operation for the AH-56 is actually an attitude hold mode in pitch and roll plus yaw axis stability augmentation. The mode was mechanized in this manner to be consistent with airspeed control used for the AH-56, i.e., hold zero pitch attitude and use the pusher-prop for airspeed control. The vehicle's pitch attitude at mode engagement is maintained by the AFCS. Mode engagement is effected by reduction of pilot-applied pitch cyclic stick force below a breakout level. Whenever the roll attitude hold mode is engaged, the AFCS commands the vehicle to return to a wings-level roll attitude. Reduction of pilot-applied roll cyclic stick force engages the mode. Again, the pilot will have to manually control all of the outer loops.

Heading Hold

UH-1 -- When this mode is engaged, the vehicle heading selected by the pilot is maintained by the AFCS through the roll axis. Minor lateral position errors can be corrected by pilot override. In addition, a switch is provided for the pilot on the control column to disengage heading hold when making turning maneuvers. The three-axis SAS is also operating during this mode. The pilot's task is to manually control airspeed and altitude and to monitor heading and make corrections as necessary to null lateral position errors.

AH-56 -- The same as for the UH-1 except that pitch, attitude hold, and yaw SAS are in operation.

Altitude Hold

UH-1 -- When the altitude hold mode is engaged, the command altitude is maintained by the AFCS with collective pitch.

The three-axis SAS is also engaged. A switch on the collective stick disengages this mode during climbing and diving maneuvers. The pilot is required to control the vehicle's airspeed and heading and to monitor altitude error.

AH-56 -- The same as for the UH-1 except that attitude hold and yaw SAS are in operation rather than three-axis SAS.

Heading and Altitude Hold

UH-1 and AH-56 -- This mode is a combination of the previous two modes. It represents the most sophisticated mode of AFCS for the SK/FF mission short of automatic control through an autopilot coupler. The pilot's tracking task is reduced to controlling longitudinal position with airspeed and monitoring heading and altitude.

Table 1 is a summary of the modes of operation for each vehicle. These modes are described in Sections IV and VI.

PILOT WORKLOAD ASSESSMENT

Since one of the primary objectives of an autopilot is to reduce pilot workload, one of the independent variables of the simulation experiment was pilot workload. It was assumed that the incorporation of pilot workload into the experiment would tend to separate performance data and to provide a clearer picture of the advantages of the various levels of flight control. A brief discussion of workload methodology follows.

Figure 1 provides a classification of the various measures which can be used for establishing the reserve capacity of an operator. Review articles by Brown (Reference 5) and Knowles (Reference 6) summarize the more important studies relating to these measures.

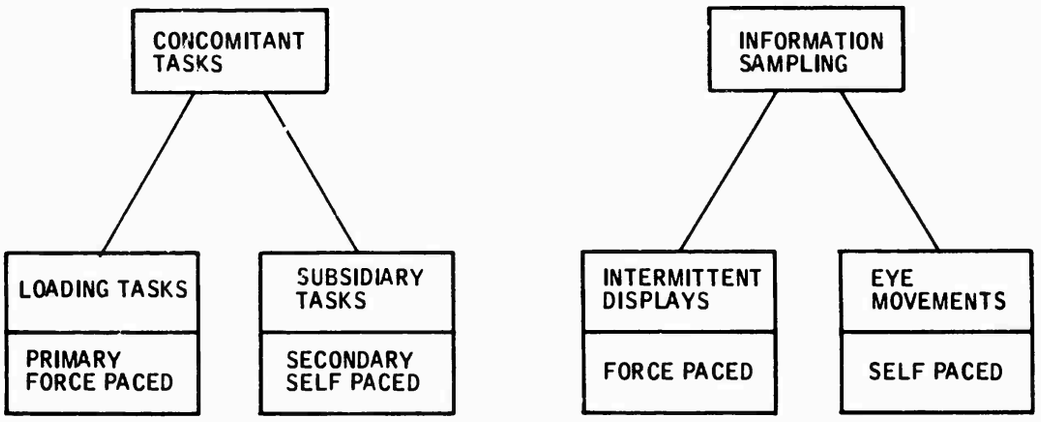

Figure 1. Methods for Measuring Information Workload

Concomitant Tasks

Concomitant tasks are of a class of tasks which are highly quantifiable in nature and are performed simultaneously with the primary tracking task. These tasks usually involve simple observable responses such as reading numbers, tapping illuminated switches, etc.

The procedure for assessing workload using concomitant tasks requires that the subject's maximum response rate be determined on the concomitant task

Table 1. Autopilot Modes of Operation

Autopilot Mode	UH-1				AH-56			
	Attitude	Airspeed	Heading	Altitude	Attitude	Airspeed	Heading	Altitude
Free Vehicle	Manual Pitch and roll with cyclic	Manual Pitch attitude	Manual roll attitude	Manual collective stick	Manual pitch and roll with cyclic	Manual pusher-prop	Manual roll attitude	Manual collective stick
Yaw SAS	↓	↓	↓	↓	↓	↓	↓	↓
Three-Axis SAS	↓	↓	↓	↓	MONITOR	↓	↓	↓
Heading Hold	Manual Pitch with cyclic	↓	MONITOR	↓	MONITOR	↓	MONITOR	↓
Altitude Hold	Manual pitch and roll with cyclic	↓	Manual roll attitude	MONITOR	MONITOR	↓	Manual roll attitude	MONITOR
Heading and Altitude Hold	Manual Pitch with cyclic	↓	MONITOR	MONITOR	MONITOR	↓	MONITOR	MONITOR

in isolation from the primary task. Then the concomitant task is introduced simultaneously with the primary task, and the subject is required to perform both tasks at the same time.

Depending on the instructions to the subject, or the manner in which the tasks are employed, the results obtained using concomitant tasks can differ significantly. Basically there are two ways the concomitant tasks can be employed -- as subsidiary tasks or as forced-pace tasks.

Subsidiary Tasks -- The rationale for the use of subsidiary tasks is that, as the information processing load of the primary task is increased, the operator's information rate on subsidiary tasks must be decreased. If it is assumed that these rates are inversely proportional, then it is possible to obtain a direct measure of primary task workload through the decrease in the information processing rate on the subsidiary task.

The subsidiary task, by instruction, is performed when the subject "feels" that he can respond with no decrement in performance on the primary task. This is the basic weakness in the use of subsidiary tasks for workload measurement. Because any subsidiary task will cause some decrement in the primary task, the subject must decide how much decrement is tolerable. The subject must resolve this question on a subjective basis, and, based on previous experience, there are wide individual differences amoung subjects as to the amount of degradation that will be accepted. This makes any evaluation of the resultant data extremely difficult.

Forced-Pace Tasks -- The rationale for using the forced-pace task is similar to that for the subsidiary task in that as the requirements of the forced-pace task increase the performance on the primary task will decrease. The basic difference between the administration of the two types of tasks is that on the subsidiary task the subject establishes his own response rate while on the forced-pace task the experimenter sets the rate at which the subject must respond, thus avoiding the problem of subject-bias. The subject is instructed to maintain his performance on the primary task at the highest possible level while responding to the forced-pace task. The experimenter adjusts the pace of the task (i. e., the rate of stimuli, etc.) over the workload levels of interest. These workload levels are then related to performance on the primary task.

Information Sampling Techniques

The rationale for the use of information sampling techniques in workload determination is that the measurement of information sampling frequencies and duration permits the quantification of operator workload on various tasks. One frequently used method in simulation to assess the required sampling frequencies and durations is the intermittent display. Intermittent displays (i. e., displays which can be taken away from the operator for short periods of time) are used to determine the amount of time that an operator has available

to sample information sources other than the primary display. Stated simply, the critical assumption inherent in this technique is that, if an operator performs the primary task at an acceptable level when the display information is available to him only 30% of the time, it is assumed that he can direct 70% of his time to other tasks.

One major weakness of this technique is that subjects can use the interval between display presentations to respond to the system. This is particularly true if the system dynamics are slow or if the display sampling cycle is short. A better arrangement is one where the subject is forced to perform another task during the interval when his primary display is interrupted. By forcing the subject to attend to a forced-pace concomitant task during the time that his primary display is interrupted, it is possible to combine the better features of both the concomitant task and interrupted display techniques. This method was used in the previous SK/FF studies. The simulation was programmed so that the display format could be interrupted (i.e., blanked out) at preselected frequencies and for preselected intervals. During the interval when the display was interrupted, random single-digit numbers were displayed sequentially in the center of the CRT at a rate of 1.25 numbers per second. The subject's task was to read the number aloud. The on-cycle of the SK/FF display format was set at 1 sec, and the display off-cycle was varied to achieve the desired workload level. (Figure 2 demonstrates the display interruption sequence for the 40 and 70% workload levels.)

The 1-sec display on-time was chosen as a compromise between display viewing time and display off-time at the highest workload level. Since the subject's eyes are always focused (reading numbers) at the center of the display area during the off-cycle, eye movement time and eye focus time do not have to be considered when setting the minimum display on-time. Therefore, the display must be on just long enough to allow for information processing and decision making. However, the display off-time depends on the display on-time when using the interrupted display technique for workload evaluation. If the display is off for a long period, the problem can become uncontrollable. If, for example, the display were on for 2 sec, the display off-cycle must be 4.67 sec in order to achieve a 70% workload level. An off-time of this magnitude is unacceptable for the helicopter formation flight control problem. Thus, the 1 sec display on-time was judged as adequate to allow time for information processing without making the display off-time unacceptable in terms of controlling the helicopter.

The following sections of this report describe the man-in-the-loop simulation program conducted to evaluate the effect of the various levels of flight control augmentation and pilot workload on the pilot's control of the UH-1 and AH-56 vehicles.

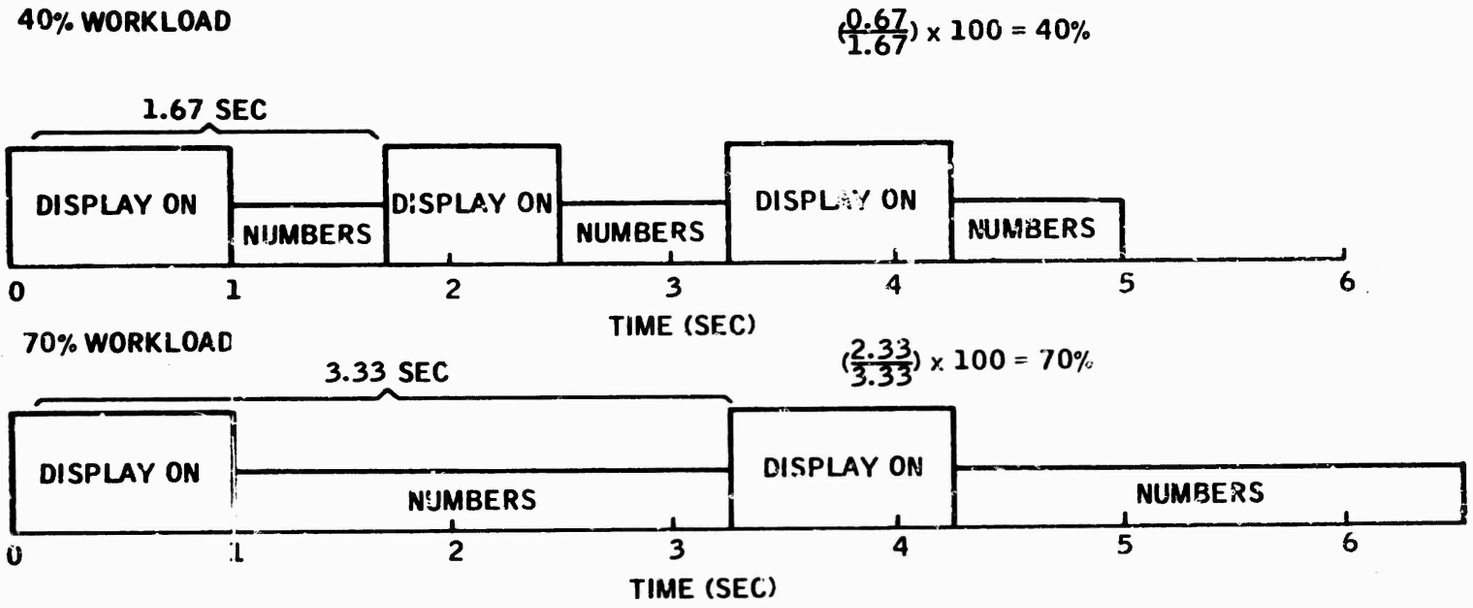

Figure 2. Display Interruption Sequence

SECTION III
SYSTEM DESCRIPTION

SIMULATION FACILITY

All simulations were performed on the Honeywell hybrid simulation facility. This facility, consisting of both digital and analog computers, was designed specifically for simulation programs where real-time performance measures are desired under varied experimental conditions. Appendix B describes the hybrid facility. Figure 3 illustrates how the facility was used in this problem. The analog portion of the facility provided the solutions to the vehicle equations of motion and the control authority calculations. The digital portion of the system performed the display calculations and controlled the total simulation.

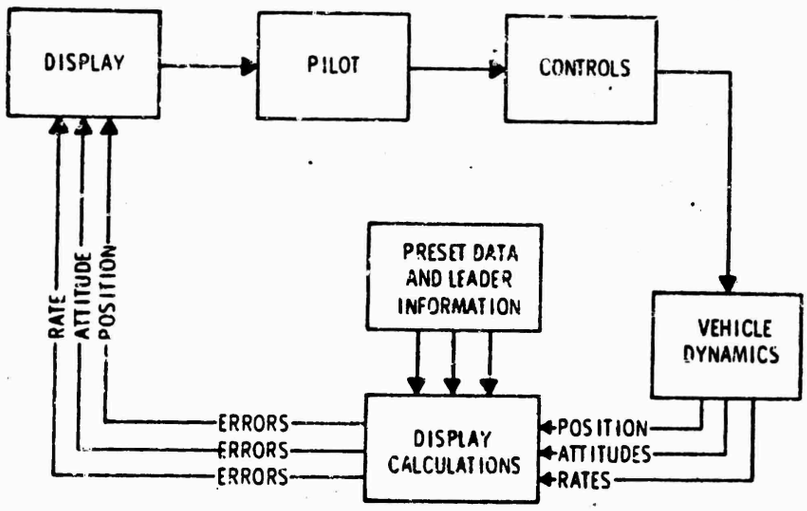

Figure 3. Simulation Block Diagram

AIRCRAFT DYNAMICS

The UH-1 Iroquois helicopter and the AH-56 Cheyenne helicopter were simulated for this study. A description of the simulation of the UH-1 is supplied in Appendix C and its autopilot modes are described in Section IV. A similar description of the AH-56 simulation is provided in Appendix D and its autopilot modes are described in Section VI.

DISPLAY AND CONTROL SYSTEM

The simulated control system consisted of a collective stick, a cyclic stick, and foot pedals mounted in a configuration with the same basic dimensions as the UH-1 pilot station. Appendix C describes the control system characteristics. The following data describe the pilot's station:

- The pilot's seat is constructed with its reference point fixed at the neutral position.
- The cyclic stick's centering position is fixed.
- The stick forces assume that the hydraulic boost is activated.

All of the alternative display formats were generated electronically and presented on a 19-inch CRT located approximately 30 in. from the subject. The layout of these controls and displays is shown in Figure 4.

FORMATION CONFIGURATION

The formation being simulated throughout this study was a four-aircraft heavy-right configuration as shown in Figure 5. The aircraft flown during simulations was the No. 3 aircraft, the first aircraft behind and to the right of the leader. It was assumed that the other three aircraft always remained in their exact commanded positions.

PLAN POSITION INDICATOR (PPI) DISPLAY FORMAT

The Plan Position Indicator (PPI) display (Figure 6) presents a plan-view of the four-aircraft, heavy-right platoon formation. The display is referenced to the lead aircraft, whose position and heading remain stationary on the display. The dimensions of the PPI are 8 in. by 8 in. The display is scaled at 1-in. equals 500 ft in both the X and Y axes and thus provides a 4000-ft-square area to the pilot. A triangle denotes the lead aircraft, while circles denote all follower aircraft, including the pilot's. A cross indicates the command position for the pilot's aircraft.

The display presents an altitude error analog showing ±100 ft of altitude error scaled at 1 in. to 100 ft.

This display was supplemented with an array of conventional flight instruments which served as backup or secondary information sources. Following are the conventional instruments included as part of the simulated display panel:

- Indicated Airspeed (IAS) - This display indicates follower's velocity over the range of 0 to 250 knots. An index marker on the perimeter of the display presents the leader's airspeed.

Figure 4. Layout of Experimental Apparatus

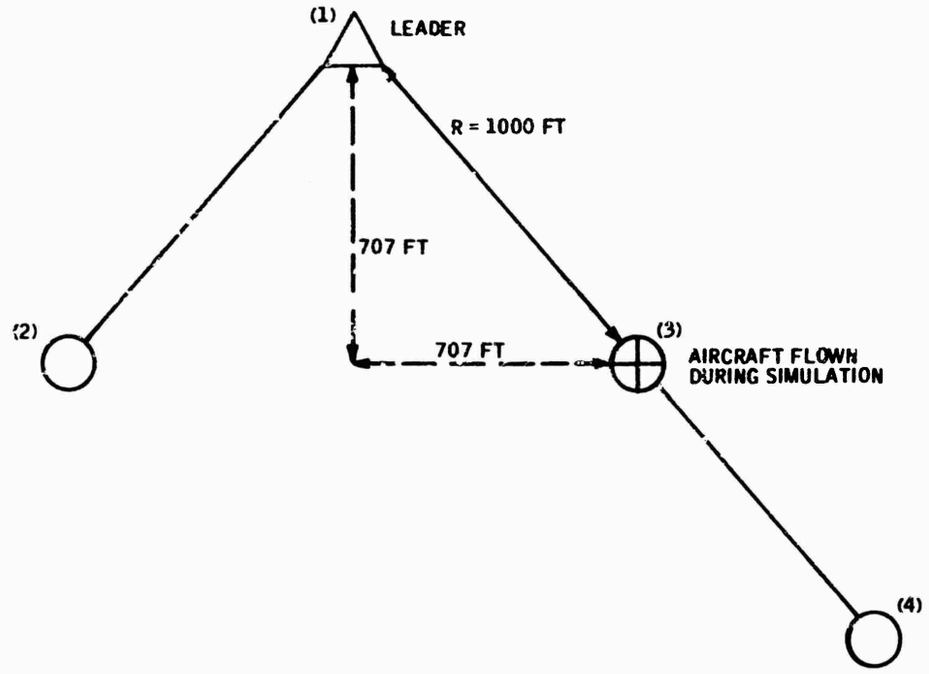

Figure 5. Heavy-Right Formation

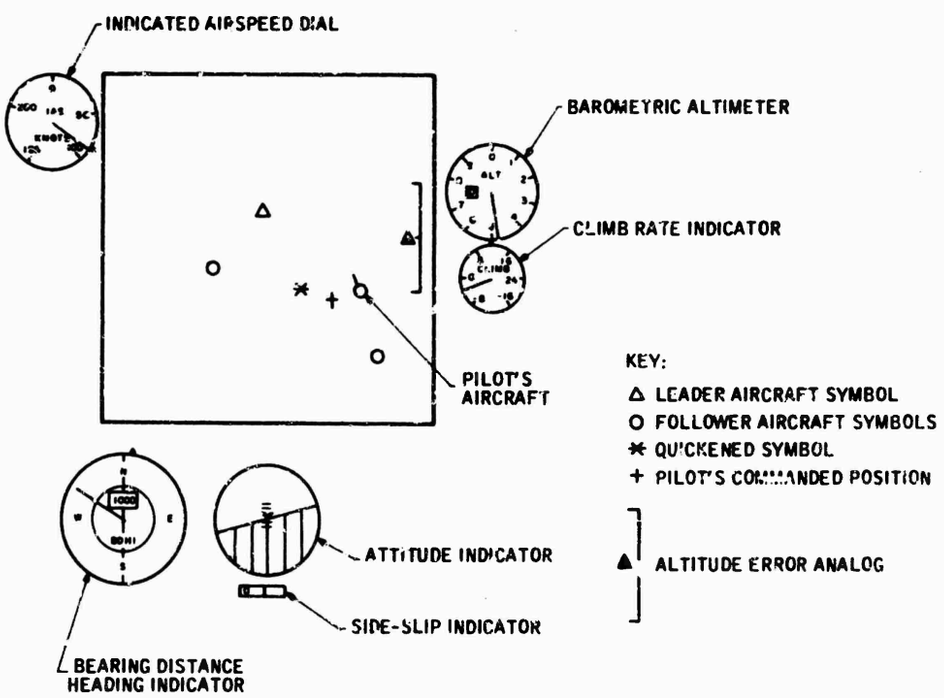

Figure 6. PPI Format

- Bearing-Distance-Heading-Indicator (BDHI) - The BDHI presents the command bearing to the leader, the actual bearing and actual range to the leader. Range is presented in feet on a drum counter. Follower aircraft heading is presented on this display in the conventional manner with a fixed lubber line over a rotating compass card. An index marker indicates lead aircraft heading.

- Barometric Altimeter - This altimeter presents follower's altitude, in feet, to 9999. Thousands of feet are displayed on a one-digit counter, and the dial is scaled from 0 to 1000 ft. An index market presents leader's altitude on the periphery of the display. In the simulation, the leader never flies at altitudes greater than 1000 ft.

- Climb Rate Indicator - This indicator presents altitude rate, in feet per minute, over a range of 0 to ±2400.

- Attitude Indicator - A two-dimensional representation of an attitude ball shows own aircraft roll and pitch; 1 in. of vertical translation of the horizon represents 20 deg of pitch.

SECTION IV
UH-1 AFCS DESCRIPTION

This section describes the various automatic modes which were simulated for the UH-1 portion of this study. These modes consisted of the following levels of autopilot assistance.

- Free vehicle
- Inner loops
  - Yaw stability augmentation
  - Three-axis stability augmentation
- Outer loops
  - Heading hold
  - Altitude hold
  - Heading and altitude hold

These UH-1 autopilot modes were defined in a study for the Army Electronics Command on advanced automatic flight control (Reference 7). Functional block diagrams of the longitudinal and lateral axis autopilot modes are shown in Figures 7 and 8 for the 88-knot flight condition.

FREE VEHICLE

The free-vehicle pitch attitude response to a cyclic step input is essentially a rate response. However, at high speed it does not maintain the steady rate response for relatively long periods after the step input. This is due to the attitude feedback nature of the stabilizer bar. The function of the stabilizer bar on the UH-1 is to improve the stability of the free vehicle. It is equivalent to providing a large time-constant lagged pitch rate feedback of low gain. A heavily lagged pitch rate appears to be similar to pitch attitude.

Free-vehicle roll attitude response to a cyclic step input is shown in Figure 9. This trace clearly shows that the vehicle has the desired rate response; however, the control authority is in excess of 20 deg/sec/in. roll cyclic. It is desirable to have the high-speed control authority fall within the range of 14 to 20 deg/sec/in. cyclic input. In addition to the large control authority, the response is characterized by large overshoots in excess of the desirable 10%.

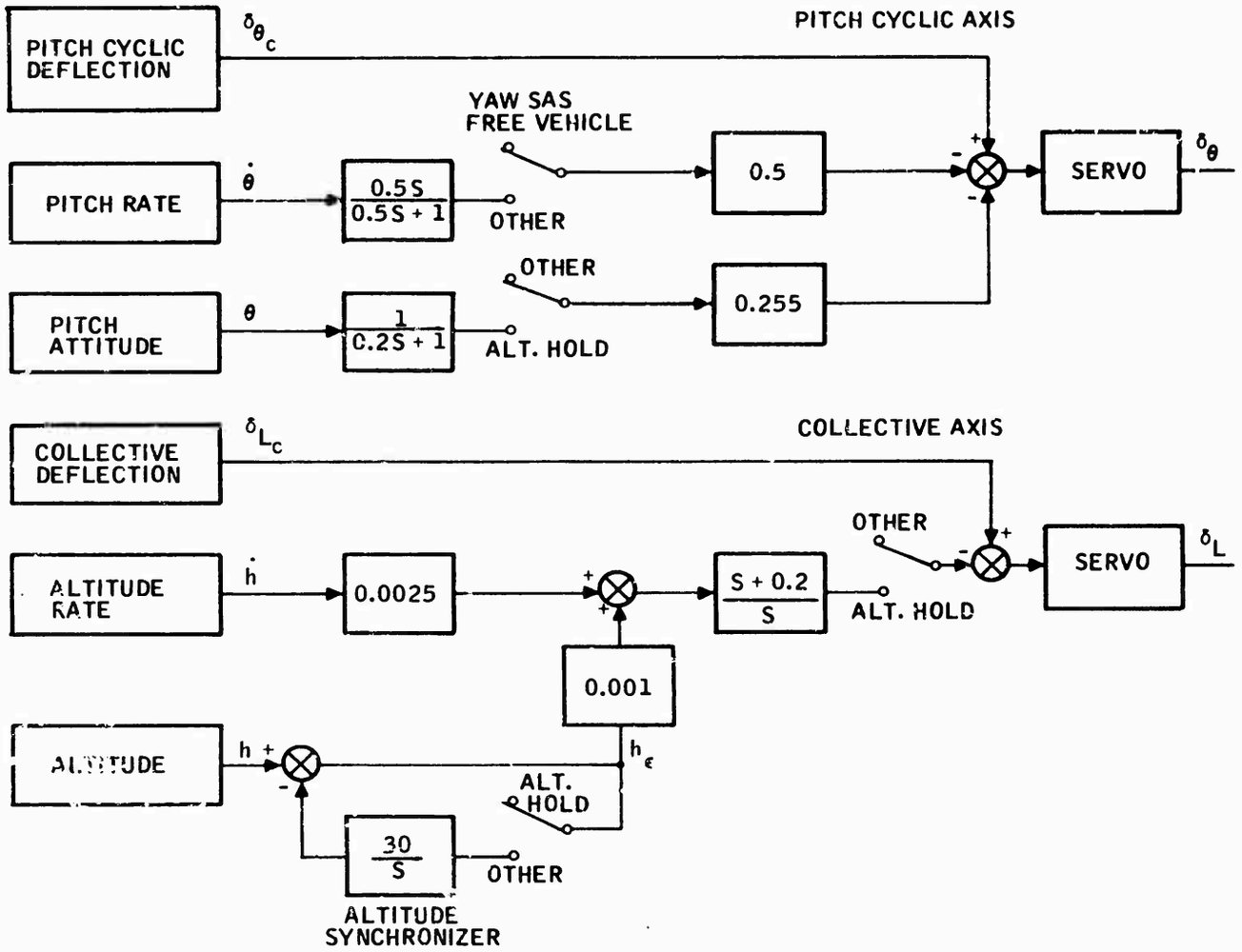

Figure 7. UH-1 Longitudinal Axis AFCS

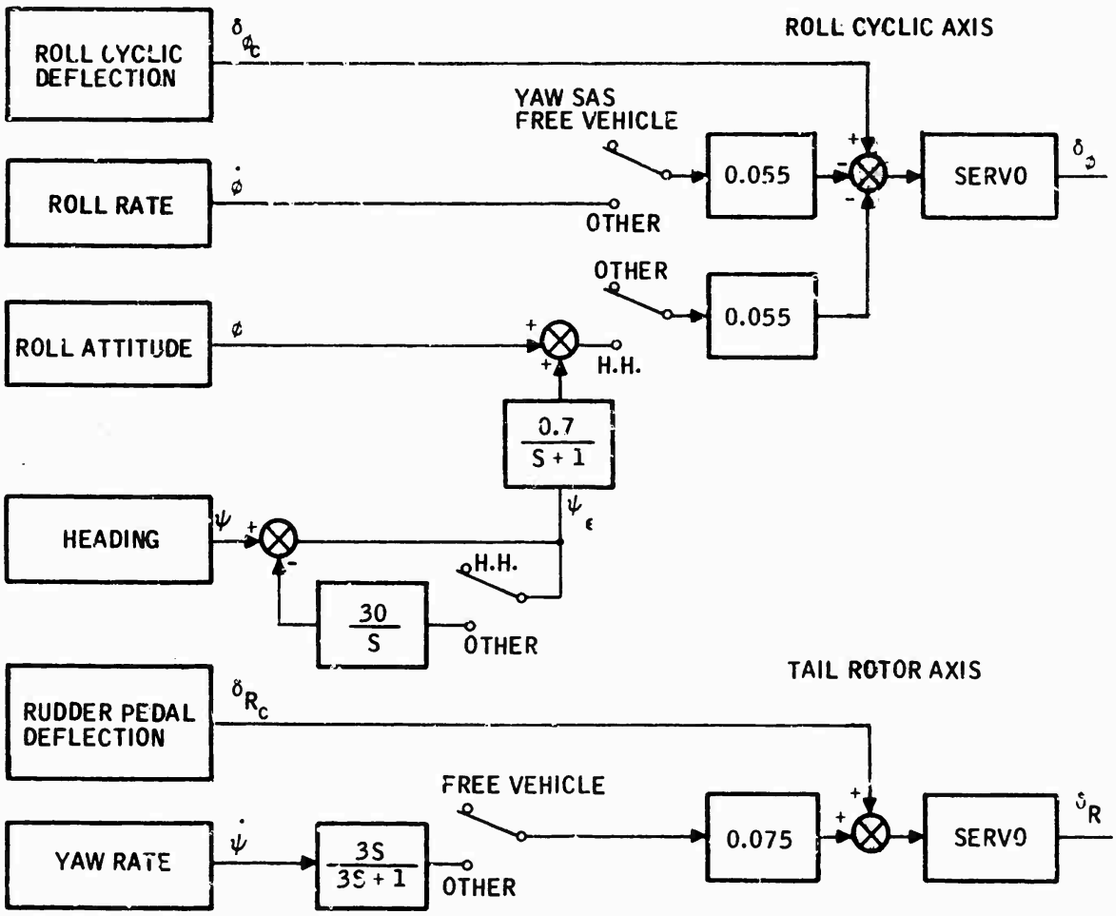

Figure 8. UH-1 Lateral Axis AFCS

YAW STABILITY AUGMENTATION

Simulation results for both the free and augmented vehicle are shown in Figure 9. Vehicle dynamics were tested with side velocity initial condition. Note that under this test condition the Dutch roll mode is obviously underdamped. The augmentation system is a conventional high-passed yaw rate feedback where K_r = 0.075 deg tail rotor per deg per sec and t_{hipass} = 3.0 sec. The yaw SAS time history of Figure 9 clearly shows that the augmentation system results in a smooth, well-damped directional axis.

THREE-AXIS STABILITY AUGMENTATION

This level of stability augmentation includes roll and pitch SAS along with yaw SAS discussed earlier.

Pitch SAS

The SAS control law used for the UH-1 pitch axis is

$$\delta_\theta = \delta_{\theta_c} - 0.5\left(\frac{0.5\,S}{0.5\,S + 1}\right)\dot{\theta}$$

Pitch attitude response of the UH-1 with SAS to a step cyclic stick input is shown in Figure 10. Note that this response is a well damped rate, and it falls within the performance criteria defined for the UH-1.

Roll SAS

The control equation used to augment the stability of the UH-1 is

$$\delta_\phi = \delta_{\phi_c} - 0.055\,\dot{\phi}$$

Roll attitude response to a cyclic step input is shown in Figure 10. The high-speed response is a well damped rate. The control authority, measured approximately 1 sec after initiation of the input command, is 15 deg/sec.

During the development of the UH-1 control laws, the desired control authority was defined to be within the range of 10 to 20 deg/sec.

HEADING HOLD

Heading hold consists of a heading error feedback that is fed to the roll axis to command bank angle changes as a function of heading error.

$$\delta_\phi = K_\phi \left[\phi + K_{\phi_\psi} \left(\frac{1}{1+S} \right) \psi_E \right] - K_p \dot{\phi}$$

where

K_ϕ = 0.055 deg/deg ϕ

K_p = 0.055 deg/deg/sec $\dot{\phi}$

K_{ϕ_ψ} = 0.7 deg roll servo/deg heading error

ψ_E = heading error

Heading error transient response is shown in Figure 9. This response is quite fast, about 9 sec to 90% of initial error reduction, and overshoots about 10%. The heading hold mode is automatically disengaged if the pilot makes a roll cyclic input. A switch on the control stick was also provided for the pilot so that he could lock out heading hold during turns.

ALTITUDE HOLD

The altitude hold mode was mechanized to control altitude through the collective pitch axis. Altitude (h) and altitude rate ($\dot{h}$) are fed through suitable gains to the collective pitch servo in addition to the SAS being engaged. The control equations used for the altitude hold mode are:

$$\delta_\theta = \delta_{\theta_c} - \left[0.5 \left(\frac{0.5S}{0.5S+1} \right) \dot{\theta} + 0.225 \left(\frac{1}{0.2S+1} \right) \theta \right]$$

$$\delta_L = -(0.0025 \dot{h} + 0.001 h) \left(\frac{S+0.2}{S} \right)$$

Note that an integrating servo is used in the collective axis. This prevents bias errors which lead to altitude hang off. Also, a pitch attitude hold mode is engaged (through the cyclic axis) to provide attitude stability. Analog simulation results for a step altitude error input are shown in Figure 10. It is seen that the altitude error transient response for this configuration is very good.

Also shown in Figure 10 is an altitude hold/pitch SAS maneuver. This maneuver was performed by engaging the pitch SAS mode, applying a simulated collective pitch command, flying to an altitude of 200 ft, and then re-engaging altitude hold. This recording clearly shows that the altitude hold maneuvering performance was very good and that large transient activity in the collective and cyclic servos. A switch on the collective control stick was used to engage the altitude hold mode.

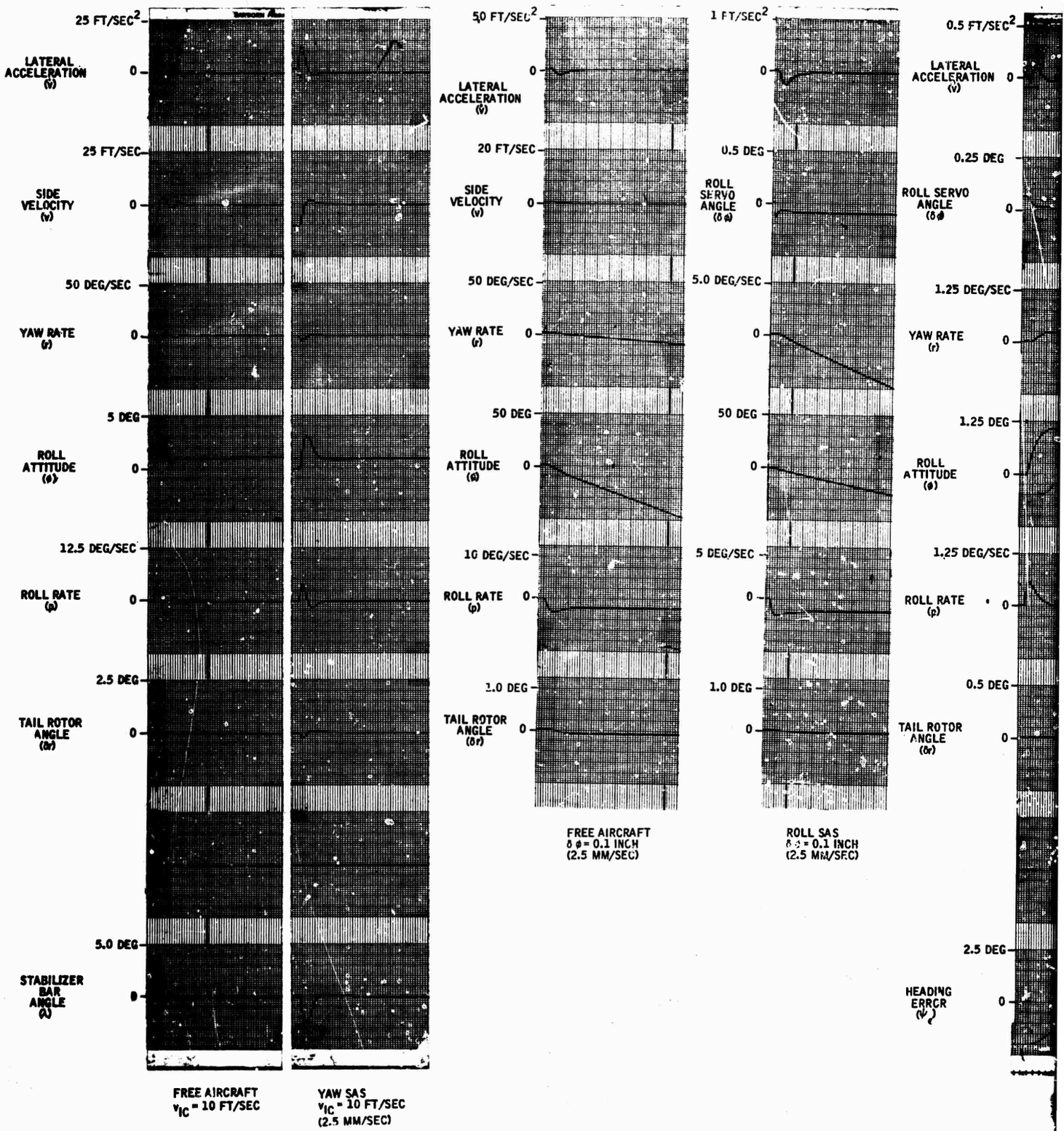

Figure 9. UH-1 Lateral-Directional Analog Responses -- Free Vehicle, Yaw and Roll SAS, and Heading Hold

A

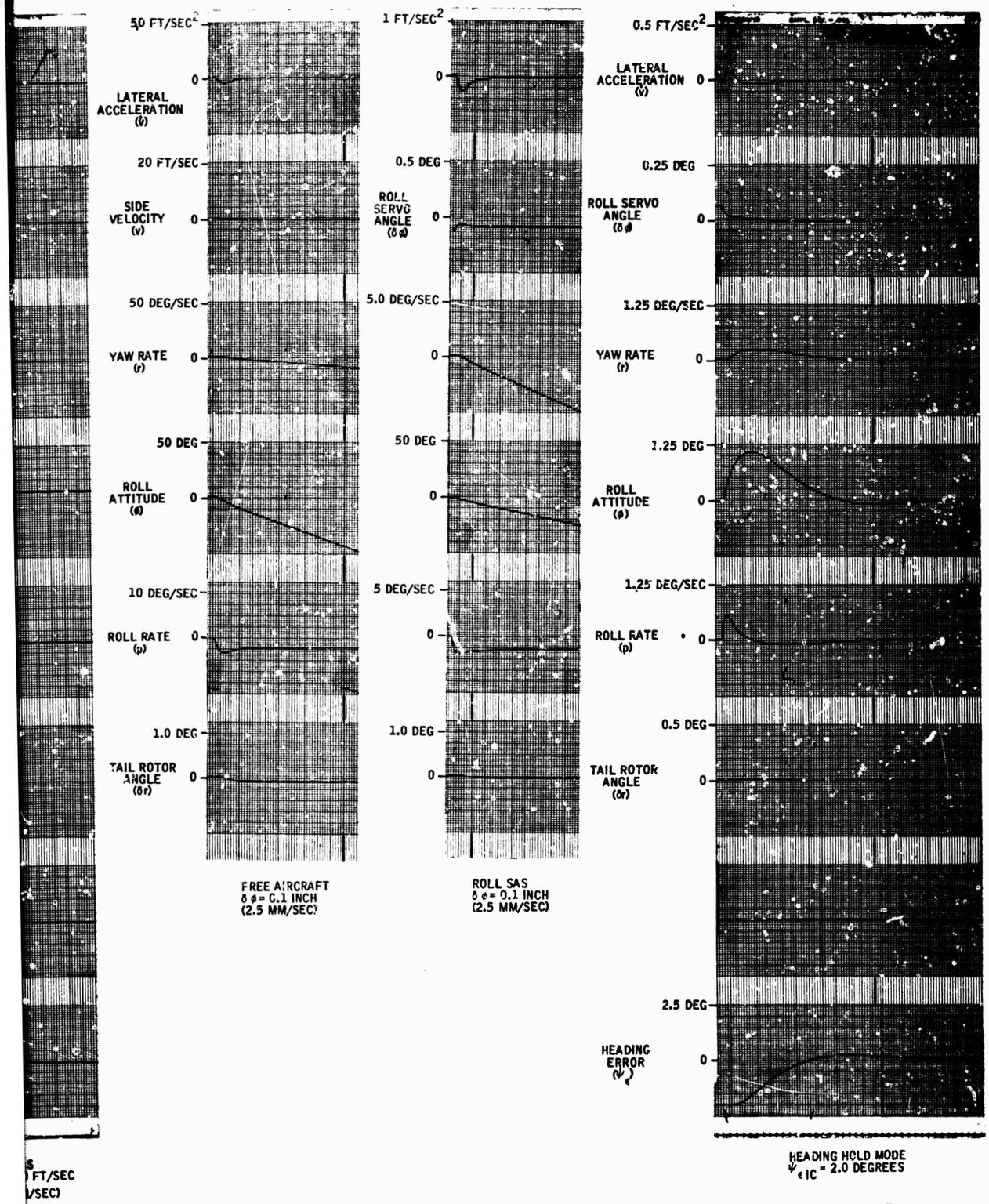

e 9. UH-1 Lateral-Directional Analog Responses -- Free Vehicle, Yaw and Roll SAS, and Heading Hold

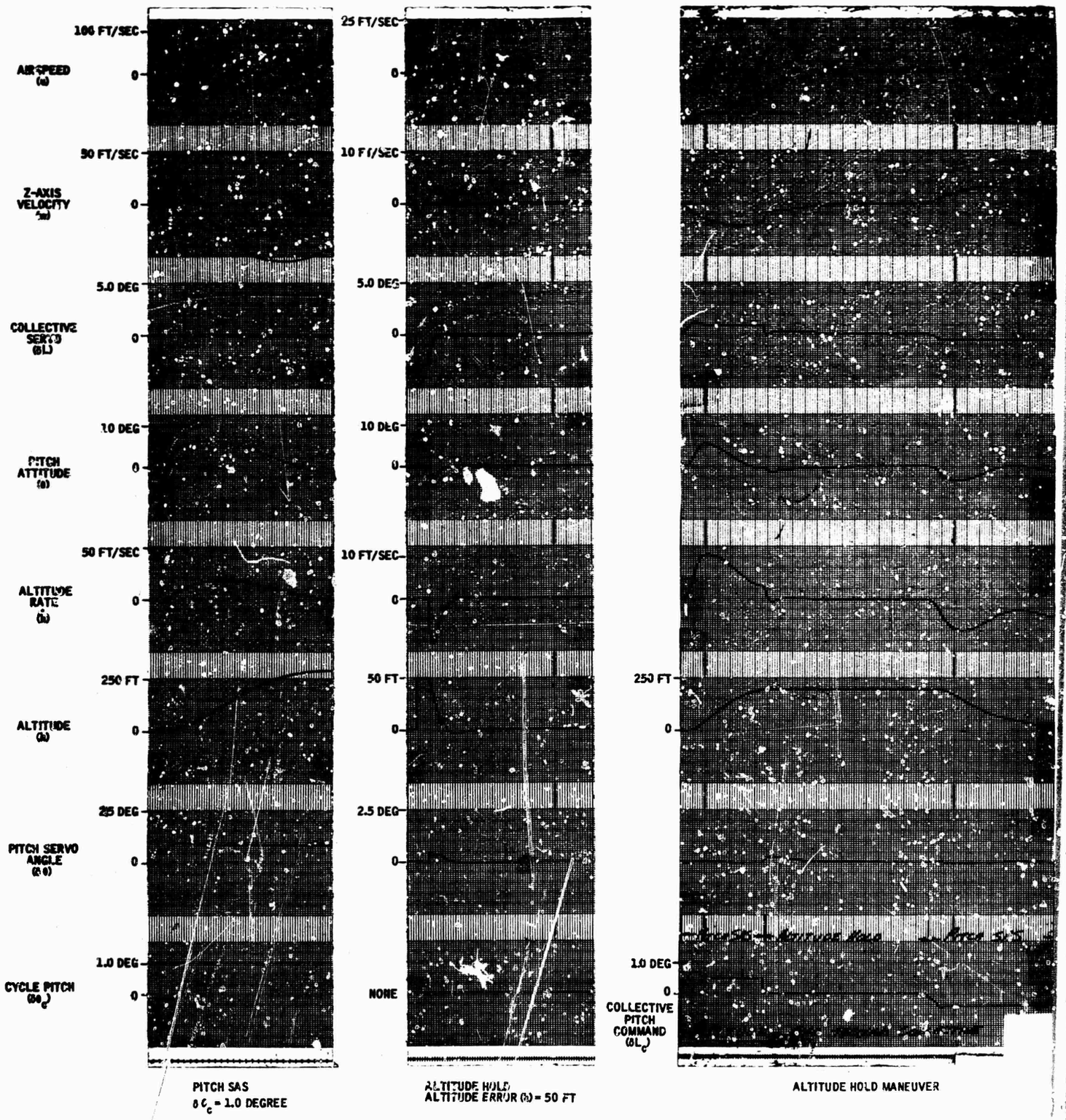

Figure 10. UH-1 Longitudinal Axis Analog Responses -- Pitch SAS and Altitude Hold

HEADING HOLD AND ALTITUDE HOLD

This configuration is a simultaneous engagement of the heading and altitude hold modes. The mode mechanization and performance is the same as described under the individual modes.

The analog simulation of the UH-1 dynamics and autopilot is described in Appendix C.

SECTION V
EVALUATION OF LEVELS OF AFCS AND WORKLOAD FOR UH-1

PRELIMINARY SIMULATIONS

Preliminary simulations were conducted to (1) determine optimum gains for the PPI quickening model, (2) select an appropriate maximum workload level, and (3) provide subject training in each autopilot mode and at each workload level prior to formal data collection.

Display Quickening

The quickening model was the same as that used in previous Honeywell studies (References 1 and 4) for the PPI display format. The equation describing this model and the gains selected for use in the UH-1 autopilot study were as defined below:

$$X_Q = K_X \Delta X + K_{\dot{X}} \Delta \dot{X} + \cos \psi_\varepsilon \left[K_\theta \theta + K_{\dot{\theta}} \dot{\theta}\right]$$

$$- \sin \psi_\varepsilon \left[K_\phi \phi + K_{\dot{\phi}} \dot{\phi} + K_\psi \psi_\varepsilon\right]$$

$$Y_Q = K_Y \Delta Y + K_{\dot{Y}} \Delta \dot{Y} + \cos \psi_\varepsilon \left[K_\phi \phi + K_{\dot{\phi}} \dot{\phi} + K_\psi \psi_\varepsilon\right]$$

$$+ \sin \psi_\varepsilon \left[K_\theta \theta + K_{\dot{\theta}} \dot{\theta}\right]$$

where

X_Q, Y_Q = distance from cross to the asterisk

K_X, K_Y = scale factor

ΔX, ΔY = follower position error

$K_{\dot{X}}$, $K_{\dot{Y}}$ = gains for velocities

$\Delta \dot{X}$, $\Delta \dot{Y}$ = velocity difference between follower and leader

θ = follower pitch attitude

$\dot{\theta}$ = follower pitch attitude rate

ϕ = follower roll attitude

$\dot{\phi}$ = follower roll attitude rate

K_θ, K_ϕ, $K_{\dot{\theta}}$, $K_{\dot{\phi}}$ = gains for attitude terms

K_ψ = gain for heading term

ψ_ϵ = ψ follower - ψ leader = heading error

The gains selected for this study were the same as those which were utilized for the previous study on data rates and accuracies (Reference 4) and were as defined below:

$K_{\dot{X}}$ = 0.1 in./fps of velocity difference

$K_{\dot{Y}}$ = 0.1 in./fps of velocity difference

K_θ = -13.3 in./rad

K_ϕ = 13.3 in./rad

$K_{\dot{\theta}}$ = -13.3 in./rad/sec

$K_{\dot{\phi}}$ = 7.8 in./rad/sec

K_{ψ} = 13.0 in./rad of heading difference

Subject Training and Maximum Workload Selection

Each subject was trained in each autopilot mode/workload combination until his performance stabilized. It was found during these training sessions that the proposed workload level of 80% consistently resulted in total loss of control. Since a 70% workload level could be handled by the subjects most of the time without total loss of control, this level (instead of the proposed 80% level) was selected for evaluation in the formal experiment.

FORMAL EXPERIMENTATION

The objective of this phase of the study was to systematically relate pilot performance during manual IFR formation flight to various levels of autopilot assistance for the UH-1 helicopter. The UH-1 was considered to be representative of the broad class of currently operationa, conventional helicopters. The levels of flight control augmentation were examined at different pilot workload levels since it was expected that the relative efficacy of the of the autopilot mode may vary with the pilot's task level.

EXPERIMENT I - EFFECT OF AUTOPILOT AND WORKLOAD ON PILOT PERFORMANCE - UH-1

The objective of this experiment was the fully factorialized evaluation of subject performance in a manual SK/FF task under six levels of autopilot assistance and three levels of subject workload.

1.0 Independent Variables

Autopilot Mode - The six levels of autopilot examined were

- Free vehicle
- Yaw axis stability augmentation
- Three-axis stability augmentation
- Heading hold (includes three-axis stability augmentation)
- Altitude hold (includes three-axis stability augmentation)
- Heading and altitude hold (includes three-axis stability augmentation)

These modes are described in Section IV.

Workload Level--The selection of the three levels of workload to be evaluated was based on the results of the workload assessment simulations that were performed during a previous Honeywell study (Reference 1) and the preliminary simulation phase of the current study. The workload consisted of a forced-pace, concomitant task presented during the interval when the primary display was interrupted. The display format was programmed so that it could be blanked out at preselected frequencies and intervals. During the interval when the display was interrupted, the computer presented a randomly selected, single-digit number in the center of the display. The off-cycle of the display was varied to provide different levels of workload, with the display on-cycle remaining constant at 1 sec. The levels of workload selected for evaluation were 0%, 40%, and 70%. The corresponding display on and off cycles were:

Workload Level	Display Off-cycle	Display On-cycle
0%	0.0 sec	continuous
40%	0.67 sec	1.0 sec
70%	2.30 sec	1.0 sec

Subjects

Subject BAO--This subject is a civilian pilot who holds a VFR helicopter rating and has approximately 40 hours of helicopter flight time. He has participated in previous Honeywell simulation programs for a total of approximately 440 hours.

Subject TR--This subject is a military pilot who holds VFR and IFR helicopter ratings and has approximately 3300 hours of helicopter flight time. He has participated in previous Honeywell simulation programs for a total of approximately 125 hours.

Subject DI--This subject is a military pilot who holds VFR and IFR helicopter ratings and has approximately 3000 hours of helicopter flight time. He has participated in previous Honeywell simulation programs for a total of approximately 50 hours.

Subject JA--This subject is a military pilot who holds VFR and IFR helicopter ratings and has approximately 5000 hours of helicopter flight time. He has participated in previous Honeywell simulation programs for a total of approximately 50 hours.

Mission Phases--The mission profile used included phases representative of typical maneuvers that might be required on a practical operational status where a broad range of task difficulties could be represented.

The various phases were:

- Phase 1 - The formation leader accelerates from 70 knots to 88 knots IAS, all formation A/C to maintain position integrity.
- Phase 2 - Formation leader climbs 250 ft at 500 ft per minute while maintaining heading, all A/C maintaining position.
- Phase 3 - The formation leader initiates a right turn of 60 deg at 1.5 deg/sec turn rate while maintaining altitude, all A/C maintaining position relative to the leader.
- Phase 4 - The formation leader descends 250 ft at 500 ft per minute while maintaining a fixed inertial heading, all A/C in the formation maintaining position with respect to leader.

- Phase 5 - The formation leader performs a left turn through 60 deg at a turn rate of 1.5 deg/sec, while maintaining altitude.

- Phase 6 - All A/C maintain position in straight and level flight.

- Phase 7 - The formation leader decelerates from 88 knots to 70 knots while maintaining altitude and heading constant.

The mission phases were flown consecutively. At the end of each phase all position errors were automatically nulled, setting the aircraft exactly on the command position. Ten seconds were then provided to allow the subject to compensate for the attitudes and rates instituted immediately prior to the automatic nulling of position errors. At the end of the 10-sec period the next mission phase was initiated.

2.0 Dependent Variables

The following variables were recorded during the simulated missions and used as the basis of comparing the various levels of autopilot and workload.

Position Error Measures--Three measures were calculated of the longitudinal (X), latersl (Y), vertical (Z), and range (R) position errors that occurred during each mission phase. The error measures computed for each phase were the mean position errors, the standard deviations of the error distributions about the mean errors, and the root-mean-square (RMS) errors. These error measures were calculated in feet, using the command position as the reference.

Activity Index--This measure was used to provide an indication of the attitude stability of the aircraft in terms of the magnitude and frequency of aircraft attitude changes. It also provides an indication of the extent to which control inputs must be instituted into the system (in terms of the magnitude and frequency of inputs made by either the pilot or autopilot) in order to maintain the correct aircraft position. It should be noted that this measure provides only an indirect measure of the pilot's input activity when automatic modes are engaged since control inputs are also instituted by the autopilot.

To allow meaningful interpretation of these measures, the average attitude, attitude rate, and frequency (Hz) associated with the activity indices are presented in Figures 11, 12, and 13. These figures show that the maximum attitude and attitude rate increase, and that the frequency decreases as the activity index increases. Since low magnitude and high frequency of control inputs and aircraft response are characteristic of a more stable control

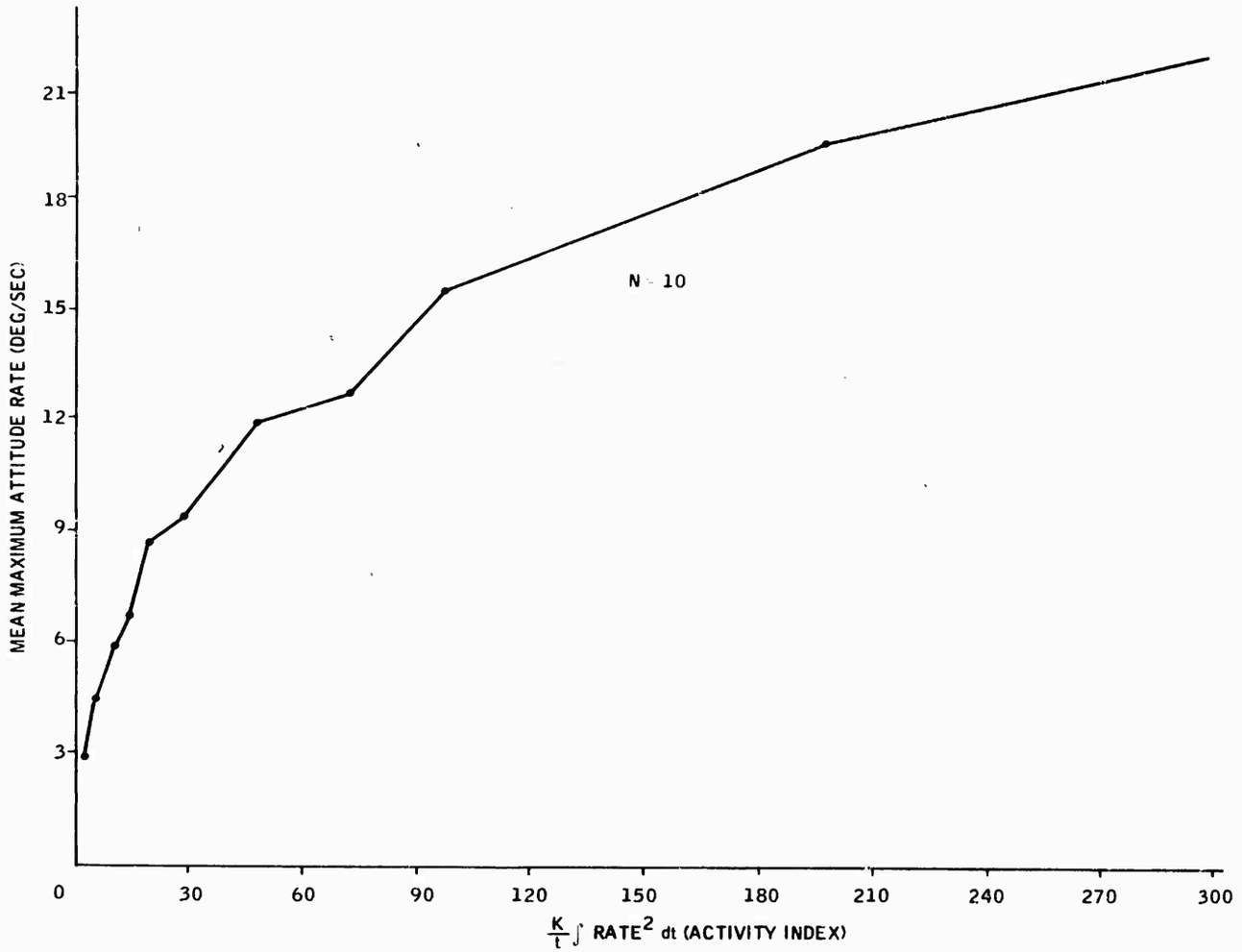

Figure 11. Mean Max. Attitude Rates versus Activity Index

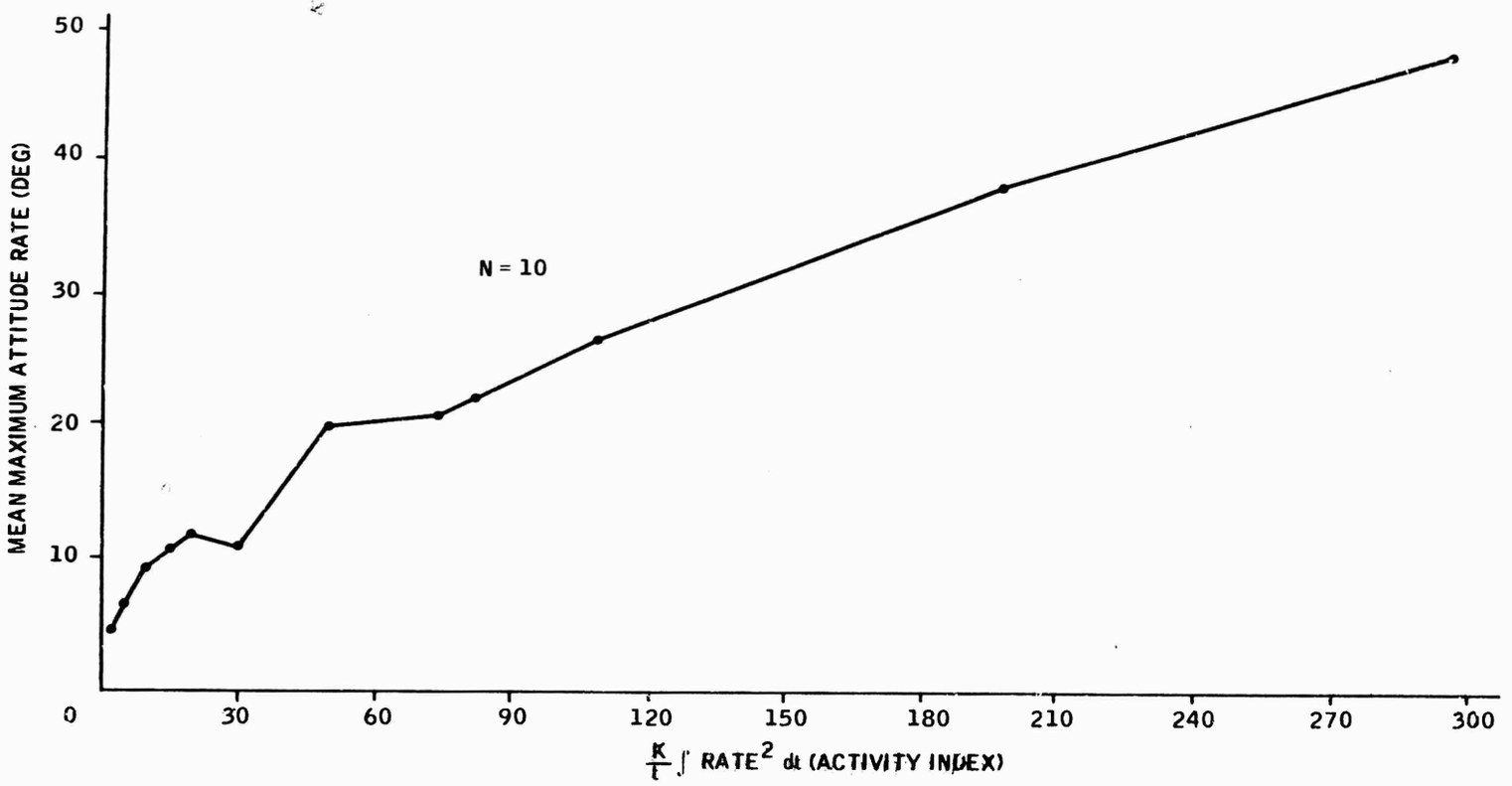

Figure 12. Mean Max. Attitudes versus Activity Index

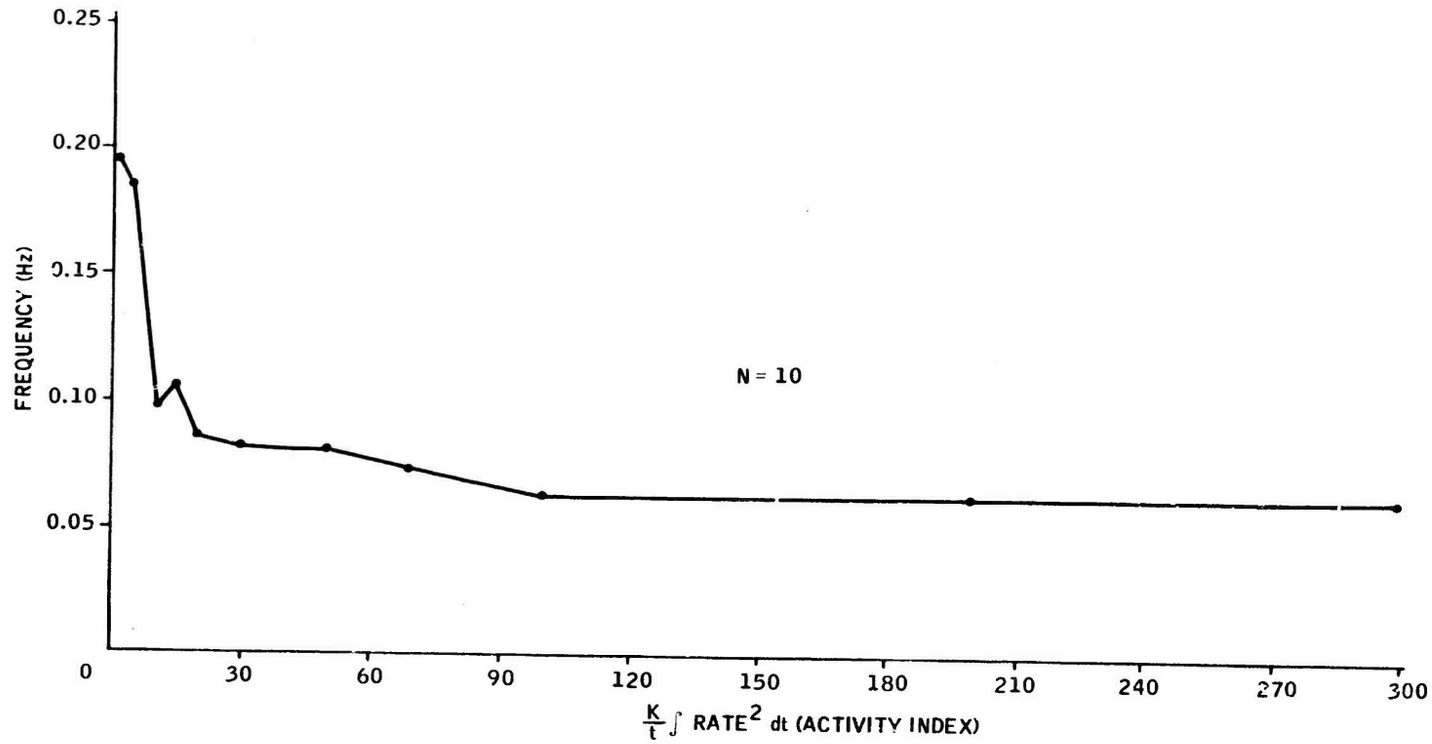

Figure 13. Frequency (CPS) versus Activity Index

system than are high-magnitude, low-frequency inputs and responses, lower activity indices were assumed to be more desirable. A more detailed description and evaluation of this measurement can be found in the final report for a previous Honeywell study on data rates and accuracies for the SK/FF system (Reference 4).

The attitude activity indices recorded were

$$\text{Pitch activity index} = \frac{K}{T}\int_{0}^{T} \dot{\phi}^{2}\, dT$$

$$\text{Roll activity index} = \frac{K}{T}\int_{0}^{T} \dot{\phi}^{2}\, dT$$

where

T = time length of specific mission phase

K = constant factor set for convenient graphical presentation

Collisions--A collision was scored any time the subject's helicopter came within 60 ft (hub-to-hub measurement) of any other helicopter in the formation. The helicopter collided with was designated on the computer printout.

Catastrophic Control Losses--Control losses which resulted in the termination of the mission due to observable collisions with the ground or which resulted from exceeding the attitude limits of the aircraft were recorded by the experimenter.

3.0 Constants

Data Rate--One rate of data update was maintained throughout the experiment. It was 4 updates/sec, found in a previous Honeywell study to be the lowest update rate yielding adequate performance (Reference 4).

Data Accuracy--One data accuracy was used throughout the experiment, as detailed below:

Measurement	SD of Gaussian Noise Distribution
bearing	N_B = 0.007 rad
elevation	N_E = 0.007 rad
range	N_R = 1.5 ft

These measurements were filtered with an alpha-beta filter ($\alpha = 0.25$) prior to display presentation. This level of measurement noise after filtering resulted in the following levels of noise in the X, Y, and Z position coordinates:

$$\sigma_X = \sigma_Y = 2.25 \text{ feet}$$

$$\sigma_Z = 3.14 \text{ feet}$$

For further details of the simulated measurement system, refer to Reference 4.

Turbulence--One level of turbulence was simulated throughout the experiment. It consisted of a zero mean wind velocity with a simulated maximum gust level of 10 knots, yielding a gust level to airspeed ratio of 0.114.

Mission Phase Sequence--The sequence of the seven mission phases was as described above and was held constant throughout the experiment.

Simulation--All characteristics of the simulation (i.e., UH-1 helicopter dynamics, formation configuration, control system, display, and display format) were as described in Section III of this report and were held constant throughout this experiment.

4.0 Experimental Plan

Figure 14 illustrates the design used for this experiment.

The schedule followed in accomplishing the experiment is presented in Table 2. The order of presentation of autopilot modes and the order of workloads within each mode were counterbalanced between subjects to control possible order effects. One seven-phase mission was flown by each subject for each combination of parameters shown in Table 2.

5.0 Analysis of Data

Analyses of variance were performed separately for each mission phase so that autopilot modes could be evaluated for each specific maneuver. The analysis for each phase was based only on the autopilot modes which were applicable for that maneuver. Some autopilot modes were not appropriate for some maneuvers; e.g., the altitude hold mode could not be used during the climb or descent phases. Thus, each analysis was performed on the complete factorial combination of the applicable autopilot modes for that phase, three levels of workload, and four subjects. The subject factor was

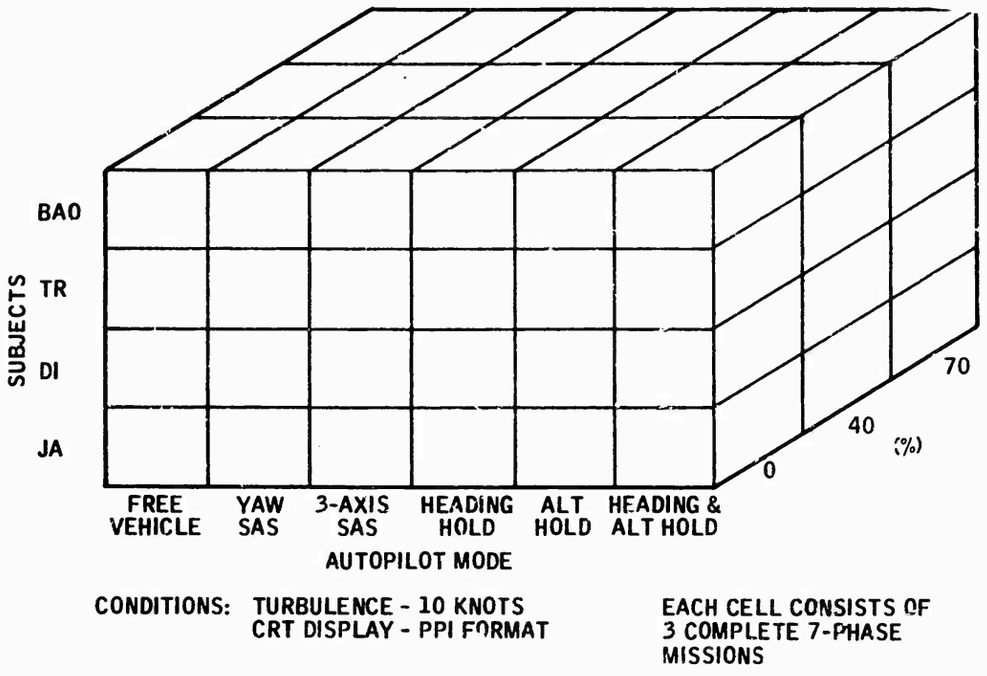

Figure 14. Experimental Design

considered to be random with all other factors fixed. Interactions of each effect with the subject factor represented the error term for the corresponding main effect being tested. For example, the workload man effect (W) was tested with the workload by subject interaction (WS).

The analysis of variance was performed on the subject cell means. The subject cell means were based on either two or three observations. A high number of control losses occurred at the 70% workload level, resulting in a considerable lengthening of data collection time. To limit the time required to complete data collection and to limit the subject frustration resulting from several consecutive control losses, it was decided to accept two replications per cell (instead of three as scheduled). Thus, although most of the subject cell means were based on three observations, some at the 70% workload level were based on only two observations. Table 3 summarizes the levels of variables and constants describing this experiment.

Table 2. Experimental Schedule (UH-1)

Subject	Mode	Workload								
BAO	3-Axis (3)	70	40	0	40	0	70	40	70	0
	Yaw-Axis (2)	40	70	0	70	40	0	0	40	70
	Heading Hold (4)	0	70	40	70	40	0	0	40	70
	Altitude Hold (5)	40	70	0	0	40	70	70	0	40
	Heading and Altitude Hold (6)	0	40	70	70	0	40	40	70	0
	Free Vehicle (1)	40	0	70	0	70	40	0	40	70
TR	3-Axis (3)	40	70	0	70	0	40	0	40	70
	Altitude Hold (5)	0	70	40	40	0	70	70	40	0
	Free Vehicle (1)	70	40	0	40	0	70	0	70	40
	Heading and Altitude Hold (6)	40	70	0	70	0	0	40	70	0
	Heading Hold (4)	0	70	40	70	0	40	40	70	0
	Yaw-Axis (2)	0	40	70	70	0	40	40	70	0
DI	Yaw-Axis (2)	0	40	70	0	70	40	40	0	70
	Altitude Hold (5)	40	70	0	70	0	40	0	40	70
	Heading and Altitude Hold (6)	70	0	40	0	40	70	40	70	0
	3-Axis (3)	0	40	70	70	40	0	40	0	70
	Free Vehicle (1)	0	40	70	0	40	70	40	70	0
	Heading Hold (4)	40	70	0	40	0	70	70	40	0
JA	Yaw Axis (2)	0	70	40	40	0	70	70	40	0
	Free Vehicle (1)	0	40	70	70	0	40	40	70	0
	Heading Hold (4)	0	40	70	70	0	40	40	70	0
	Heading and Altitude Hold (6)	40	70	0	70	0	40	0	40	70
	Altitude Hold (5)	70	40	0	40	0	70	0	70	40
	3-Axis (3)	40	70	0	70	0	40	0	70	40

Table 3. Experiment Summary (UH-1)

1. Controlled Parameters	Levels
a. Subjects (S)	4
b. Workloads (W)	3
c. Autopilot Modes (M)	6
d. Mission Phases (P)	7

2. Measured Parameters
   a. Position Error Measures (12)
      1) RMS error for X, Y, Z, and R
      2) Mean error for X, Y, Z, and R
      3) Standard deviation for X, Y, Z, and R
   b. Collisions with other aircraft
   c. Catastrophic Control Losses
   d. Activity Indices (2)
      1) Roll activity index
      2) Pitch activity index

3. Experimental Constants
   a. Turbulence level of 10 knots
   b. Mission phase sequence
   c. Data Rate
   d. Data Accuracy
   e. All characteristics of the simulation (helicopter dynamics, formulation configuration, PPI display format, quickening model, etc.)

4. Total Number of Cell Means

   $S \times Q \times M \times P = 4 \times 3 \times 6 \times 7 = 504$

6.0 Results - Experiment I

Analyses of variance were performed on the RMS_X, RMS_Y, RMS_Z position error data and on the pitch and roll activity indices recorded during this experiment. These analyses, summarized in Appendix A for three representative phases, indicate the statistical significance of differences in pilot performance associated with the various autopilot modes and workload levels.

6.1 Effect of Workload on Performance -- Overall mean RMS errors and activity indices by mission phase for each of the workloads tested are shown in Figures 15 through 28. Increasing the workload level resulted in increased longitudinal (X), lateral (Y), and altitude (Z) RMS position errors and in higher pitch and roll activity indices for all seven mission phases. The differences in the RMS position errors resulting from increasing the workload were statistically significant for all three axes (RMS_X, RMS_Y, RMS_Z) for all seven phases. The differences in the roll activity index were also statistically significant for all phases.

The pitch activity index also increased with the increase in workload level in all seven phases, although the differences due to this increased workload were not significant for two of the seven mission phases. In the left turn and the straight-and-level phases the same trend was noted, but the resultant increase in the pitch activity index was not great enough to result in statistical significance.

It can be noted from Figures 15 through 28 that the extent of performance degradation resulting from increasing the workload varies with the mission phase. For example, the percentage of increase in RMS_X errors associated with the increase in workload from 40% to 70% ranges from 75% in the straight-and-level phase (Figure 25) to 160% in the climb phase (Figure 17), with corresponding percentage increases in the roll activity index ranging from 200% in the straight-and-level phase to 350% in the climb phase. This variation in the extent of performance degradation between the mission phases is as expected due to the varying levels of difficulty of these maneuvers.

The relationship between performance degradation and the workload level appears to be exponential in nature, with the increase from 40% to 70% resulting in a much sharper rise in RMS errors and activity indices than that from 0% to 40%.

In summary, increasing the pilot workload results in significant performance degradation in terms of increasing RMS position errors and demanding a greater extent of control inputs to maintain position. These results verify those obtained in a previous Honeywell study on the evaluation of various display formats at different workload levels (Reference 1).

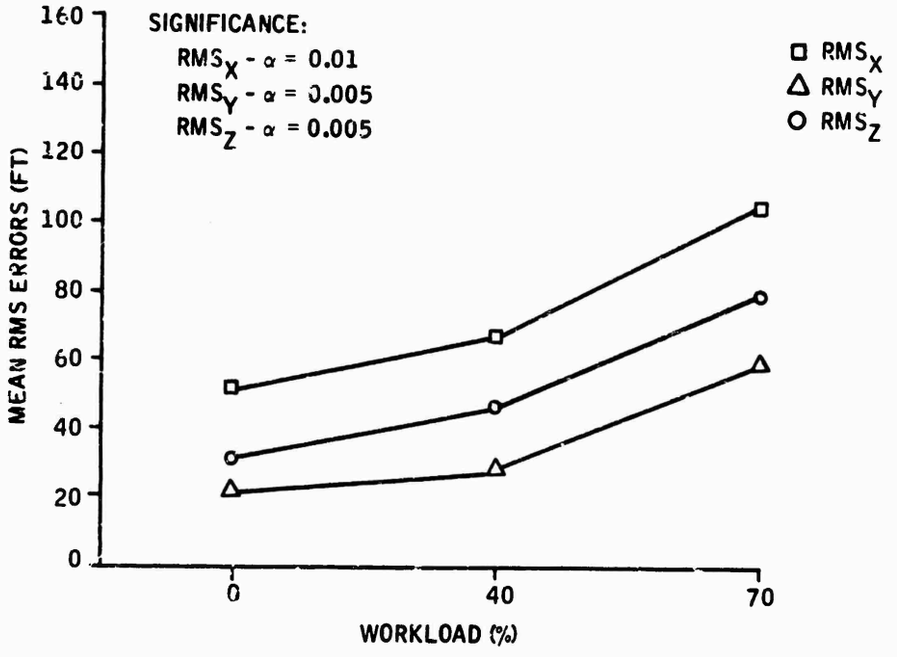

Figure 15. Phase 2 (Acceleration): RMS Errors versus Workload

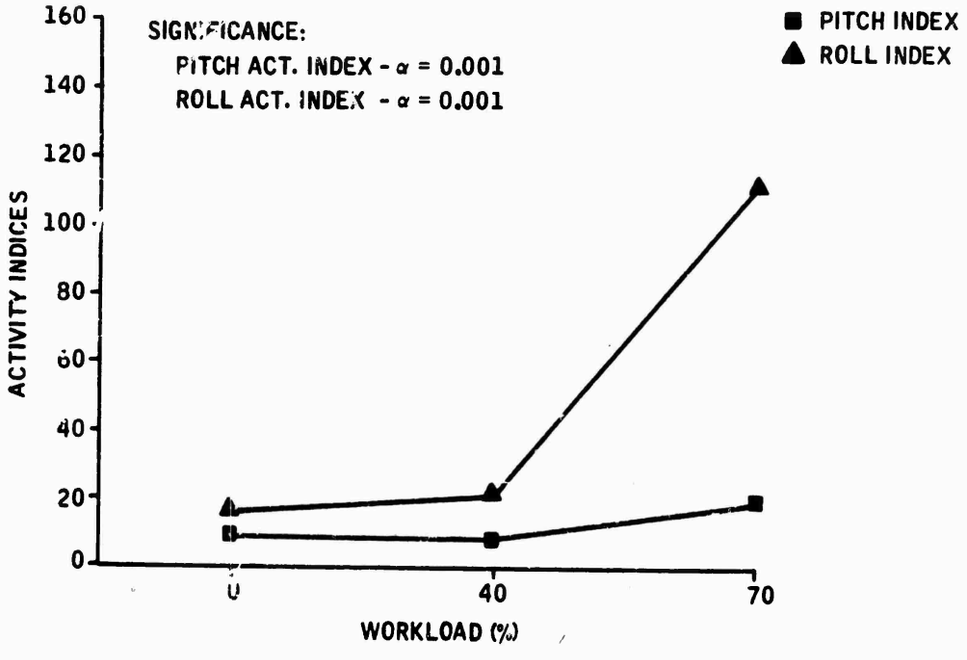

Figure 16. Phase 2 (Acceleration): Activity Indices versus Workload

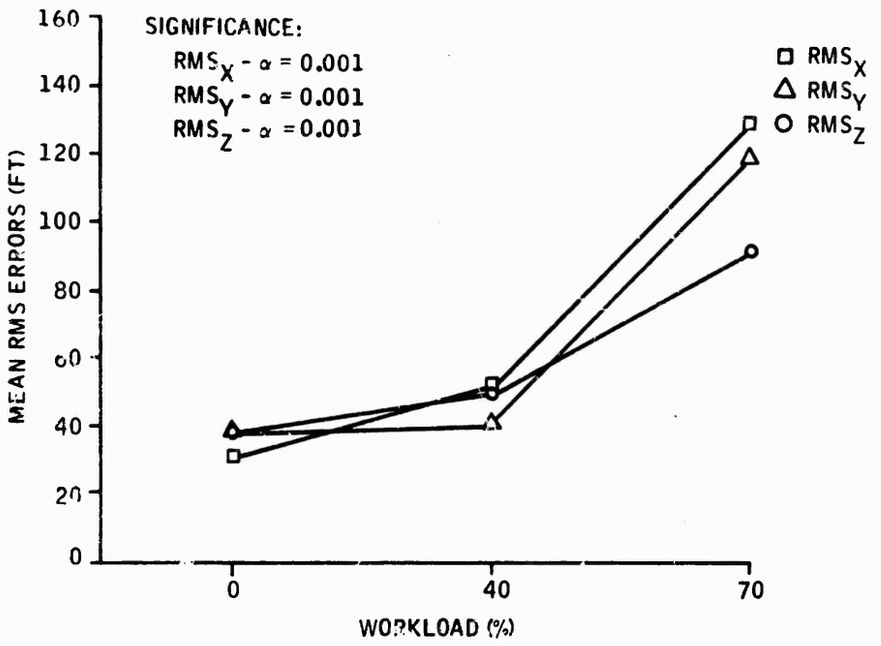

Figure 17. Phase 3 (Climb): RMS Errors versus Workload

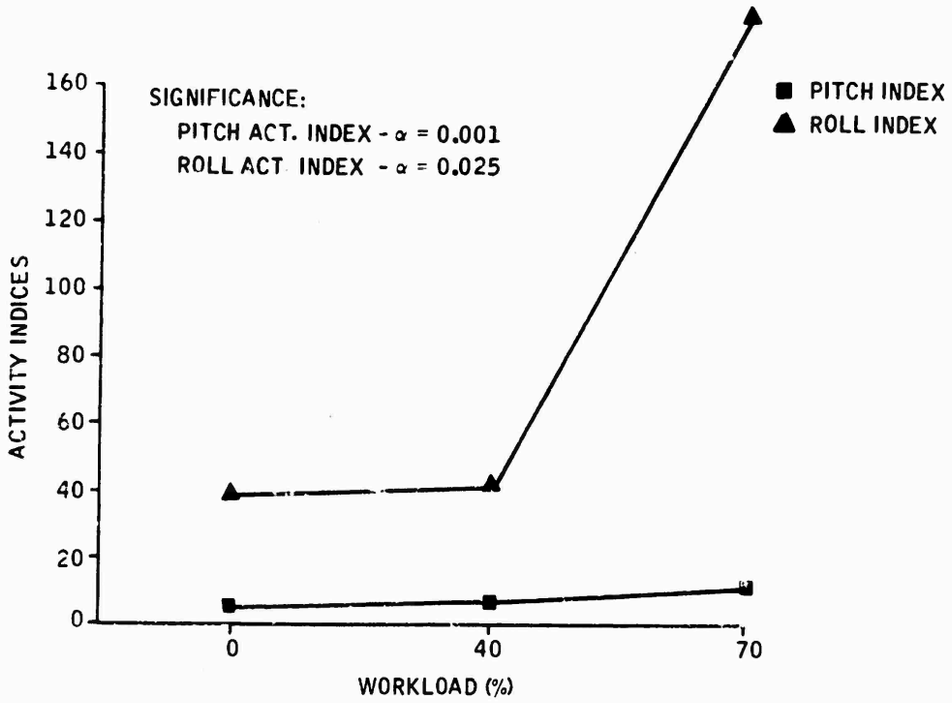

Figure 18. Phase 3 (Climb): Activity Indices versus Workload

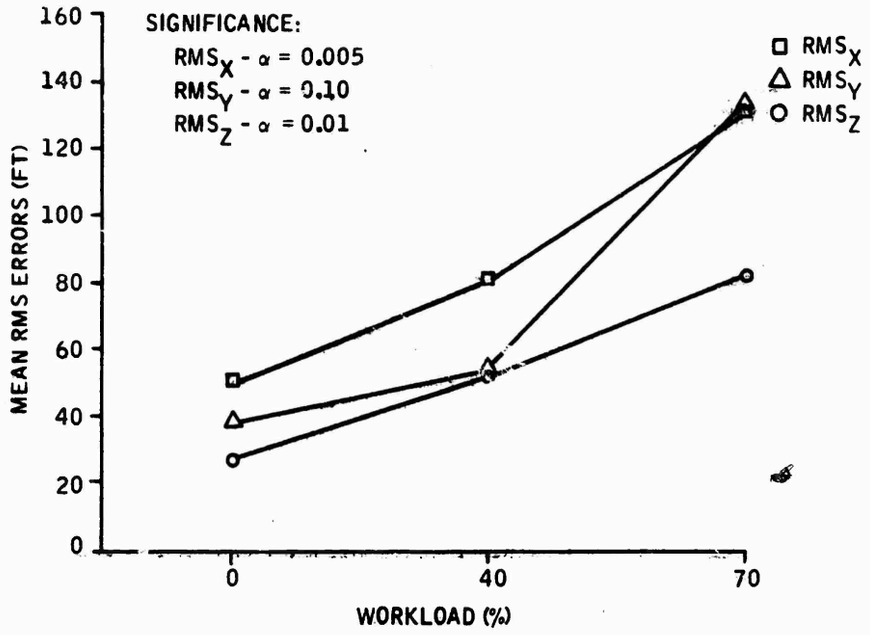

Figure 19. Phase 4 (Right Turn): RMS Errors versus Workload

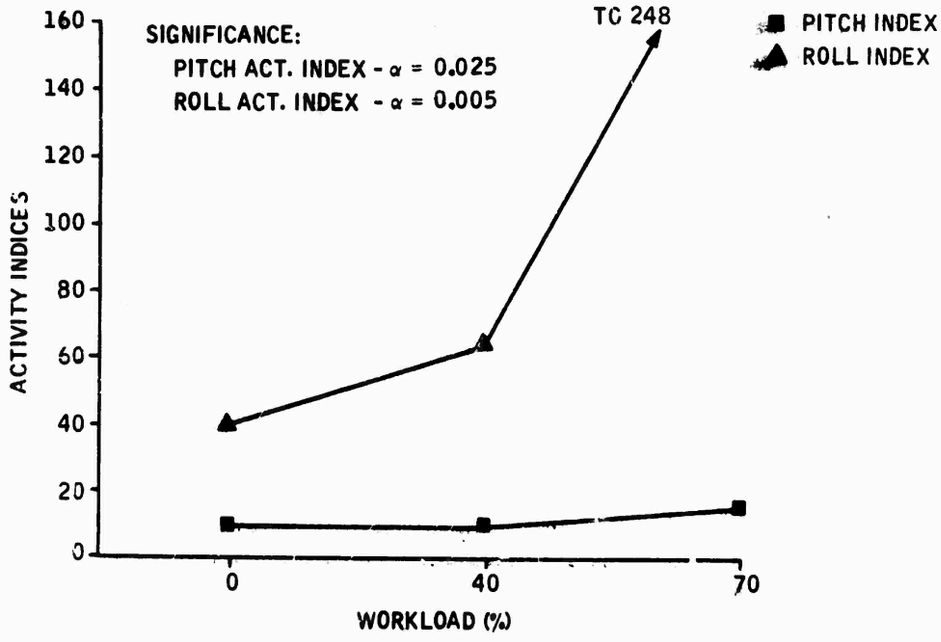

Figure 20. Phase 4 (Right Turn): Activity Indices versus Workload

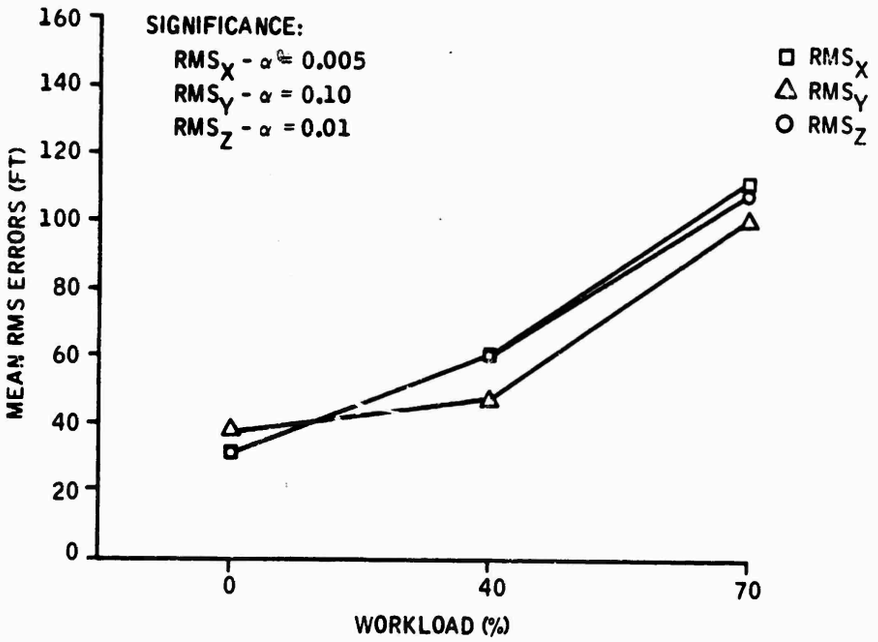

Figure 21. Phase 5 (Descent): RMS Errors versus Workload

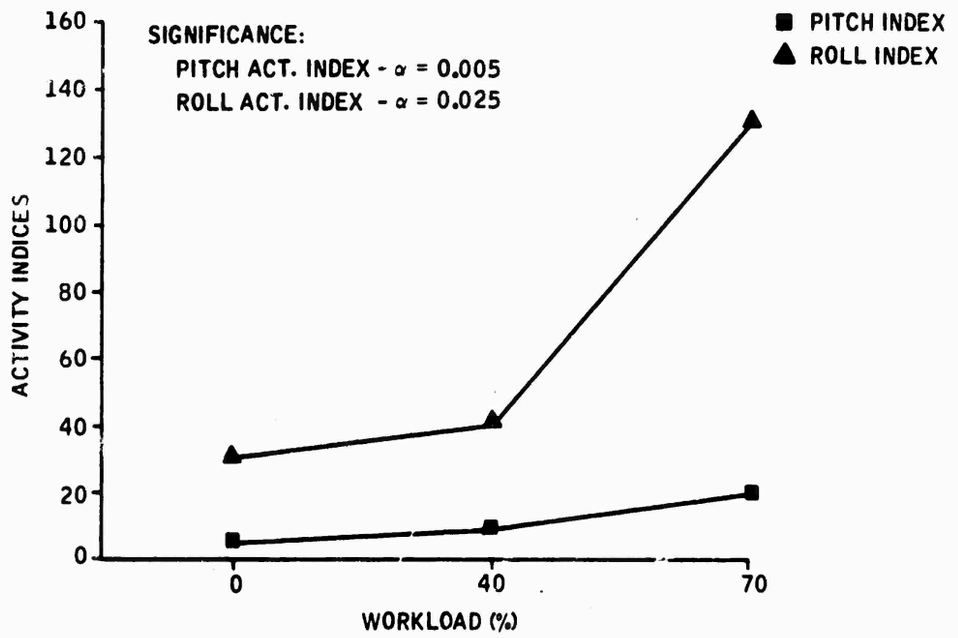

Figure 22. Phase 5 (Descent): Activity Indices versus Workload

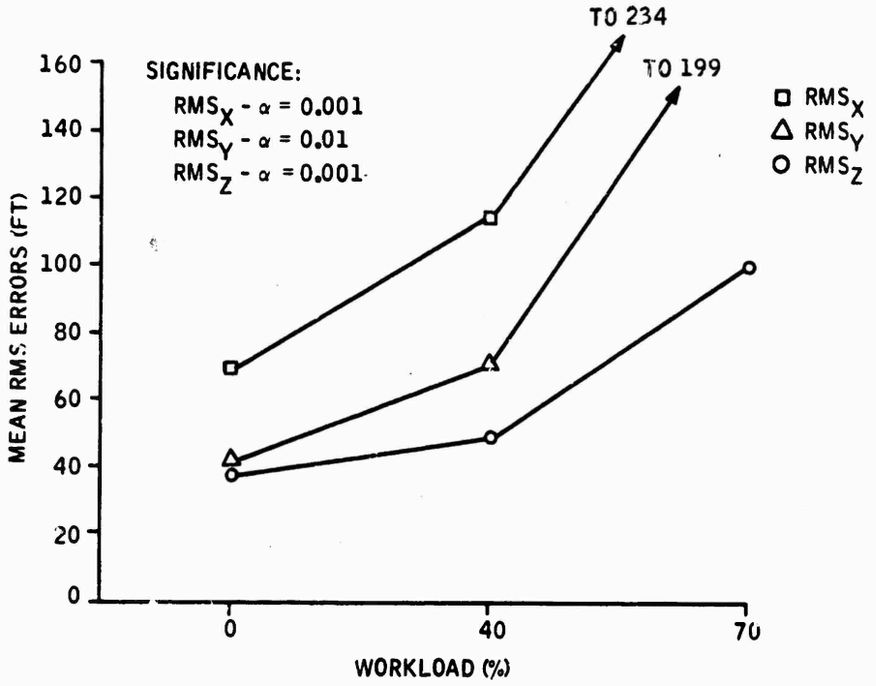

Figure 23. Phase 6 (Left Turn): RMS Errors versus Workload

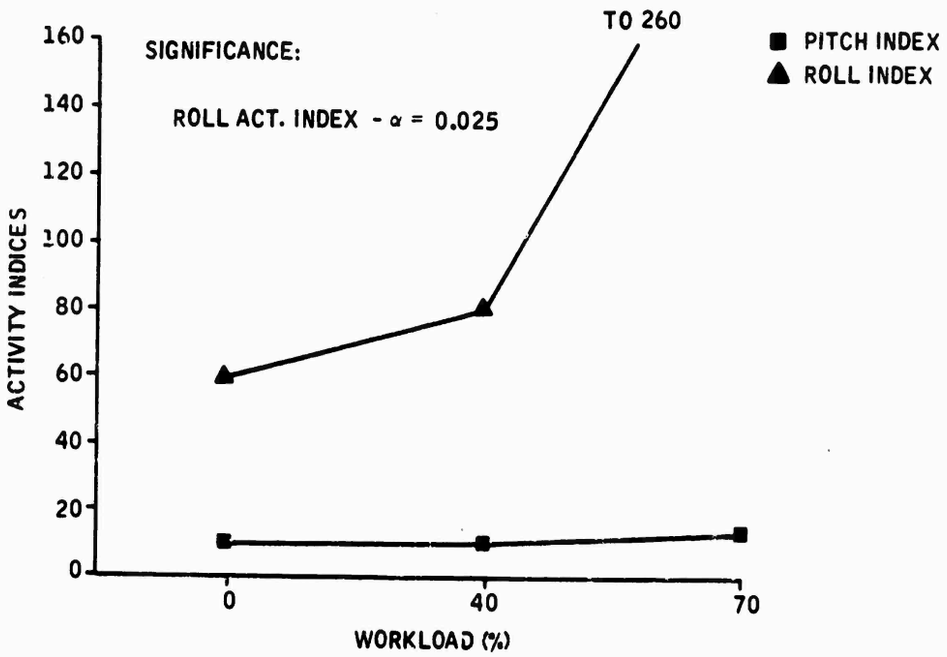

Figure 24. Phase 6 (Left Turn): Activity Indices versus Workload

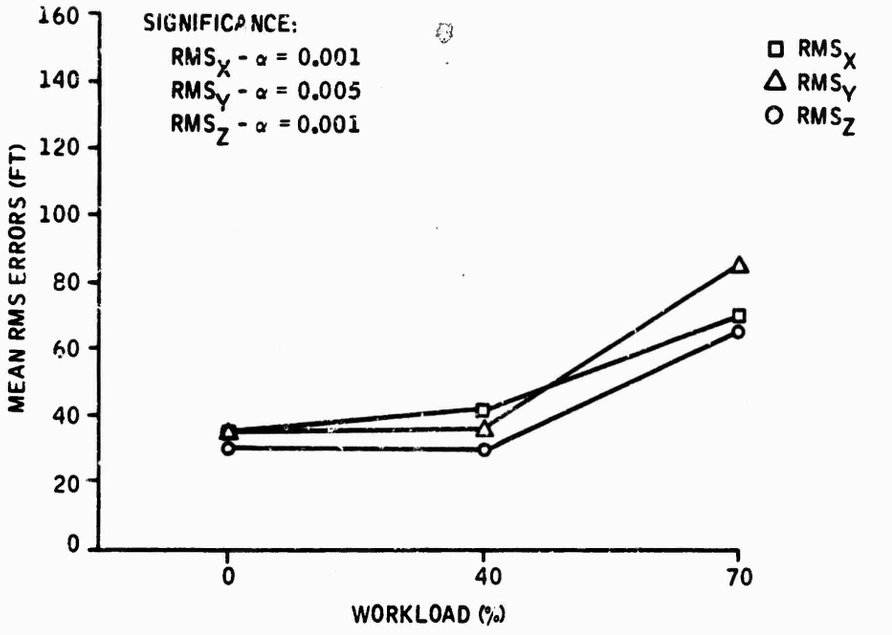

Figure 25. Phase 7 (Straight and Level): RMS Errors versus Workload

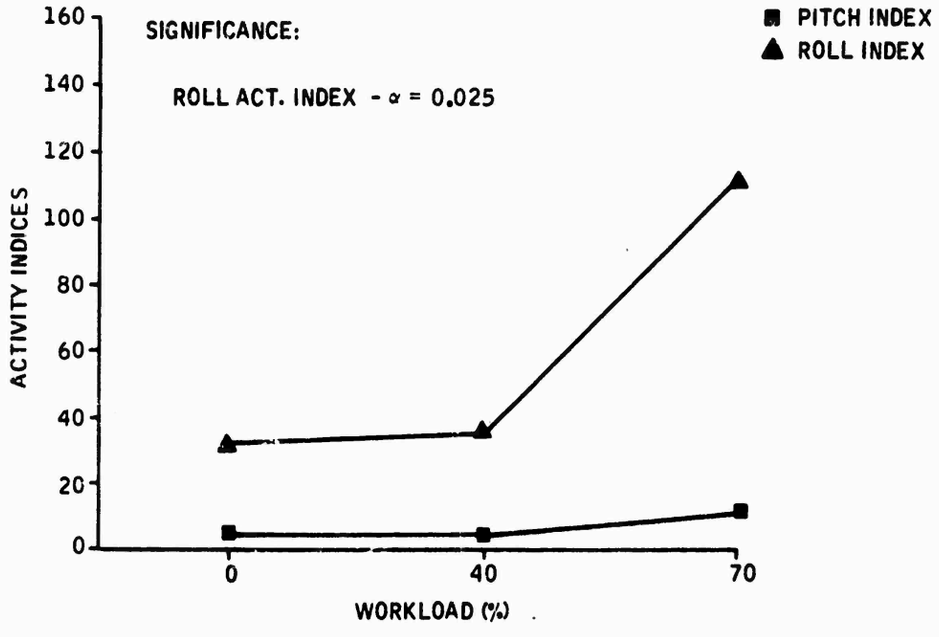

Figure 26. Phase 7 (Straight and Level): Activity Indices versus Workload

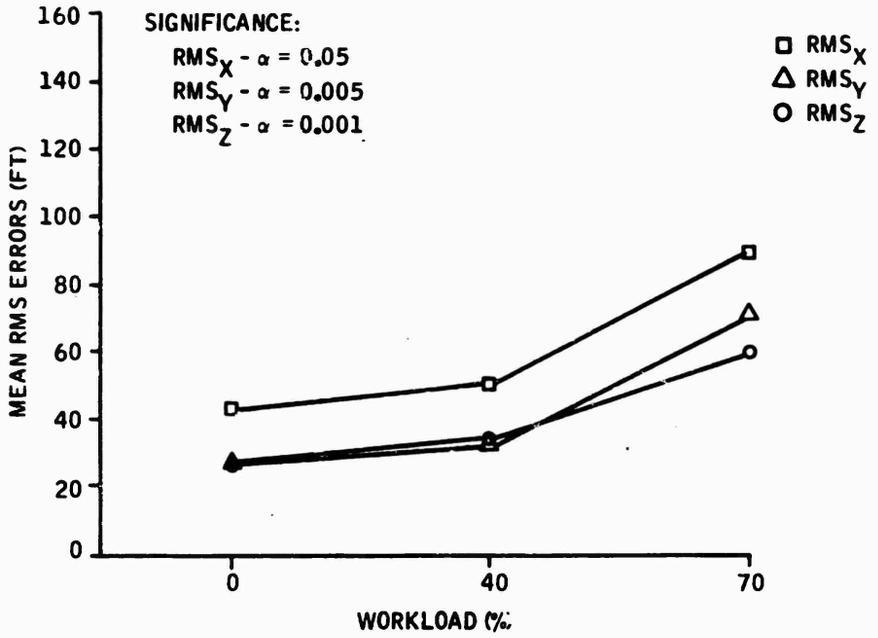

Figure 27. Phase 8 (Deceleration): RMS Errors versus Workload

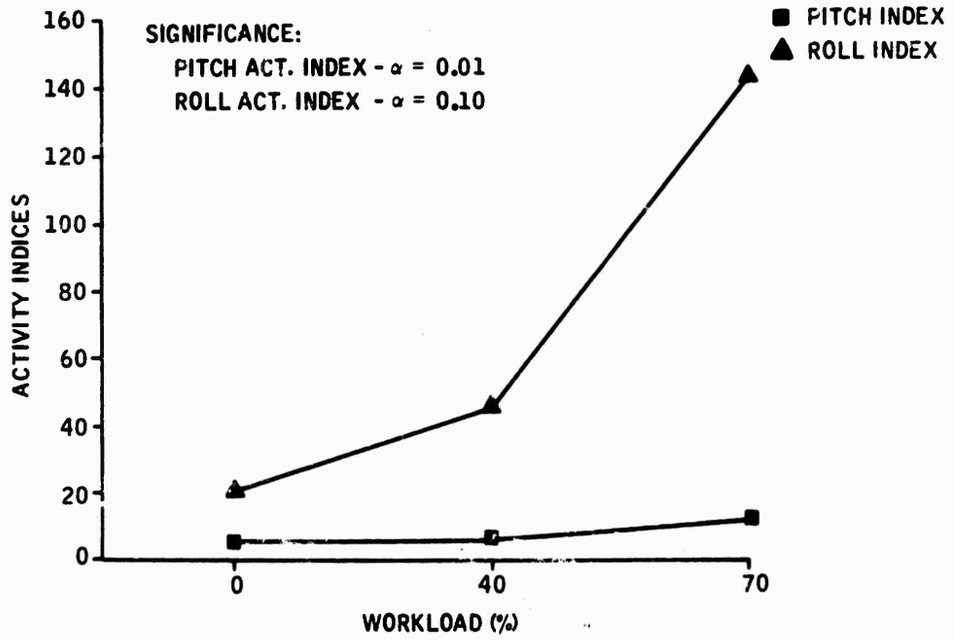

Figure 28. Phase 8 (Deceleration): Activity Indices versus Workload

6.2 Effect of Varying Degrees of Autopilot Assistance on Pilot Performance--

During some maneuvers certain autopilot modes could not be used -- e.g., the altitude hold mode could not be engaged during the climb or descent maneuvers. For this reason the analyses for the different phases were not all based on the same autopilot modes. The modes tested in each phase were

Phase	Applicable Autopilot Modes
Acceleration	Modes 1 to 6
Climb	Modes 1 to 4 (Modes 5 and 6 excluded because of altitude hold)
Right Turn	Modes 1 to 3, 5 (Modes 4 and 6 excluded because of heading hold)
Descent	Modes 1 to 4 (Modes 5 and 6 excluded because of altitude hold)
Left Turn	Modes 1 to 3, 5 (Modes 4 and 6 excluded because of heading hold)
Straight and Level	Modes 1 to 6
Deceleration	Modes 1 to 6

Overall mean RMS errors and activity indices for applicable autopilot modes are shown for each mission phase in Figures 29 through 42. Those parameters which were controlled by the autopilot are represented by cross-hatching (e.g., RMS_Z in the altitude hold modes). These parameters were not included in the tests of statistical significance since evaluation of pilot rather than autopilot performance was of primary concern in this study. The means shown in these figures are averaged over workload levels and subjects.

RMS Position Errors--It can be observed from Figures 29 through 41 that the autopilot mode generally did not have a statistically significant effect on the RMS position errors, except in the axis actually being controlled by the autopilot. For example, the altitude hold mode resulted in a considerable decrease in RMS_X errors. The RMS_X errors were not significantly different for the various levels of autopilot in any of the phases except the straight-and-level phase (Figure 39). The difference in RMS_X errors for this phase was statistically significant. This significance appears to be a result of the higher RMS_X errors obtained in the yaw SAS and 3-axis SAS modes. The RMS_Y errors were not significantly different as a function of the autopilot mode for any of the seven mission phases. RMS_Z errors obtained in all

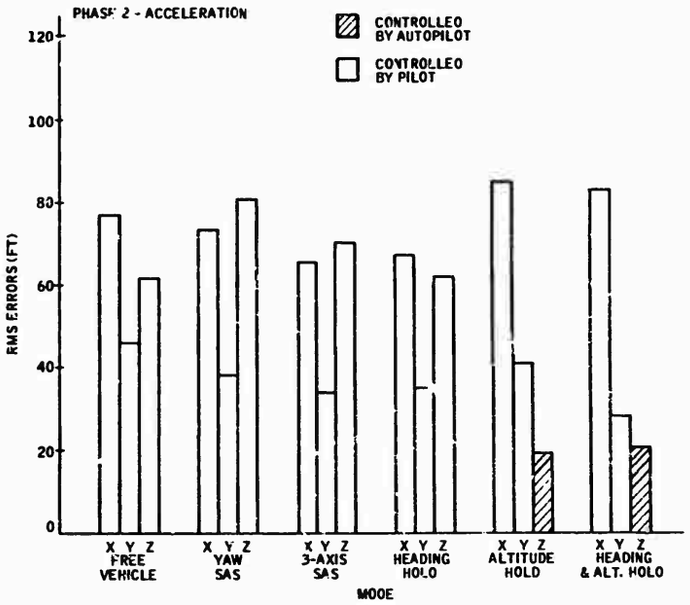

Figure 29. Phase 2 (Acceleration): RMS Errors versus Mode

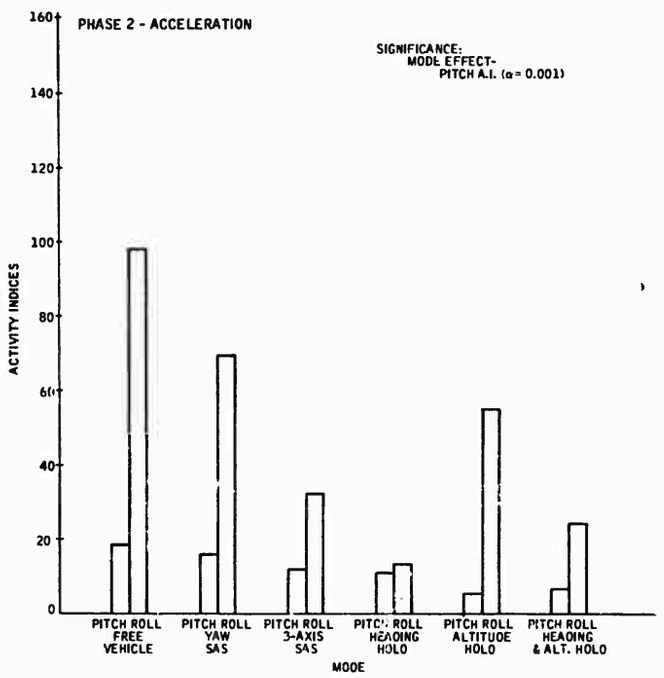

Figure 30. Phase 2 (Acceleration): Activity Indices versus Mode

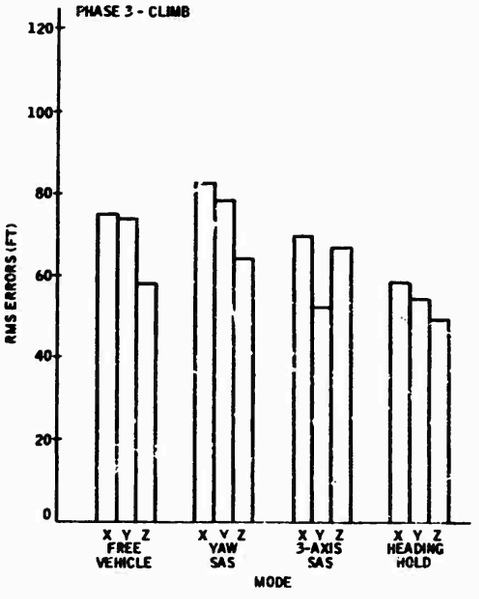

Figure 31. Phase 3 (Climb): RMS Errors versus Mode

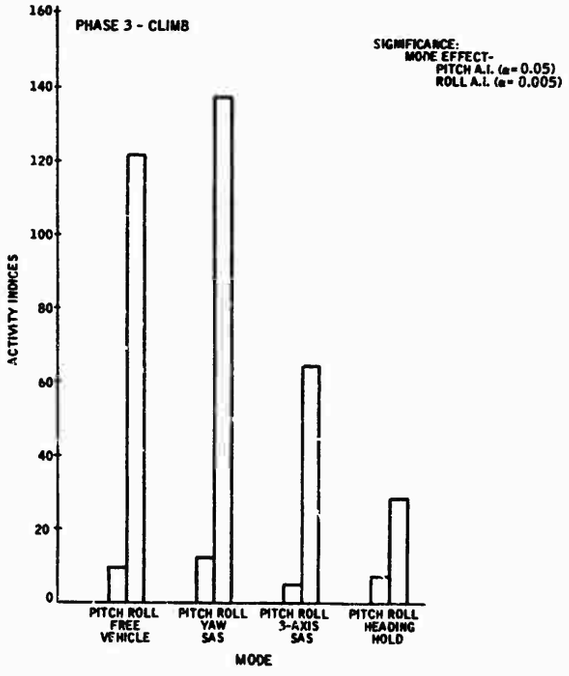

Figure 32. Phase 3 (Climb): Activity Indices versus Mode

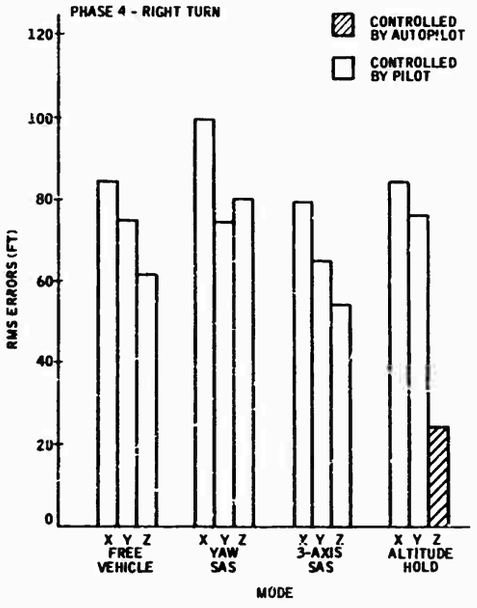

Figure 33. Phase 4 (Right Turn): RMS Errors versus Mode

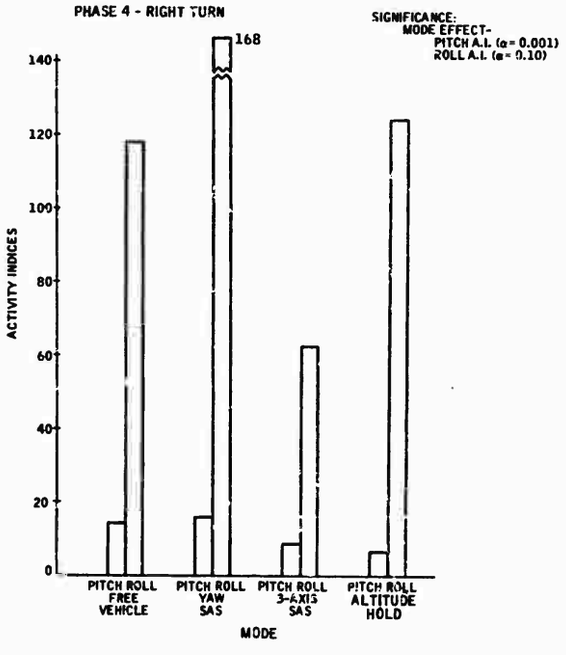

Figure 34. Phase 4 (Right Turn): Activity Indices versus Mode

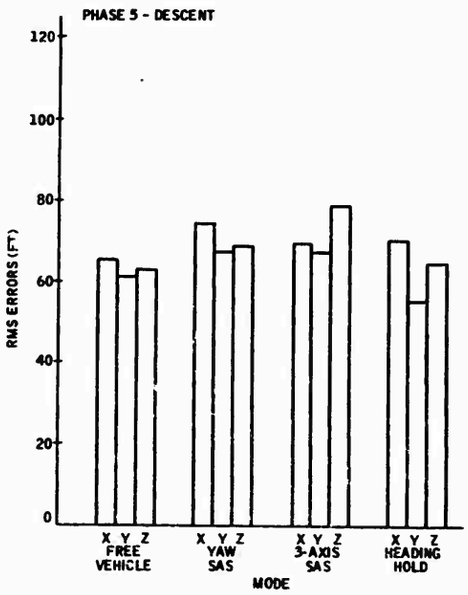

Figure 35. Phase 5 (Descent): RMS Errors versus Mode

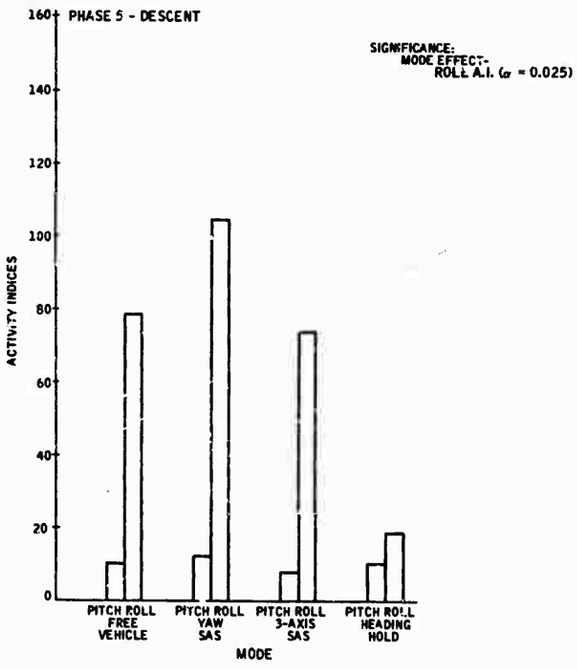

Figure 36. Phase 5 (Descent): Activity Indices versus Mode

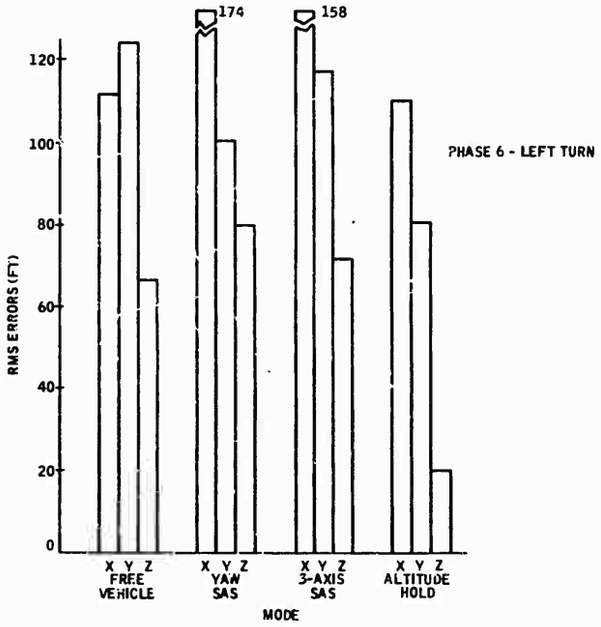

Figure 37. Phase 6 (Left Turn): RMS Errors versus Mode

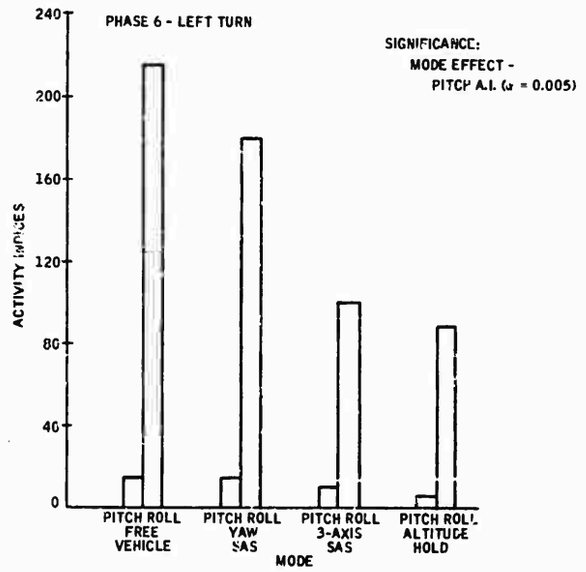

Figure 38. Phase 6 (Left Turn): Activity Indices versus Mode

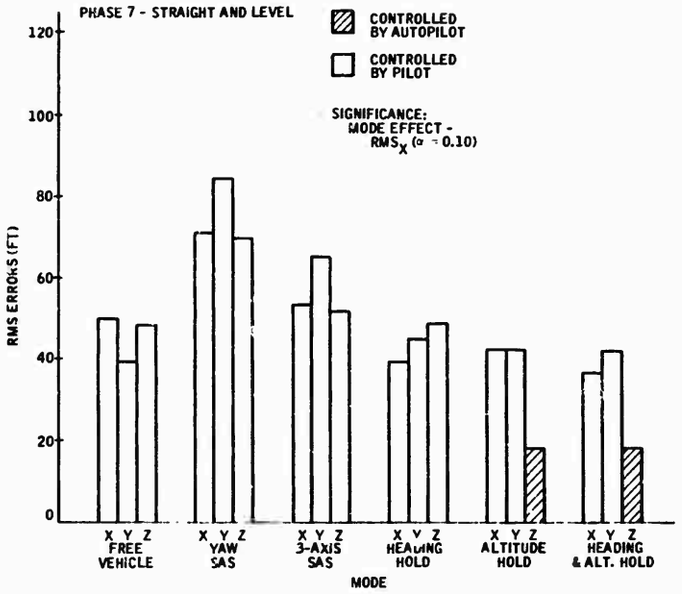

Figure 39. Phase 7 (Straight and Level): RMS Errors versus Mode

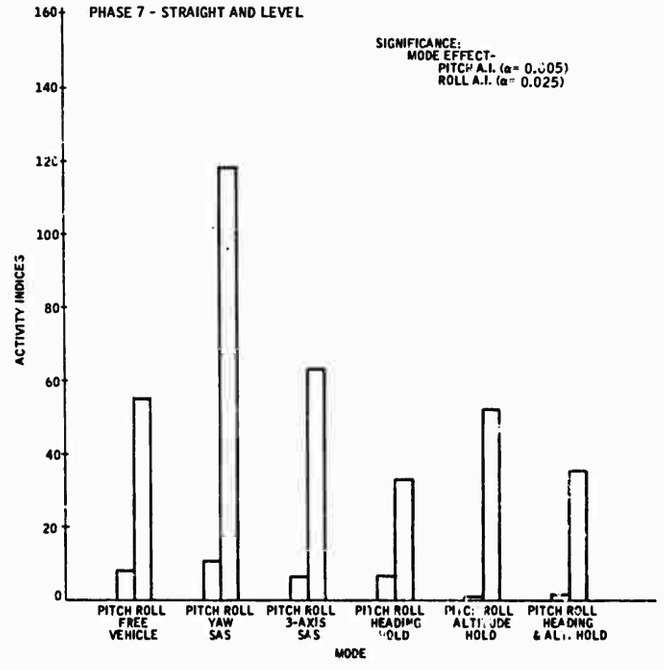

Figure 40. Phase 7 (Straight and Level): Activity Indices versus Mode

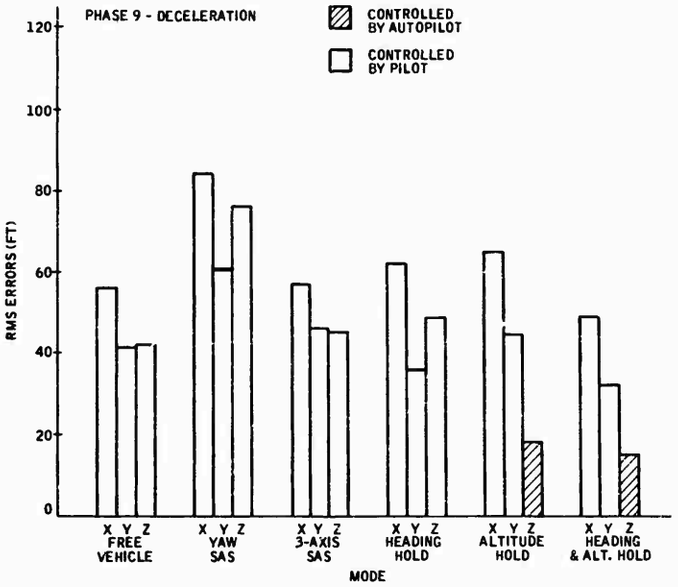

Figure 41. Phase 8 (Deceleration): RMS Errors versus Mode

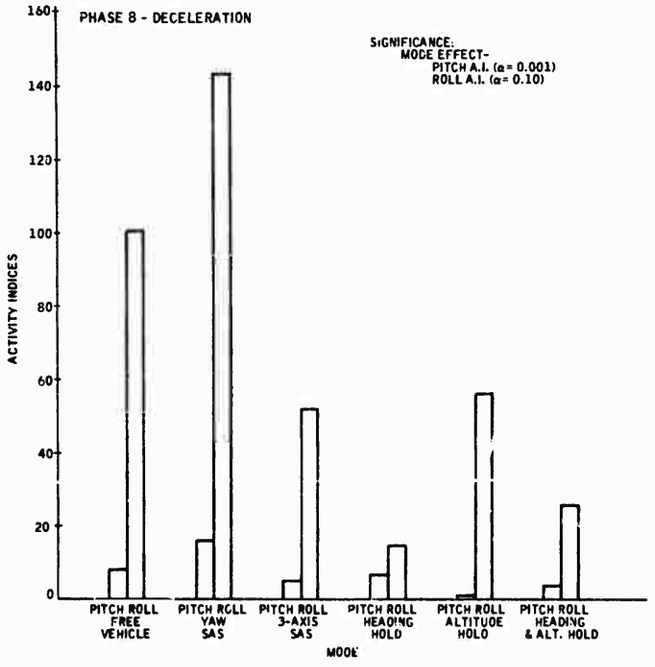

Figure 42. Phase 8 (Deceleration): Activity Indices versus Mode

modes tested resulted in the same general level of position errors when performance data were averaged over the three workloads.

Activity Indices -- The pitch and roll activity indices consistently resulted in significant performance differences for the varying levels of autopilot assistance. The pitch activity index was significantly affected by the autopilot level in five of the seven mission phases (phases 2, 3, 6, 7, and 8 -- Figures 30, 32, 38, 40, and 42). The roll activity index was significantly affected by the autopilot level in four of the seven phases (phases 3, 5, 7, and 8 -- Figures 32, 36, 40, and 42).

The free-vehicle mode resulted in the highest pitch activity index (lowest performance level) in four of the seven mission phases, and the yaw SAS mode resulted in poorest performance in the other three phases. In every phase where the altitude hold mode could be used it resulted in the best performance in terms of decreasing the pitch activity index. In the other two phases where the altitude hold mode could not be used (climb and descent) the 3-axis SAS resulted in the lowest pitch activity index. The following ranking of the autopilot modes in terms of the pitch activity index was noted quite consistently over the seven phases:

Rank	Autopilot Mode
1	Altitude hold (includes 3-axis SAS)
2	Heading and altitude hold (includes 3-axis SAS)
3	Three-axis SAS
4	Heading hold (includes 3-axis SAS)
5	Free vehicle
6	Yaw SAS

Summary -- Varying the levels of autopilot assistance had a significant effect on overall subject performance in terms of the activity indices but not in terms of RMS position errors. The altitude hold mode (Mode 5) resulted in the lowest pitch activity indices and the heading hold mode (Mode 4) resulted in the lowest roll activity indices. Since the heading and altitude hold mode (Mode 6) resulted in pitch activity indices nearly as low as those for Mode 4 and roll activity indices nearly as low as those for Mode 5, it appears that Mode 6 is optimal in terms of both activity indices. In summary, it appears that (1) the heading and altitude hold mode resulted in the best overall performance in terms of aircraft attitude stability and the extent of control inputs required by the pilot to maintain aircraft position, and (2) all autopilot modes except those with altitude hold were not significantly different for any of the seven mission phases.

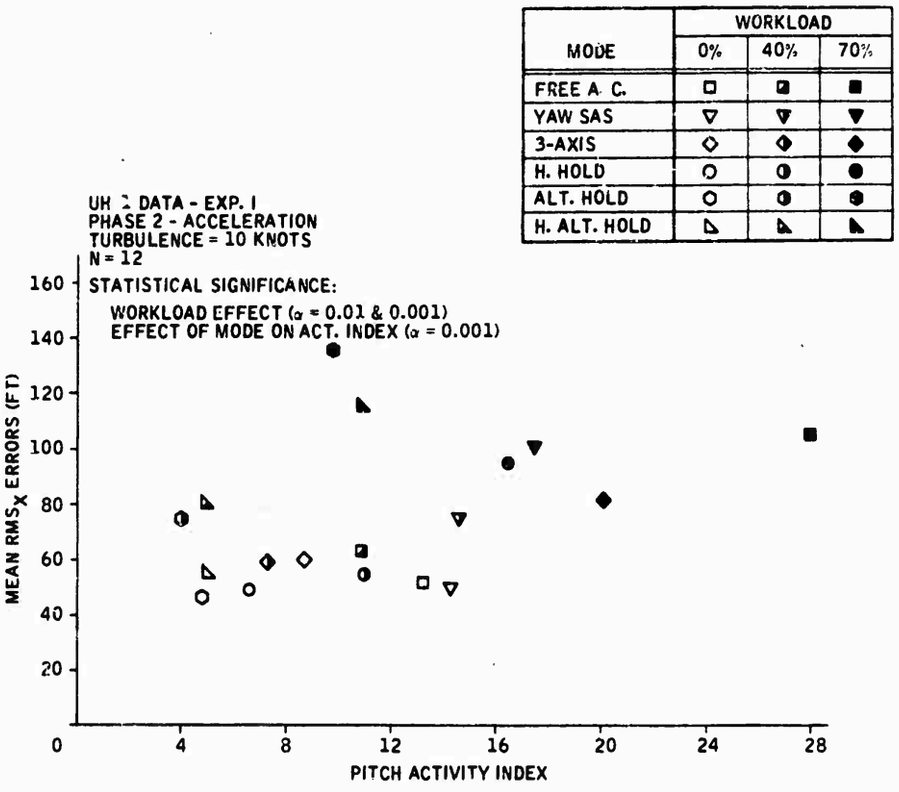

Figure 43. Phase 2 (Acceleration): RMS_X Errors versus Pitch Activity by Mode and Workload

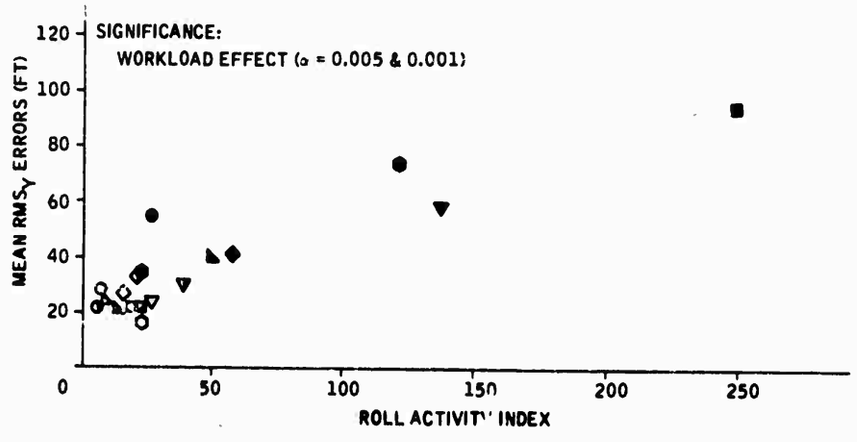

Figure 44. Phase 2 (Acceleration): RMS_Y Errors versus Roll Activity by Mode and Workload

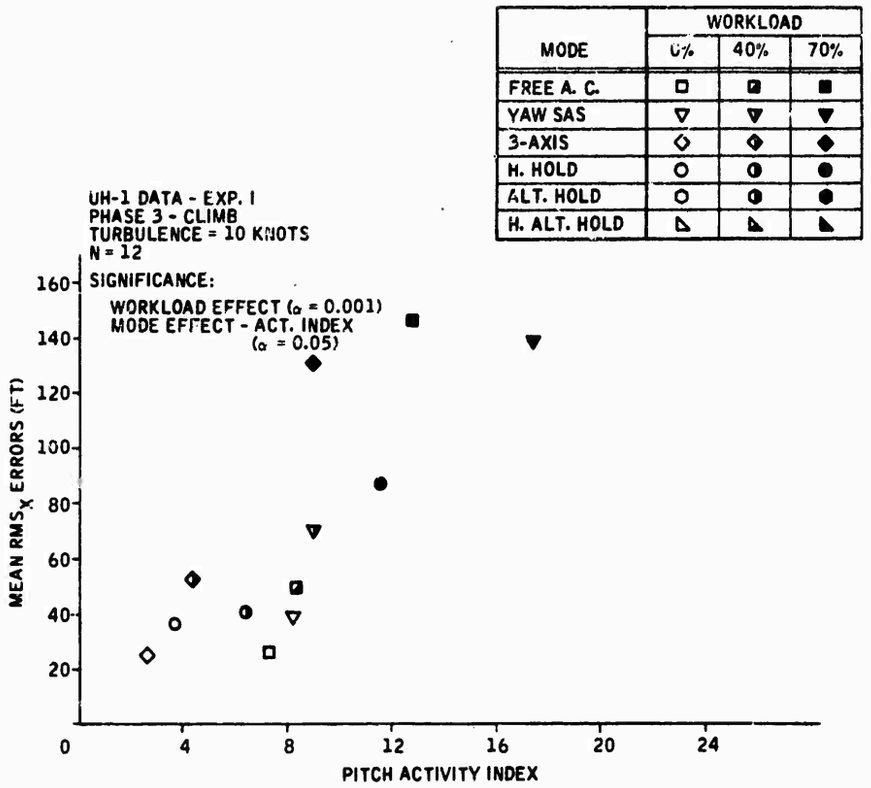

Figure 45. Phase 3 (Climb): RMS$_X$ Error versus Pitch Activity by Mode and Workload

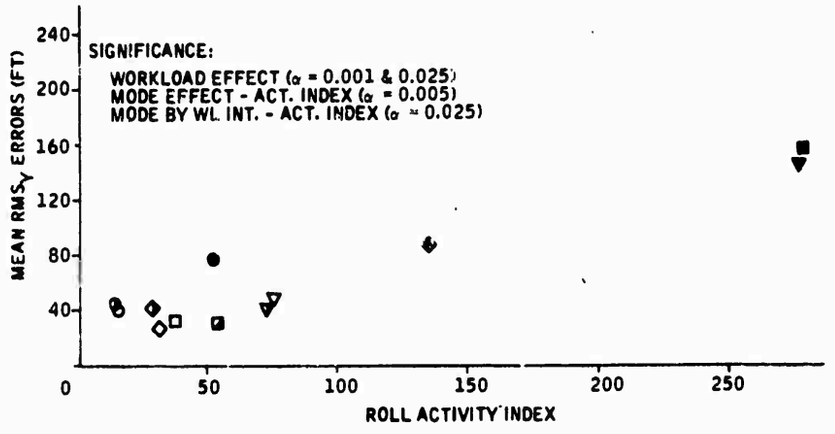

Figure 46. Phase 3 (Climb): RMS$_Y$ Errors versus Roll Activity by Mode and Workload

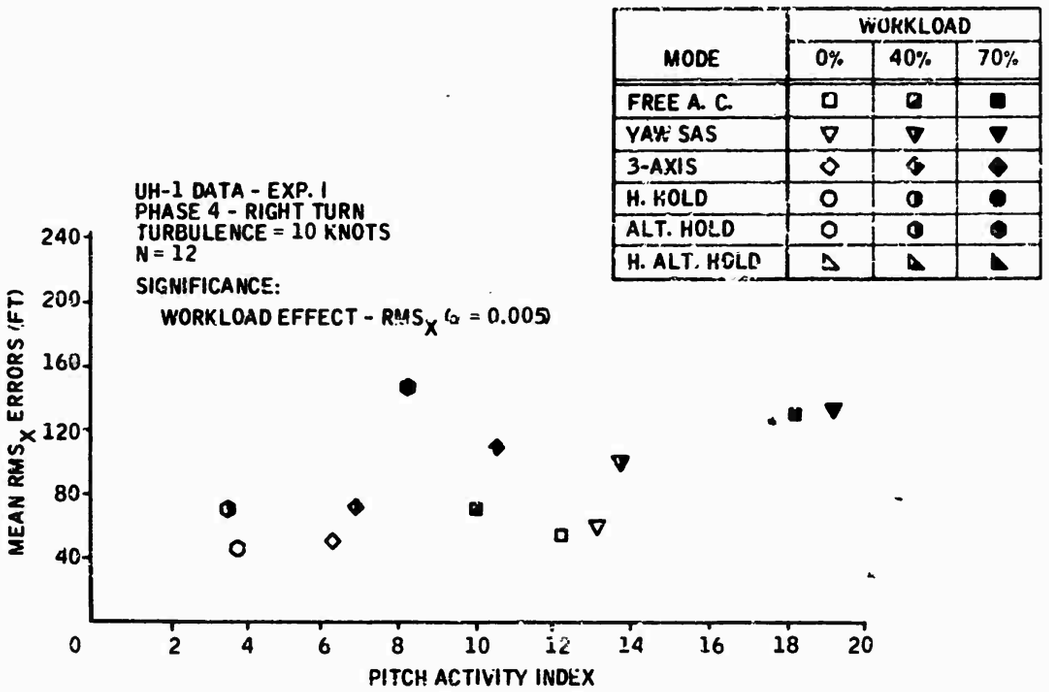

Figure 47. Phase 4 (Right Turn): RMS_X Errors versus Pitch Activity by Mode and Workload

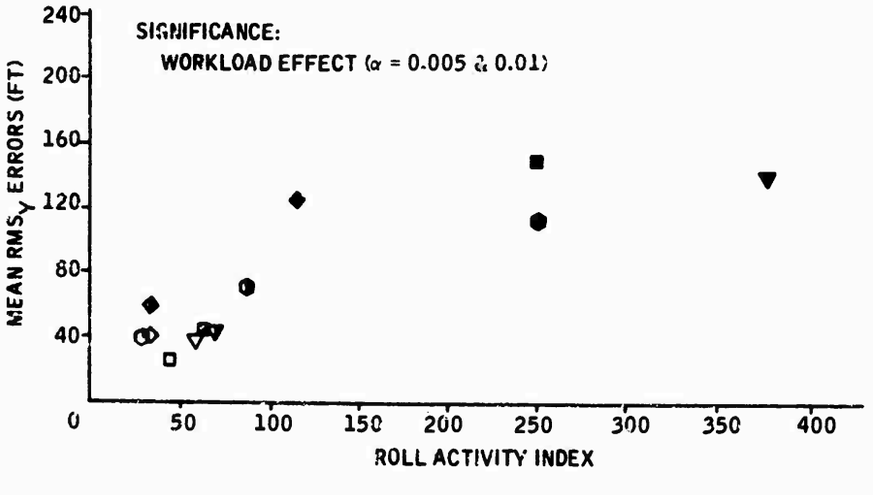

Figure 48. Phase 4 (Right Turn): RMS_Y Error versus Roll Activity by Mode and Workload

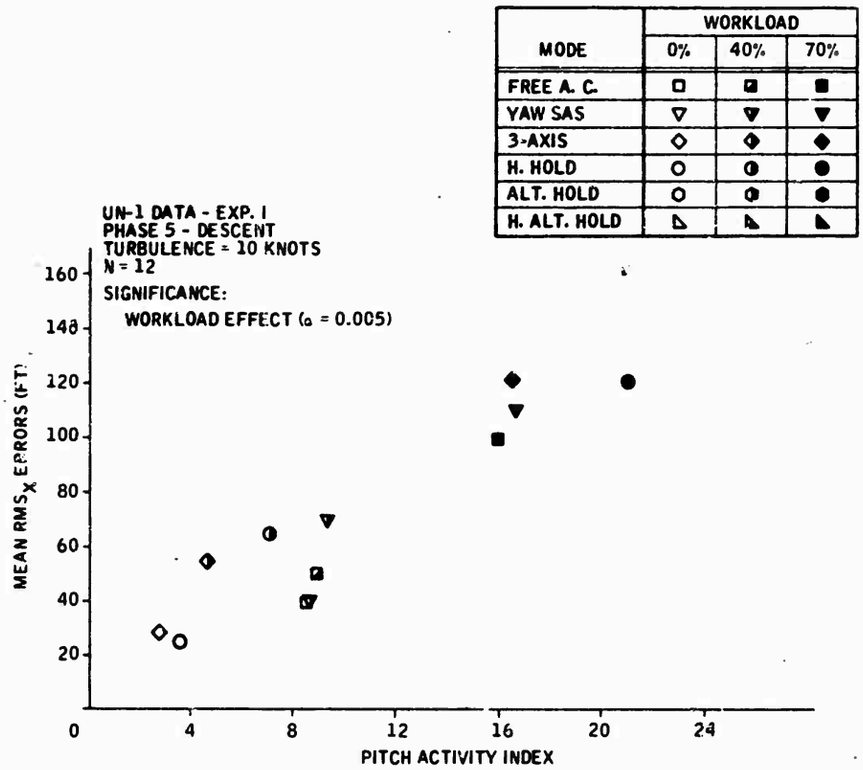

Figure 49. Phase 5 (Descent): RMS_X Error versus Pitch Activity by Mode and Workload

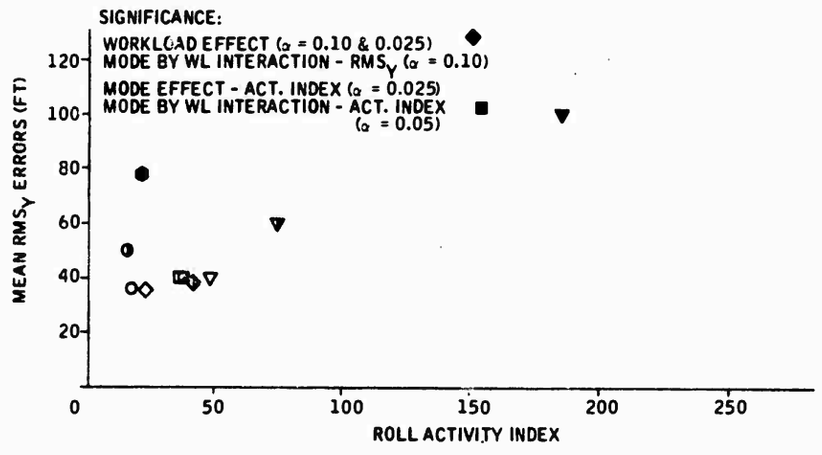

Figure 50. Phase 5 (Descent): RMS_Y Errors versus Roll Activity by Mode and Workload

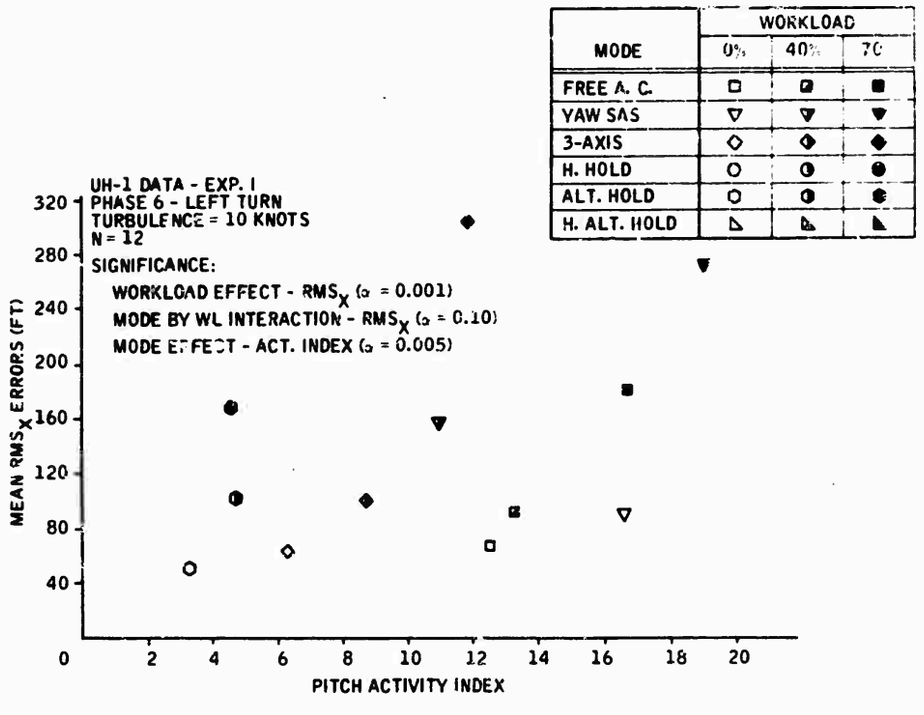

Figure 51. Phase 6 (Left Turn): RMS_X Errors versus Pitch Activity by Mode and Workload

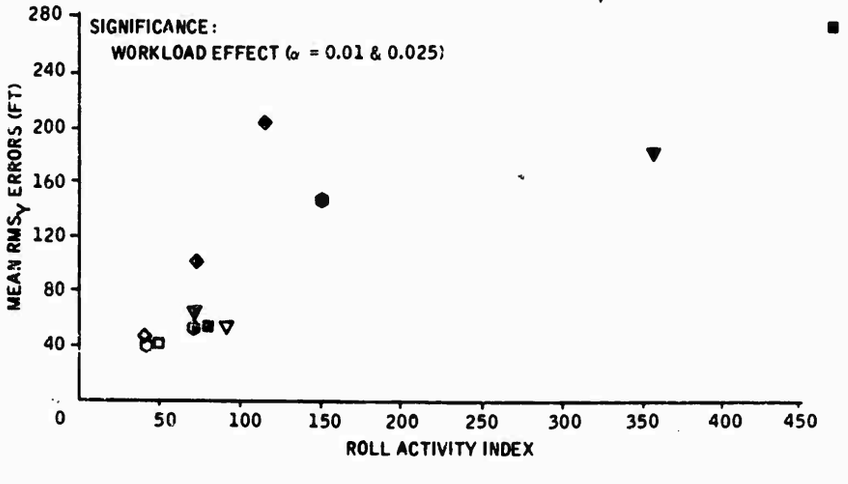

Figure 52. Phase 6 (Left Turn): RMS_Y Errors versus Roll Activity by Mode and Workload

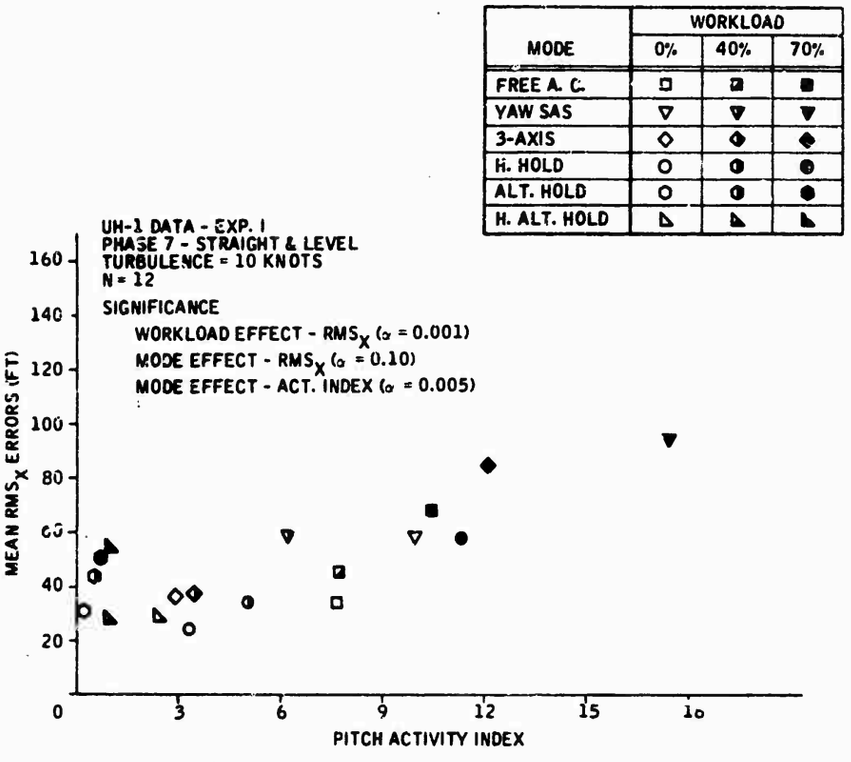

Figure 53. Phase 7 (Straight and Level): RMS$_X$ Errors versus Pitch Activity by Mode and Workload

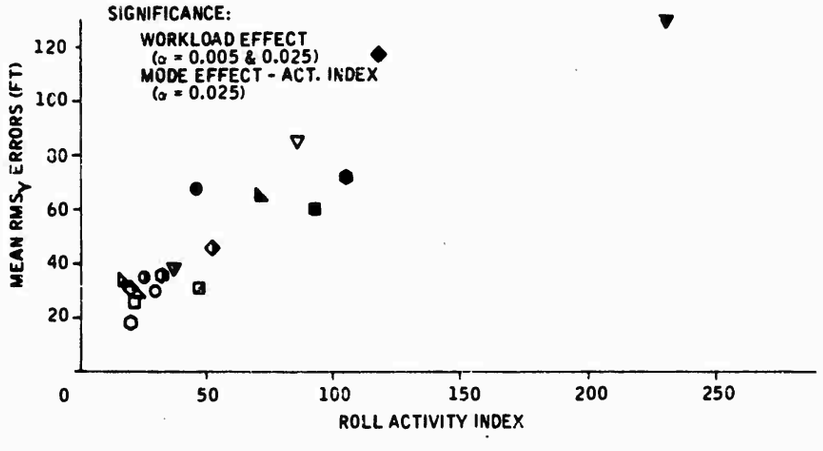

Figure 54. Phase 7 (Straight and Level): RMS$_Y$ Error versus Roll Activity by Mode and Workload

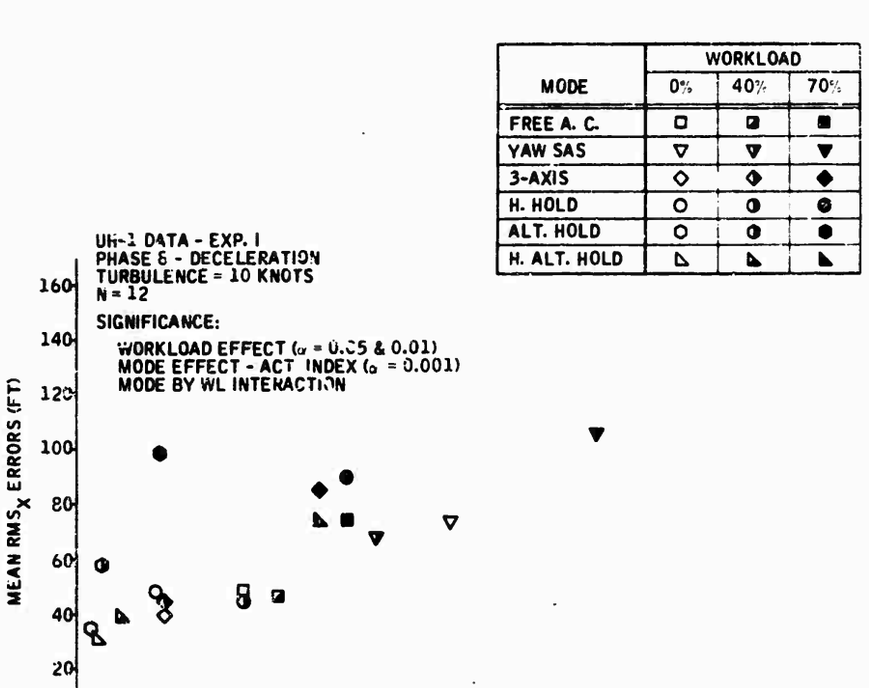

Figure 55. Phase 8 (Deceleration): RMS_X Errors versus Pitch Activity by Mode and Workload

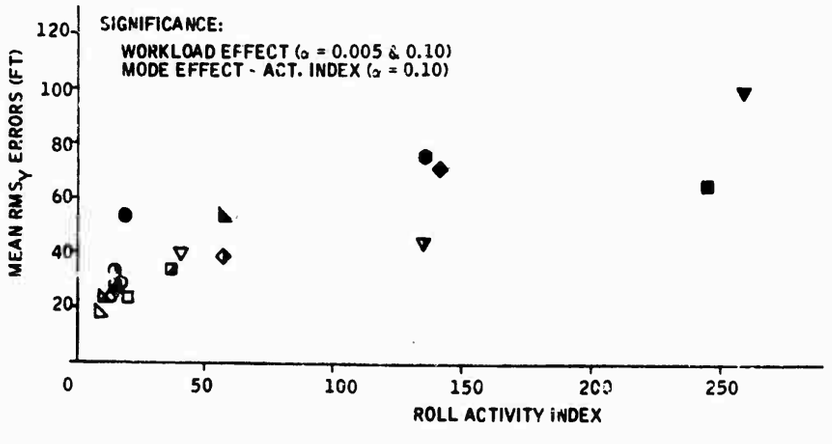

Figure 56. Phase 8 (Deceleration): RMS_Y Errors versus Roll Activity by Mode and Workload

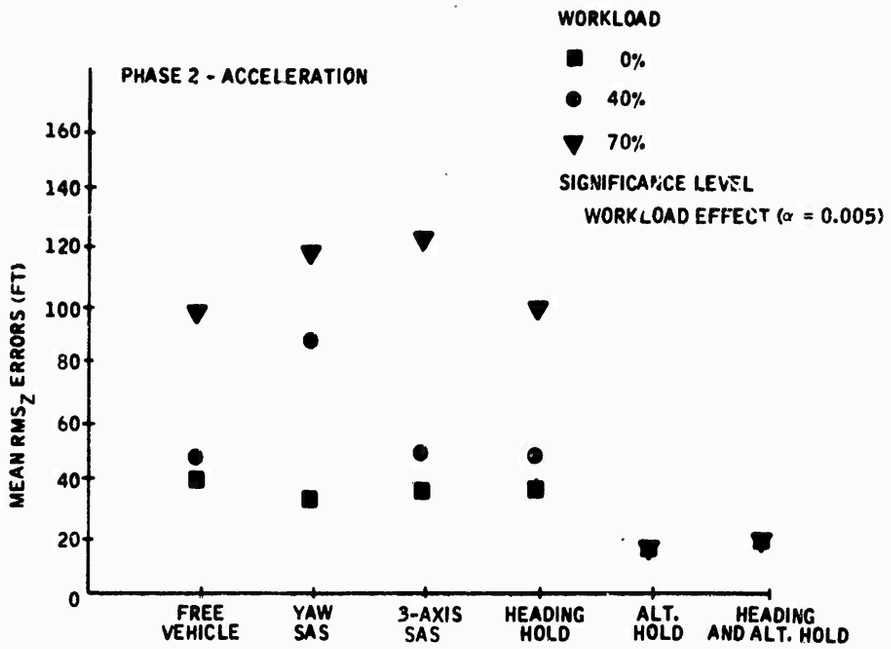

Figure 57. Phase 2 (Acceleration): RMS_Z Errors versus Mode by Workload

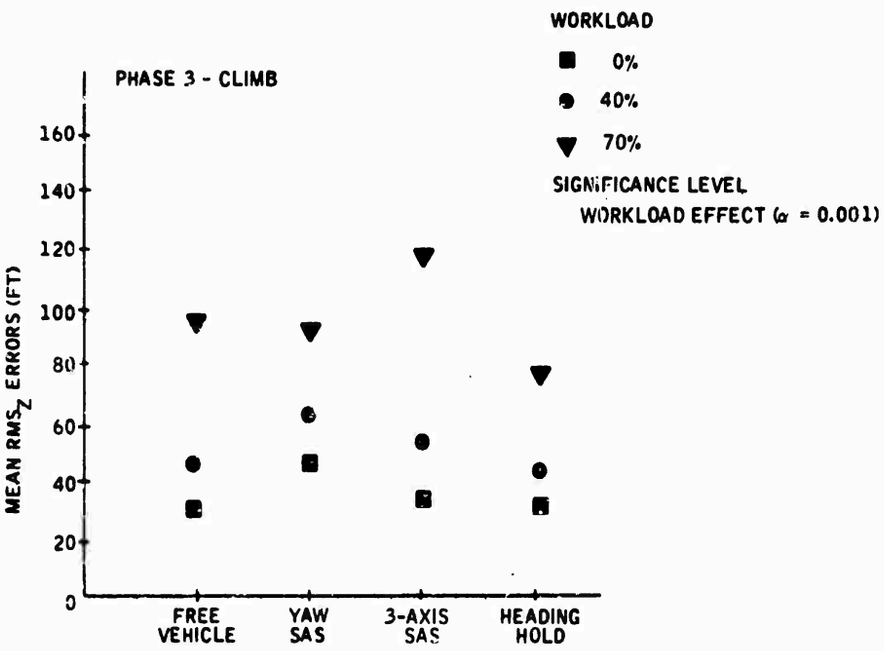

Figure 58. Phase 3 (Climb): RMS_Z Errors versus Mode by Workload

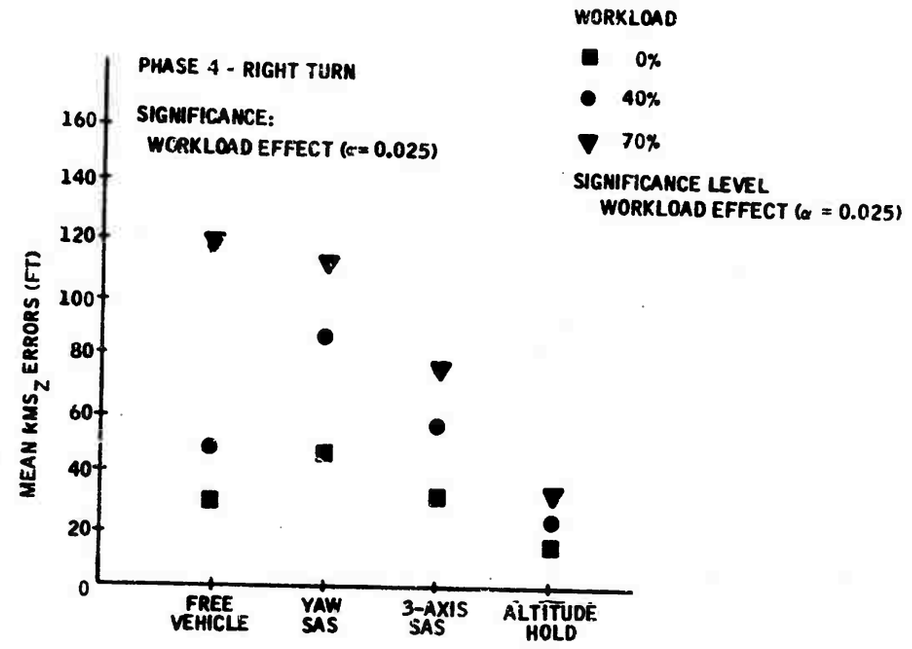

Figure 59. Phase 4 (Right Turn): RMS_Z Errors versus Mode by Workload

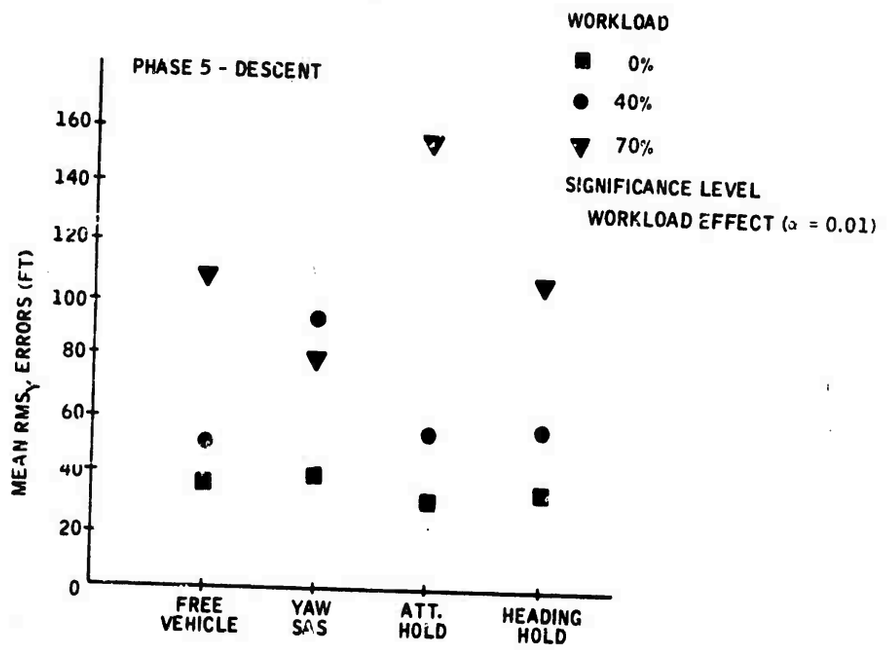

Figure 60. Phase 5 (Descent): RMS_Z Errors versus Mode by Workload

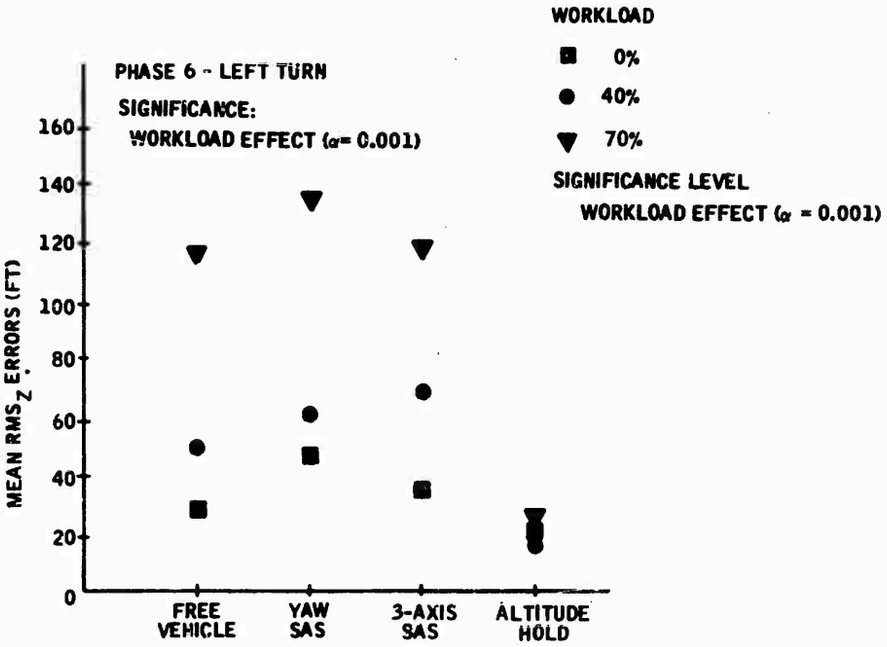

Figure 61. Phase 6 (Left Turn): RMS_Z Errors versus Mode by Workload

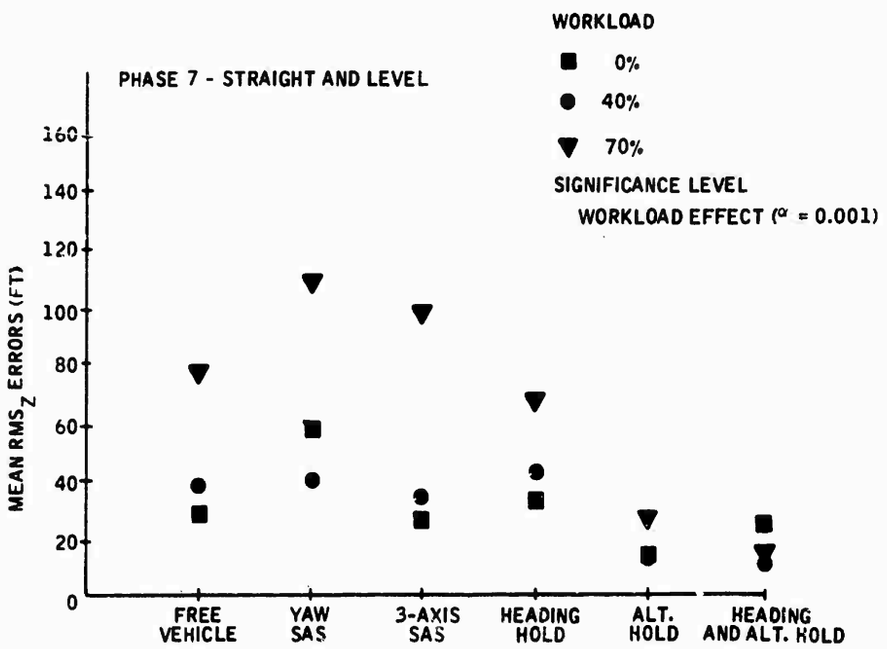

Figure 62. Phase 7 (Straight and Level): RMS_Z Errors versus Mode by Workload

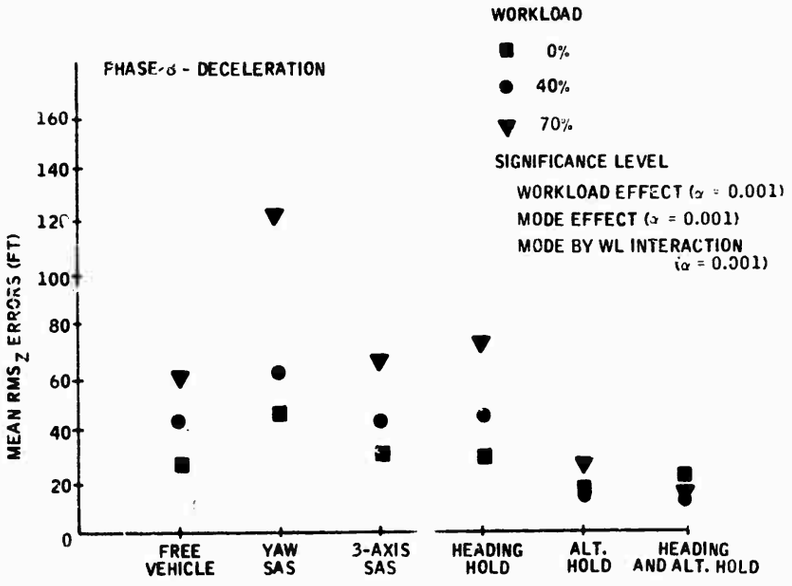

Figure 63. Phase 8 (Deceleration): RMS_Z Errors versus Mode by Workload

The only statistically significant differences in RMS_Y which could be attributed to the autopilot mode by workload interaction were noted for the descent phase (Figure 50). This significance appears to result primarily from the different relationship between workload levels noted for the four autopilot modes. While the free vehicle and three-axis SAS modes result in the same level of RMS_Y errors for the 0% and 40% workloads, the other two modes result in approximately a 50% increase in RMS_Y errors. Conversely, while the percentage increase in RMS_Y errors corresponding to the increase in workload from 40% to 70% is approximately 150% for the free vehicle and 200% for the three-axis SAS mode, it ranges from only 60 to 70% for the other two modes. Although the differences in RMS_Y errors for the other six mission phases were not statistically significant, a consistent trend was noted over these phases.

Activity Indices -- The interaction of the autopilot mode and the workload did not have a significant effect on the pitch activity index. In five of the seven mission phases the same relationship between autopilot modes is noted for each of the workload levels (Figures 47, 49, 51, 53, and 55). In the other two phases [i.e., acceleration and climb (Figures 43 and 45)] there is a tendency toward greater heterogeneity in the pitch activity index for the various autopilot modes with the increase in workload level, although this trend was not statistically significant.

6.3 Effect of Autopilot Mode by Workload Interaction on Performance -- It should be noted that all recorded data were based only on those flights which did not result in total loss of aircraft control. When the subject lost control, he was required to repeat his attempts to fly that mission phase until he completed it without a control loss. Several control losses occurred at the 70% workload level. This forced the data to appear somewhat better than was actually the case for the 70% workload level and tended to make data for the various autopilot modes more homogenous. For example, if RMS errors obtained for Mode 1 (free vehicle) at the 70% workload were the same as those obtained for Mode 6 (altitude and heading hold plus 3-axis SAS) although 50 control losses were recorded for Mode 1 and only 5 for Mode 6, it would be obvious that Mode 6 resulted in significantly better performance. For this reason, the analysis of the various levels of autopilot assistance at the 70% workload level must be based on the number of recorded control losses as well as the position error and activity index data. The analysis of recorded control losses follows this analysis of position errors and activity indices.

Mean RMS_X and RMS_Y errors and pitch and roll activity indices by autopilot mode and workload level are shown for each phase in Figures 43 through 56. These figures describe performance in terms of both RMS position errors and activity indices. Since a high quality of performance is defined by low position errors and low activity indices, the quality of performance is indicated by the proximity of the symbols to the lower left-hand corner of the graph. Mean RMS_Z errors by autopilot mode and workload level are shown for each phase in Figures 57 through 63.

RMS Position Errors -- The differences in RMS position errors resulting from the various combinations of autopilot mode and workload were generally not statistically significant.

The only statistically significant differences in the RMS_X errors were found for the left-turn phase (Figure 51). This significance appears to be due to the relatively higher increase in RMS_X errors for the 70% workload level noted for the three-axis SAS autopilot mode. The percentage increase in RMS_X resulting from the increase in workload from 40% to 70% is 200% for the three-axis SAS mode while it ranges from 60% to 100% for the other three modes. The difference in RMS_X errors noted for the other six phases do not result in statistical significance. The acceleration and climb phases (Figures 43 and 45) do, however, show a tendency for greater heterogeneity in RMS_X errors to occur for various autopilot modes at the highest workload level. This trend is not noted for the other four phases (right turn, descent, straight-and-level, and deceleration). For these phases the same general level of RMS_X errors was obtained for all autopilot modes at each specific workload. The increase in RMS_X errors noted in Figure 47, 49, 53, and 55 for these phases appears to be a function only of the workload level.

The interaction of the autopilot mode and the workload has a significant effect on the roll activity index in two of the seven mission phases. The significant results for the climb phase appear to be due to the much higher activity indices obtained for the free vehicle and the Yaw SAS modes at the 70% workload level. The activity index for the heading hold mode also appears to be significantly less than that for the three-axis mode at the 70% workload level. The significant results for the descent phase appear to be due to the relatively low roll activity index obtained for the heading hold mode at the 70% workload level. Although the differences in the roll activity index for the other mission phases were not statistically significant, a consistent trend was noted for all of these phases. The heterogeneity of the activity indices for the various autopilot modes was considerably greater for the 70% workload than for the lower workloads. Although this trend was not statistically significant for any one of these phases, its consistent occurrence over all phases provides reason to assume that higher workloads do actually result in greater heterogeneity in roll activity indices for the various modes.

Means and Standard Deviations -- Figures 64 through 70 present bounds which describe the lateral and longitudinal position error envelopes resulting for the applicable autopilot modes by mission phase. Since greater differences were noted between modes at the 70% workload level, the position error envelopes are presented for that workload. Center points in each rectangle are defined as coordinates of mean longitudinal and lateral errors for specific phases with rectangle dimensions defined by ± three times the mean standard deviation actually obtained for this phase. The mean X and Y errors defining this position are averages over all mean position errors obtained for this phase and are assumed to provide a good estimate of the mean aircraft location under the given conditions. The X and Y standard deviations presented are averages of all X and Y standard deviations recorded during the experiment under the same treatment conditions and are assumed to provide a good estimate of the standard deviation of the error distribution which has the mean X and ;Y errors described above. When these assumptions are made, each rectangle can be assumed to describe the bounds within which the aircraft is expected to remain at least 99% of the time (since they are presented as mean locations ± three standard deviations around the mean).

The number of control losses occurring for each phase and each mode was also presented in Figures 64 through 70 since the analysis of differences between autopilot modes at the 70% workload level would not be complete without this information. It can be observed that the performance trend in terms of the error envelopes was somewhat inconsistent, with the higher levels of autopilot resulting in the smallest envelopes in some phases and the free vehicle resulting in the smallest in others. When the number of control losses are considered, however, it is noted consistently that the higher levels of autopilot result in a lower number of control losses.

The number of losses associated with the various autopilot modes (totals over all mission phases) at the 70% workload level was

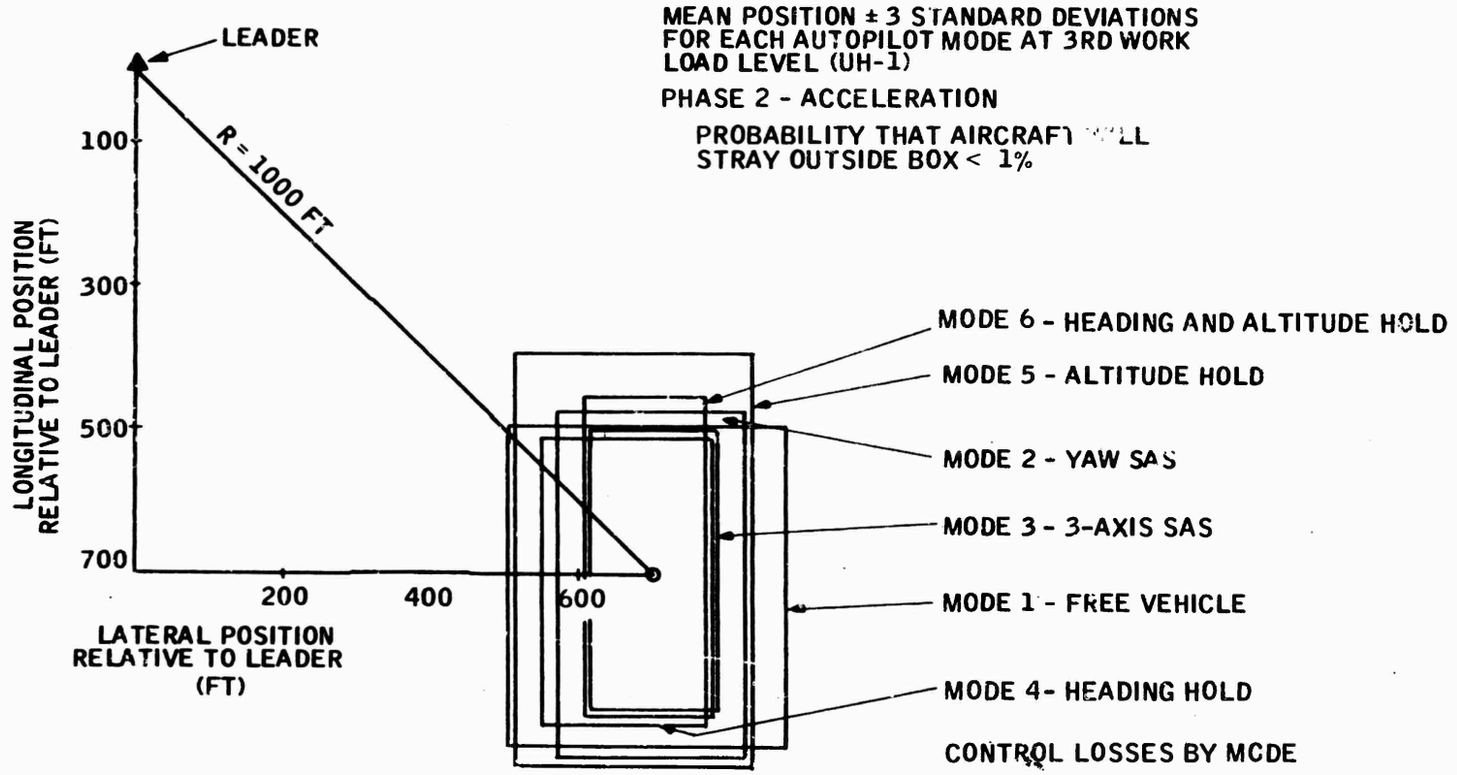

CONTROL LOSSES BY MODE

MODE	NO. OF LOSSES
1	1
2	1
3	1
4	0
5	0
6	0

Figure 64. Phase 2 (Acceleration): Lateral and Longitudinal Position Error by Mode

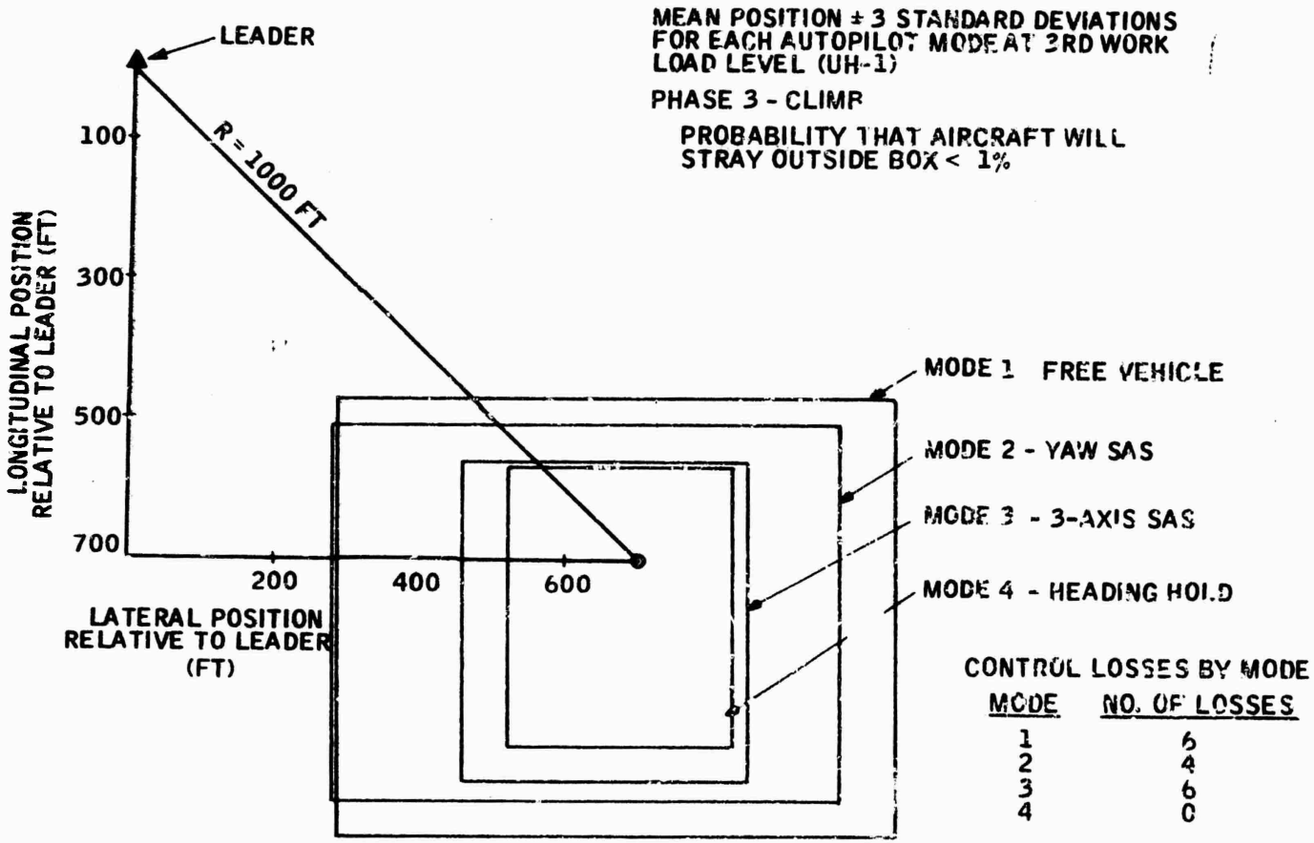

Figure 65. Phase 3 (Climb): Lateral and Longitudinal Position Error by Mode

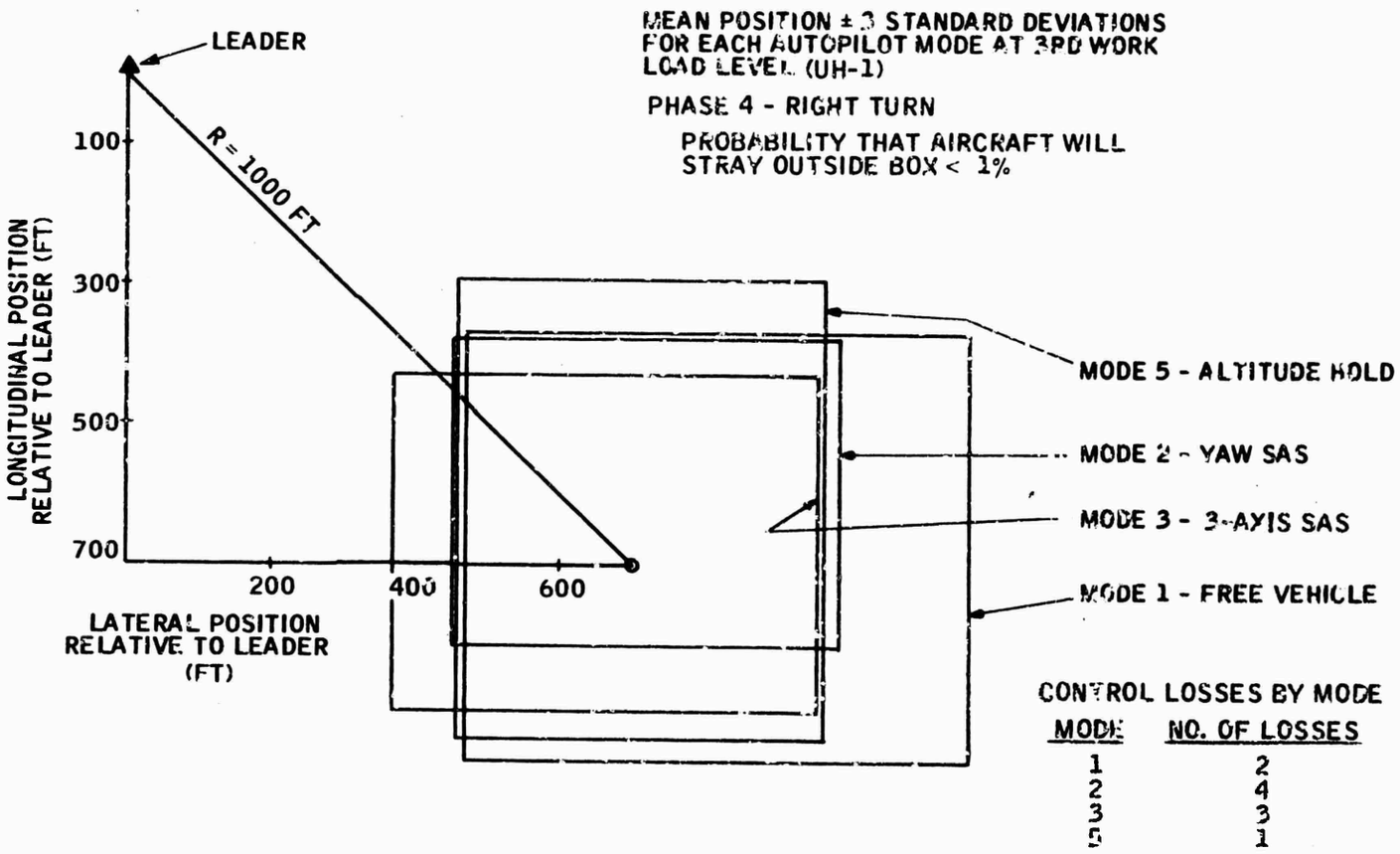

Figure 66. Phase 4 (Right Turn): Lateral and Longitudinal Position Error by Mode

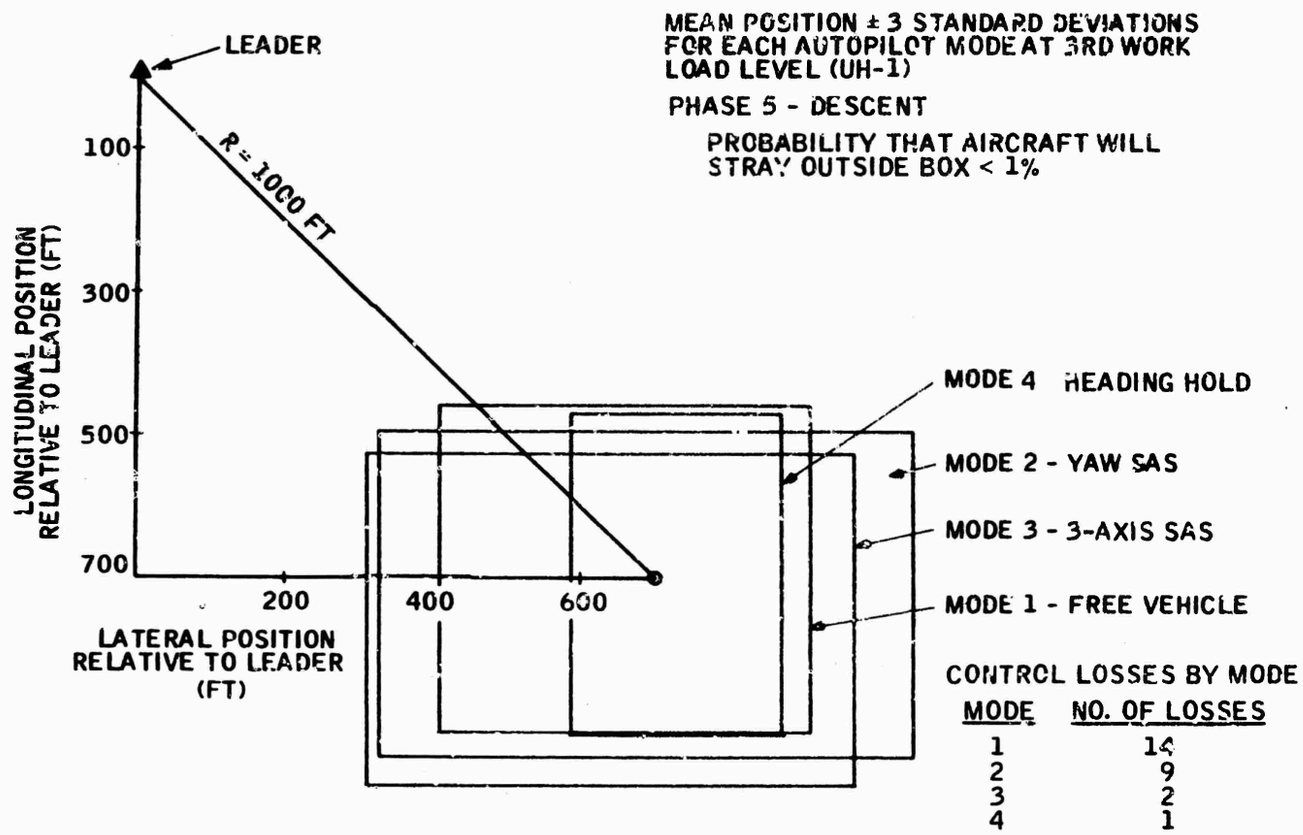

Figure 67. Phase 5 (Descent): Lateral and Longitudinal Position Error by Mode

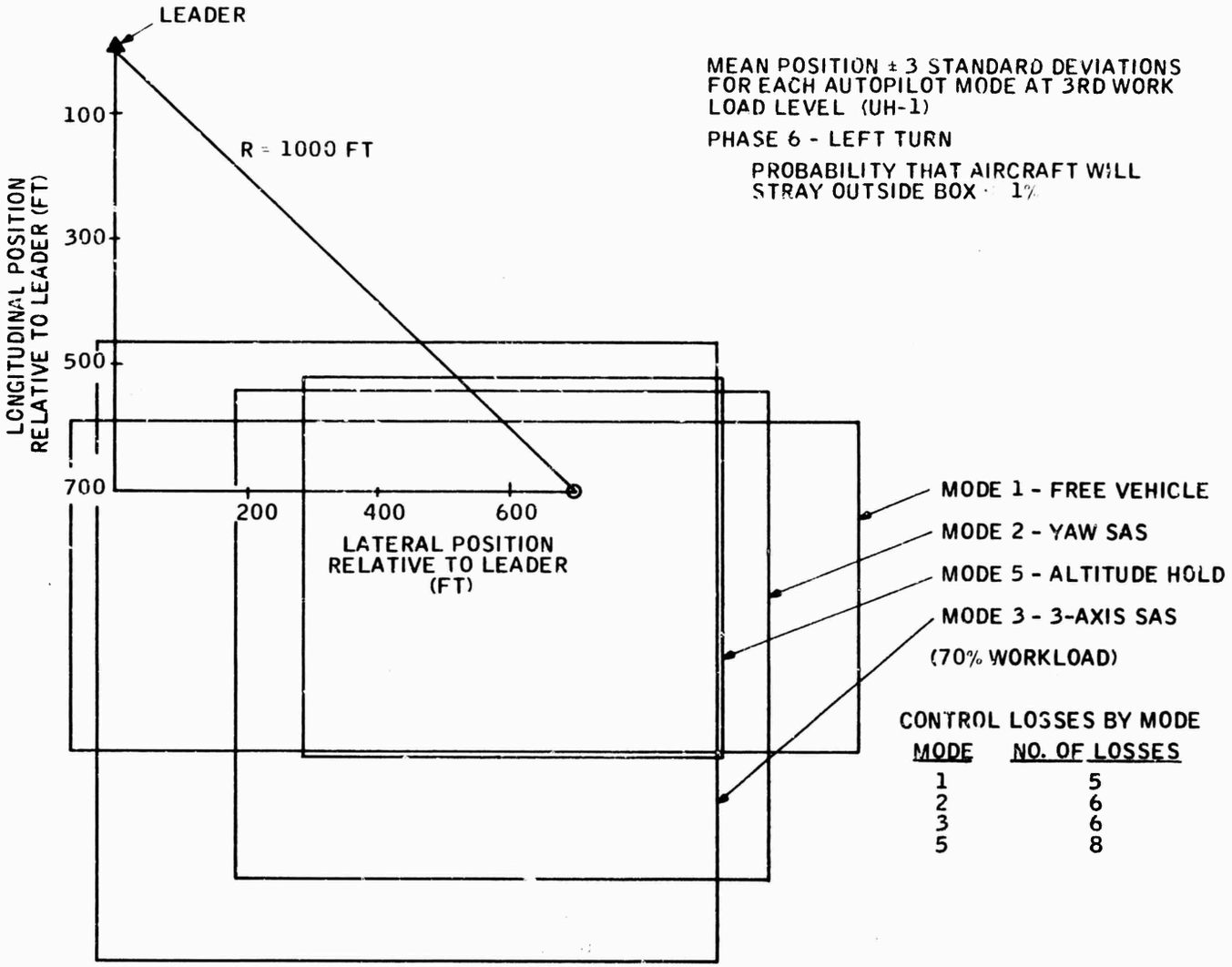

Figure 68. Phase 6 (Left Turn): Lateral and Longitudinal Position Error by Mode

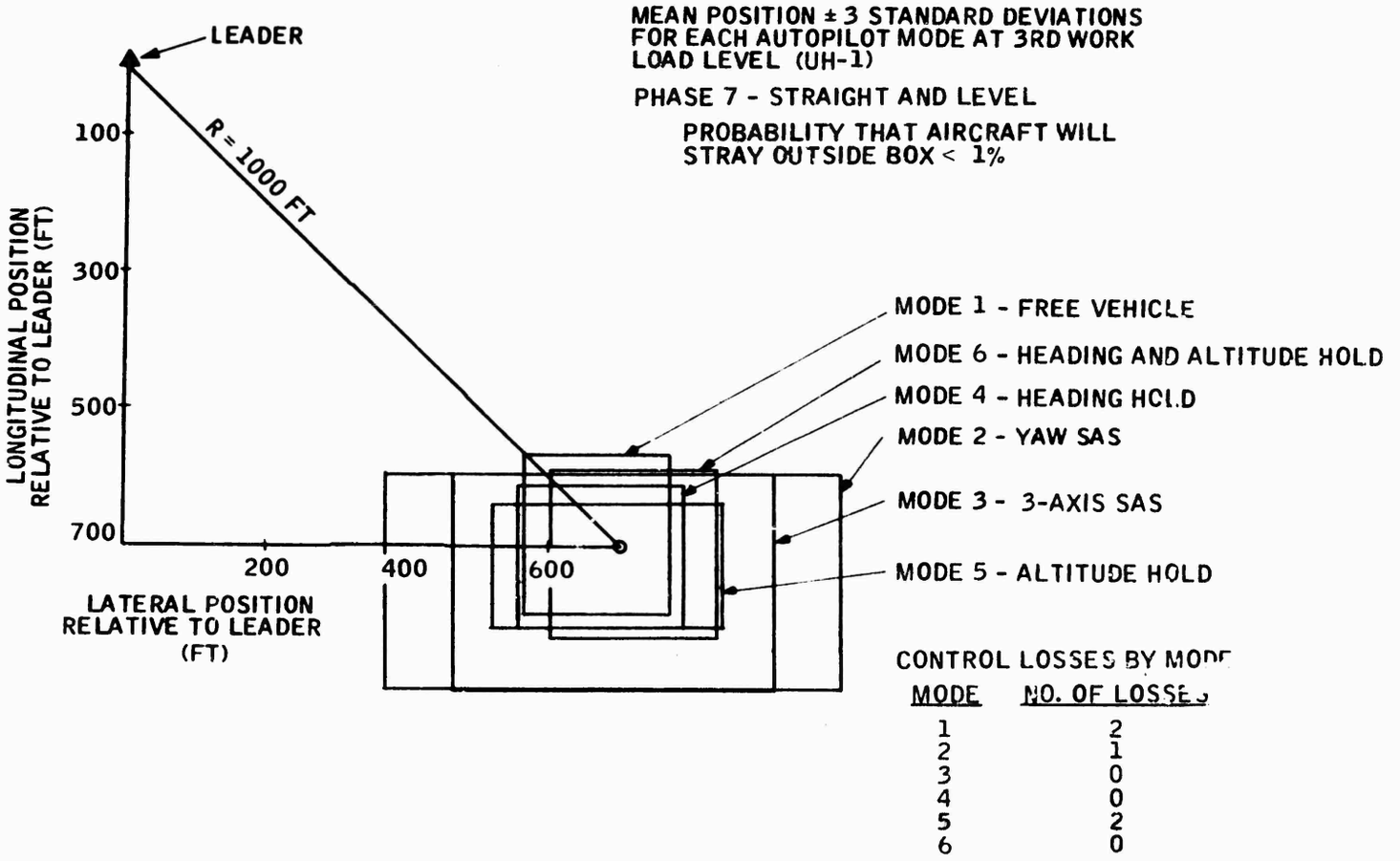

CONTROL LOSSES BY MODE

MODE	NO. OF LOSSES
1	2
2	1
3	0
4	0
5	2
6	0

Figure 69. Phase 7 (Straight and Level): Lateral and Longitudinal Position Error by Mode

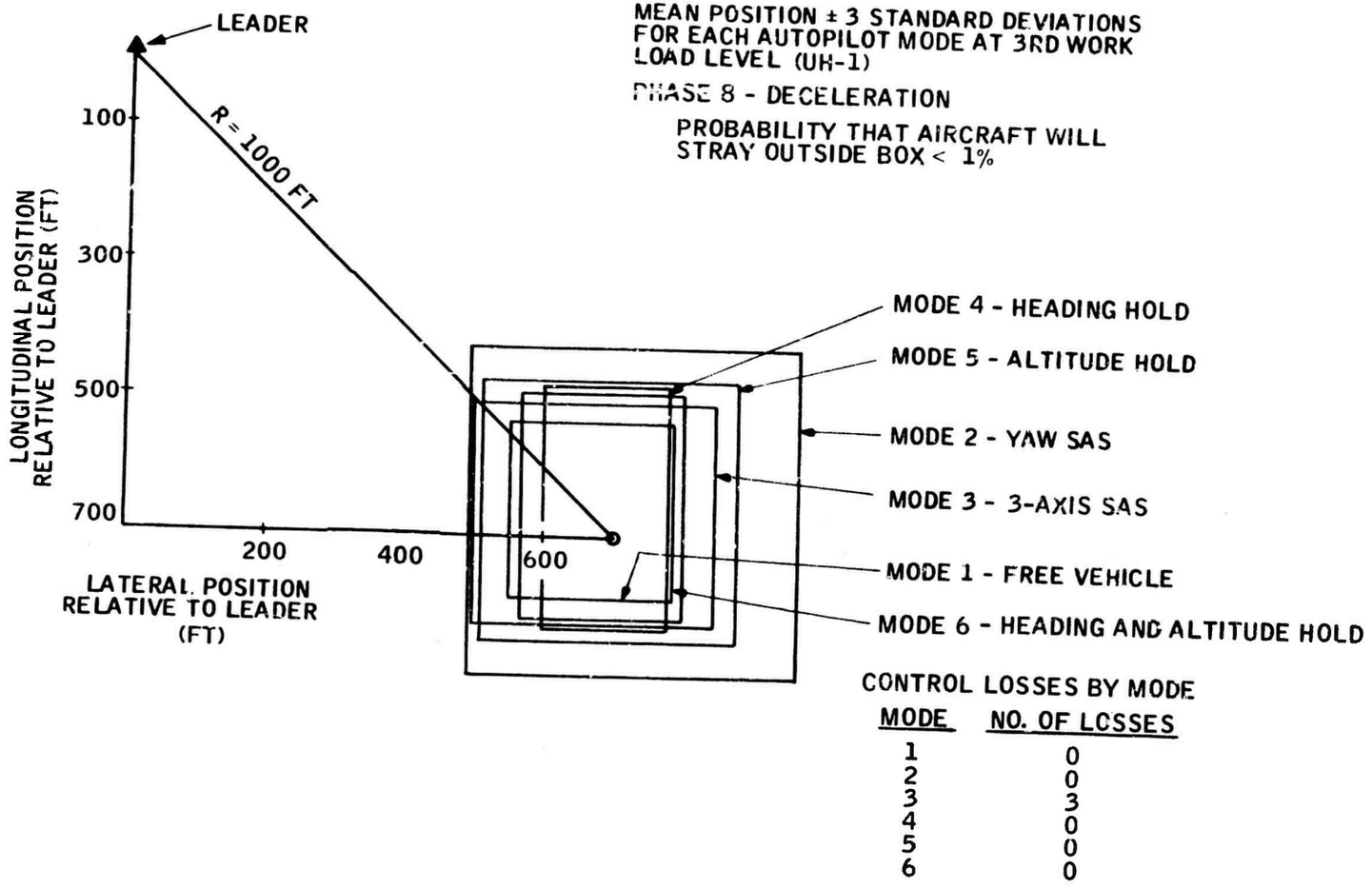

CONTROL LOSSES BY MODE

MODE	NO. OF LOSSES
1	0
2	0
3	3
4	0
5	0
6	0

Figure 70. Phase 8 (Deceleration): Lateral and Longitudinal Position Error by Mode

- Free vehicle - 30
- Yaw SAS - 24
- Three-axis SAS - 20
- Heading hold - 3
- Altitude hold - 11
- Heading and Altitude hold - 0

(A complete analysis of control losses is presented in the following subsection.)

From simultaneous examination of these error envelopes and control losses, the three higher level autopilot modes resulted in better overall performance at the 70 percent workload level.

Catastrophic Control Losses and Collisions -- Since the number of control losses recorded for this experiment was very high for the 70 percent workload level, the analysis of control losses was critical in the evaluation of the autopilot modes at this workload level. All control losses recorded are presented in Table 4. A total of 90 control losses was recorded during the experiment, with 88 of these at the 70 percent workload level. It is obvious that the number of control losses was affected by the workload level. Of the 90 control losses, 83 were recorded for only two of the subjects. The further analysis of control losses was, therefore, based primarily on the reactions of these two subjects. It was found that the more difficult maneuvers resulted in a considerably higher number of control losses; e.g., ranging from 10 to 27 for the climb, descent, and turn phases and from 3 to 5 for the acceleration, deceleration, and straight-and-level phases. The number of control losses was considerably higher for the free vehicle, the yaw SAS, and the three-axis SAS modes than for the three higher-level autopilot modes. This breakdown of control losses indicates significant performance differences between levels of autopilot modes at the 70 percent workload level. These differences did not show up in the RMS position errors, probably because performance in the free vehicle, yaw SAS, and three-axis autopilot modes was forced to the same level achieved in the other three modes. No collisons were recorded during this experiment.

Summary -- The autopilot mode by workload interaction generally did not have a significant effect on subject performance in terms of either RMS position errors or activity indices. The only consistent trends noted were that the RMS_Y errors and roll activity indices for the various autopilot modes became more heterogeneous with the increase in workload and that the heading hold mode resulted in significant lateral control performance improvement at the 70 percent workload level. The only significant differences in subject performance noted for the various autopilot mode/workload combinations were the

Table 4. Control Loss Record (UH-1)

Subject	Mode	Workload	Phase	Number of Losses
BAO	Yaw SAS	70%	Descent	4
	3-Axis SAS	70%	Left Turn	2
TR	Heading Hold	70%	Descent	1
DI	Free Vehicle	70%	Acceleration	1
			Climb	5
			Descent	9
			Left Turn	3
			Straight and Level	2
	Yaw SAS	40%	Left Turn	1
		70%	Climb	3
			Right Turn	3
			Descent	3
			Left Turn	3
			Straight and Level	1
	3-Axis SAS	40%	Left Turn	1
		70%	Acceleratic	1
			Climb	4
			Right Turn	3
			Deceleration	3
	Altitude Hold		Right Turn	1
			Left Turn	3

Table 4. Control Loss Record (UH-1) (Continued)

Subject	Mode	Workload	Phase	Number of Losses
JA	Free Vehicle	70%	Climb	1
			Right Turn	2
			Descent	5
			Left Turn	2
	Yaw SAS	70%	Acceleration	1
			Climb	1
			Right Turn	1
			Descent	2
			Left Turn	2
	3-Axis SAS	70%	Climb	2
			Descent	2
			Left Turn	3
	Altitude Hold		Left Turn	5
			Straight and Level	2

Control Loss by Parameter Variation:

Phases	Number of Losses
Acceleration (2)	3
Climb (3)	16
Right Turn (4)	10
Descent (5)	26
Left Turn (6)	27

Table 4. Control Loss Record (UH-1) (Concluded)

Control Loss by Parameter Variation: (cont.)	
Phase	Number of Losses
Straight and Level	5
Deceleration (8)	3
Modes	
Free Vehicle	30
Yaw SAS	25
Three-Axis SAS	21
Heading Hold	3
Altitude Hold	11
Heading and Altitude Hold	0
Workload	
0%	0
40%	2
70%	88
Subject	
BAO	6
TR	1
DI	50
JA	33

differences in frequency of control loss at the 70 percent workload level. The number of control losses decreased considerably for the three highest autopilot levels, thus indicating an increase in control precision with the increase in autopilot capability at the 70 percent workload level.

6.4 Pilot Comments and Reactions -- At the conclusion of the formal data-gathering phase of the study, the subjects were questioned to ascertain reactions to the various combinations of workloads and autopilot modes and to elicit comments on the study. In addition, record was kept of relevant comments made in the course of the simulation sessions.

The most salient point made was that the two autopilot modes which incorporated altitude hold (Modes 5 and 6) were "easier" to fly. This opinion was expressed by all of the subjects although they differed on whether Mode 5 or Mode 6 was easier. One subject stated that the addition of heading hold (Mode 6) made the simulation slightly more difficult to fly, due to the interaction of pilot and heading hold autopilot corrections for errors caused by gust loading. This subject was of the opinion that Mode 5 was the easiest to fly. The other subjects agreed on Mode 6.

These data are quite strongly supported by the analysis of the pitch and roll activity indices. In other words, it was found that the extent of pilot control inputs demanded to maintain aircraft position decreased with the increase in the autopilot capability.

6.5 Analog Traces of Stick Inputs -- Figures 71A and 71B present samples of the analog traces of pitch and roll cyclic inputs for the three phases of straight-and-level (Phase 7), climb (Phase 3), and left turn (Phase 4), at the highest workload level. The three traces on the left of each figure are from the modes ranked best in terms of the applicable activity index (pitch or roll), and the traces on the right are from the modes ranked lowest. These traces are illustrative of the rankings derived from the statistical analysis of the activity indices over all subjects, all workloads, and all phases.

6.6 Summary of Results - Experiment I --

Task Difficulty and Aircraft Response Stability -- The most significant improvements in pilot performance resulting from increasing levels of autopilot capability were seen in the increase in the ease of the control task and in the stability of the aircraft response. The pitch and roll activity indices, which indicate the extent of control inputs/aircraft responses required to maintain aircraft position, were significantly lower for the three highest autopilot levels (i.e., heading hold, altitude hold, heading, and altitude hold modes). Aircraft position was maintained with lower-amplitude, higher-frequency control inputs and aircraft responses, thus indicating a more stable system as well as a less-demanding task for the pilot.

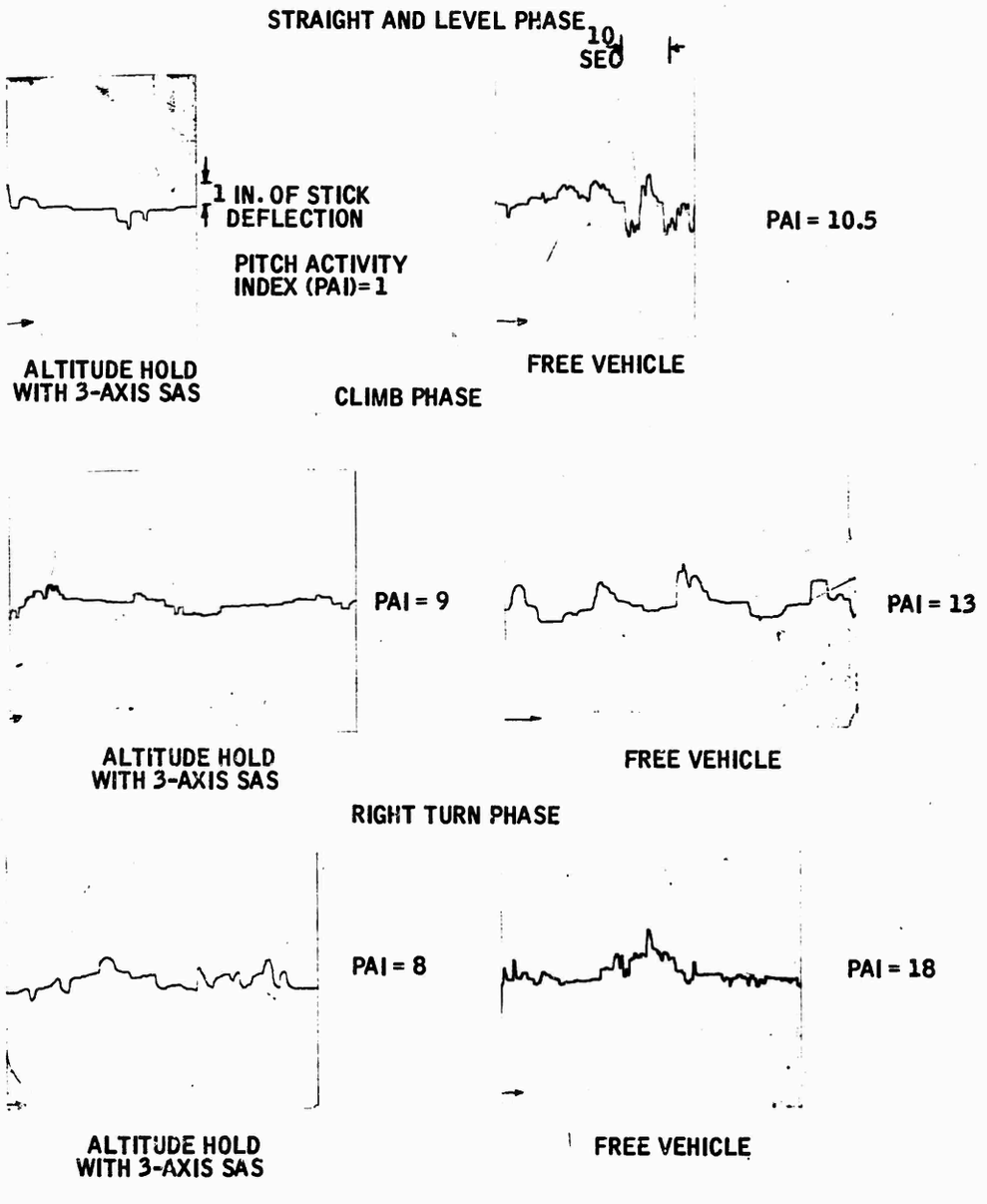

Figure 71A. Analog Traces of Pitch and Roll Activity Indices

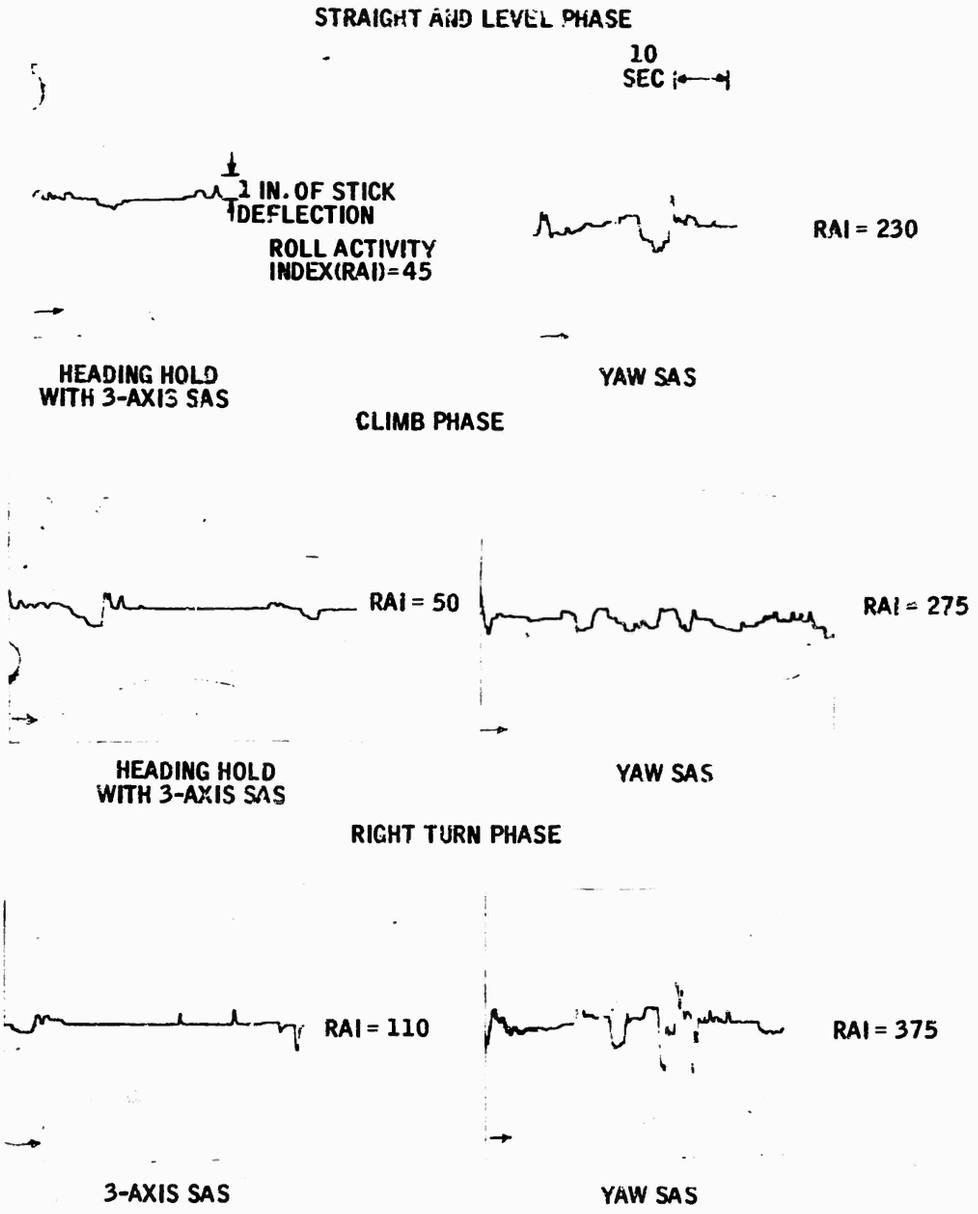

Figure 71B. Analog Traces of Pitch and Roll Activity Indices

The heading and altitude hold mode resulted in the best overall performance in terms of the activity indices, with altitude hold being more critical to reduction of the pitch activity index and the heading hold more critical to reduction of the roll activity index (Figures 30, 40, and 12).

Pilot opinion substantiated the increasing ease of the control task with the increase in autopilot capability. Three of the four subjects selected the heading and altitude hold mode, and the other selected the altitude hold mode as the "easiest" to fly.

In conclusion, the increase in autopilot capability in the helicopter SK/FF task resulted in an increase in system control stability and a decrease in the difficulty of the pilots' control task.

Control Precision -- The most significant decrease in RMS errors was noted for the altitude parameter, which was being controlled primarily by the autopilot and monitored by the pilot. The RMS altitude error (RMS_Z) was significantly lower when either of the modes with altitude hold was engaged (Figures 39 and 41).

The primary purpose of this study, however, was to evaluate the pilot's precision at varying workloads in controlling manually those parameters not being controlled by the autopilot. Evaluation of those parameters being manually controlled by the pilot revealed that varying the levels of autopilot assistance did not significantly affect subject performance in terms of position errors which were averaged over the three workload levels. This could possibly be explained by the pilot's ability to maintain a maximal degree of control precision, without autopilot assistance, with the aid of a quickened display. This display enables him to close all the outer loops, thus performing the same function as an autopilot. Even though additional levels of autopilot assistance made the task easier, it may not have been possible for the pilot to achieve a higher level of control precision (i.e., lower RMS errors). It was expected for this reason that greater performance differences due to varying autopilot levels would show up at higher workload levels.

While the analysis of autopilot modes by workload level did not show significant performance differences in terms of position errors, significant differences were noted in terms of the frequency of control losses. It was found that the number of control losses decreased considerably with the increase in autopilot capability at the 70 percent workload level. Since so many control losses occurred at this workload level, thus requiring the subjects to repeat the maneuvers until completed successfully, the RMS position errors for the various modes were forced to become more homogeneous. Inasmuch as the upper limit of the pilot's capability to control the aircraft appears to have been exceeded by this high workload level, the frequency of control losses was assumed to provide a more accurate evaluation of differences between autopilot modes at the 70 percent workload than that provided by the position errors.

In conclusion, improvement in control position in terms of position errors averaged over all workloads was noted primarily in those parameters which were controlled by the autopilot. The pilots' control precision based on position errors averaged over all workloads did not improve significantly with the increase in autopilot capability. Evaluation of autopilot modes by workload, however, revealed that the increased autopilot capability enabled the pilot to perform considerably better under the highest workload condition tested. At this high workload level the pilot in many cases was unable to maintain control of the vehicle without more autopilot assistance than that provided by the three-axis SAS.

SECTION VI
AH-56 AFCS DESCRIPTION

Presented in this section is a functional description of the AH-56 compound helicopter and its Honeywell-developed AFCS. This description is presented for the AH-56/AFCS, configured for the mid-range portion (60 knots airspeed) of the stationkeeping operational flight envelope. This discussion details the AH-56 modes of operation (as applied to the SK/FF study), a description of the stability loops which define these modes, and time histories demonstrating performance characteristics of the AH-56/AFCS.

PITCH ATTITUDE HOLD

The vehicle's pitch attitude at mode engagement is maintained by the AFCS. Mode engagement is effected by initial AFCS engagement or by reduction of pilot-applied pitch cyclic stick force below the break-out level with the AFCS engaged.

A functional block diagram of the pitch attitude hold mode is shown in Figure 72. The mode consists of six major elements -- the pitch attitude reference, a pitch synchronizer, error signal shaping, pitch rate and attitude feedback loops, servo input shaping, and an AFCS servo. Prior to engagement the synchronizer is driven by the attitude error signal and nulls the error. Upon engagement, the synchronizer input is grounded and the output provides the reference attitude at the time of engagement. The attitude error signal is shaped by fixed, time-lag network with a variable gain. The gain, $K\theta$, is scheduled with dynamic pressure. For the purposes of this study this gain is fixed for the flight condition of interest to a value of 2.7 in X_R/rad θ_E. Basic vehicle stability is augmented by high-passed pitch rate and pitch attitude feedbacks to provide a fast, well damped inner loop for the attitude hold mode. The sum of the shaped error and high-passed rate and attitude signals are fed to the proportional plus integral shaping network sum point of the pitch cyclic parallel servo. This signal is used to control the transfer value and mod piston, which comprise the AFCS servo. The servo output is used to position the boost control valve and actuator piston. The actuator position is transmitted as a force to the vehicle control gyro which, in turn, creates a change in the cyclic pitch of the main rotor blades.

Figure 73 shows the pitch attitude response to a 0.1-rad pitch attitude command. Note that the pitch attitude response time is approximately 3.0 sec and overshoots less than 5.0%. The performance characteristics shown are well within specification limits with respect to pitch attitude hold response.

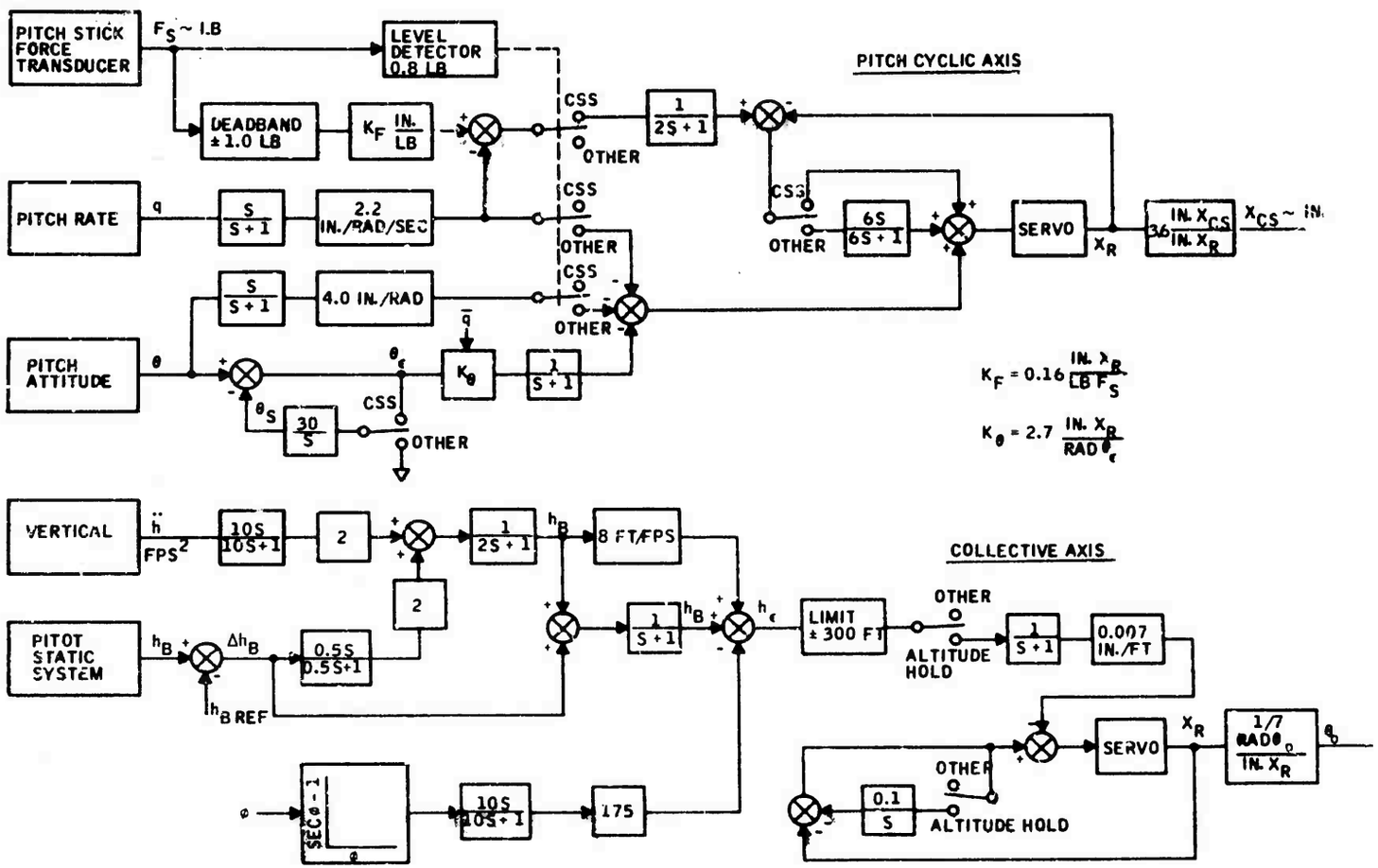

Figure 72. AH-56 Longitudinal Axis

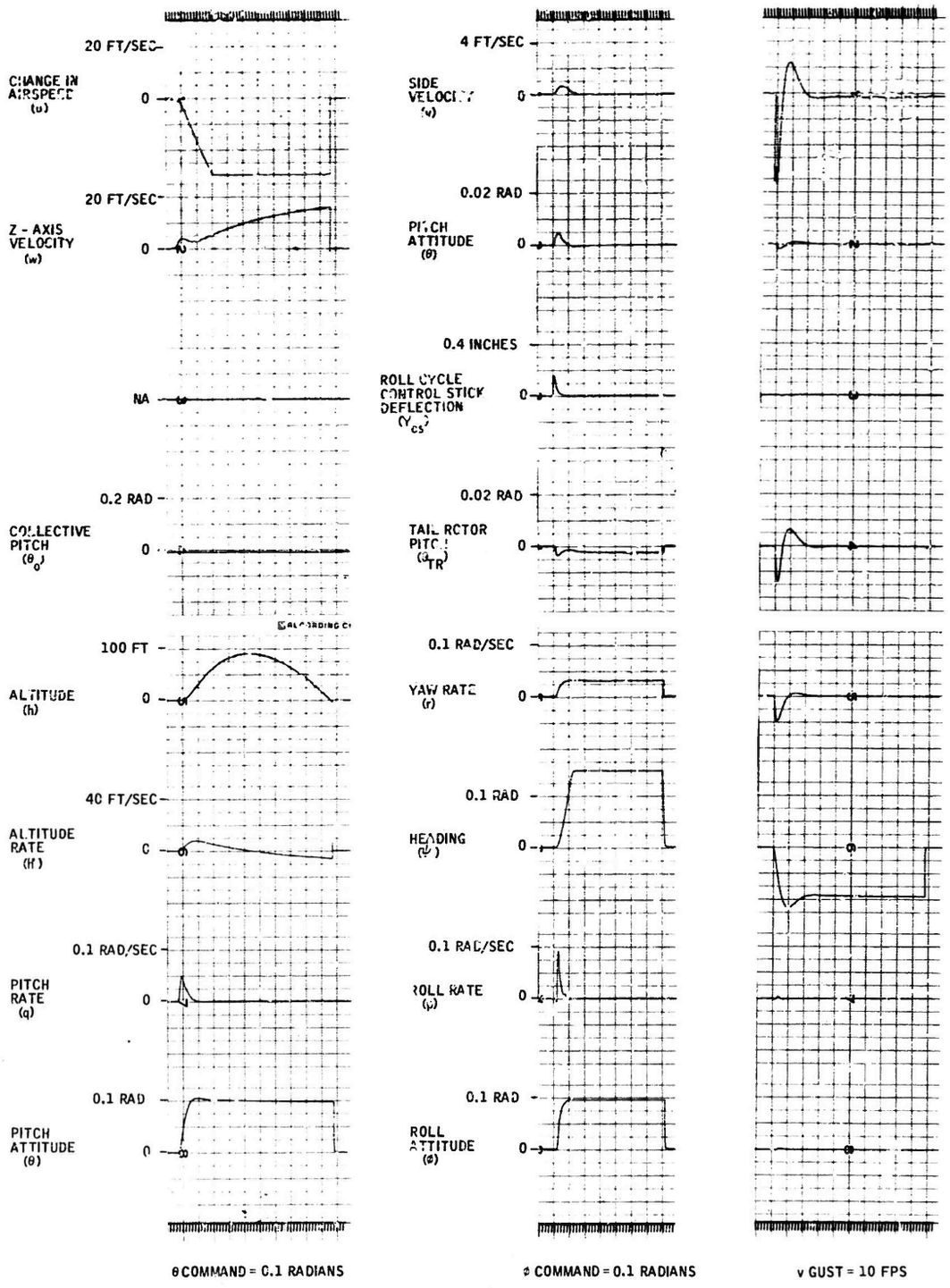

Figure 73. Pitch and Roll Attitude Hold

ROLL ATTITUDE HOLD

Whenever the roll attitude hold mode is engaged, the AFCS commands the vehicle to return to a wings-level roll attitude. Mode engagement is by initial AFCS engagement or by reduction of pilot-applied roll cyclic stick forces below the breakout level with the AFCS engaged.

The functional block diagram of the roll attitude hold mode is shown in Figure 74. Roll attitude control is accomplished by feeding the roll attitude error through a fixed and scheduled gain (K_2) into the servo input shaping networks. The output signals of the servo shaping networks are used to control the transfer valve and mod piston of the AFCS servo. The servo output is used to position the boost control valve and actuator piston. The actuator positions are transmitted as a force to the vehicle control gyro which, in turn, creates a change in the lateral cyclic pitch of the main rotor blades.

It should be noted at this point that roll rate feedback is not incorporated in the roll cyclic axis. The free vehicle along with the mechanical gyro provides acceptable roll attitude hold performance which eliminates the need for a roll rate gyro and its associated feedback networks.

The roll attitude hold performance characteristics are shown in Figure 73. This figure shows that for a roll attitude command of 0.1 rad the roll attitude response time was less than 3.0 sec and the overshoot was less than 5.0%. These performance characteristics are well within specification limits.

HEADING HOLD

When this mode is engaged, vehicle heading at engagement is maintained by the AFCS. Mode engagement is effected if the vehicle roll angle is within ±7 deg by initial AFCS engagement or by reduction of pilot-applied forces to the roll cyclic stick below the breakout levels with the AFCS engaged. When this mode is engaged, the AFCS initiates roll attitude changes to correct for heading errors caused by wind gusts, cross-coupling effects, etc., and then returns the vehicle to wings-level attitude.

A functional block diagram of the heading hold mode is shown in Figure 74. At the flight condition studied during the manual stationkeeping problem, the heading hold function is accomplished via the roll cyclic control axis. This function is accomplished by commanding roll angle changes proportional to heading error. Heading error is provided by locking the heading synchronizer at the instant of heading hold engagement. Elements of the roll attitude command loop are similar to elements of the roll attitude hold mode described previously. The proportionality between commanded roll attitude and heading error is scheduled as a function of dynamic pressure. For the purpose of this study this gain is fixed for the flight condition of interest to a value of 0.4 x X_R/rad. Since tight, responsive control of heading is desired, additional

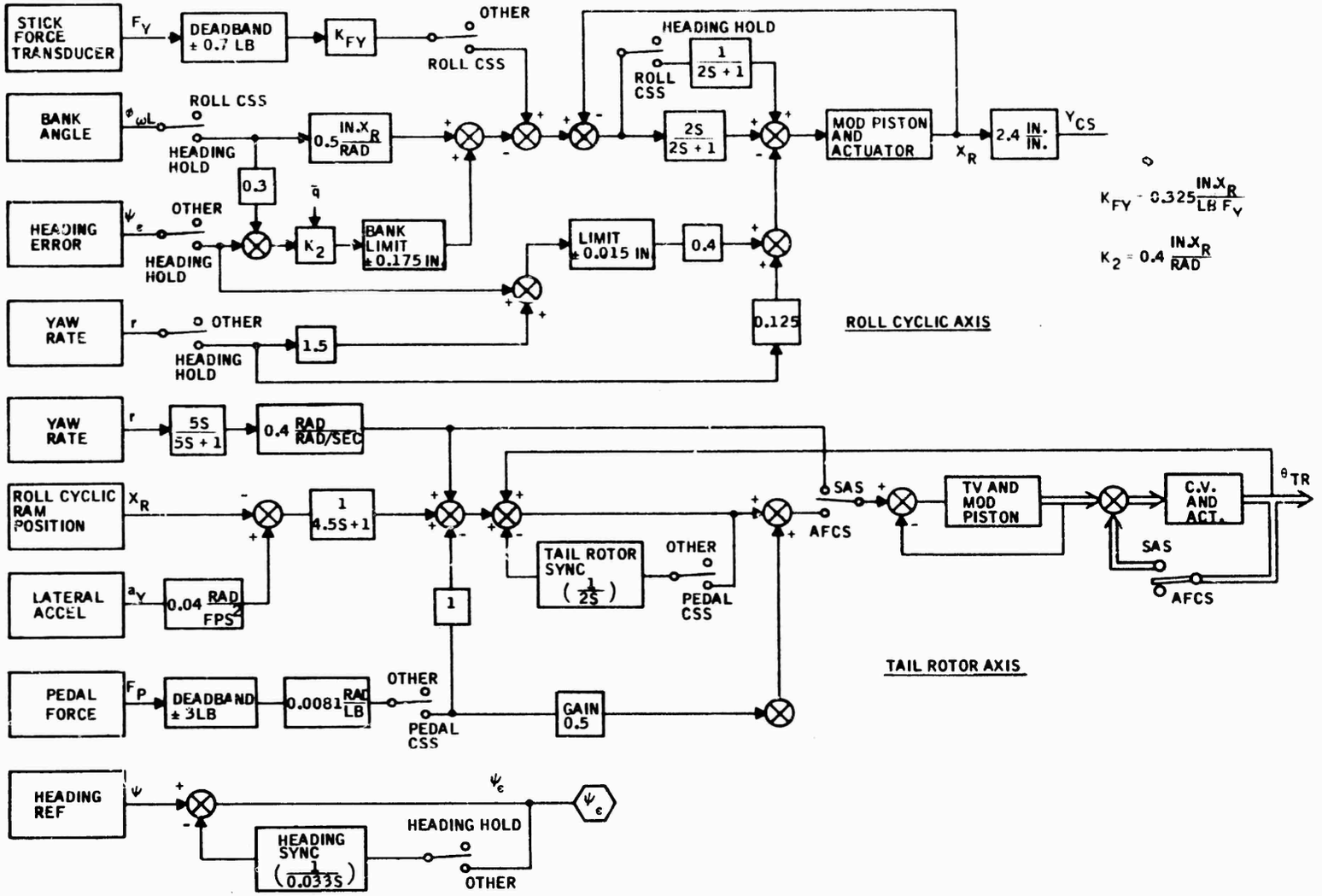

Figure 74. AH-56 Lateral Axis

unfiltered yaw rate is also fed to the roll cyclic servo. Since this signal is removed when heading hold is not engaged, it does not hinder turn coordination at higher speeds. To maintain heading hold accuracy and turn coordination, proportional-plus-integral control is obtained by high-pass filtering the major servo feedback loop.

Heading hold performance for various input conditions and mode configurations are shown in Figure 75. Note that for an initial heading error of 0.1 rad the response time to 90% reduction of the initial error signal is approximately 5.0 sec and the overshoot is 5.0%. These performance characteristics are well within the specification limits with respect to the heading hold function. Also, note that for the same type of input command, heading hold mode engaged, and with the pitch axis in a CSS (control stick steering) configuration, that over the long term the pitch and roll axes drift from their zero reference. This is a normal condition and is due to the aerodynamic cross-coupling of the AH-56 vehicle. It should be further noted that the drift rates are small and the pilot should experience little difficulty in controlling the vehicle to the desired roll and pitch attitudes.

Recordings for a side gust input (υ_g = 10 fps) are included to show that the transient recovery from this input command is smooth and well damped.

Also shown in Figure 75 are various heading hold maneuvers. These maneuvers were performed by simulating a lateral stick force input (F_Y), which engaged the CSS mode in the roll axis, flying to a desired heading, and then removing the F_Y command which re-engaged the heading hold mode. These recordings clearly show that the AH-56A vehicle, under control of the autopilot, will undergo a heading change maneuver in a smooth and well-controlled manner.

ALTITUDE HOLD

The altitude hold mode is selectable when the AFCS is engaged. The altitude existing at mode engagement is maintained by the AFCS.

Upon engagement of the altitude hold mode tha altitude error signals are converted to command collective pitch changes of the main rotor blades. Figure 72 is a functional block diagram of the altitude hold mode.

The basic concept of deriving the altitude error signal is to use an electronic blending circuit. Normal acceleration, ($N_Z \approx \ddot{h}$) is high passed and summed with high-passed static pressure and then shaped to produce a blended altitude rate signal ($\dot{h}$). In a similar manner the blended rate, $\dot{h}_B$, is summed and shaped with the error in static pressure to produce a blended altitude error, h_B. This configuration has two major advantages:

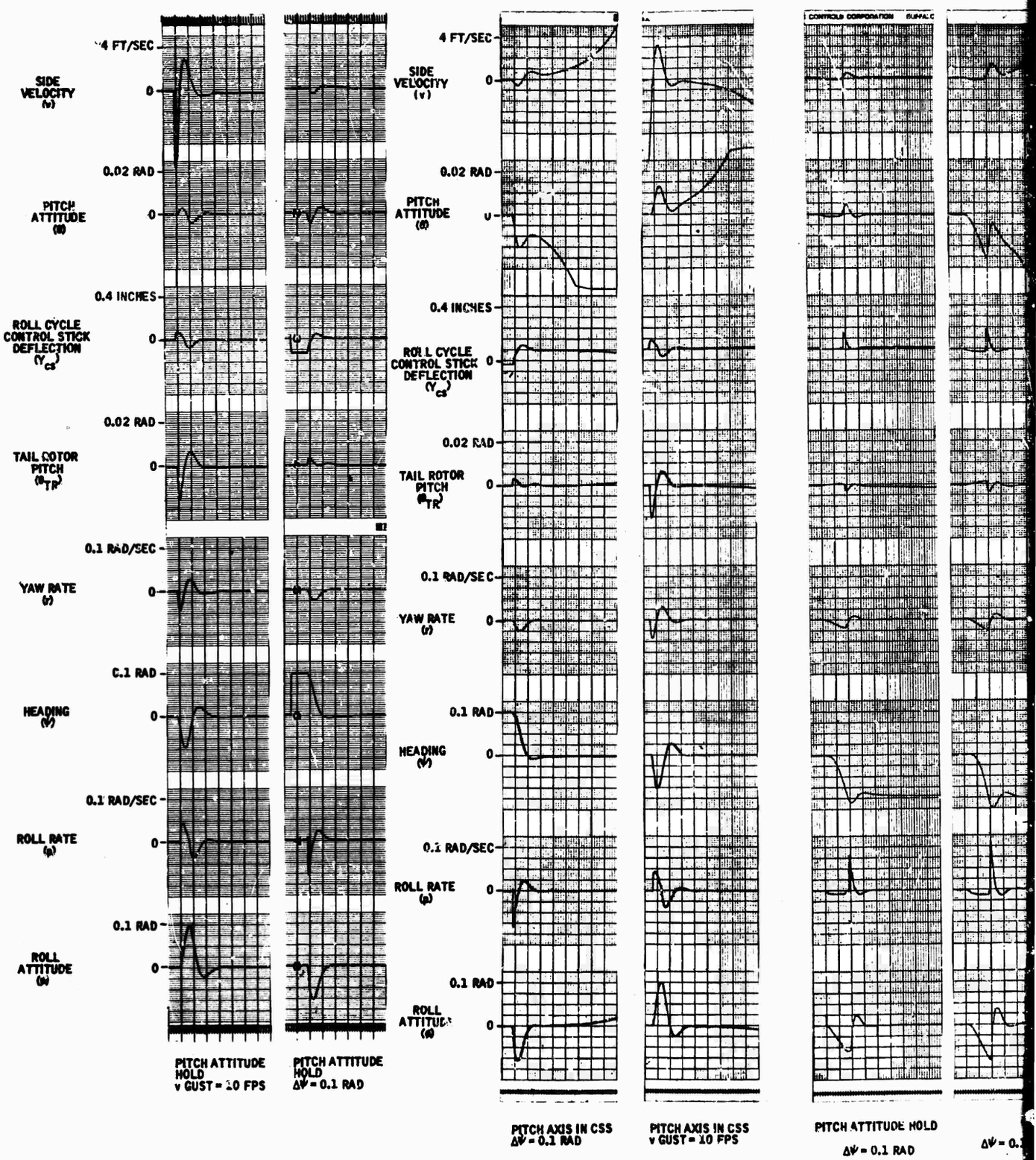

A

Figure 75. Heading Hold

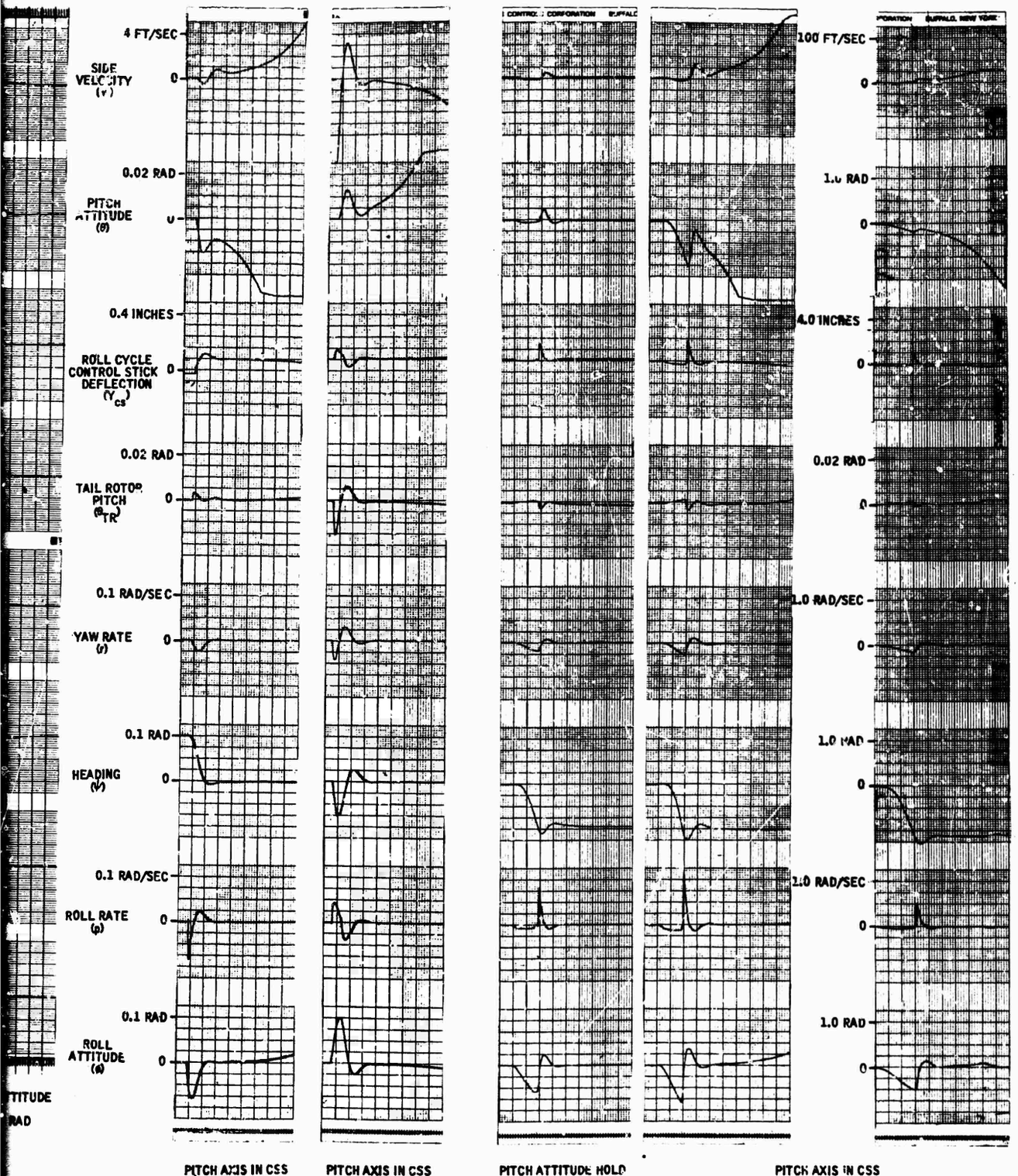

Figure 75. Heading Hold

- The noise content of the air data signals is heavily filtered
- The oscillations due to ADC nonlinearities are minimized.

The blended altitude and blended altitude rate are summed to develop an altitude error signal which is converted to a collective pitch command. Integration of the altitude error is provided by the altitude synchronizer in the feedback of the collective actuator.

The performance characteristic of the altitude hold mode in response to an altitude command are shown in Figure 76. As shown, for an altitude command of 100 ft, the change in altitude was made in a smooth and well-controlled manner. The response time to achieve steady state is approximately 30 sec with no overshoot. These performance characteristics are well in the specification limits for altitude hold. Also shown in Figure 76 are several altitude change maneuvers. These maneuvers were performed by disengaging the latitude hold mode and applying a collective stick input to establish a climbing rate of approximately 5.0 ft/sec, climbing to the desired altitude of 100 ft, and then engaging the altitude hold mode. This maneuver was performed two different ways. First, when the desired altitude was reached, the collective command was faded and altitude hold engaged. Second, when the desired altitude was reached, altitude hold was engaged and the collective command faded. The maneuvers were performed in this manner because the simulated control stick is not driven as a function of the servo output position as it is in the actual vehicle. This makes it necessary for the collective commands to be faded manually upon engagement of the altitude hold mode. A review of these two maneuvers shows that acceptable altitude hold performance can be achieved for small collective imputs, by having the subject assume the feedback function of an actual parallel servo.

YAW SAS

The functional description and computer analysis results of the yaw SAS are presented in this section.

Figure 74 is a functional block diagram of the tail rotor axis. The yaw SAS portion of the tail rotor axis is a conventional high passed yaw rate feedback commanding proportional control of the tail rotor blade pitch through a limited authority series, hydraulic servo. The yaw rate feedback is high passed to allow steady turns without the SAS "fighting" the turn. As shown in the block diagram the gain and time constant chosen are:

K_r = 0.4 rad tail rotor/rad/sec yaw rate

TrH = 5.0 sec

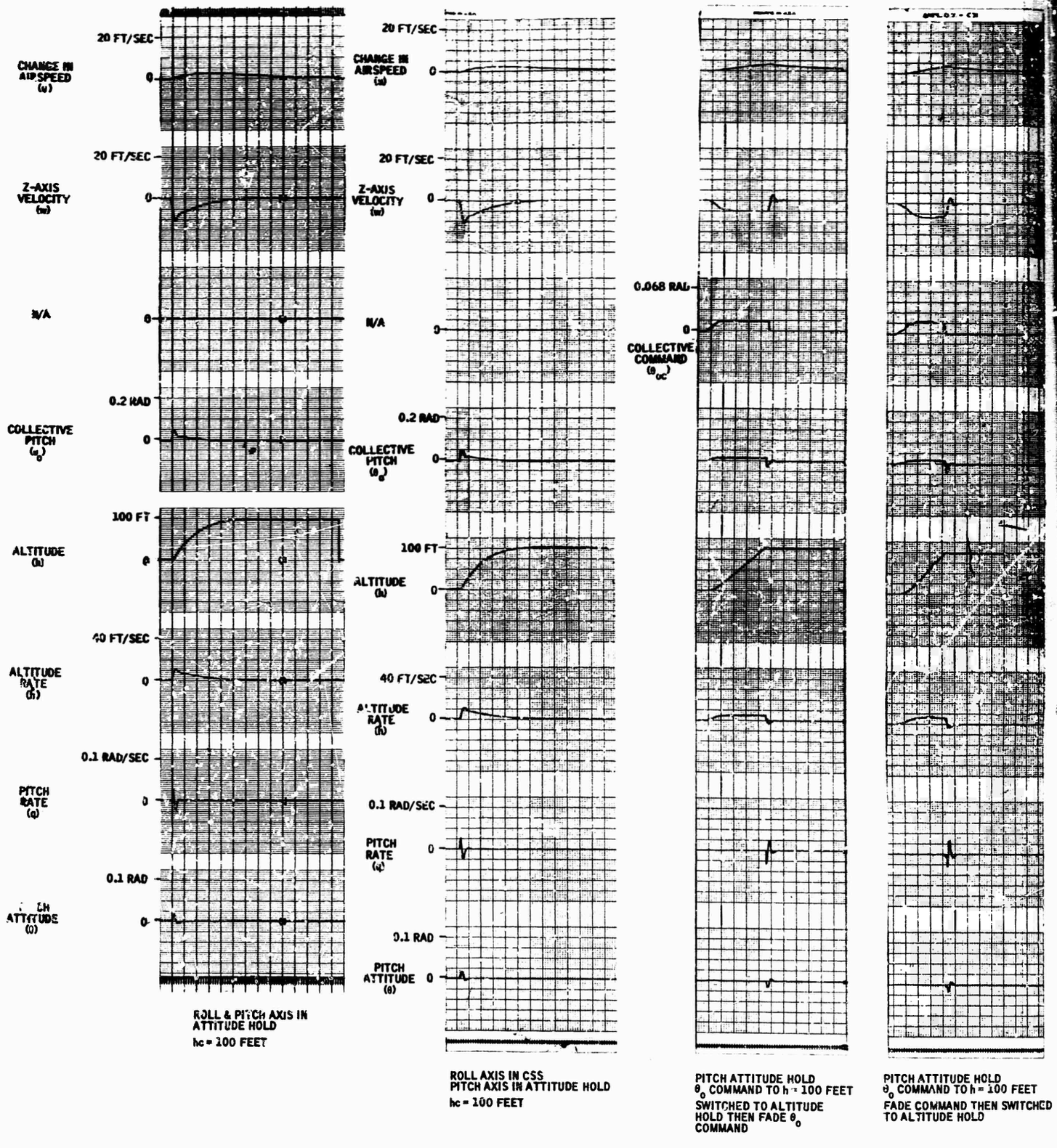

Figure 76. Altitude Hold

The results of analog computer simulation of the AH-56 helicopter equipped with a yaw SAS mode are shown in Figure 77. Performance was evaluated for side velocity disturbances. Note that the responses, with the yaw SAS engaged, are well damped (overshoot about 15%) and that the roll angle excursion is negligible for these 10 ft/sec lateral velocity disturbances. The performance characteristics shown on these recordings are well within specification limits with respect to yaw damping.

CONTROL STICK STEERING (CSS)

When the AFCS is engaged, application of forces to the cyclic stick or rudder pedal beyond the breakout levels results in a rate of change in vehicle attitude or heading, respectively. The angular rate of change is directly proportional to the applied force. The pitch, roll, and yaw control steering modes are engaged by applying force to the pitch cyclic stick, roll cyclic stick, or yaw axes, respectively.

Pitch

Figure 72 is a functional block diagram of pitch CSS. This mode contains three major elements -- a stick force element, a rate gyro block, and the servo-actuator combination.

The pilots' pitch stick force is measured with a force transducer, summed with high passed pitch rate, and fed through a shaping network to the servo input. The gain and time constants of the rate loop are identical to those used in the pitch attitude hold mode. The gain, KF, is set to give the desired pitch rate per pound of stick force. During the CSS mode, the loop integration is both unnecessary and undesirable. Thus, the high pass at the servo input is switched out during CSS operation.

The time history of a pitch CSS manuever is shown in Figure 77. This maneuver was performed by applying a simulated pitch cyclic input (Fs) which engaged the CSS mode, maneuvering to an attitude of 0.4 rad, and then removing the input command and reverting to the pitch attitude hold mode. Shown in Figure 77 are the free vehicle characteristics. As shown, the pitch rate response to a pitch cyclic step input (Xcs) is a well damped rate.

Roll

Elements of the roll CSS mode as shown in Figure 74 are a stick force transducer, a scheduled gain, and the hydraulic servo actuator. Lateral Stick force as measured by a force transducer is used both to engage the CSS mode when a preset breakout force level is exceeded, and to proportionally drive the hydraulic actuator following CSS engagement. Note that

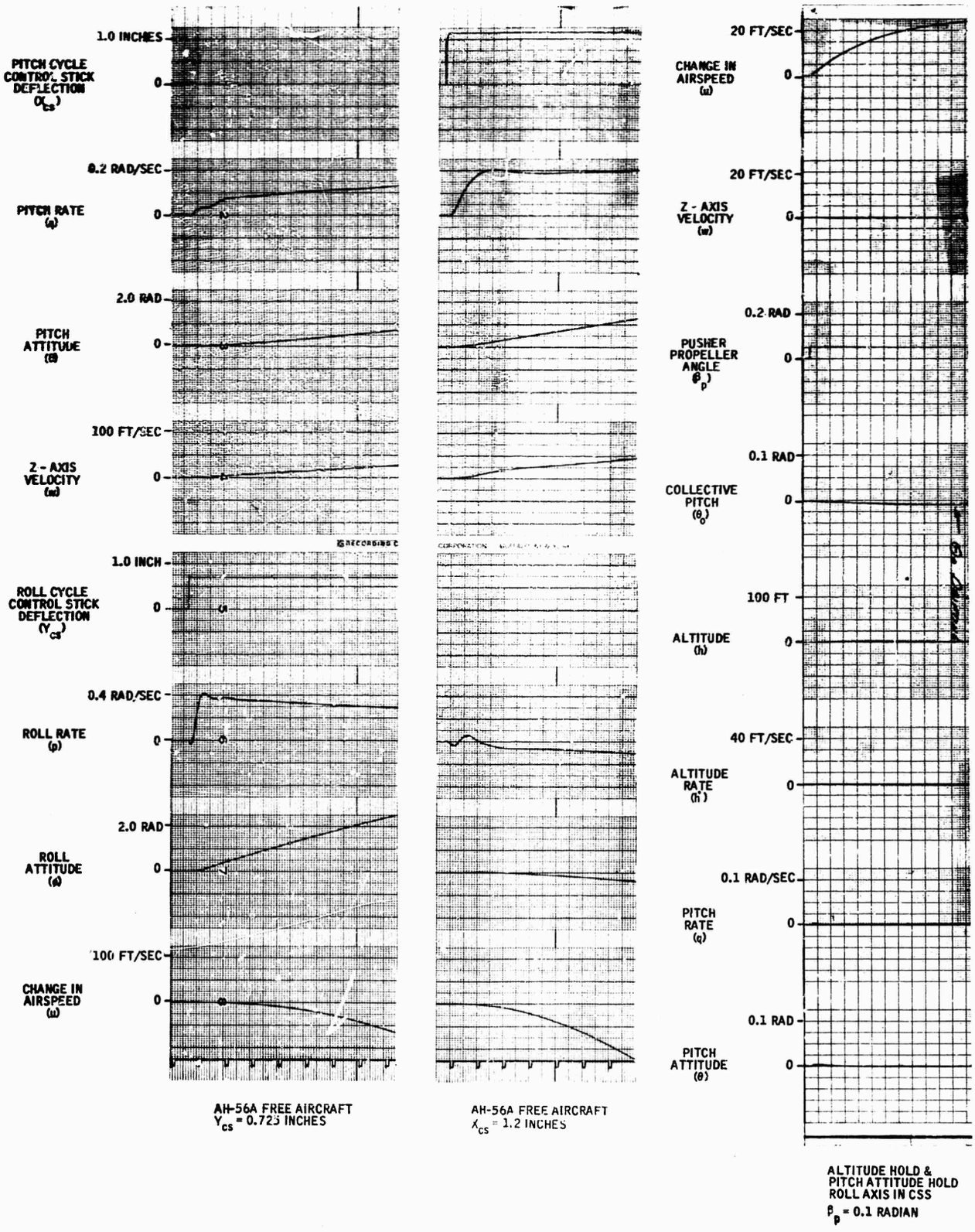

Figure 77. AH-56 Free Aircraft and Pusher Propeller Response (β_p)

upon roll axis CSS engagement the roll axis is controlled as a function of the free vehicle characteristics. During the autopilot analysis it became apparent that the free-vehicle rolling response is sufficiently well damped and that additional stability augmentation is unnecessary. Free vehicle characteristics of the roll axes for a cyclic stick input is shown in Figure 77. Note that for a roll cyclic stick (Ycs) input the vehicle's response is a well damped rate. Roll axis CSS maneuvers are presented in Figure 78. These maneuvers were performed by engaging heading hold and applying a simulated roll cyclic stick input that engaged the roll CSS mode, flying to a roll attitude of 0.1 rad, and then removing the input command and reverting back to a heading hold mode. As shown in Figure 78, the transition to the new heading was smooth and well controlled.

Note that during this type of maneuver and with the pitch axis in the CSS configuration the pilot will have to manually control to the desired pitch attitude.

Yaw

Yaw CSS is configured, as shown in Figure 72, to allow pedal force to command a sideslip at high speeds. Elements of the system are a pedal force channel, rate channel, a turn coordination channel consisting of lateral acceleration (Ay) and roll cyclic ram position (Xr), and the tail rotor hydraulic servo actuator loop.

A net pedal force signal derived from the left and right pedal force transducers is used to engage yaw CSS at a preset breakout force level, and to command a proportional tail rotor servo displacement. Upon engagement the tail rotor synchronizer is placed in a sync mode which removes the high passed yaw rate and turn coordination terms and allows the vehicle to sideslip. At CSS disengagement the synchronizer reverts to a hold mode, and the tail rotor angle existing at that instant becomes the new tail rotor reference.

PUSHER PROP COMMANDS

The AH-56 is a compound helicopter; that is, a fifth axis of control is available. This pusher-propeller axis provides control of airspeed independent of attitude control. The pusher propeller is used both to change airspeed and hold a given airspeed. Hence, the use of a pusher-propeller control should provide performance capabilities not obtainable from conventional helicopters. Manual pusher-prop commands are put in via a twist grip on the collective control lever. These manual commands are fed directly to the hydraulic servo, which results in porportional pusher-propeller blade angle changes.

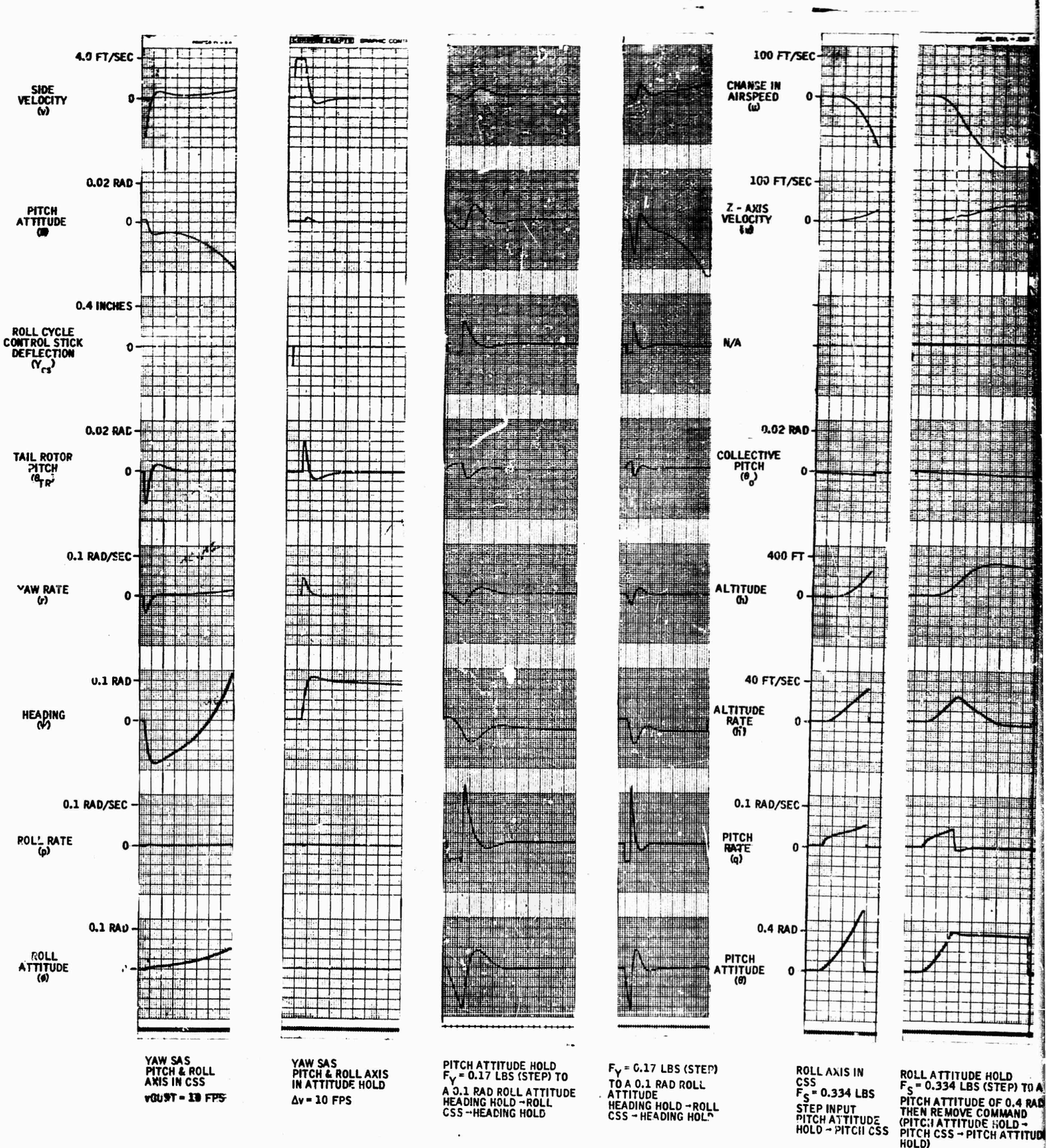

YAW SAS
PITCH & ROLL AXIS IN CSS
vGUST = 10 FPS

YAW SAS
PITCH & ROLL AXIS IN ATTITUDE HOLD
Δv = 10 FPS

PITCH ATTITUDE HOLD
F_Y = 0.17 LBS (STEP) TO A 0.1 RAD ROLL ATTITUDE
HEADING HOLD → ROLL CSS → HEADING HOLD

F_Y = 0.17 LBS (STEP)
TO A 0.1 RAD ROLL ATTITUDE
HEADING HOLD → ROLL CSS → HEADING HOLD

ROLL AXIS IN CSS
F_S = 0.334 LBS
STEP INPUT
PITCH ATTITUDE HOLD → PITCH CSS

ROLL ATTITUDE HOLD
F_S = 0.334 LBS (STEP) TO A
PITCH ATTITUDE OF 0.4 RAD
THEN REMOVE COMMAND
(PITCH ATTITUDE HOLD → PITCH CSS → PITCH ATTITUDE HOLD)

Figure 78. Yaw SAS and CSS Responses

Figure 78 shows the vehicle response to a step pusher-propeller command. As shown, the forward velocity response is similar to a first-order lag. Note that there is very little coupling into the other axes.

SK/FF AUTOPILOT MODES MECHANIZED

The AH-56/AFCS analog simulation was mechanized to allow the manual SK/FF problem to be studied with either of six levels of stability augmentation. These six levels of stability augmentation are as follows: Free aircraft, yaw SAS, three-axis stability augmentation/attitude hold, heading hold, altitude hold, and the combination of heading hold and altitude hold.

Free Aircraft

When in this configuration all feedbacks and shaping network are removed from the vehicle, and control stick inputs are fed directly to the simulated actuators.

Yaw SAS

Yaw axis stability augmentation is provided whenever the AFCS is engaged. During this level of augmentation, the pilot must manually control vehicle attitude, heading, airspeed, and altitude.

Three-Axis Stability Augmentation/Attitude Hold

When this mode is engaged, pitch attitude and wings-level roll attitude is maintained by the AFCS. The CSS mode in pitch and roll is engaged when the pilot makes pitch or roll cyclic stick commands. Under this level of augmentation the pilot must manually control vehicle heading, airspeed, and altitude.

Heading Hold

When this mode is engaged, vehicle heading at the time of mode engagement will be maintained by the AFCS. Yaw SAS and pitch attitude hold are engaged when this mode is selected. The pilot's task will be to manually control airspeed and altitude and to monitor heading and make corrections as required to null lateral position errors.

Altitude Hold

When this mode is engaged, the altitude existing at the time of mode engagement will be maintained by the AFCS. Three-axis stability augmentation/attitude hold will be engaged when this mode is selected. The pilot will be required to manually control airspeed and heading, and to monitor altitude.

Heading and Altitude Hold

This mode is a combination of the previous two modes. When this mode is engaged, the AFCS will automatically hold vehicle heading and altitude. The pilot must control his longitudinal position via airspeed control.

A description of the AH-56 free-vehicle and autopilot simulation is presented in Appendix D.

SECTION VII

EVALUATION OF LEVELS OF AFCS AND WORKLOAD FOR AH-56

PRELIMINARY SIMULATIONS

Preliminary simulations were conducted to (1) determine optimum gains for the PPI quickening model (2) select an appropriate maximum workload level, and (3) provide subject training in each autopilot mode and at each workload level prior to formal data collection.

Display Quickening

It was found during these preliminary sessions that the use of the pusher prop for control of longitudinal position required a modification to the PPI quickening model used in previous studies and in the UH-1 autopilot study (described in Section V). A longitudinal acceleration term was added to relate the display quickening symbol movement more directly to pusher-prop inputs, since these inputs result directly in changes in longitudinal velocity. The resultant modified PPI quickening model and the gains selected during these preliminary sessions were defined as

$$X_Q = K_X \Delta X + K_{\dot{X}} \Delta \dot{X} + \cos \psi_E \left[K_\theta \theta + K_{\dot{\theta}} \dot{\theta} + K_{\ddot{X}} \ddot{X}\right]$$

$$- \sin \psi_E \left[K_\phi \phi + K_{\dot{\phi}} + K_\psi \psi_E\right]$$

$$Y_Q = K_Y \Delta Y + K_{\dot{Y}} \Delta \dot{Y} + \cos \psi_E \left[K_\phi \phi + K_{\dot{\phi}} \dot{\phi} + K_\psi \psi_E\right]$$

$$+ \sin \psi_E \left[K_\theta \theta + K_{\dot{\theta}} \dot{\theta} + K_{\ddot{X}} \ddot{X}\right]$$

X_Q, Y_Q = distance from cross to the asterisk

K_X, K_Y = scale factor

ΔX, ΔY = follower position error

$K_{\dot{X}}$, $K_{\dot{Y}}$ = gains for velocities

$\Delta \dot{X}$, $\Delta \dot{Y}$ = velocity difference between follower and leader

$\ddot{X}$ = longitudinal acceleration

θ = follower pitch attitude

$\dot{\theta}$ = follower pitch attitude rate

ϕ = follower roll attitude

$\dot{\phi}$ = follower roll attitude rate

$K_\theta, K_\phi, K_{\dot{\theta}}, K_{\dot{\phi}}$ = gains for attitude terms

K_ψ = gain for heading term

$K_{\ddot{X}}$ = gain for acceleration term

ψ_E = ψ follower ψ leader = heading error

The gains which were selected during the preliminary experimental sessions were

$K_{\dot{X}}$ = 0.1 in./ft/sec of velocity difference

$K_{\dot{Y}}$ = 0.06 in./ft/sec of velocity difference

K_θ = -13.3 in./rad

K_ϕ = 9.5 in./rad

$K_{\dot{\theta}}$ = -13.3 in./rad/sec

$K_{\dot{\phi}}$ = 5.7 in./rad/sec

K_ψ = 4.8 in./rad of heading differences

$K_{\ddot{X}}$ = 0.25 in./ft/sec/sec of longitudinal acceleration

Subject Training and Maximum Workload Selection

Each subject was trained in each autopilot mode/workload combination until his performance stabilized. It was found during these training sessions that the 70% maximum workload level used in the UH-1 study resulted in a high frequency of control losses, also noted in the control loss record for the

formal UH-1 study (Section V). It was decided, therefore, to set the maximum workload level for this study at 60% for evaluation in the formal experiment.

FORMAL EXPERIMENTATION

The objective of this phase of the study was to systematically relate pilot performance during manual IFR formation flight to various levels of autopilot assistance and pilot workload for the AH-56 Cheyenne helicopter. This aircraft was selected to represent the advanced class of high-speed, high-performance helicopters envisioned to be in operation during the 1970s.

Experiment II was conducted to evaluate pilot performance on the AH-56 as a function of autopilot and workload levels. This experiment and its results are described in detail as follows.

EXPERIMENT II - AH-56 AUTOPILOT EVALUATION

Objective

The objective of this experiment was the fully-factorialized evaluation of subject performance in a manual SK/FF task under six levels of autopilot assistance and three levels of subject workload.

1.0 Independent Variables

Autopilot Mode -- The six levels of autopilot examined were

1) Free vehicle
2) Yaw stability augmentation
3) Attitude hold: Yaw SAS, pitch and roll attitude holds
4) Heading hold (includes attitude holds and yaw SAS)
5) Altitude hold (includes attitude holds and yaw SAS)
6) Heading and altitude hold (includes attitude holds and yaw SAS)

These modes are described in Section VI.

Workload Level -- Workload is defined as described for Experiment I, Section V. The off-cycle of the display was varied to provide different levels of workload. Those selected for evaluaton were

Workload Level	Display Off-Cycle	Display On-Cycle
0%	0.0 sec	Continuous
40%	0.67 sec	1.0 sec
60%	1.50 sec	1.0 sec

Subjects -- The same four subjects described for Experiment I also participated in this experiment.

Mission Phases -- Same as described for Experiment I with the exception that at the end of the 10-sec period straight-and-level flight was commanded until (or unless) the aircraft was within ±75 ft of commanded position in all three axes. Only when the aircraft was within this envelope was the next phase started.

2.0 Dependent Variables

The following variables were recorded during the simulated missions:

Position Error Measures -- RMS errors, means, and standard deviations of the position errors as described for Experiment I, were recorded during this experiment.

Activity Index -- The pitch and roll activity indices described for Experiment I were recorded during this experiment.

Collisions -- Collisions, as defined for Experiment I, were also recorded for this experiment.

Catastrophic Control Losses -- Control losses resulting in mission termination were recorded.

3.0 Constants

Turbulence -- One level of turbulence was simulated throughout the experiment. It consisted of a zero mean wind velocity with a simulated maximum gust level of 10 knots, yielding a gust level to airspeed ratio of 0.167, which is significantly higher than the comparable UH-1 ratio.

Mission Phase Sequence -- The sequence of the seven mission phases was as described for Experiment I and was held constant throughout the experiment.

Simulation -- All characteristics of the simulation (i.e., AH-56 helicopter dynamics, formation configuration, control system, display, and display format) were as described in Section III of this report and were held constant throughout the experiment.

Data Rate -- One rate of data update was maintained throughout the experiment. It was 4 updates/sec, found in a previous Honeywell study to be the lowest update rate yielding adequate performance. (Reference 4)

Data Accuracy -- One level of sensor measurement noise was simulated and used throughout the experiment.

Measurement	SD of Gaussian Noise Distribution
Bearing	$N_B = 0.007$ rad
Elevation	$N_E = 0.007$ rad
Range	$N_R = 1.5$ ft

These measurements were filtered with an alpha-beta filter ($\alpha = 0.25$) prior to display presentation. This level of measurement noise after filtering resulted in the following levels of noise in the x, y, and z position coordinates:

$$\sigma_x = \sigma_y = 2.25 \text{ ft}, \quad \sigma_z = 3.14 \text{ ft}$$

For further details of the simulated measurement system, see Reference 4.

4.0 Experimental Plan

Figure 78 illustrated the design used for this experiment:

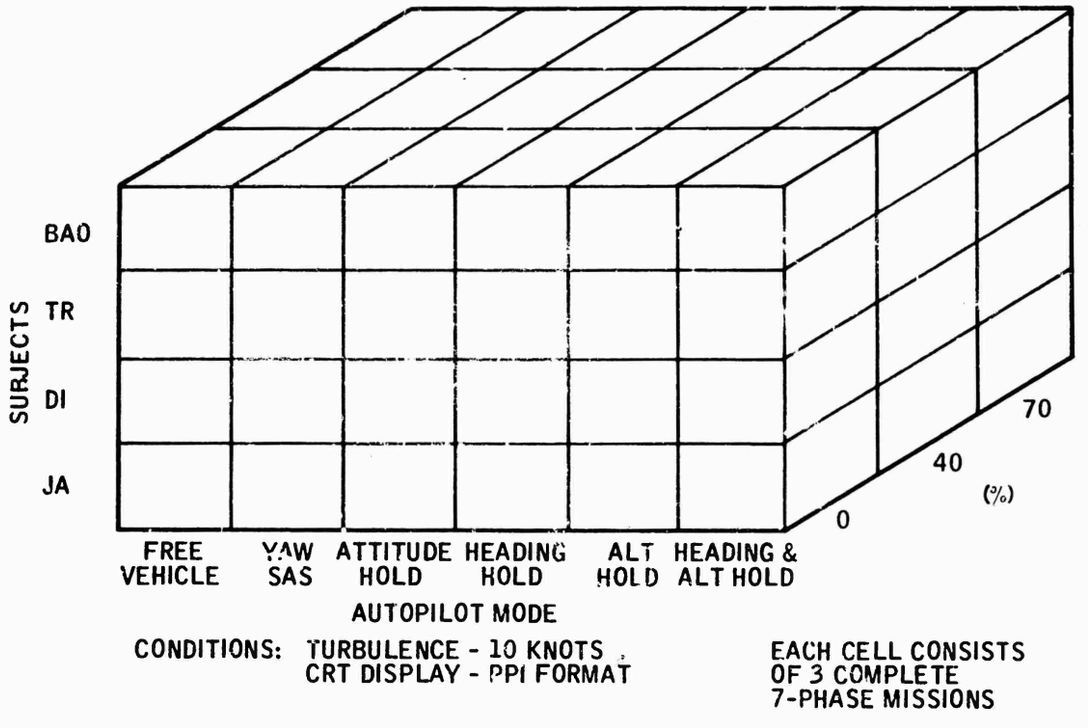

Figure 79. Experimental Design

The schedule followed in accomplishing the experiment is presented in Table 5. The order of presentation of autopilot modes and the order of workloads within each mode were counterbalanced between subjects to control possible order effects. One seven-phase mission was flown by each subject for each combination of parameters shown in Table 5.

5.0 Analysis of Data

Analyses of variance were performed for each mission phase separately in order that autopilot modes could be evaluated for each specific maneuver. The analysis for each phase was based only on the autopilot modes applicable for that maneuver. Some autopilot modes were not appropriate for some mission phases; e.g., the altitude hold mode could not be used during the climb or descent phases. Thus, each analysis was performed on the complete factorial combination of the applicable autopilot modes for that phase, three levels of workload, and four subjects. The subject factor was considered to be random with all other factors fixed. Interactions of each effect with the subject factor represented the error term for the corresponding main effect being tested. Table 6 summarizes the levels of variables and constants describing this experiment.

Table 5. Experimental Schedule

Subject	Mode									
BAO	Yaw Axis (2)	0	40	60	0	60	40	40	0	60
	Heading Hold (4)	40	60	0	60	0	40	0	40	60
	Heading and Alt. Hold (6)	60	0	40	0	40	60	40	60	0
	Attitude Hold (3)	0	40	60	60	40	0	40	0	60
	Free Vehicle (1)	0	40	60	60	40	0	40	60	0
	Altitude Hold (5)	40	60	0	40	0	60	60	40	0
TR	Heading and Alt. Hold (6)	40	60	0	60	0	40	0	40	60
	Free Vehicle (1)	40	60	0	60	0	40	0	60	40
	Heading Hold (4)	0	40	60	60	0	40	40	60	0
	Yaw Axis (2)	0	60	40	40	0	60	60	40	0
	Attitude Hold (3)	0	40	60	60	0	40	40	60	0
	Altitude Hold (5)	60	40	0	40	0	60	0	60	40
DI	Free Vehicle (1)	60	40	0	40	0	60	40	60	0
	Yaw Axis (2)	40	60	0	60	40	0	0	40	60
	Attitude Hold (3)	40	0	60	60	40	0	0	40	60
	Altitude Hold (5)	40	60	0	0	40	60	60	0	40
	Heading and Alt. Hold (6)	0	40	60	60	0	40	40	60	0
	Heading Hold (4)	40	0	60	0	60	40	0	40	60
JA	Altitude Hold (5)	0	60	40	40	0	60	60	40	0
	Attitude Hold (3)	40	60	0	60	0	40	0	40	60
	Free Vehicle (1)	60	40	0	40	0	60	0	60	40
	Heading and Alt. Hold (6)	40	60	40	60	0	40	0	40	60
	Heading Hold (4)	0	60	40	60	0	40	40	60	0
	Yaw Axis (2)	0	40	60	60	0	40	40	60	0

Table 6. Experiment Summary

	Levels
1. Controlled Parameters	
a. Subjects (S)	4
b. Workloads (W)	3
c. Autopilot Modes (M)	6
d. Mission Phases (P)	7
e. Replications per cell (R)	3
2. Measured Parameters	
a. Position Error Measures (12)	
1) RMS error for X, Y, Z and R	
2) Mean error for X, Y, Z and R	
3) Standard deviation for X, Y, Z and R	
b. Collisions with other aircraft	
c. Catastrophic Control Losses	
d. Activity Indices (2)	
1) Roll activity index	
2) Pitch activity index	
3. Experimental Constants	
a. Turbulence level of 10 knots	
b. Mission phase sequence	
c Data Rate	
d. Data Accuracy	
e. All characteristics of the simulation (helicopter dynamics, formation configuration, PPI display format and quickening model, etc.)	
4. Total Number of Observations:	
S x W x M x P x R = 4 x 3 x 6 x 7 x 3 = 1512	

6.0 Results - Experiment II

Analyses of variance were performed on the RMS_X, RMS_Y, RMS_Z position error data and on the pitch and roll activity indices recorded during this experiment. These analyses, summarized in Appendix A for three representative phases, indicate the statistical significance of differences in pilot performance associated with the various autopilot modes and workload levels.

6.1 Effect of Workload on Performance -- Overall mean RMS errors and activity indices for each of the workloads tested are shown by phase in Figures 80 through 93. With one exception, increasing the workload level resulted in increased longitudinal (X), lateral (Y), and altitude (Z) RMS position errors, and in higher pitch and roll activity indices for all seven mission phases. The lone exception is the RMS_Z error in phase 2 (Figure 80) which decreased with the increase in workload from 40% to 60%, although it remained well above the RMS_Z error for that phase at 0% workload.

With two exceptions, all differences in the pitch and roll indices and in the RMS position errors (RMS_X, RMS_Y, RMS_Z) were statistically significant for all phases. The two exceptions, RMS_Z error in phase 8 (Figure 92) and pitch activity index in phase 7 (Figure 91), while not statistically significant do increase with the increase in workload and fall just short of formal statistical significance, especially in the case of the pitch activity index, at the 0.10 level of confidence. On the figures, the scaling necessary to include both the roll and pitch indices on the same graph tends to deemphasize the magnitude of the changes in the pitch index across workloads, but the percentage change in the pitch index is approximately the same as that in the roll indes, and the differences in the pitch index were statistically significant in all but one phase, as noted above.

It is apparent from Figures 80 through 93 that the extent of performance degradation in any given axis varies with mission phase, as was true of the UH-1 simulation (Experiment I). For example, the percentage of increase in RMS_Y errors associated with the increase in workload from 40% to 60% ranged from slightly over 10% in the acceleration phase (Figure 80) to nearly 100% in the descent phase (Figure 86). The roll activity index in general increased more with the increase in workload from 40% to 60% than from 0% to 40% in all phases. The variations in the extent of performance degradation between mission phases is as expected, and is due to the varying levels of difficulty of the maneuvers and to the emphasis in any given phase (except straight and level) on change in one axis, which may contribute to degradation of performance in the other two axes.

In summary, increasing the pilot workload results in significant performance degradation in terms of increasing RMS position errors and demanding an increase in control inputs to maintain position. These results verify those obtained in a previous Honeywell study on the evaluation of various display formats at different workload levels (Reference 1) and the results obtained in Experiment I of this study (Section V).

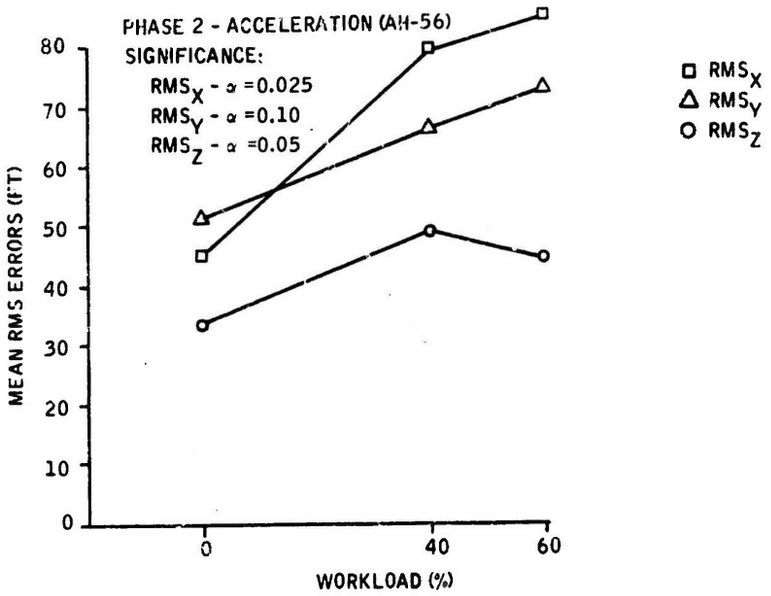

Figure 80. Phase 2 (Acceleration): RMS Errors versus Workload

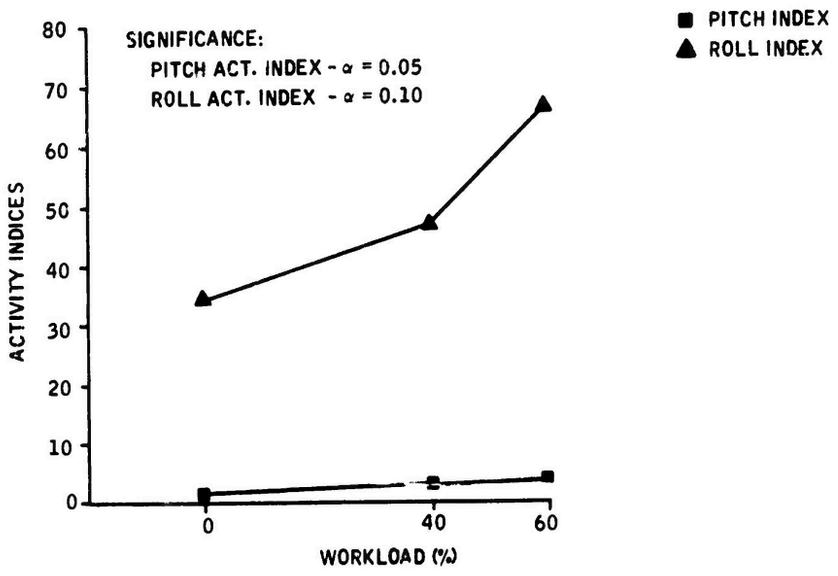

Figure 81. Phase 2 (Acceleration): Activity Indices versus Workload

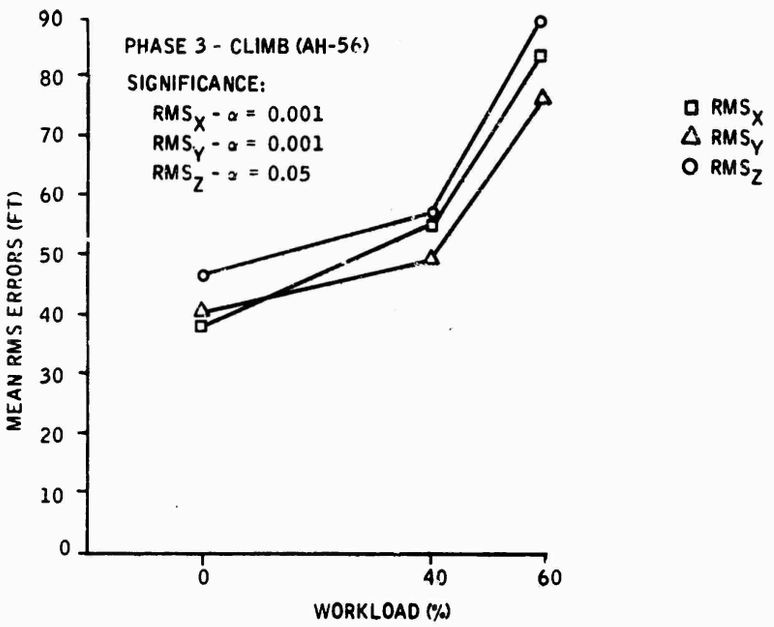

Figure 82. Phase 3 (Climb): RMS Errors versus Workload

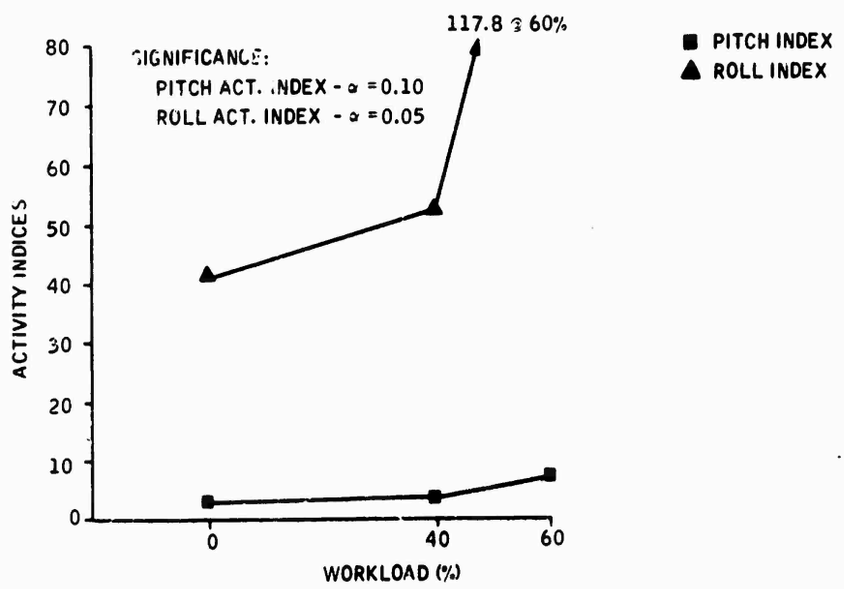

Figure 83. Phase 3 (Climb): Activity Indices versus Workload

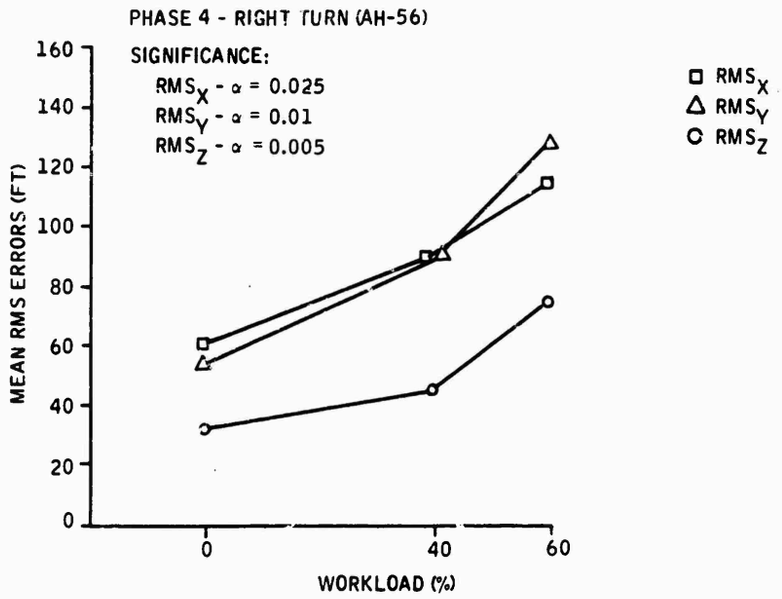

Figure 84. Phase 4 (Right Turn): RMS Errors versus Workload

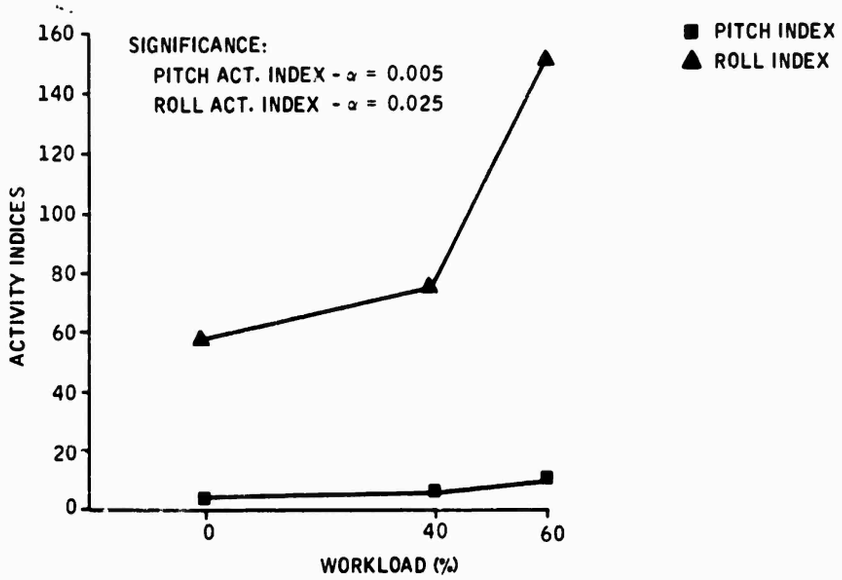

Figure 85. Phase 4 (Right Turn): Activity Indices versus Workload

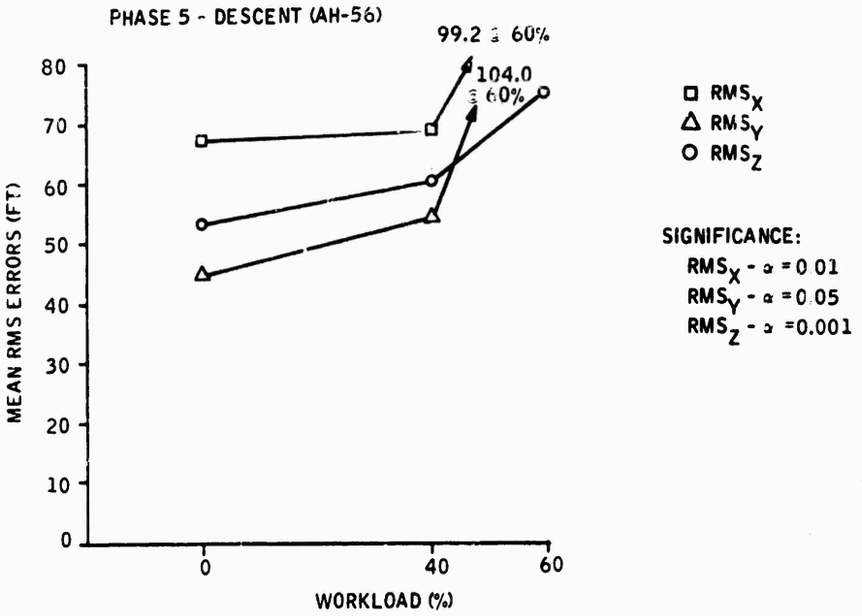

Figure 86. Phase 5 (Descent): RMS Errors versus Workload

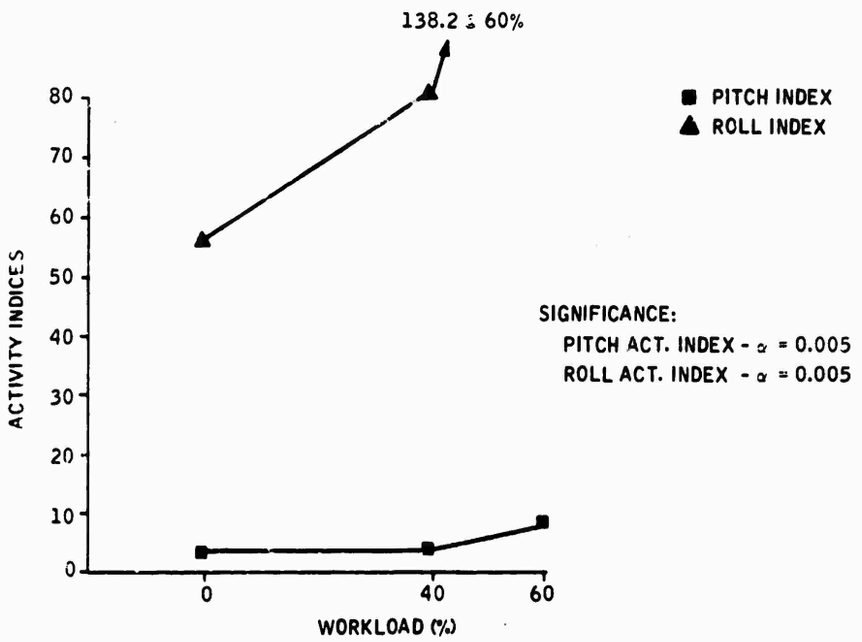

Figure 87. Phase 5 (Descent): Activity Indices versus Workload

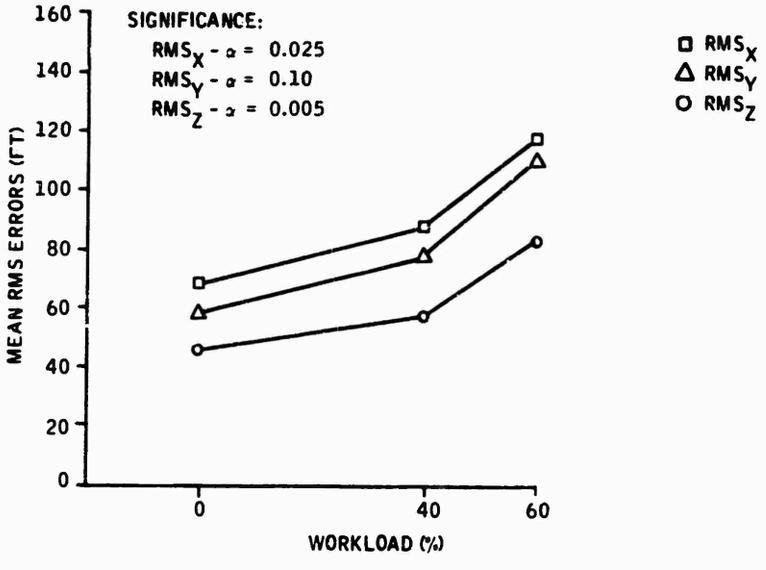

Figure 88. Phase 6 (Left Turn): RMS Errors versus Workload

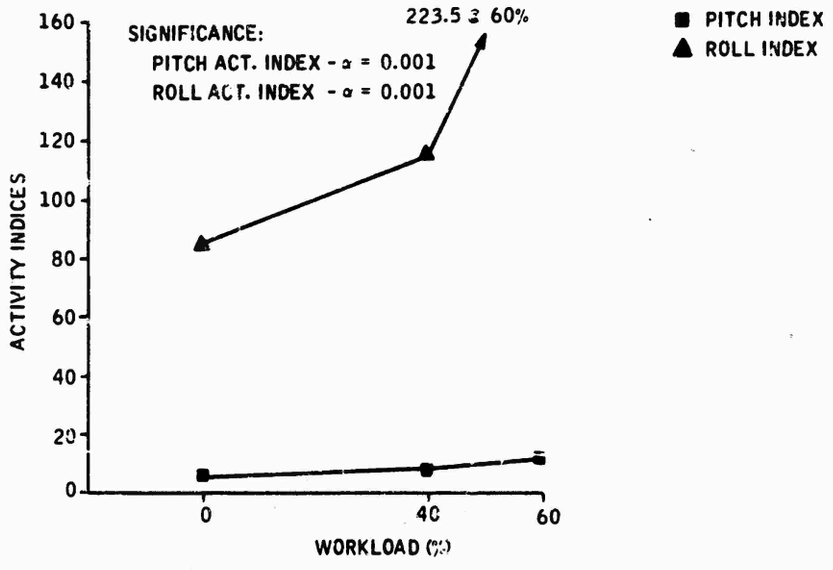

Figure 89. Phase 6 (Left Turn): Activity Indices versus Workload

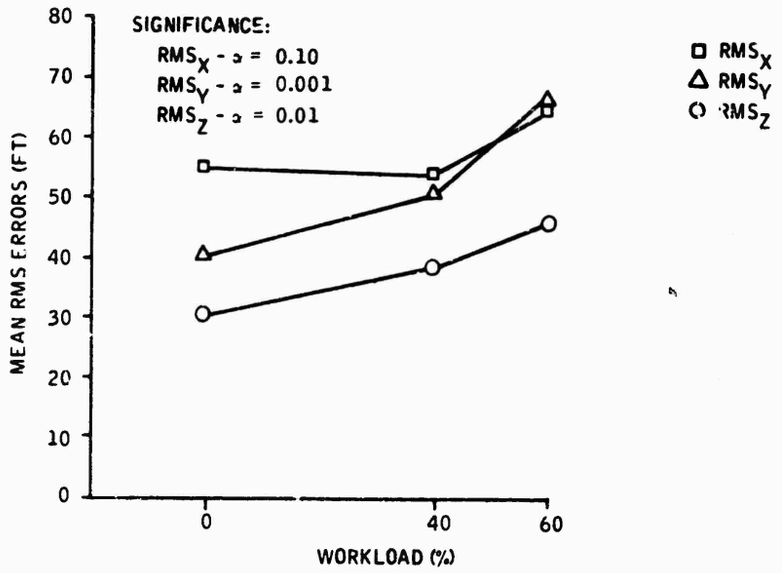

Figure 90. Phase 7 (Straight and Level): RMS Errors versus Workload

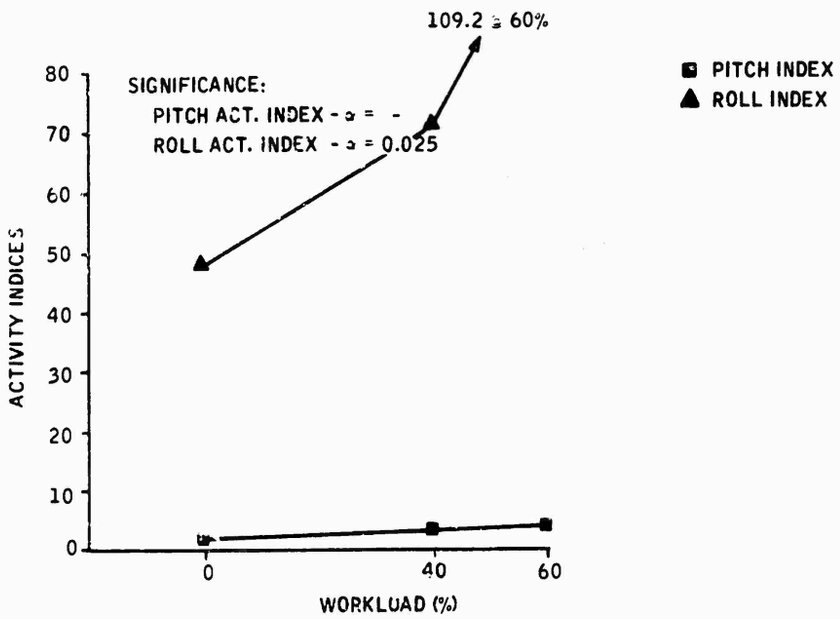

Figure 91. Phase 7 (Straight and Level): Activity Indices versus Workload

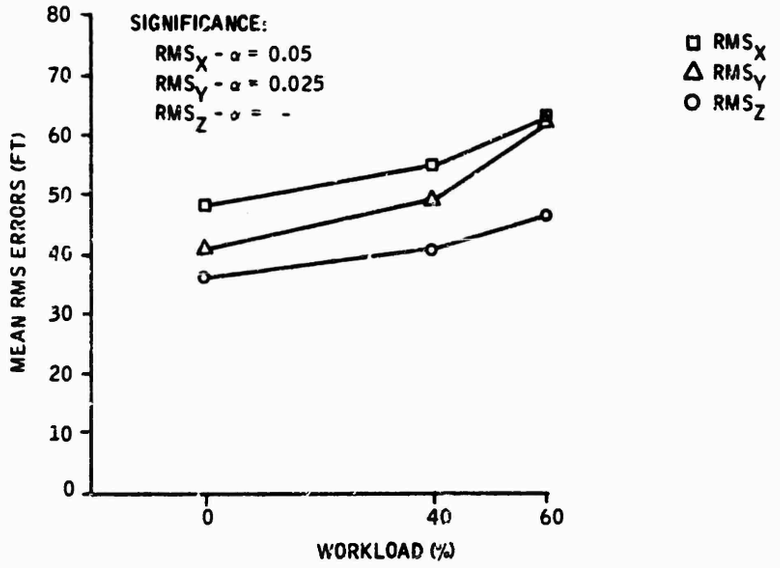

Figure 92. Phase 8 (Deceleration): RMS Errors versus Workload

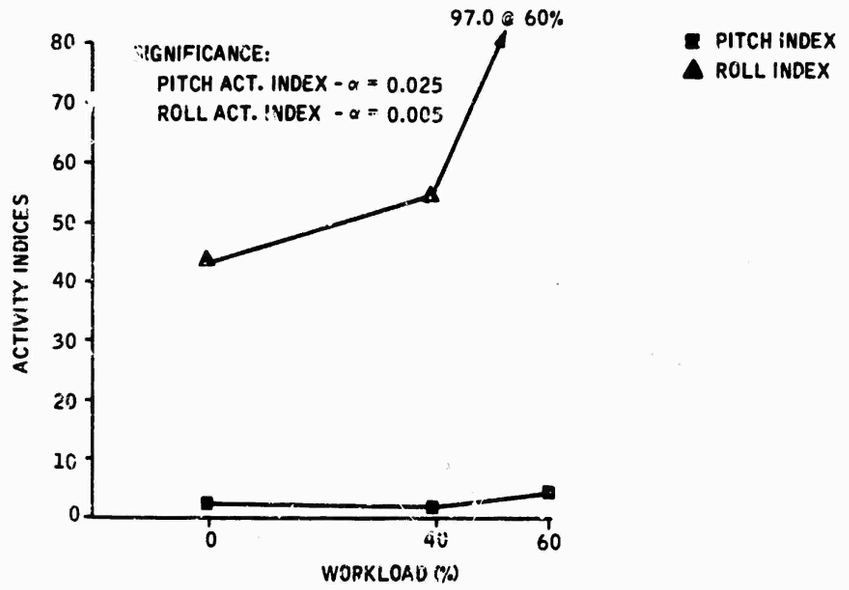

Figure 93. Phase 8 (Deceleration): Activity Indices versus Workload

6. 2 Effect of Varying Degrees of Autopilot Assistance on Pilot Performance -- As stated in the UH-1 study, certain autopilot modes were not applicable for all maneuvers. The modes tested in each phase were as indicated in the UH-1 study.

Overall mean RMS errors and activity indices for applicable autopilot modes are shown for each mission phase in Figures 94 through 107. Those parameters which were controlled by the autopilot are represented by crosstracking. These parameters were not included in the tests of statistical significane, since evaluation of pilot rather than autopilot performance was of primary concern in this study.

RMS Position Errors -- It can be observed from even-numbered Figures 94 through 106 that the level of autopilot capability generally did not have a statistically significant effect on RMS position errors, except in those axes actually being controlled by the autopilot. In other words the control of altitude by the autopilot resulted in lower RMS altitude errors but did not improve pilot performance in controlling lateral and longitudinal position.

No statistically significant performance differences were noted in control of the longitudinal position errors. The same general level of RMS_X errors was obtained for all mission phases.

The only statistically significant performance differences in control of the lateral position error occurred in the descent phase (Figure 100). In this phase the yaw SAS mode resulted in considerably higher RMS_Y errors, with the other three modes resulting in the same general level of errors. In the other six mission phases all modes yielded the same general level of performance in terms of the RMS_Y error control. No statistically significant performance differences were noted for any of these phases.

The RMS errors in altitude, as mentioned previously, were decreased considerably by either of the autopilot modes with altitude hold. The same general level of position errors was obtained for all the other autopilot modes in all phases except the climb phase. Statistically significant performance differences were obtained for this phase as a result of the considerably higher errors obtained for the heading hold mode. The other six mission phases did not yield any significant overall performance differences as a result of variation in autopilot capability.

Activity Indices -- The pitch and roll activity indices consistently resulted in significant performance differences for the varying levels of autopilot assistance. The pitch activity index was significantly affected by the autopilot level in all seven mission phases (Figures 95 through 107). The roll activity index was significantly affected by the autopilot level in five of the seven phases (phases 2, 3, 5, 6, and 7, Figures 95, 97, 101, 103. and 105). Although differences in the pitch activity indices in Figures 95 through 107 appear to be minimal because of the scaling required for the roll activity

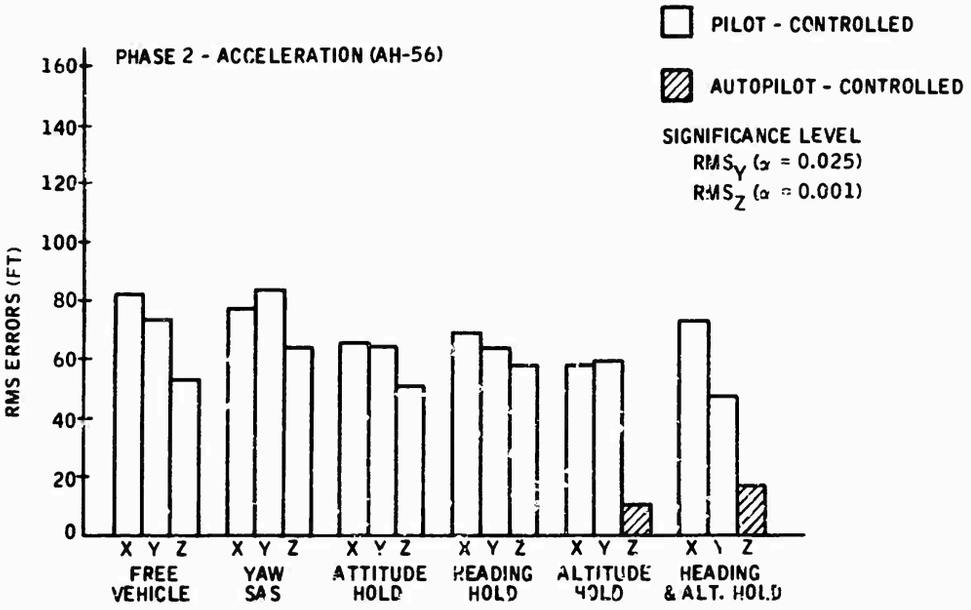

Figure 94. Phase 2 (Acceleration): RMS Errors versus Mode

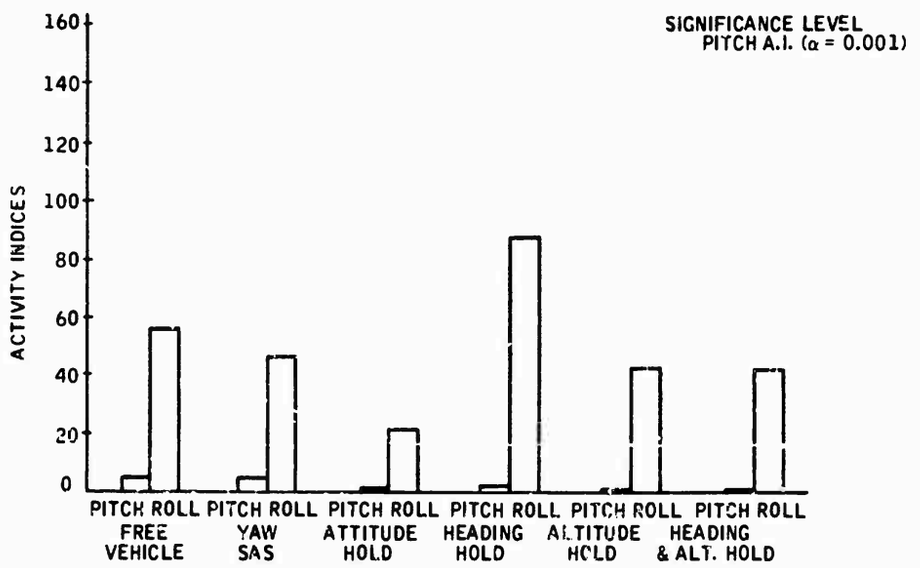

Figure 95. Phase 2 (Acceleration): Activity Indices versus Mode

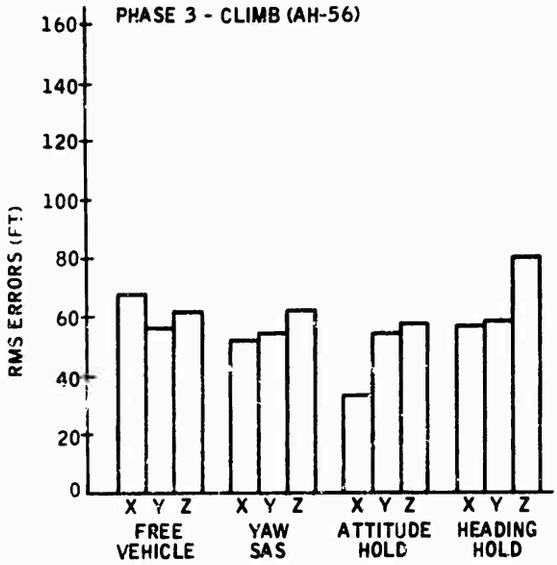

Figure 96. Phase 3 (Climb): RMS Errors versus Mode

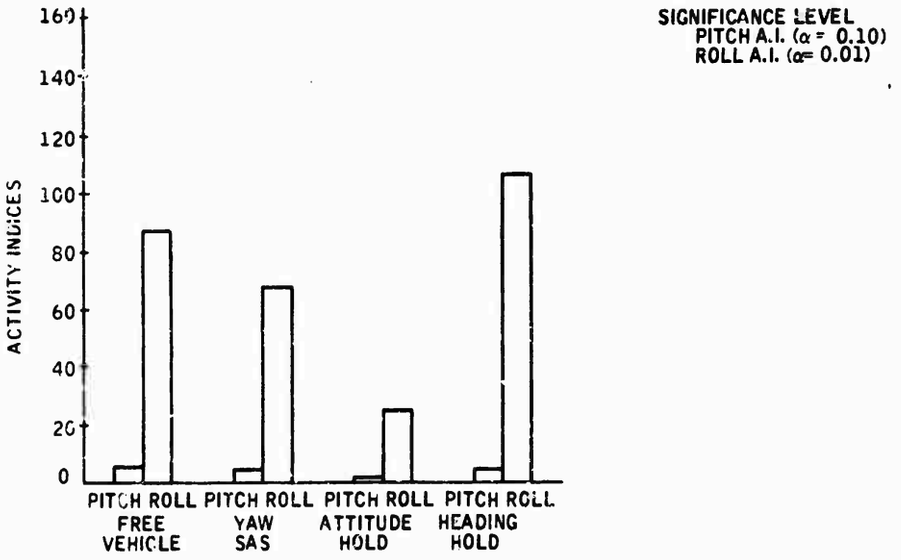

Figure 97. Phase 3 (Climb): Activity Indices versus Mode

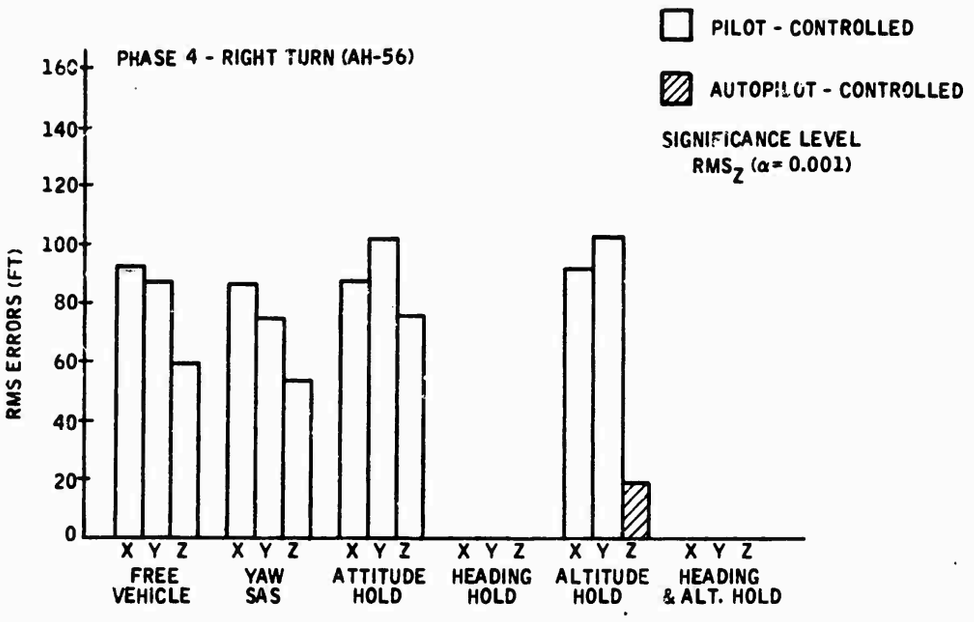

Figure 98. Phase 4 (Right Turn): RMS Errors versus Mode

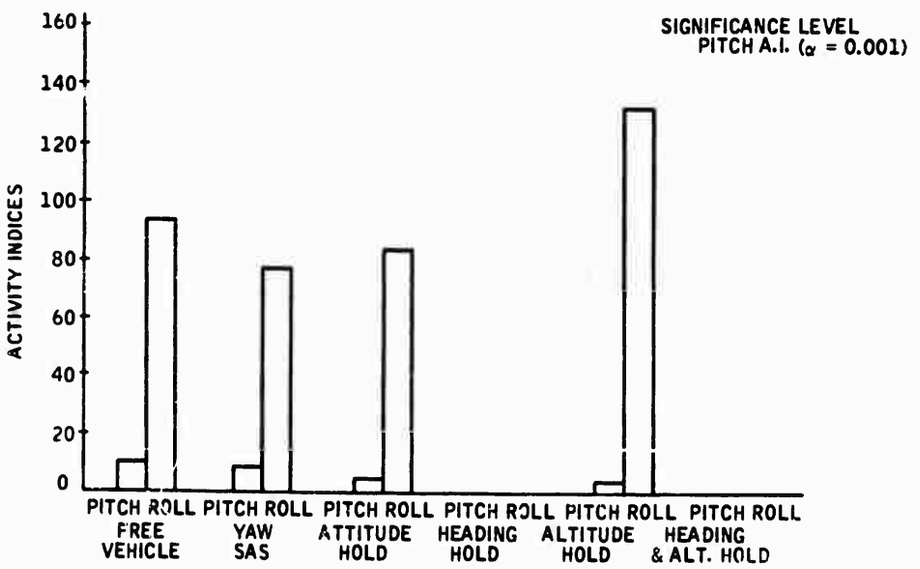

Figure 99. Phase 4 (Right Turn): Activity Indices versus Mode

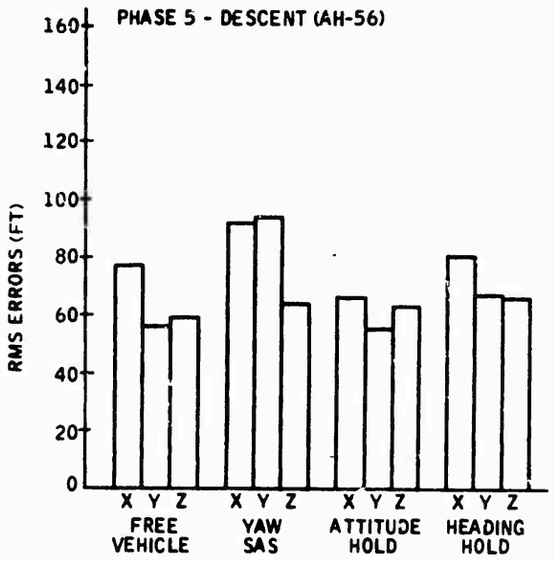

Figure 100. Phase 5 (Descent): RMS Errors versus Mode

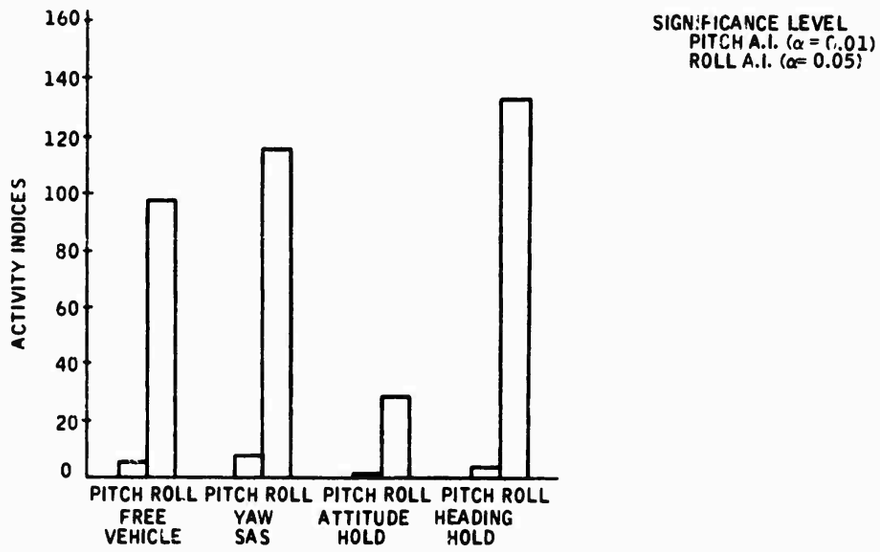

Figure 101. Phase 5 (Descent): Activity Indices versus Mode

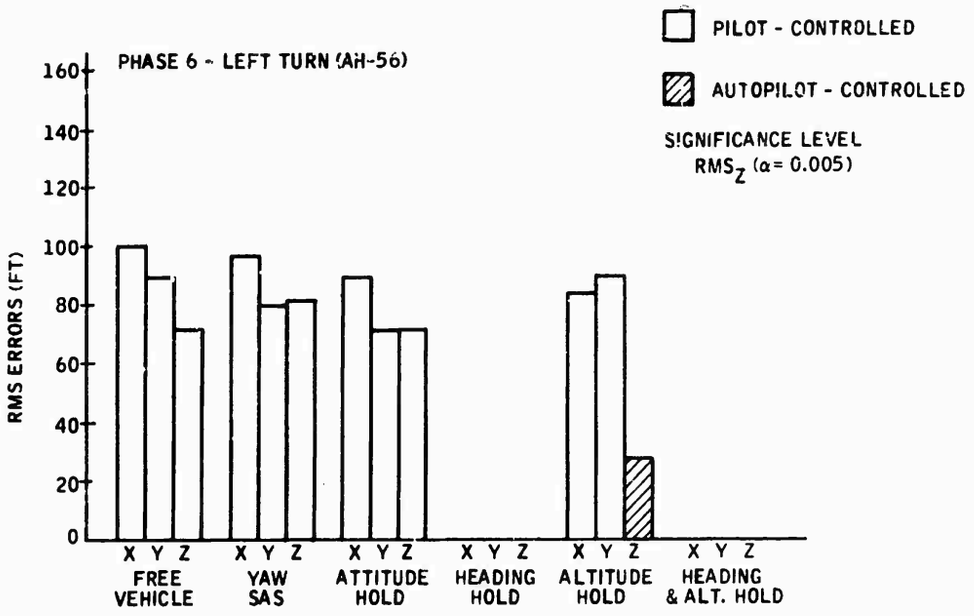

Figure 102. Phase 6 (Left Turn): RMS Errors versus Mode

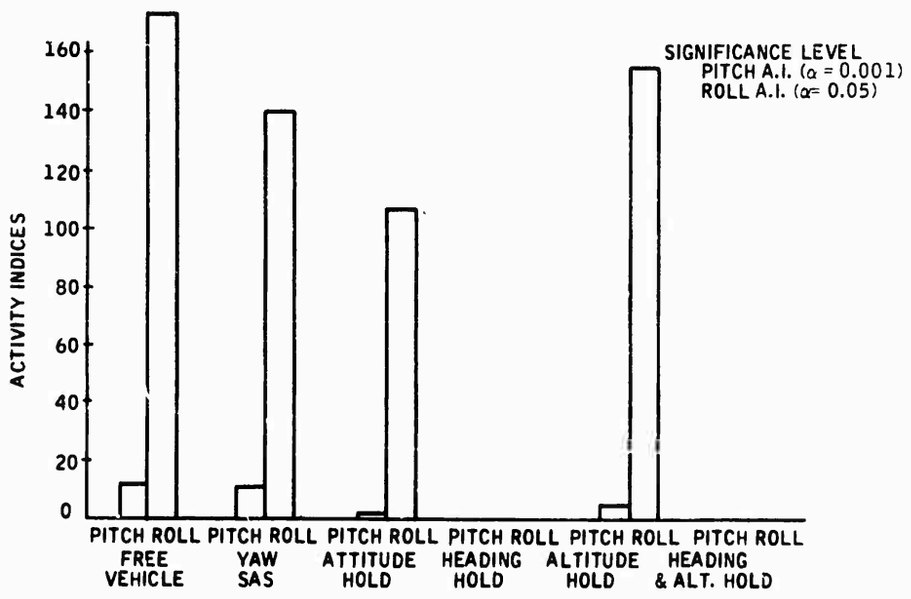

Figure 103. Phase 6 (Left Turn): Activity Indices versus Mode

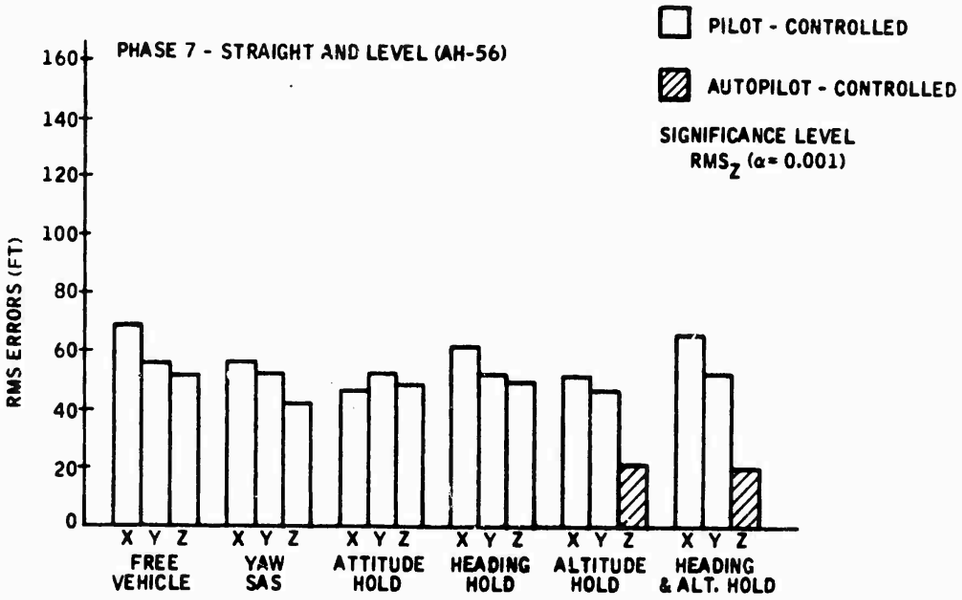

Figure 104. Phase 7 (Straight and Level): RMS Errors versus Mode

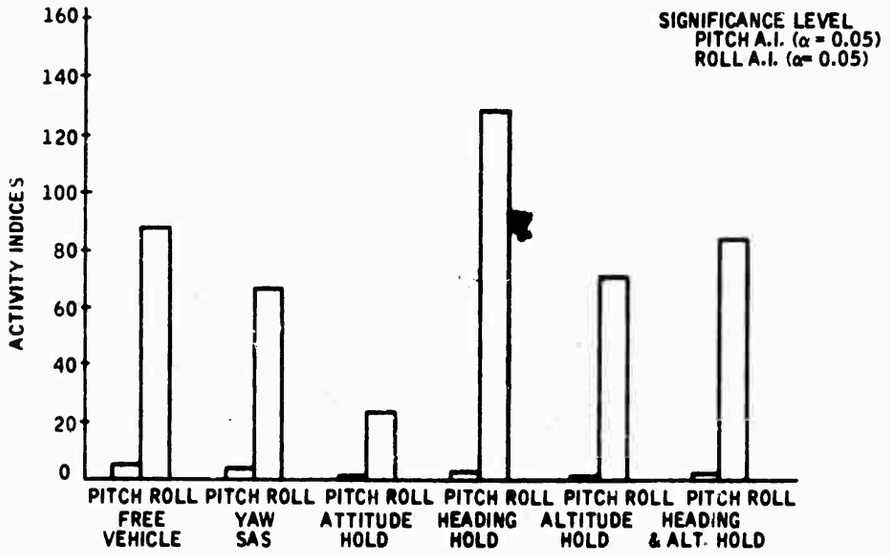

Figure 105. Phase 7 (Straight and Level): Activity Indices versus Mode

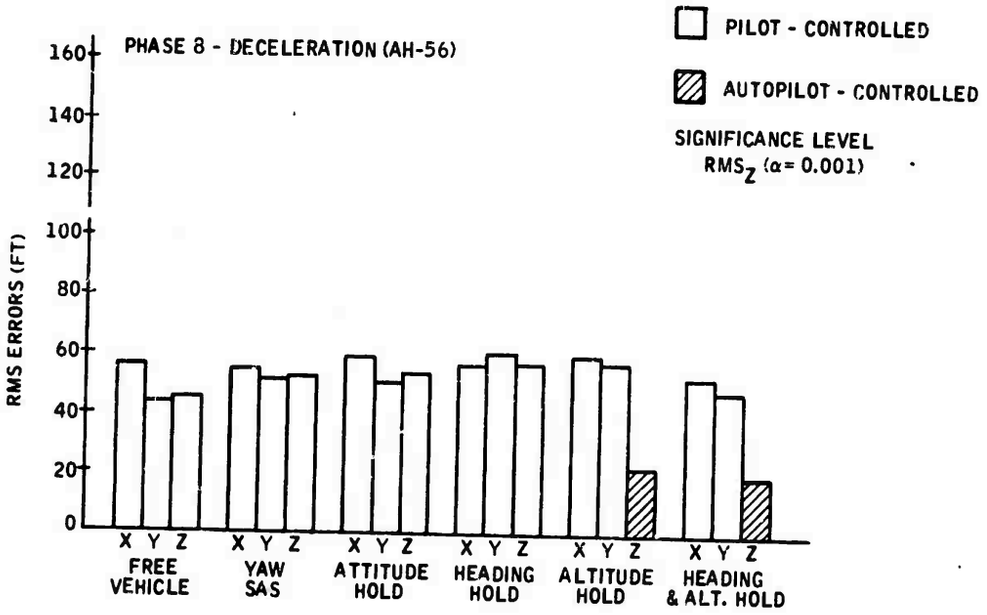

Figure 106. Phase 8 (Deceleration): RMS Errors versus Mode

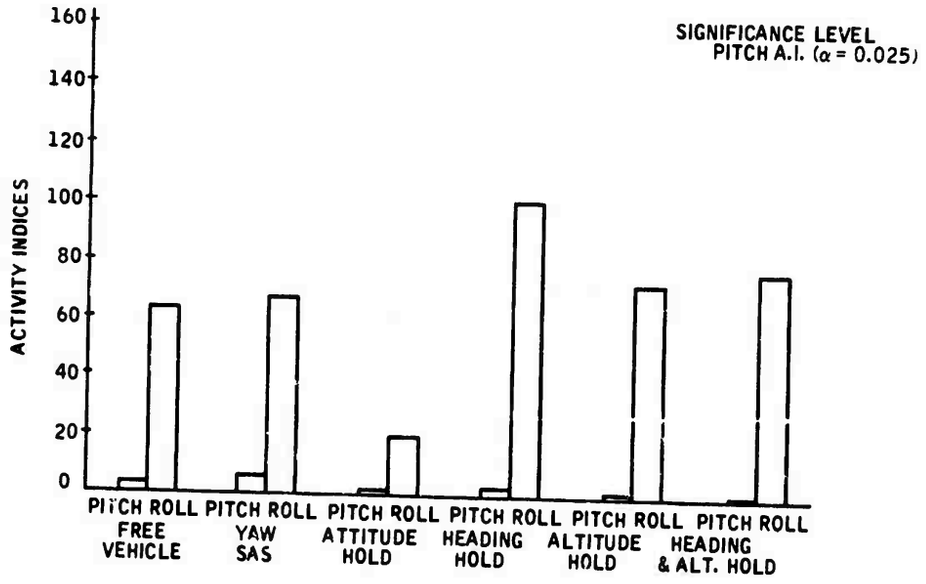

Figure 107. Phase 8 (Deceleration): Activity Indices versus Mode

indices the percentage change in the pitch index is approximately the same as that observed for the roll activity index.

The attitude hold, altitude hold, and the altitude and heading hold modes (Modes 3, 5, and 6, respectively) resulted in the best overall performance in terms of the pitch activity index (Figures 97, 101, and 103). The free vehicle resulted in poorest performance (highest activity indices). The following ranking of autopilot modes (where the best performance is denoted by the lowest number) in terms of the pitch activity index was noted quite consistently over the seven phases:

Rank	Autopilot Mode
1	Heading and altitude hold (includes attitude hold and yaw SAS)
1	Altitude hold (includes attitude hold and yaw SAS)
1	Attitude hold (includes yaw SAS)
2	Heading hold (includes attitude hold and yaw SAS)
3	Yaw SAS
4	Free vehicle

The attitude hold mode consistently resulted in the best overall performance in terms of the roll activity index, yielding the lowest activity index in six of the seven mission phases. The heading hold mode resulted in the poorest performances in terms of this index, resulting in higher roll activity indices than the free vehicle. The ranking of the various autopilot modes in terms of the roll activity index which appeared quite consistently over the seven phases was

Rank	Autopilot Mode
1	Attitude hold (includes yaw SAS)
2	Yaw SAS
3	Altitude hold (includes attitude hold and yaw SAS)
3	Heading and altitude hold (includes attitude hold and yaw SAS)
4	Free vehicle
5	Heading hold (includes attitude hold and yaw SAS)

The low ranking of the heading hold mode in terms of this index was probably due to the reaction of this mode to simulated gusts. Its response to gusts results in more control inputs than does the pilot's response when the other autopilot modes were engaged; i.e., this was the only mode which resulted in automatic correction for lateral gust effects. The heading hold mode evaluated for the UH-1 resulted in better performance in terms of the activity index. This can be explained by the greater effect of the simulated turbulence on the AH-56. Although the same gust loading (10 knots) as that used in the UH-1 autopilot study (Section V) was used in this study, the difference in the nominal cruise speeds of the two aircraft simulated resulted in varying turbulence effects. The relative effect of the turbulence on the two aircraft is indicated by the gust level to airspeed ratio, with an increase reflecting an increase in the gust effect. The ratio of the 10-knot gust level to the AH-56 nominal cruise spped of 60 knots was 50% higher than the corresponding ratio for the UH-1 with its cruise speed of 88 knots.

Summary -- Varying the levels of autopilot assistance had a significant effect on overall subject performance in terms of the activity indices. The attitude hold, altitude hold, and heading and altitude hold modes resulted in the lowest pitch activity indices and the attitude hold mode in the lowest roll activity indices. Since the attitude hold mode yielded better performance in terms of both indices, it appeared that this mode would be optimal for overall performance in terms of aircraft response stability and the extent of control inputs required to maintain aircraft position.

Variation of the autopilot capability did not significantly affect the level of control precision in terms of the RMS position errors averaged over the three workloads. The same general level of overall performance was obtained for all modes. It was expected, however, that more significant performance differences in terms of position errors would occur at the higher workload levels. The following subsection of this report presents the analysis of autopilot modes by workload.

6.3 Effect of Autopilot Mode by Workload Interaction on Performance -- Figures 108 through 121 present RMS longitudinal errors and pitch activity indices by workload for each of the mission phases. RMS lateral errors and roll activity indices by workload are presented in Figures 122 through 135. The RMS errors in altitude are shown by workload and mission phase in Figures 136 through 142.

RMS Position Errors -- Statistically significant differences in RMS_X errors attributable to the autopilot mode by workload interaction were found for three of the seven mission phases. The significance noted for the descent phase (Figure 114) results from the different relationships between workload for the four autopilot modes. For the free vehicle, yaw SAS, and attitude hold modes the 40% workload results in lower RMS_X errors than no workload. For the heading hold mode this relationship reversed. Also the 70% workload for the heading hold mode results in lower RMS_X errors than

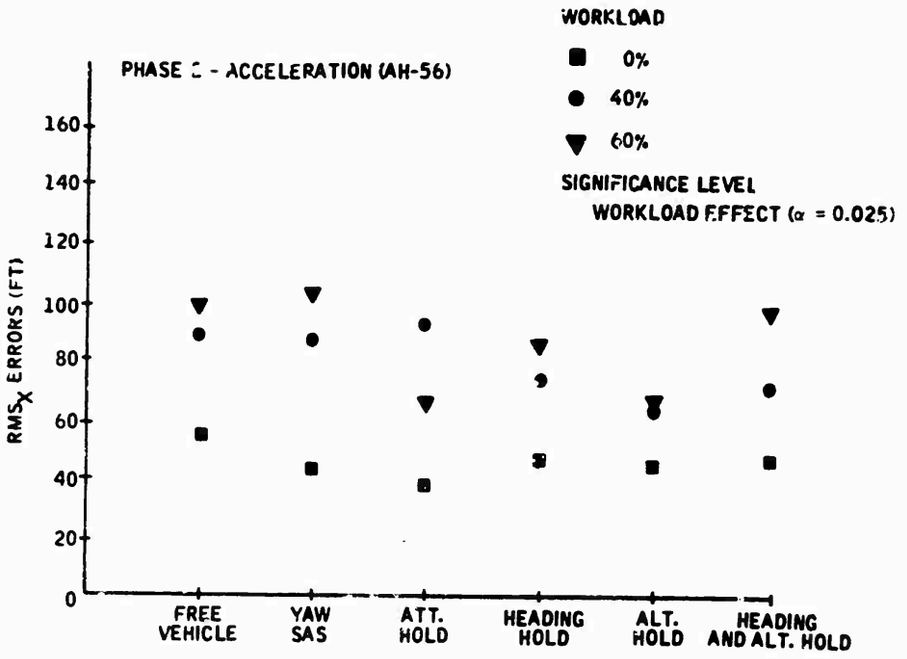

Figure 108. Phase 2 (Acceleration): RMS$_X$ Error versus Mode by Workload

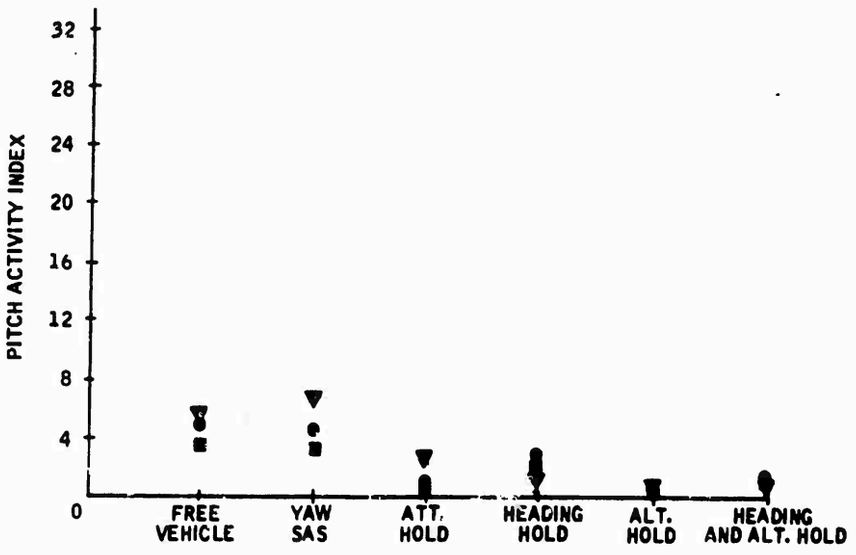

Figure 109. Phase 2 (Acceleration): Pitch Activity Index versus Mode by Workload

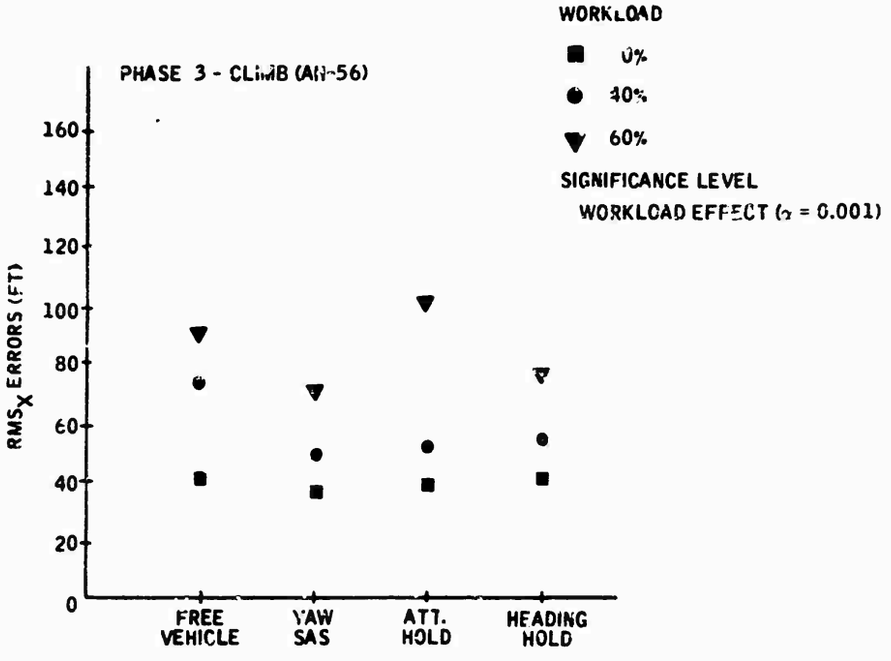

Figure 110. Phase 3 (Climb): RMS$_X$ Error versus Mode by Workload

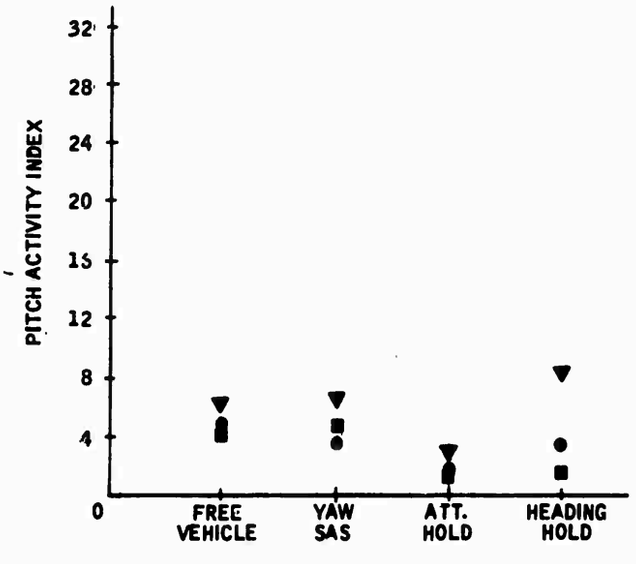

Figure 111. Phase 3 (Climb): Pitch Activity Index versus Mode by Workload

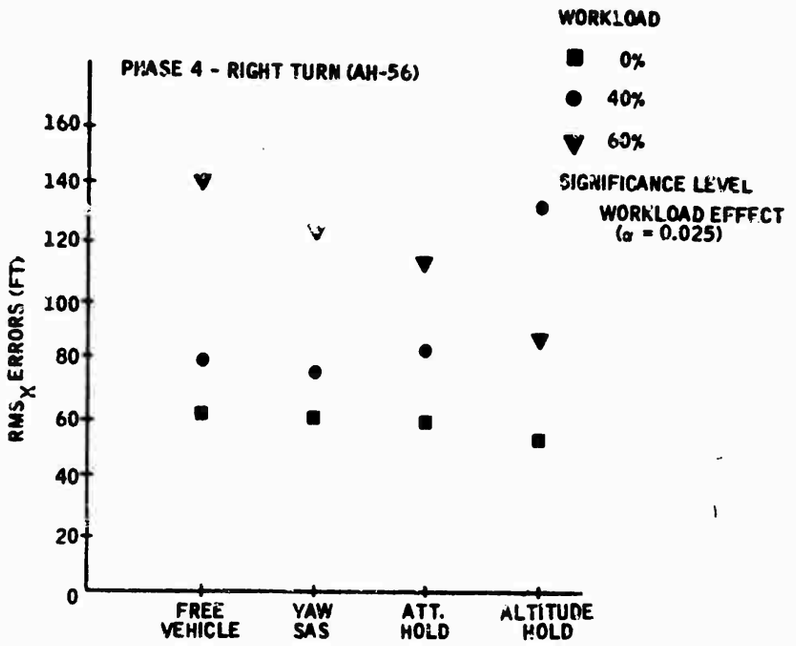

Figure 112. Phase 4 (Right Turn): RMS$_X$ Error versus Mode by Workload

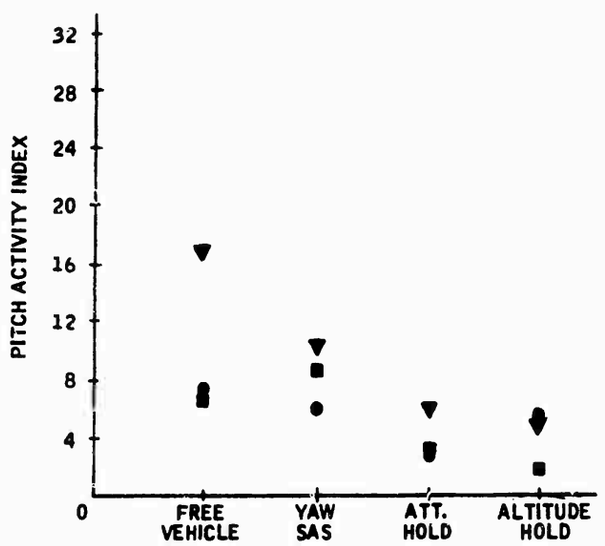

Figure 113. Phase 4 (Right Turn): Pitch Activity Index versus Mode by Workload

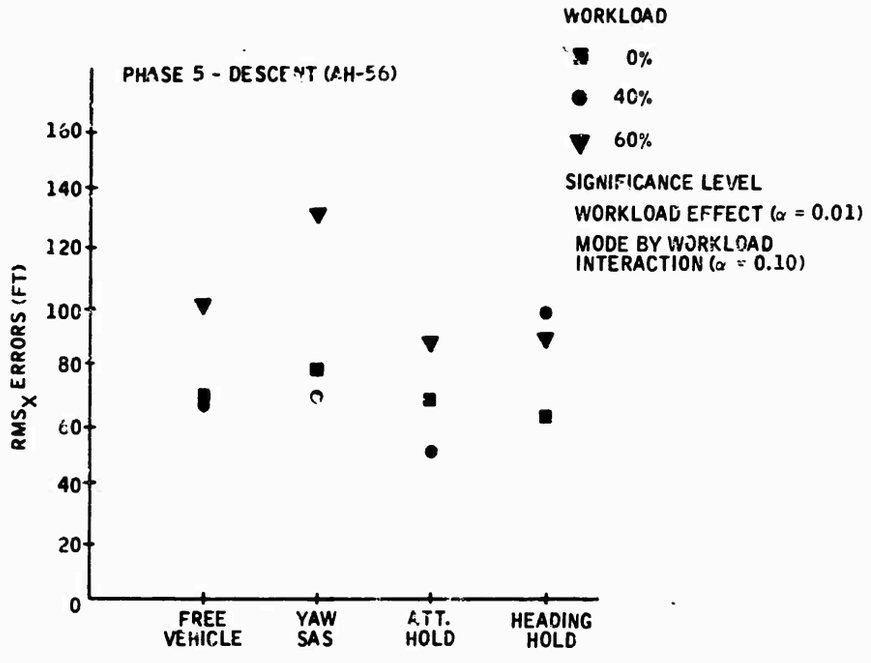

Figure 114. Phase 5 (Descent): RMS_X Error versus Mode by Workload

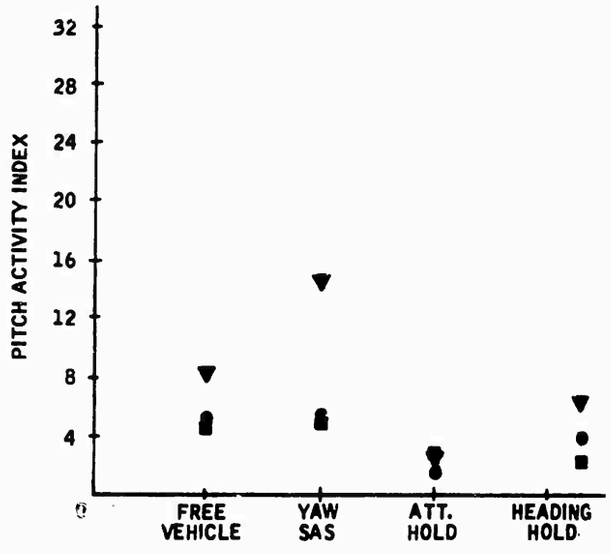

Figure 115. Phase 5 (Descent): Pitch Activity Index versus Mode by Workload

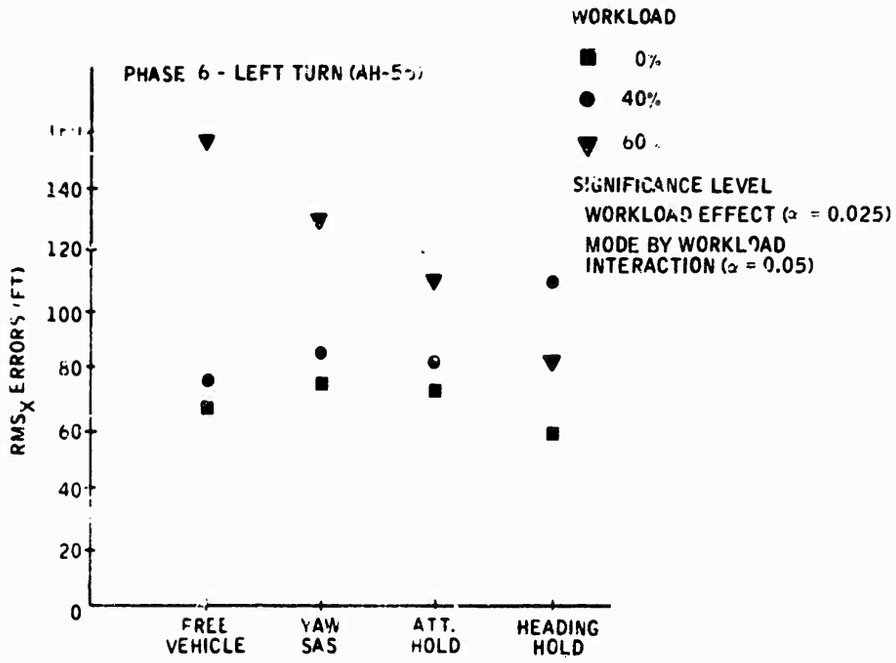

Figure 116. Phase 6 (Left Turn): RMS_X Error versus Mode by Workload

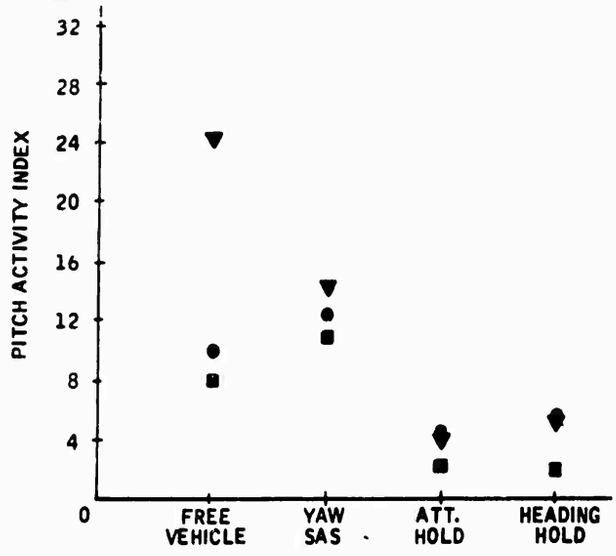

Figure 117. Phase 6 (Left Turn): Pitch Activity Index versus Mode by Workload

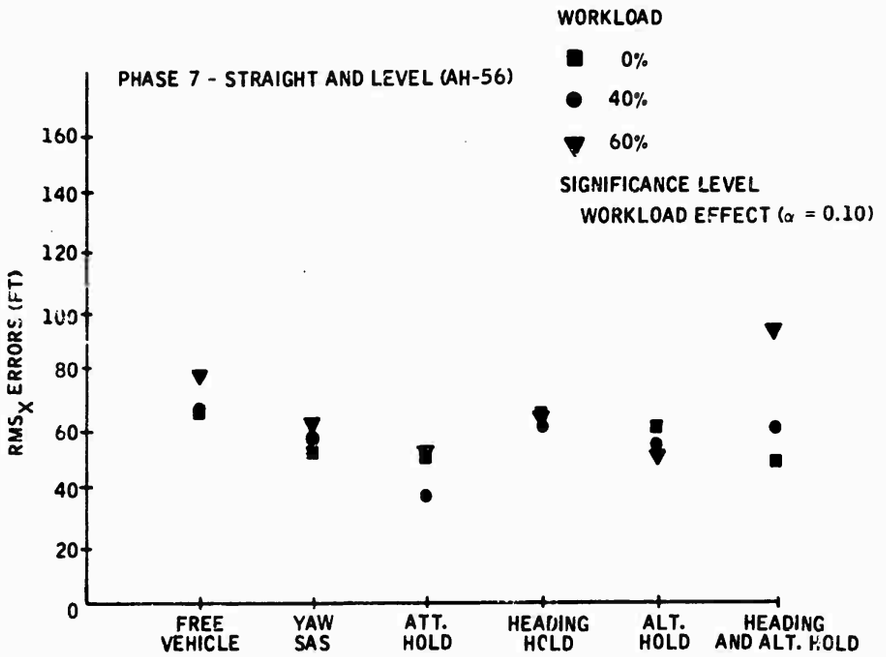

Figure 118. Phase 7 (Straight and Level): RMS$_X$ Error versus Mode by Workload

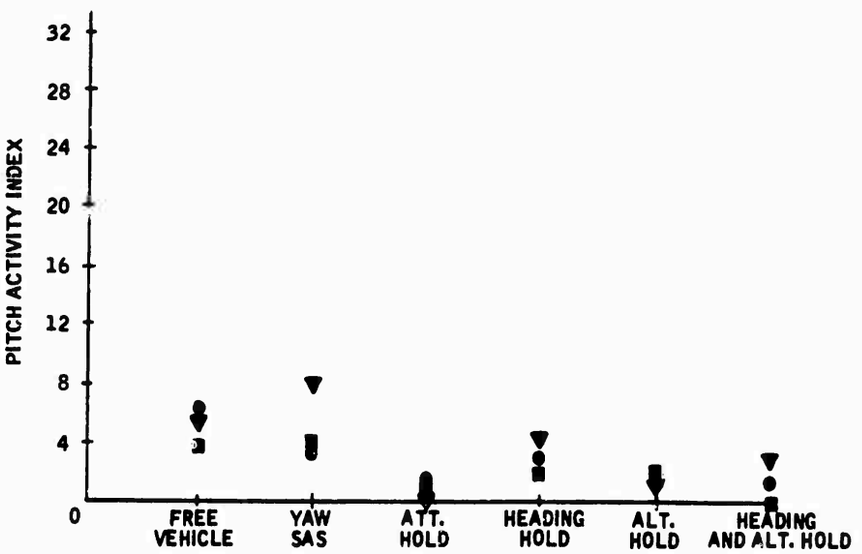

Figure 119. Phase 7 (Straight and Level): Pitch Activity Index versus Mode by Workload

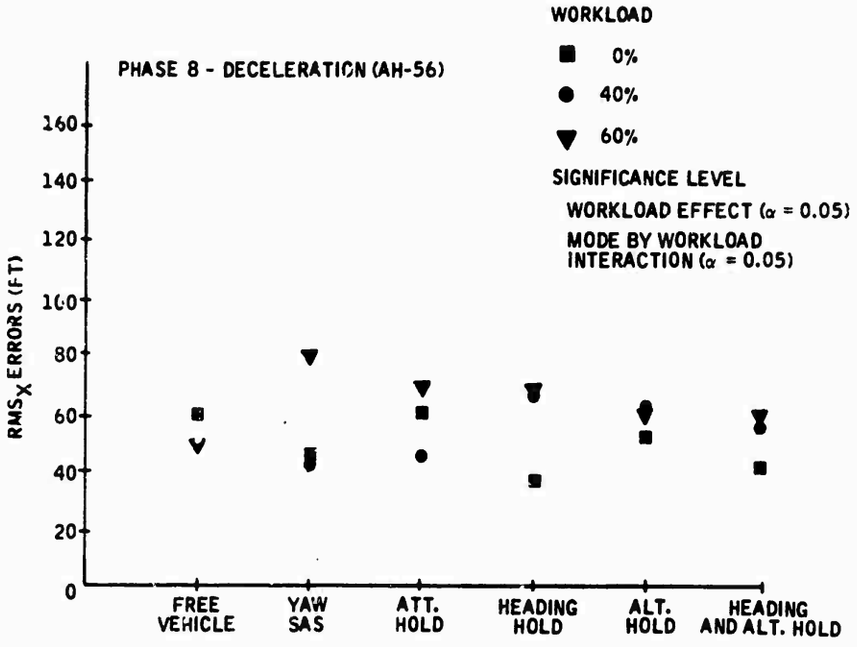

Figure 120. Phase 8 (Deceleration): RMS_X Error versus Mode by Workload

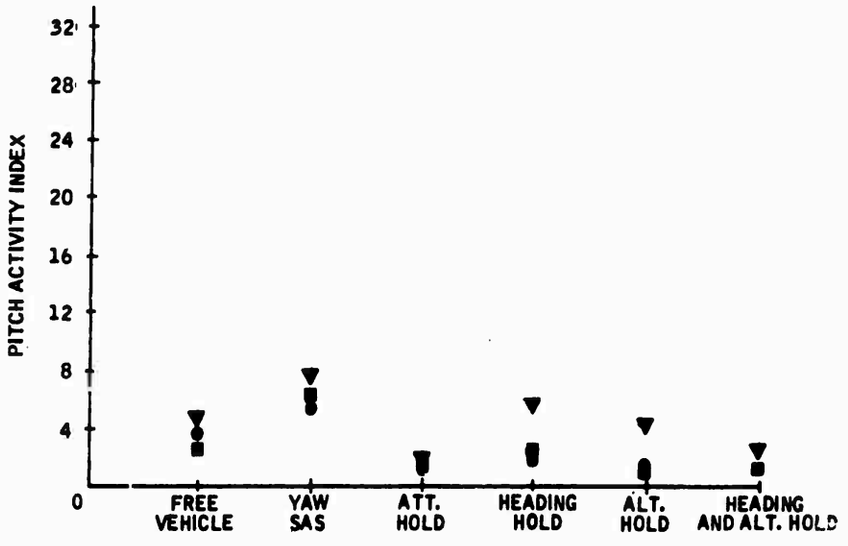

Figure 121. Phase 8 (Deceleration): Pitch Activity Index versus Mode by Workload

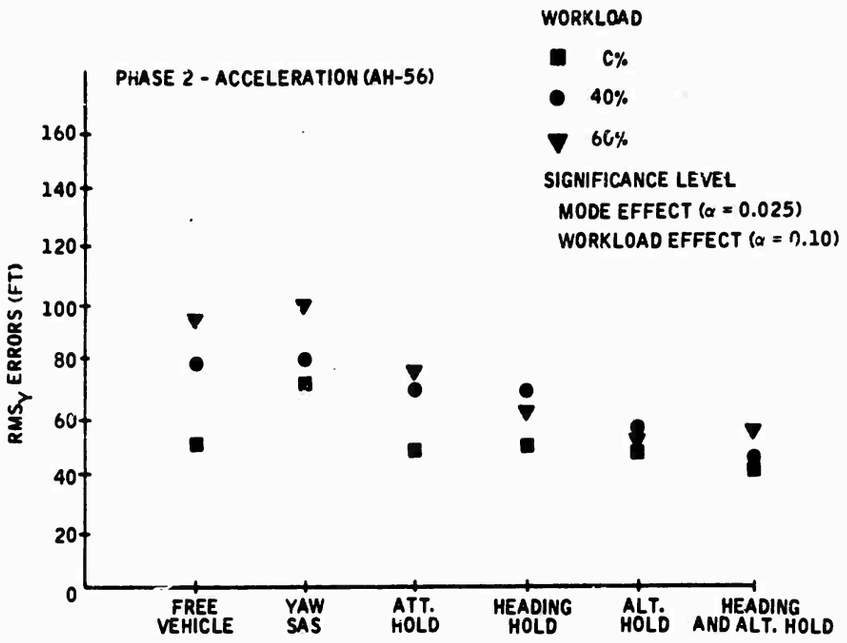

Figure 122. Phase 2 (Acceleration): RMS$_Y$ Errors versus Mode by Workload

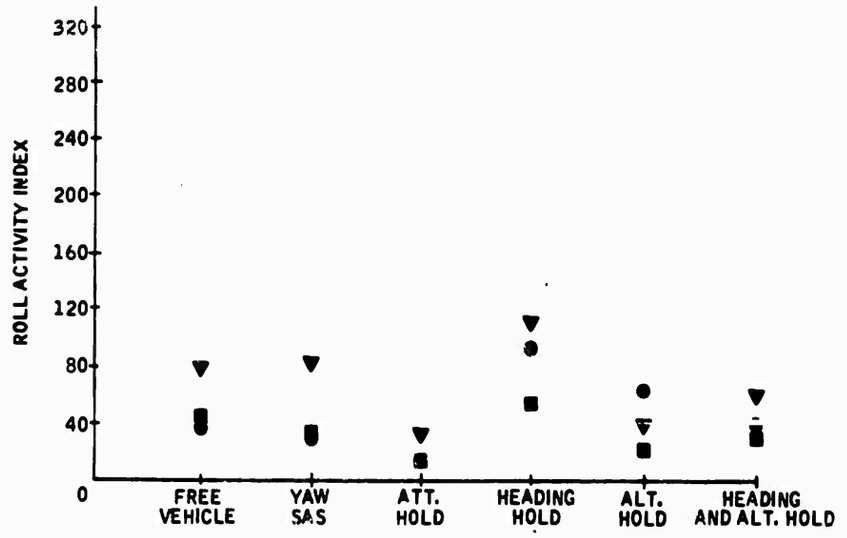

Figure 123. Phase 2 (Acceleration): Roll Activity Index versus Mode by Workload

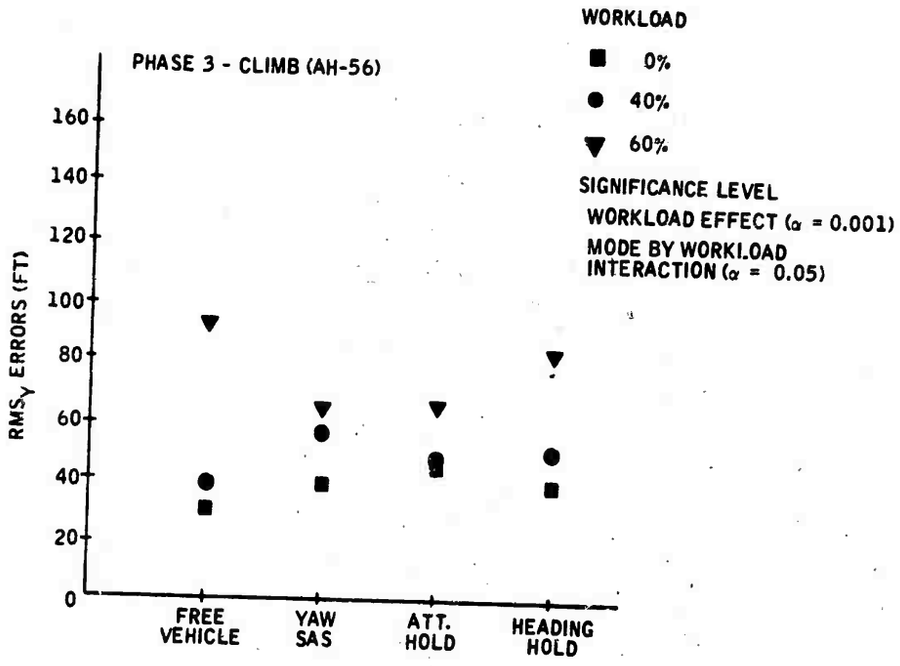

Figure 124. Phase 3 (Climb): RMS$_Y$ Errors versus Mode by Workload

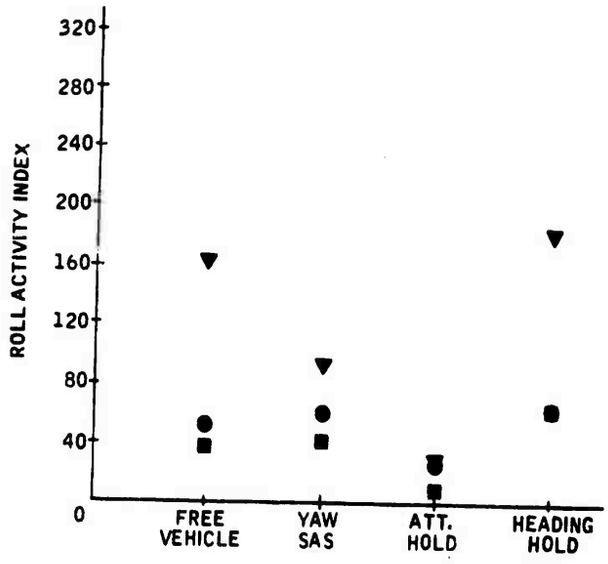

Figure 125. Phase 3 (Climb): Roll Activity Index versus Mode by Workload

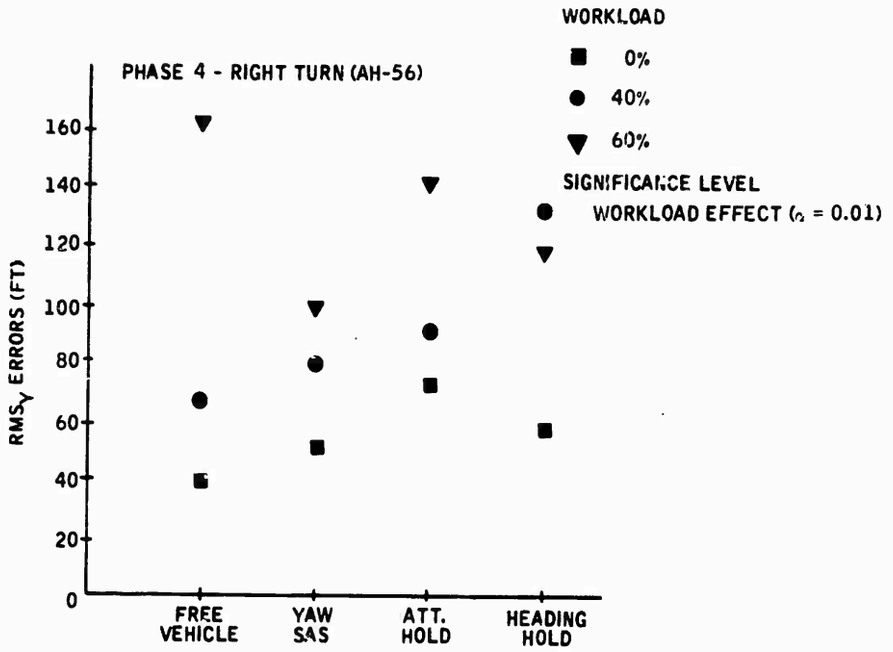

Figure 126. Phase 4 (Right Turn): RMS$_Y$ Errors versus Mode by Workload

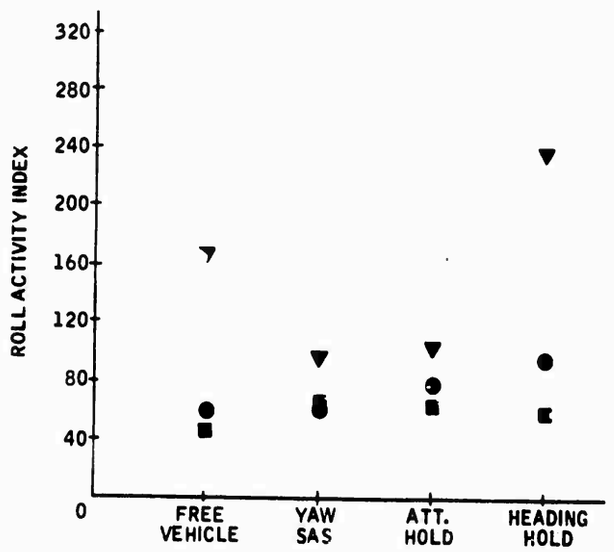

Figure 127. Phase 4 (Right Turn): Roll Activity Index versus Mode by Workload

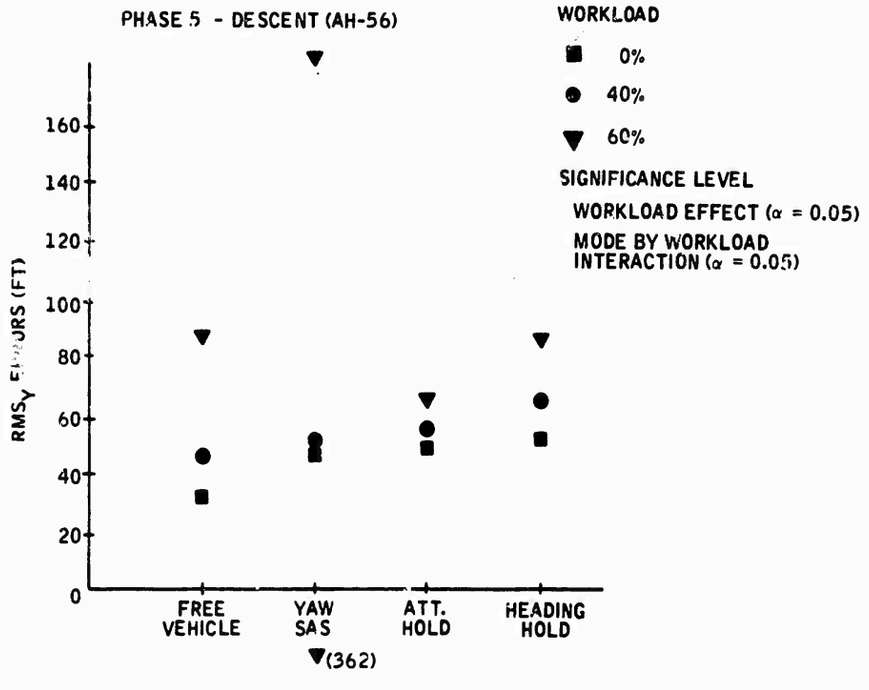

Figure 128. Phase 5 (Descent): RMS$_Y$ Errors versus Mode by Workload

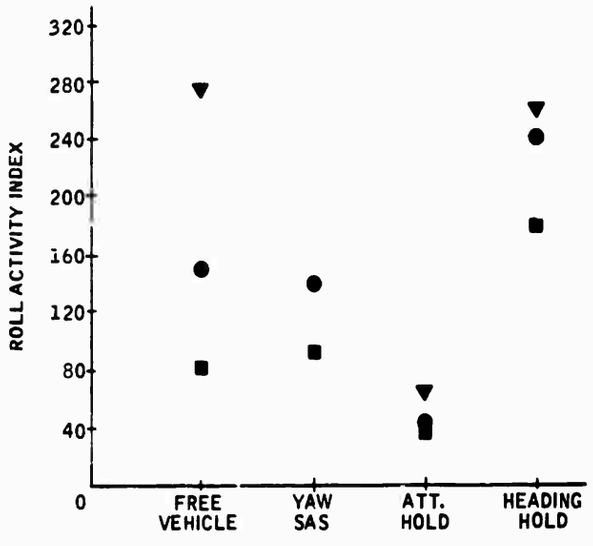

Figure 129. Phase 5 (Descent): Roll Activity Index versus Mode by Workload

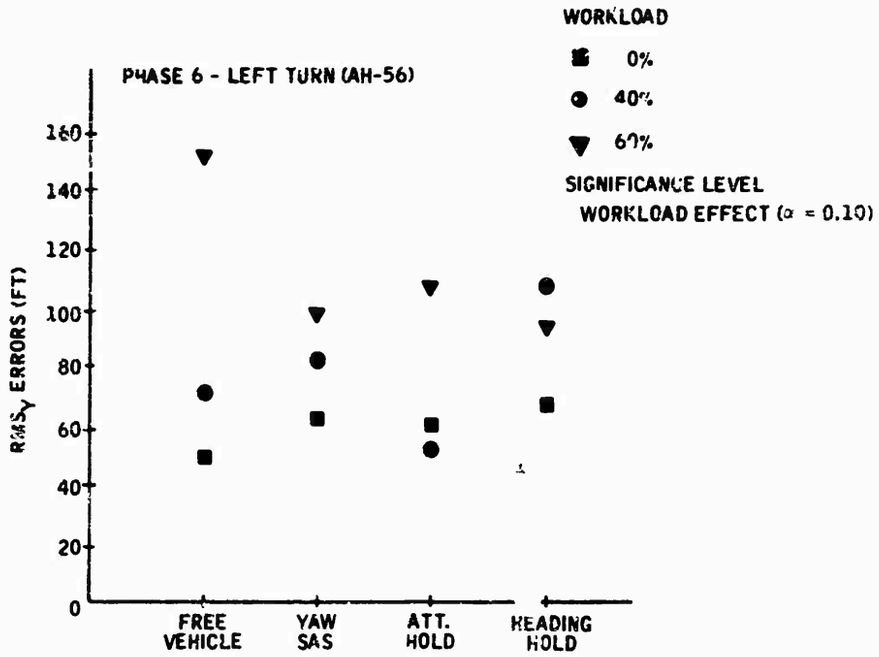

Figure 130. Phase 6 (Left Turn): RMS_Y Errors versus Mode by Workload

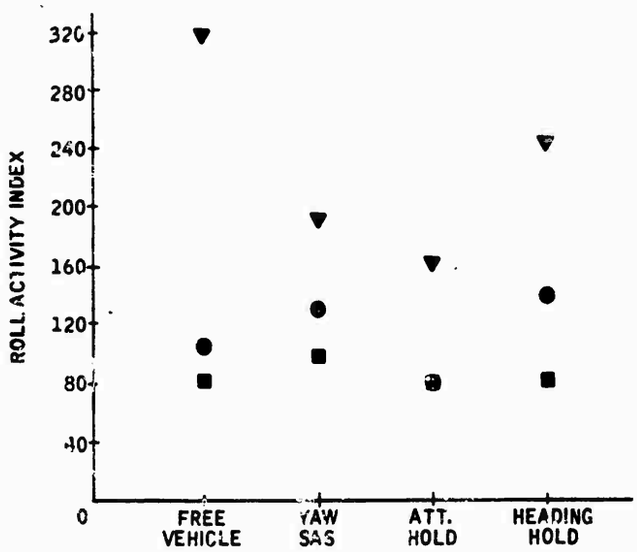

Figure 131. Phase 6 (Left Turn): Roll Activity Index versus Mode by Workload

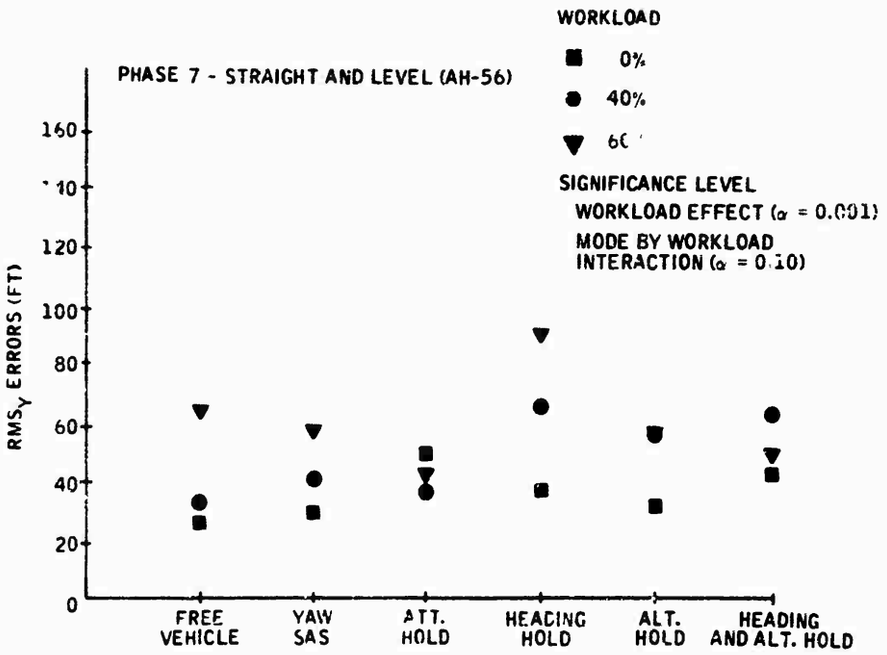

Figure 132. Phase 7 (Straight and Level): RMS$_Y$ Errors versus Mode by Workload

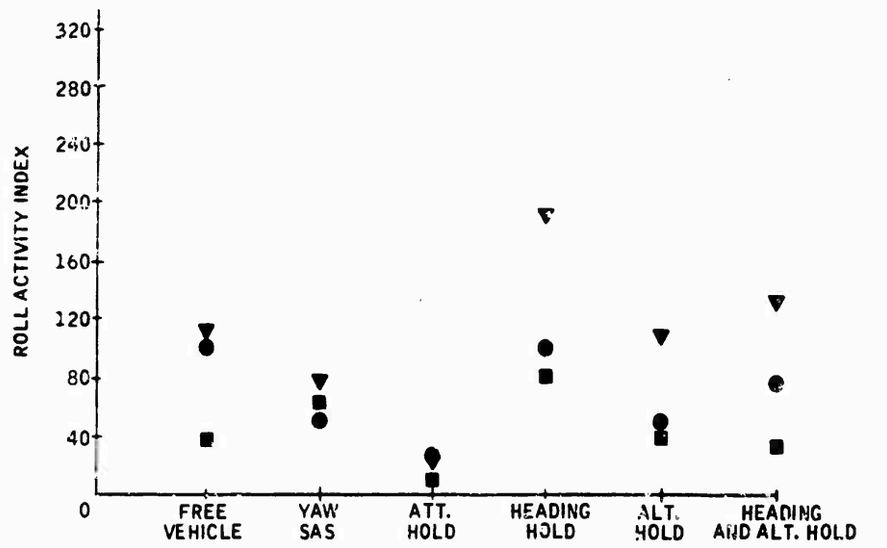

Figure 133. Phase 7 (Straight and Level): Roll Activity Index versus Mode by Workload

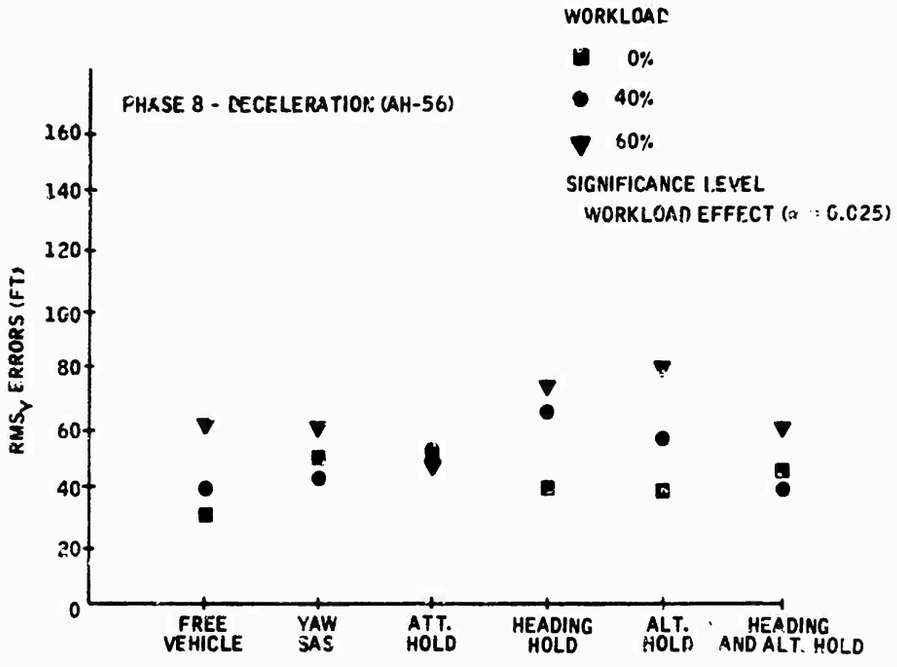

Figure 134. Phase 8 (Deceleration): RMS$_Y$ Errors versus Mode by Workload

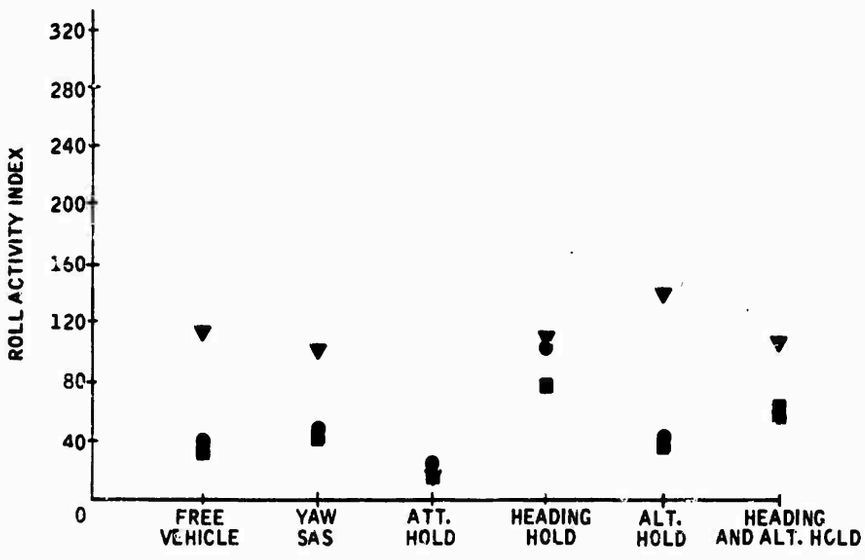

Figure 135. Phase 8 (Deceleration): Roll Activity Index versus Mode by Workload

the 40% workload. The statistical significance of the performance differences for the left-turn phase (Figure 116) appears to be due to the different relationship between workloads for the altitude hold mode. Unlike the other three modes this mode resulted in higher RMS_Y errors for the 40% than for the 70% workload. The statistical significance noted for the deceleration phase (Figure 120) also appears to result from differences in the relationship between workloads for the various autopilot modes. The lowest RMS_Y errors were obtained under the no-workload condition for only three of the modes. For two of the other three the 40% workload condition results in lowest errors and for the other mode the 60% level results in lowest errors.

Although the other four mission phases (Figures 108, 110, 112, and 120) did not result in statistically significant differences in RMS_X errors, a consistent trend was noted for the 60% workload. In five of the seven mission phases the attitude and altitude hold modes resulted in the best performance at this workload level.

The following ranking of the modes in terms of the RMS_X errors was observed quite consistently over the seven phases for the 60% workload:

Rank	Autopilot Mode
1	Altitude hold (includes attitude hold and yaw SAS)
1	Attitude hold (includes yaw SAS)
2	Heading hold (includes attitude hold and yaw SAS)
2	Heading and altitude hold (includes attitude hold and yaw SAS)
3	Yaw SAS
3	Free vehicle

No consistent trends were noted for the 40% workload level. The no-workload condition resulted in the same general level of RMS_X errors.

Statistically significant differences in RMS_Y errors attributable to the various combinations of autopilot mode and workload were found for three of the seven mission phases. The statistical significance noted for the climb phase appears to result from the relatively higher percentage increase in RMS_Y errors noted for the 60% workload in the free-vehicle mode (Figure 124). The percentage increase in RMS_Y errors for the corresponding workload increase from 40% to 60% was 125% for the free vehicle, while the highest increase obtained for any of the other three autopilot modes was 60%. This same result was obtained for the left-turn phase (Figure 130) and appears to explain the significance of those RMS_Y differences. There is also wide variation in RMS_Y errors for the 40% workload in the left-turn phase, with an

approximate 60-ft difference between errors for the attitude and altitude hold modes. The statistical significance noted for the descent phase (Figure 128) apparently results from the extremely high increase in RMS$_Y$ errors noted for the 60% workload in the yaw SAS mode. The percentage increase in RMS$_Y$ errors associated with the workload increase from 40% to 60% was 260% for this mode, compared to the 100% which was the highest increase noted for any of the other modes.

Although differences in RMS$_Y$ noted for the other four phases (Figures 122, 126, 132, and 134) were not statistically significant, consistent relationships between autopilot modes at the specific workload levels were noted for all seven phases. In six of the seven phases the free vehicle resulted in the best performance under the no-workload and 40% workload conditions. On the contrary, in five of the seven phases the free vehicle resulted in the poorest performance at the 60% workload level, with the attitude hold, altitude hold, and heading and altitude hold modes resulting in the best performance. The ranking of modes in terms of RMS$_Y$ errors at this 60% workload condition which was noted quite consistently was

Rank	Autopilot Mode
1	Attitude hold (includes yaw SAS)
1	Heading and altitude hold (includes attitude hold and yaw SAS)
1	Altitude hold (includes attitude hold and yas SAS)
2	Heading hold (includes attitude hold and yaw SAS)
2	Yaw SAS
3	Free vehicle

It appears that the levels of autopilot tested significantly improved performance in terms of RMS lateral errors at the highest workload level.

The RMS altitude errors (Figures 136 through 144) were consistently and significantly lower for those autopilot modes which resulted in autopilot control of altitude (Modes 5 and 6). Otherwise, the differences in RMS altitude errors attributable to the interaction of autopilot mode and workload were not statistically significant. However, consistent relationships between autopilot modes were noted across mission phases for each of the workload levels. At the no-workload condition it was obvious that increasing the autopilot capability did not decrease the RMS$_Z$ error (except in those modes where the autopilot controlled the altitude). The free vehicle resulted in the best in five of seven mission phases under this no-workload condition. At the 40% workload level the yaw SAS and attitude hold modes resulted in the best performance. At the highest workload (60%) the attitude hold mode

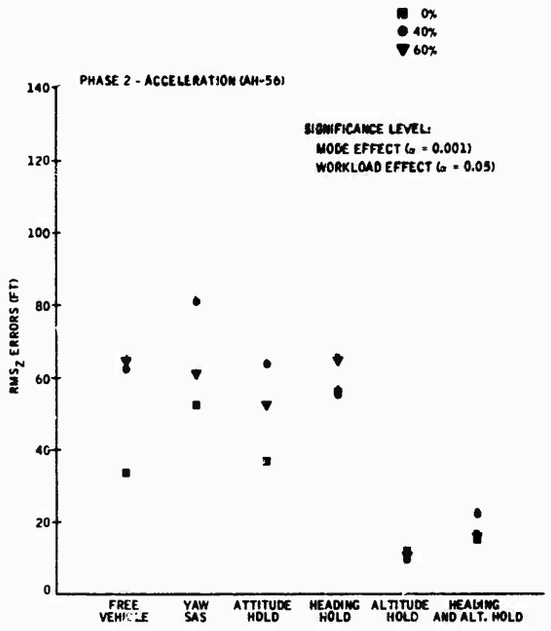

Figure 136. Phase 2 (Acceleration): RMS$_Z$ Errors versus Mode by Workload

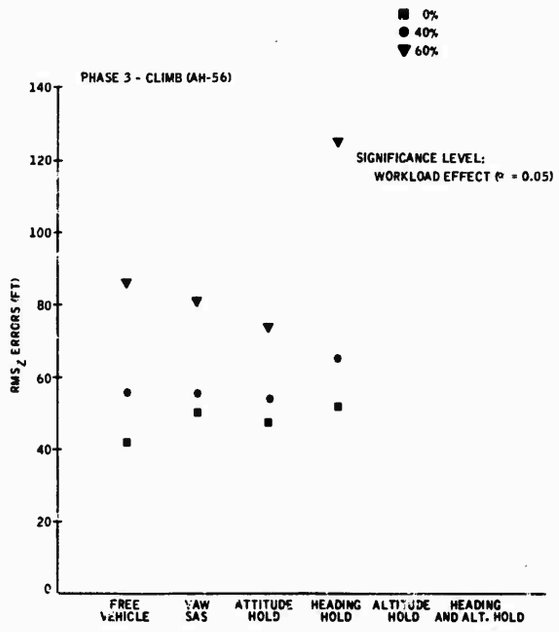

Figure 137. Phase 3 (Climb): RMS$_Z$ Errors versus Mode by Workload

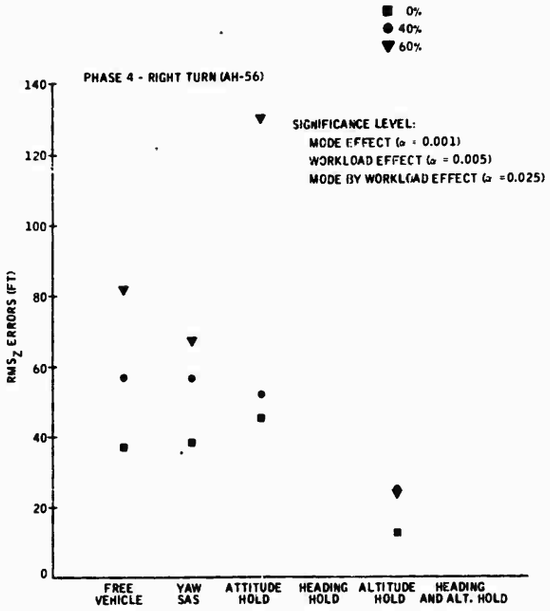

Figure 138. Phase 4 (Right Turn): RMS_Z Errors versus Mode by Workload

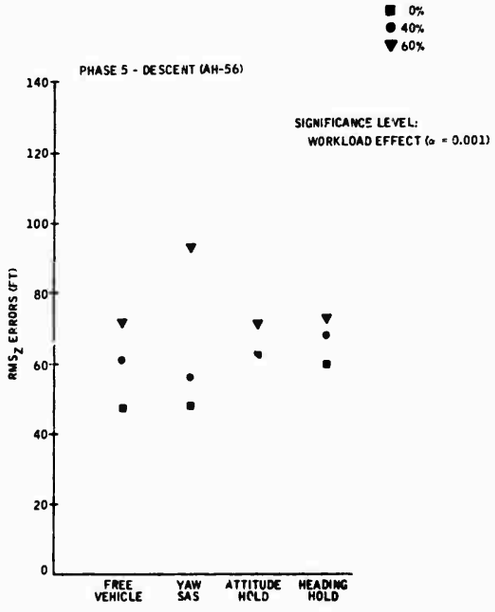

Figure 139. Phase 5 (Descent): RMS_Z Errors versus Mode by Workload

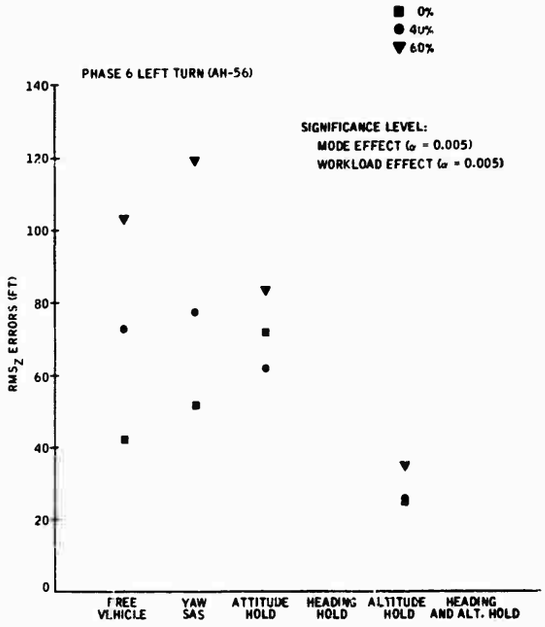

Figure 140. Phase 6 (Left Turn): RMS_Z Errors versus Mode by Workload

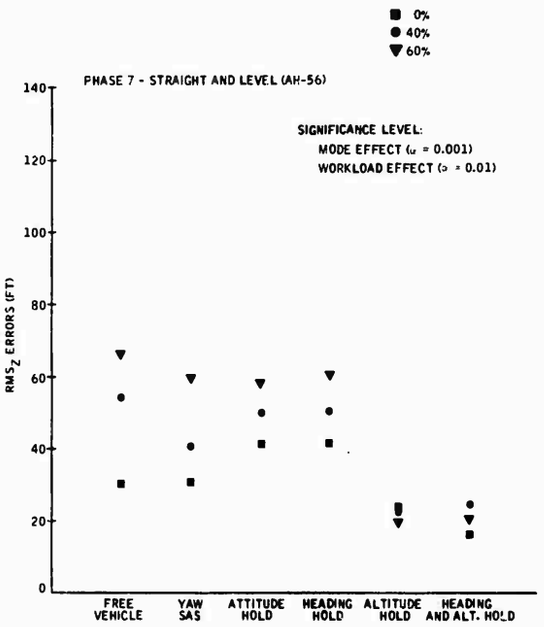

Figure 141. Phase 7 (Straight and Level): RMS_Z Errors versus Mode by Workload

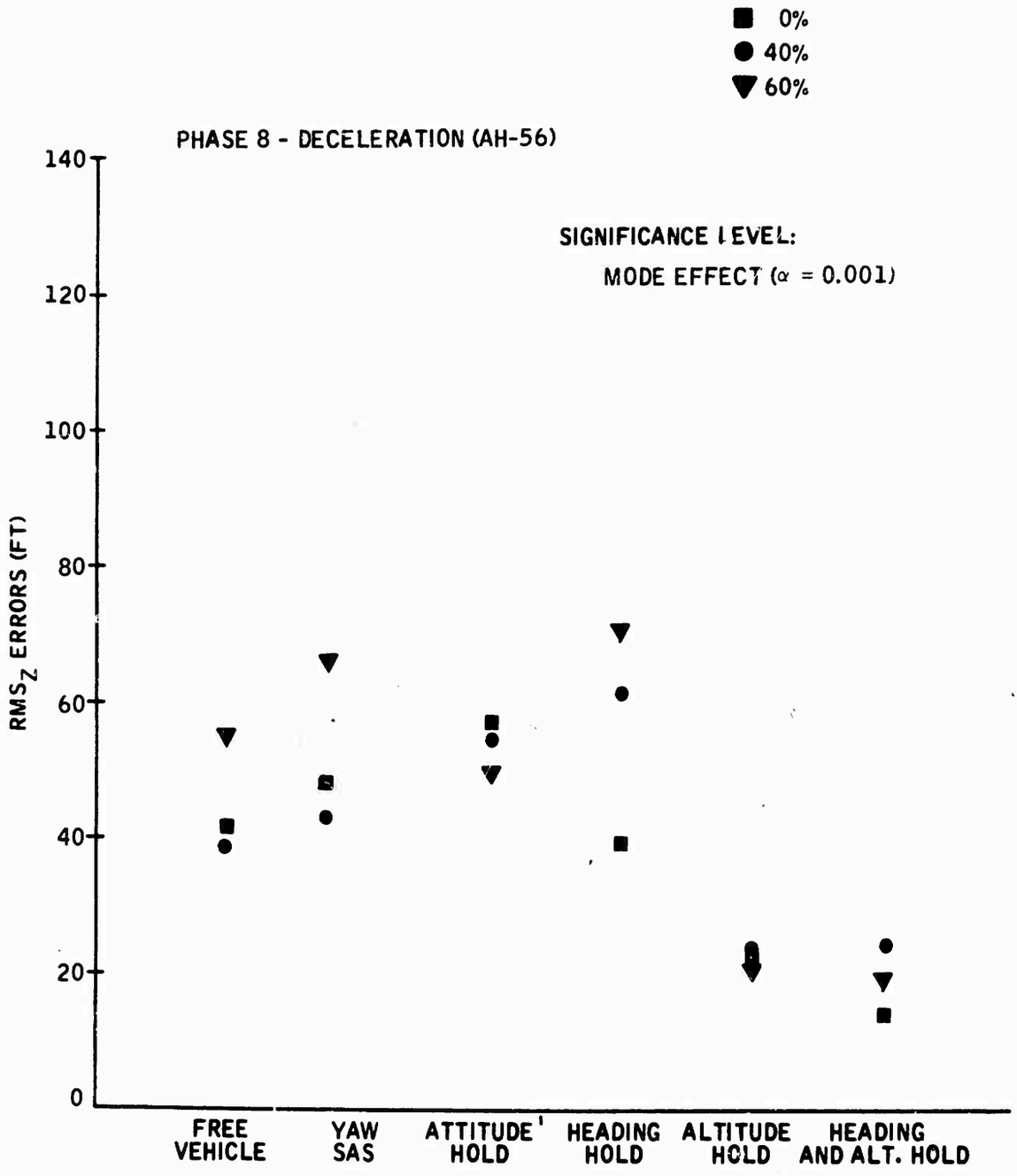

Figure 142. Phase 8 (Deceleration): RMS_Z Errors versus Mode by Workload

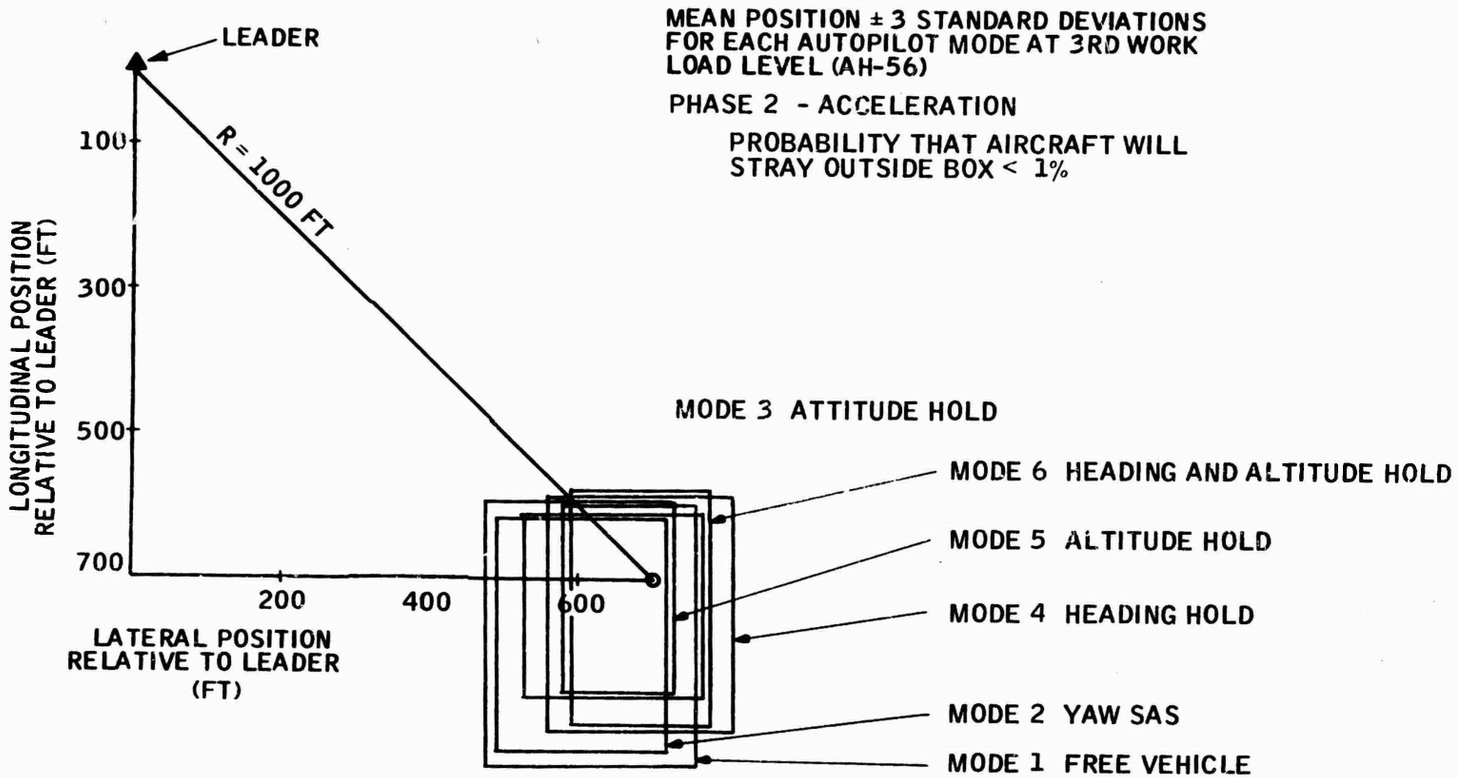

Figure 143. Phase 2 (Acceleration): Lateral and Longitudinal Position Error by Mode

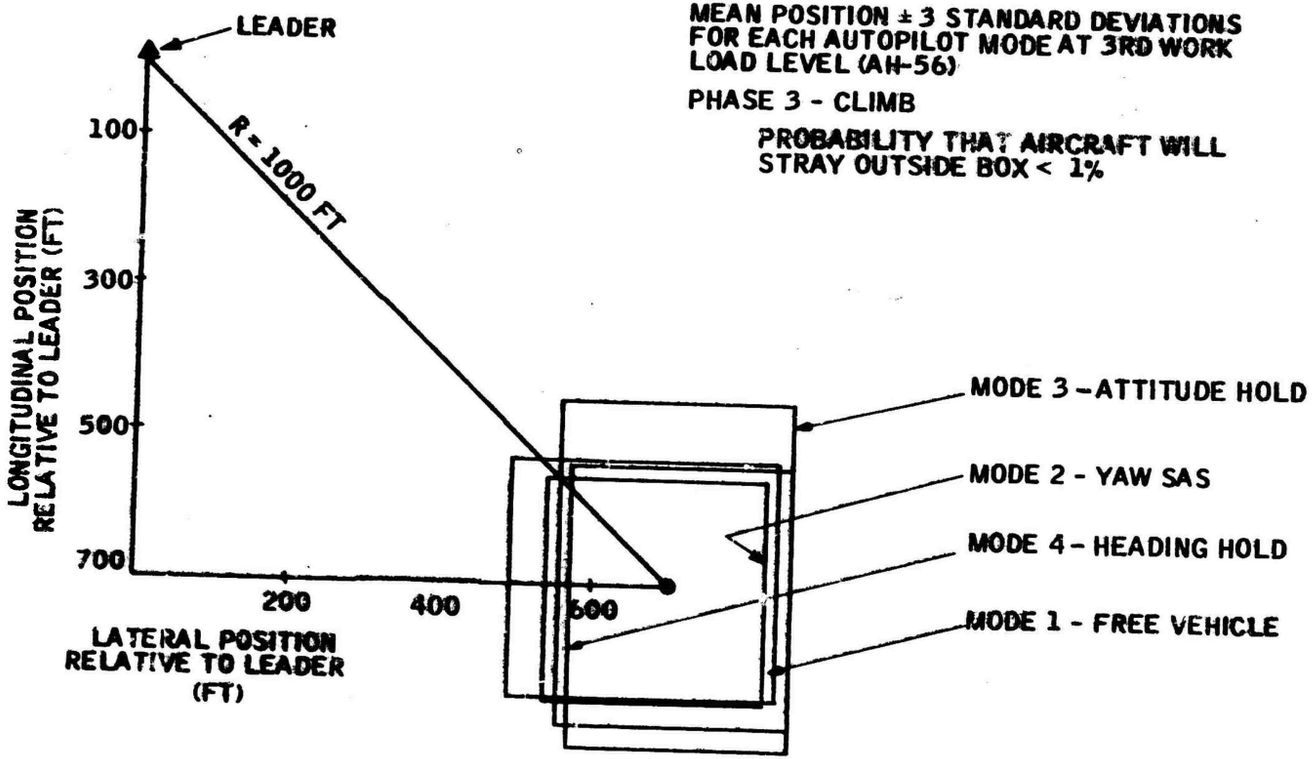

Figure 144. Phase 3 (Climb): Lateral and Longitudinal Position Error by Mode

resulted in the lowest RMS_Z errors controlled by the pilot in five of the seven mission phases. Therefore, at the higher workload levels it appears that increasing autopilot assistance in controlling other parameters did result in better control of the altitude error. The ranking of all six modes with respect to altitude errors for the highest workload which appeared to be quite consistent over the seven phases was as follows:

Rank	Autopilot Mode
1	Altitude hold (includes attitude hold and yaw SAS)
2	Heading and altitude hold (includes attitude hold and yaw SAS)
3	Attitude hold (includes yaw SAS)
4	Heading hold (includes attitude hold and yaw SAS)
4	Yaw SAS
5	Free vehicle

Activity Indices -- The effect of the autopilot mode by workload interaction on the pitch activity index is statistically significant in three of the seven mission phases. In the right-turn phase (Figure 113) the significance appears to result from the relatively high index obtained for the free vehicle for the 60% workload. The percentage increase associated with the workload increase from 40% to 60% for the free vehicle is approximately 125%, as compared to a maximum of 70% for the other three modes. The statistical significance noted for the descent phase (Figure 115) appears to result from the relatively higher index obtained for the yaw SAS mode at the 60% workload. In this case the percentage increase in the index associated with the workload increase from 40% to 60% is 200% for the yaw SAS mode, compared to approximately 70% for the other modes. The left-turn phase (Figure 117) shows the same trend as that described for the right-turn phase. The significance apparently was due to the greater increase in the index resulting from the workload increase from 40% to 60% for the free vehicle. This percentage increase was approximately 140%, compared to the maximum of 15% for the other three modes. The other four mission phases (Figures 109, 111, 119, and 121) exhibit the same general relationship between autopilot modes for all three workloads. These relationships are those shown by the rankings presented in the previous discussion of the main effect of autopilot mode on performance.

The effect of the various combinations of autopilot mode and workload on the roll activity index was statistically significant in three of the seven mission phases. The significance noted for the climb phase (Figure 125) appears to be due to the differences in the relationship between workloads for the four modes. The free vehicle and the heading hold mode result in relatively

greater increase in the index with the workload increase from 40% to 60%. Both result in percentage increases of approximately 150%, compared to the 5% and 50% increases noted for the attitude hold and yaw SAS modes, respectively. The variable relationship between workloads for the four modes examined for the descent phase (Figure 129) appears to have caused statistical significance for this phase. The heading hold mode resulted in much higher errors for 0% and 40% workloads. The free-vehicle and the yaw SAS mode resulted in greater percentage increases in the index for the workload increase from 40% to 60%. The attitude hold mode resulted in significantly lower indices for all three workloads. The statistical significance noted for the left turn also resulted from variable relationships between worklodas for the specific autopilot modes (Figure 131). Again, the percentage increase in the index associated with the workload increase from 40% to 60% varied greatly, with increases of 250% for the free vehicle as compared to a maximum of 70% for the other three modes. The other four mission phases (Figures 123, 127, 133, and 135) exhibit the same general relationship between autopilot modes for all three workloads. These relationships are those shown by the rankings presented in the previous discussion of the main effect of autopilot mode on performance.

Means and Standard Deviations -- Figures 143 through 149 present bounds which describe the lateral and longitudinal position error envelopes resulting for the applicable autopilot modes by mission phase. Since greater differences were noted between modes at the 70% workload level, the position error envelopes are presented for that workload. Center points in each rectangle are defined as coordinates of mean longitudinal and lateral errors for a specific phase with rectangle dimensions described by ±3 times the mean standard deviation for that phase. In general, the rectangles appear to be smaller for higher levels of autopilot, with either the free vehicle or the yaw SAS mode resulting in the largest rectangles. In the acceleration, straight-and-level, and deceleration phases the error envelopes do not vary considerably in size. In the more complex maneuvers, however, the size varies considerably with the autopilot mode (Figures 144 through 147).

Summary -- No notable improvement in performance in terms of RMS position errors resulted from additional autopilot capability under the no-workload or 40% workload conditions. At the 60% workload level, however, the advantages of additional autopilot assistance were obvious, with RMS position errors decreasing for the higher levels of autopilot and increasing considerably for the free vehicle. Although the free vehicle had resulted in RMS errors which were as low or lower than those for the other modes at the lower workload conditions, at the 60% workload the free vehicle resulted in the worst performance in terms of RMS errors. The altitude and attitude hold modes consistently resulted in the best performance in terms of RMS errors at this workload level. Thus, it was found that additional autopilot assistance resulted in improved control precision at the highest pilot workload tested.

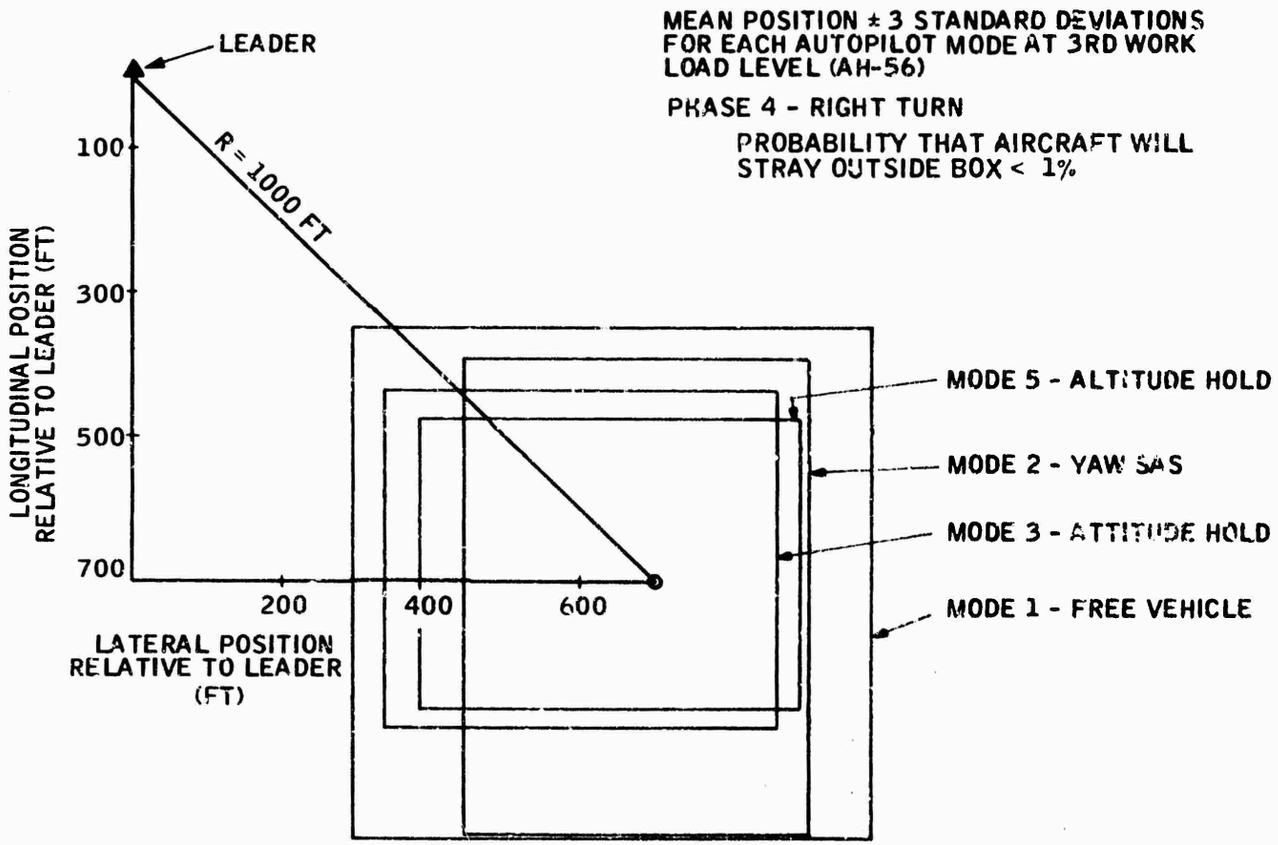

Figure 145. Phase 4 (Right Turn): Lateral and Longitudinal Position Error by Mode

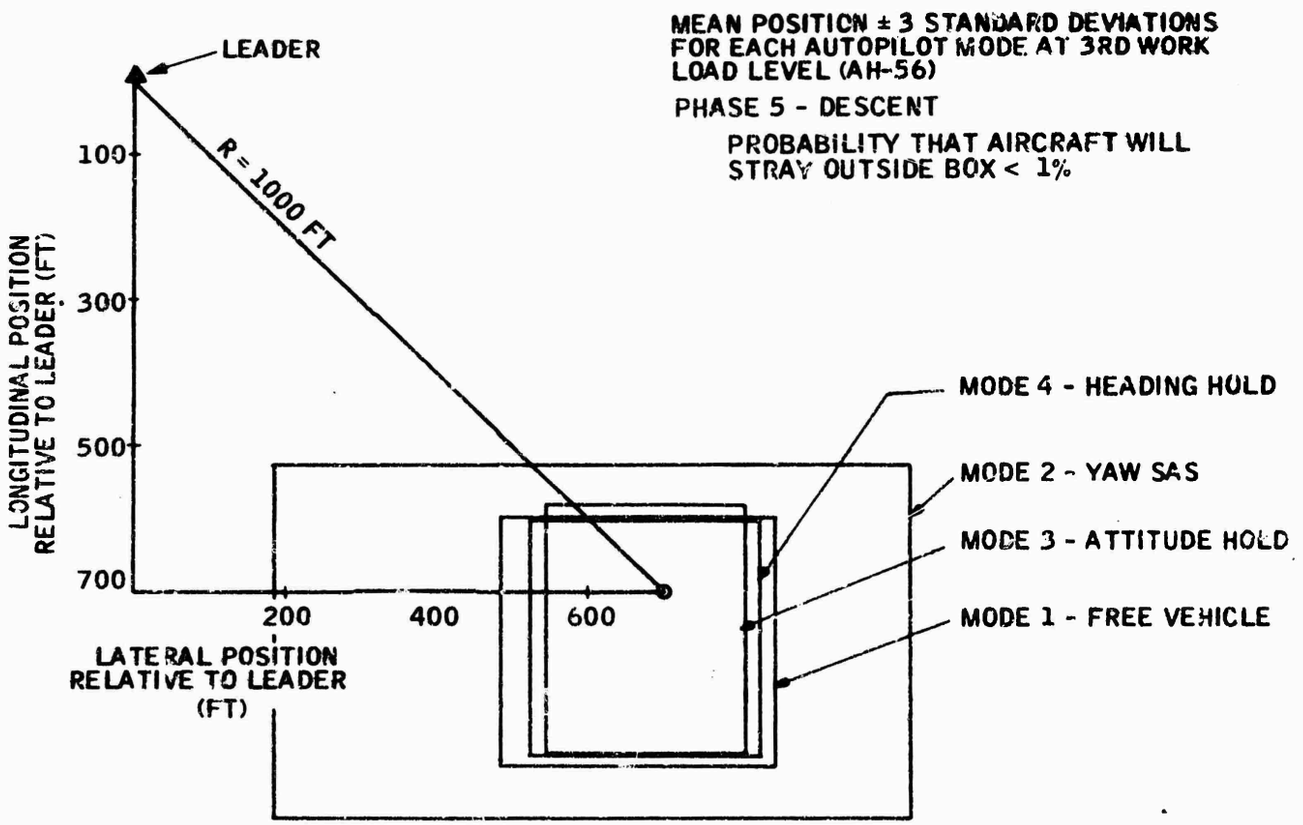

Figure 146. Phase 5 (Descent): Lateral and Longitudinal Position Error by Mode

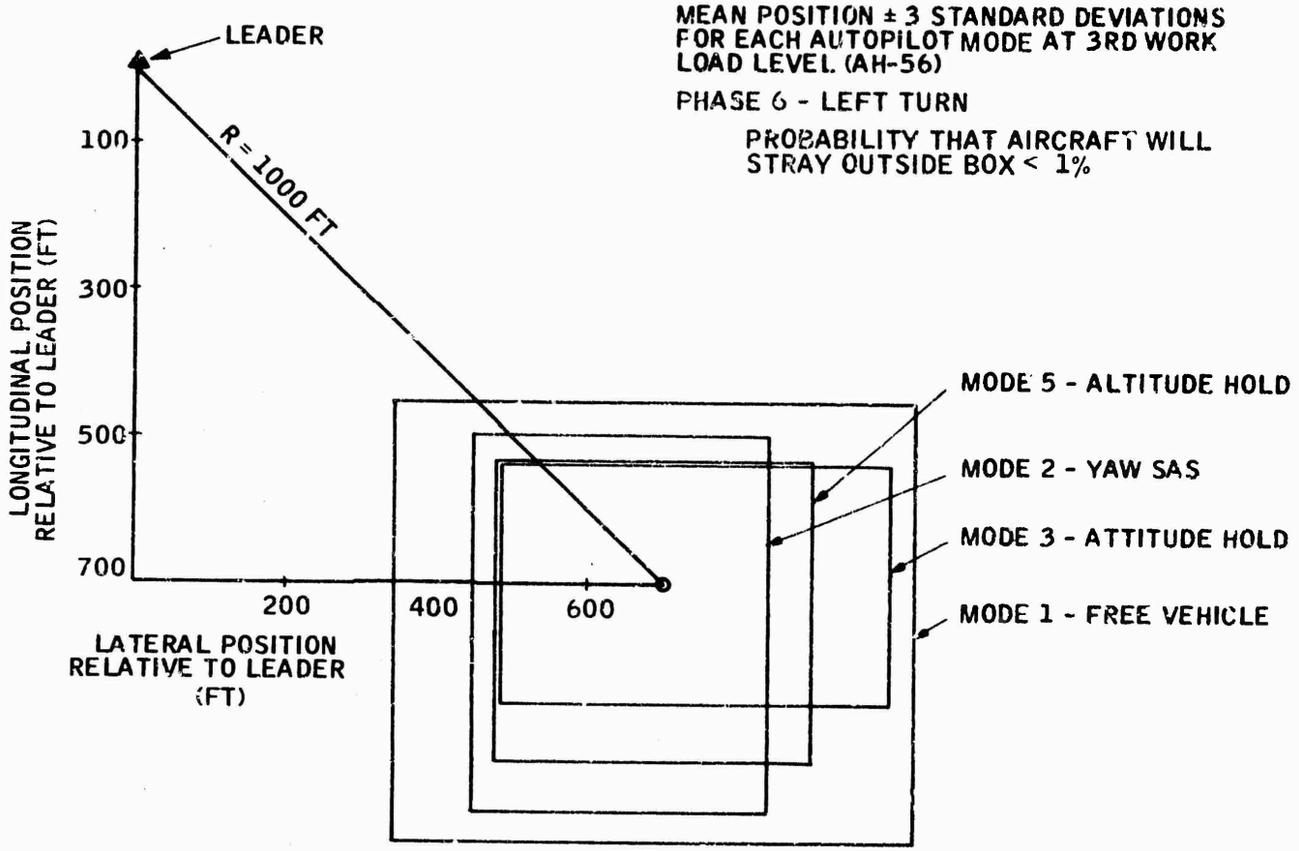

Figure 147. Phase 6 (Left Turn): Lateral and Longitudinal Position Error by Mode

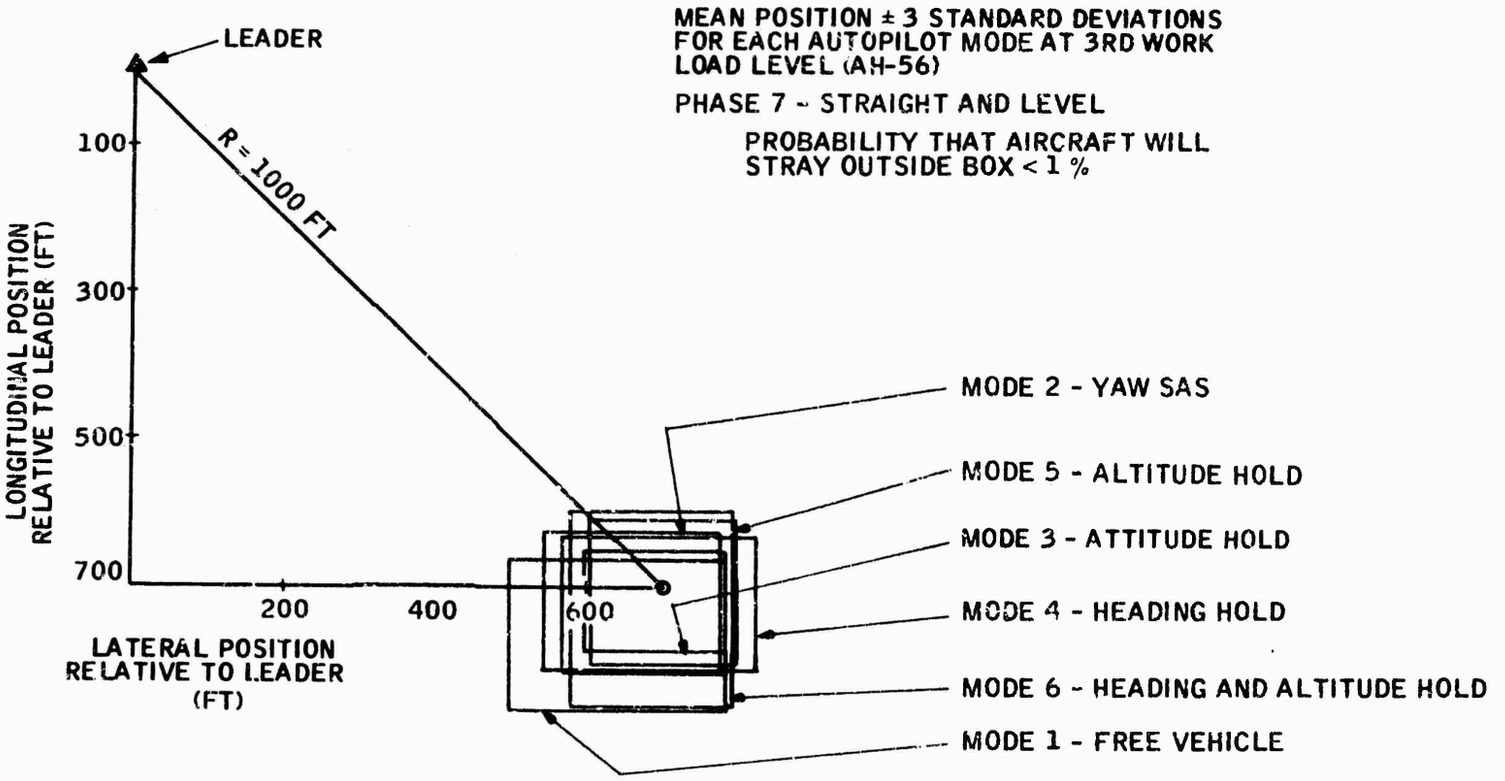

Figure 148. Phase 7 (Straight and Level): Lateral and Longitudinal Position Error by Mode

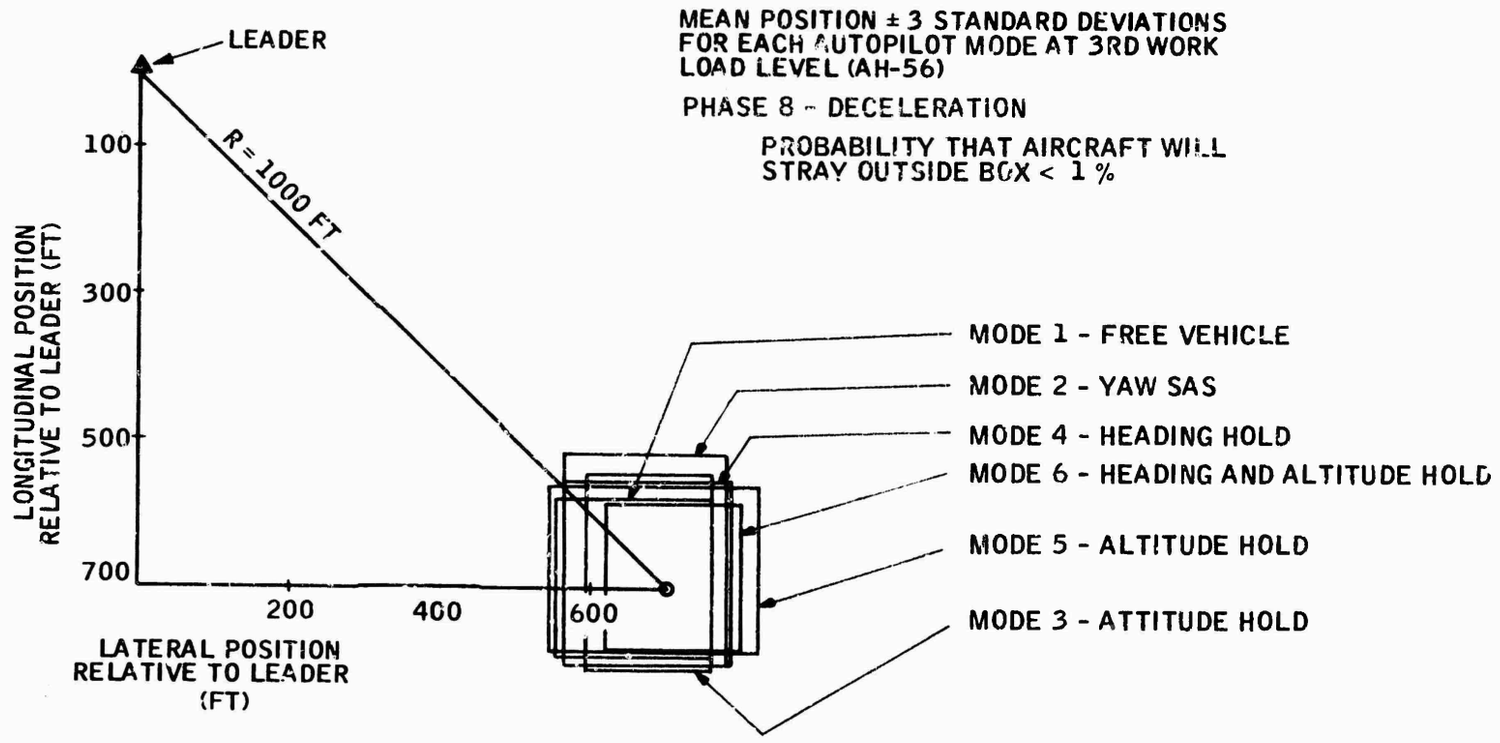

Figure 149. Phase 8 (deceleration): Lateral and Longitudinal Position Error by Mode

The relationship between autopilot modes in terms of the activity indices generally was the same as indicated by the rankings presented in the previous discussion of the main effect of autopilot mode on activity indices. The attitude and altitude hold modes were superior in reduction of the pitch activity index and the attitude hold and yaw SAS modes in the reduction of the roll activity index. The most notable difference observed in the analyses of these modes by workload was that the increase in activity indices resulting from workload increases was relatively greater for the free vehicle in three of the seven mission phases.

6.4 Catastrophic Control Losses and Collisions -- A detailed breakdown of the control losses in this experiment is presented in Table 7. Only 16 control losses were encountered in the experiment, making any analysis or interpretations of the losses speculative. It was noted that of the control losses, 15 (93.75%) were at the 60% workload level, indicating the importance of workload in performance degradation. It was also noted that one maneuver, the left turn, accounted for 12 (75%) of the control losses, and that one subject (DI) accounted for 12 (75%) of the control losses. In addition, the same subject (DI) had the only collision occurring in the experiment.

6.5 Pilot Reactions and Comments -- Following the completion of formal data collection, the pilot/subjects were questioned to determine their reactions to the simulation and to the various autopilot modes.

When asked to rank the various autopilot modes according to the subject's opinion of his own "ability to fly" them, Mode 6 (heading hold and altitude hold) was ranked first (easiest) by three of the four subjects; the other subject ranked it second. The three subjects who ranked Mode 6 first ranked Mode 5 (altitude hold) second. The other subject ranked Mode 5 third. This subject's first-ranked mode was Mode 3 (pitch and roll attitude holds). Mode 4 (heading hold) was, however, ranked very low--sixth (last) by two subjects, fifth by another, and fourth by another.

One can conclude from this that the altitude hold was the important factor in the high ranking of Modes 5 and 6. The low ranking of Mode 4 is probably due to the "looseness" of the hold in light of the simulated turbulence and the reference of the display to the leader's heading.

Two of the subjects also commented on the transition from the UH-1 simulation to the AH-56 simulation with reference to the shift in necessary corrective action for a given error. This is a problem which will be considered in a Honeywell follow-on study (Reference 8). The present study served to illustrate and better define the variables involved in error-information versus necessary-corrective-action information, and it is anticipated that a definition of the considerations necessary will emerge from the follow-on study.

Table 7. Control Loss Record

Control Loss Record				
Subject	Mode	Workload (%)	Phase	No. of Losses
BAO	Yaw SAS	60	Left Turn	1
	Heading hold	60	Ascent	1
TR	Yaw SAS	60	Left Turn	1
DI	Free vehicle	60	Ascent	1
		60	Left Turn	4
	Yaw SAS	60	Left Turn	2
	Heading hold	60	Right Turn	1
	Alt and head hold	60	Left Turn	3
		40	Descent	1 (Collided with A/C 4)
JA	Heading hold	60	Left Turn	1

Control Loss by Parameter Variation	
Phases	No. Of Losses
Accel. (2)	0
Ascent (3)	2
R. Turn (4)	1
Descent (5)	1
L. Turn (6)	12
S and L (7)	0
Decel (8)	0
Modes	**No. Of Losses**
Free vehicle	5
Yaw SAS	4
Three-Axis SAS	0
Heading hold	3
Altitude hold	0
Heading and Alt. Hold	4
Workload	**No. Of Losses**
0%	0
40%	1
60%	15
Subject	**No. Of Losses**
BAO	2
TR	1
DI	12
JA	1

6.6 Analog Traces of Stick Inputs -- Figures 150A and 150B present samples of the analog traces of pitch and roll cyclic inputs for three phases, straight and level (phase 7), climb (phase 3), and left turn (phase 4), at the highest workload level. The three traces on the left of each figure are from the modes ranked best in terms of the applicable activity index (pitch or roll), and the traces on the right are from the modes ranked lowest. These traces are illustrative of the rankings derived from the statistical analysis of the activity indices over all subjects, all workloads, and all phases.

6.7 Summary of Results -- Experiment II

Task Difficulty and Aircraft Response Stability -- The most significant improvements in pilot performance resulting from increasing levels of autopilot assistance were seen in the increased ease of the control task and the greater stability of aircraft response. The pitch and roll activity indices, which indicate the extent of control inputs/aircraft response required to maintain position, were significantly lower for the higher levels of autopilot capability. The increased autopilot assistance allowed the aircraft to be maintained with lower-amplitude, higher-frequency control inputs and aircraft responses, thus indicating a more stable system as well as a less-demanding control task.

The altitude hold, heading and altitude hold, and the attitude hold modes resulted in the best performance in terms of the pitch activity index. The lowest roll activity indices were obtained for the attitude hold mode. Due to the response of the heading hold mode to gusts, it did not perform as well in terms of the roll activity index as did those modes with the roll attitude hold engaged. Since the attitude hold mode resulted in activity indices as low or lower than the other modes in both pitch and roll, it would appear to be optimal in terms of both activity indices.

The increasing ease of the control task with the increase in autopilot capability was substantiated by pilot opinion. Three of the four subjects selected the attitude hold mode as "easiest" to fly.

In conclusion, the increased autopilot assistance resulted in increased system control stability and decreased difficulty of the pilot's control task.

Control Precision -- The performance improvements in terms of aircraft position errors resulting from increasing the autopilot capability were noted primarily at the highest workload. At the 60% workload level the attitude hold, altitude hold, and heading and altitude hold modes quite consistently resulted in lower position errors than did the free-vehicle, yaw SAS, or heading hold modes. The primary benefit appeared to be gained from the attitude and altitude holds. When the heading hold was added to the altitude and attitude hold mode, it did not result in further performance improvement. Under the no-workload and 40% workload conditions very few significant differences were noted for the varying levels of autopilot capability, with the free vehicle generally resulting in errors as low as those obtained in any of the autopilot

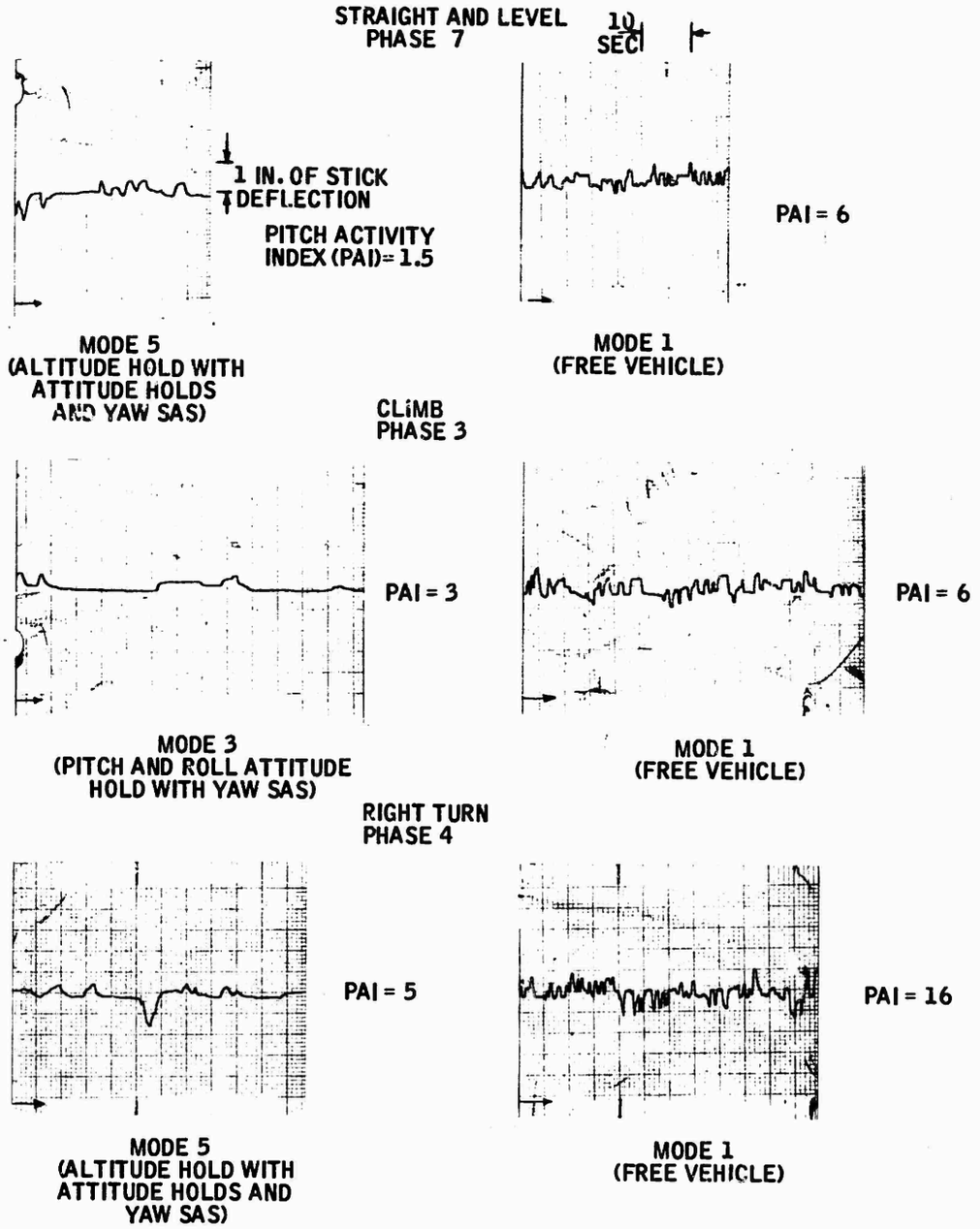

Figure 150A. Analog Traces of Pitch and Roll Activity Indices: Pilot Pitch Control Inputs

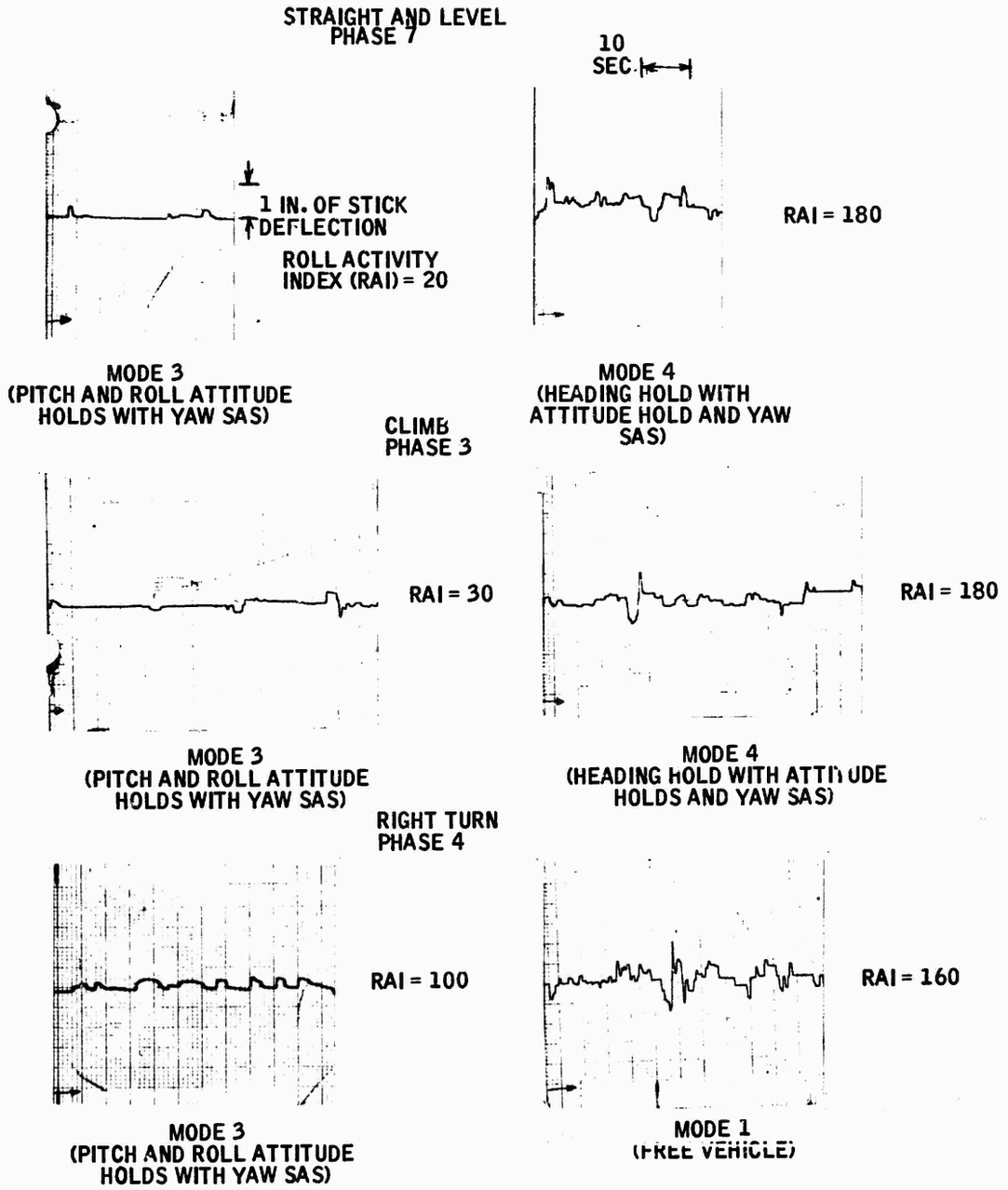

Figure 150B. Analog Traces of Pitch and Roll Activity Indices: Pilot Roll Control Inputs

modes. This was not true for the altitude error, which was substantially decreased for those modes with altitude hold, even under these lower workload conditions. This resulted from the control of altitude error by the autopilot when these two modes were engaged.

In conclusion, increasing the autopilot capability resulted in significant improvement in pilot control precision only at the highest workload tested. Apparently, as suggested previously in the summary of the UH-1 results (Section V), the level of control precision which can be attained by the pilot with the aid of a quickened display cannot be exceeded, even with the addition of autopilot assistance, as long as the pilot can focus most of his attention on the control task. When it is necessary for the pilot to focus a great deal of attention on other tasks, however, the autopilot assistance becomes valuable in increasing control precision.

SECTION VIII
SUMMARY AND CONCLUSIONS

The primary objective of this study was to relate pilot performance during manual IFR formation flight to various levels of autopilot assistance. For convenience, the autopilot modes investigated are listed below for each of the study helicopters:

UH-1	AH-56A
• Free vehicle	• Free vehicle
• Yaw SAS	• Yaw SAS
• Three-axis SAS	• Attitude hold (pitch and roll)
• Heading hold	• Heading hold
• Altitude hold	• Altitude hold
• Heading and altitude hold	• Heading and altitude hold

SUMMARY OF RESULTS

UH-1

The most significant improvements in pilot performance resulting from increasing autopilot sophistication were seen in the ease of the control task and general system stability. Pilot control inputs and aircraft responses required for position control were significantly lower when the outer-loop hold modes of the autopilot were engaged. This result agrees with the pilot/subjects' ranking of the autopilot modes according to their ability to fly a particular mode (Section V).

Position errors were generally not significantly improved for the lower workload levels (0% and 40%) as the autopilot level increased, although a definite improvement in altitude error was observed when altitude hold was engaged. However, at the 70% workload level, position control showed improvement when the level of autopilot sophistication was increased, as indicated by the control losses (see Table 4).

AH-56A

As with the UH-1 the most significant improvements in pilot performance with the AH-56 vehicle resulting from additional autopilot sophistication were observed in the ease of the control task and system stability. The attitude hold mode resulted in the lowest control activity. These results were substantiated by pilot/subject opinion. Three of the four pilots chose the altitude hold mode (which includes attitude hold) as being the "easiest" to fly.

This result of attitude hold improving performance is consistent with the piloting technique for the AH-56; i.e., to hold zero pitch attitude and control airspeed with the pusher prop.

For the 0% and 40% workload levels, position errors were generally constant across all autopilot modes. At the highest workload level (60%), however, some improvement is noted in X and Y position errors when the autopilot outer-loop hold modes were engaged. Heading hold by itself did not improve position errors. This is probably due to the relatively high level of turbulence simulated for the AH-56 vehicle. The heading hold mode did not provide tight enough control, and the pilot was required to make frequent manual corrections. [The absolute level of turbulence was the same for both the UH-1 and AH-56; however, since the AH-56 was operating at a lower airspeed (60 knots) than the UH-1 (88 knots), the effect of turbulence on the AH-56 was greater].

CONCLUSIONS

The following general conclusions were reached during this investigation:

- For both helicopters, the most significant improvements in pilot performance due to increasing the level of autopilot sophistication were observed in the ease on the control task and general system stability. This result is indicated by the pitch and roll activity indices, pilot control inputs, and pilot opinion.

- Position errors were generally not reduced as the autopilot level was increased. This can be explained by the pilot's ability to maintain a high degree of control precision with just the quickened display. It appears that the limiting factor is the vehicle's basic position response. The quickened display enables the pilot to close all the outer loops, thus performing the same function as the autopilot. Apparently, the quickened display masked the effects of the autopilot in terms of position errors, although the autopilot made the control task easier by adding system stability. At the highest workload level for each vehicle some improvement is noted in position errors for the autopilot outer-loop hold modes.

- The heading hold mode did not reduce lateral errors as expected. In the presence of turbulence, the response of the heading hold was not fast enough to provide precise lateral control.

- Performance with the AH-56 in the SK/FF mode could possibly be improved if a display format were developed specifically for that vehicle and consistent with its control system. For this study, the same display format and form of the quickening law were used for both simulated helicopters, although the control tasks were different.

- The benefits from autopilot assistance in terms of position control would probably be greater if pilot fatigue over long periods of time were considered. For this study, relatively short missions were simulated, and no measurement of pilot fatigue was made.

- To significantly improve position errors over the level obtained with a manual/quickened display system, some level of autopilot/coupler is probably required where signals from the measurement system are fed directly into the autopilot.

GLOSSARY

Activity Indices	Mean-square pitch and roll rates of the simulated aircraft. These values are used as performance measures and provide an indication of the pilot's activity as he controls the simulated vehicle.
Alpha-Beta Filter	Name of the digital filter used in this study to provide smoothed estimates of position and rate from the assumed measurements.
Analysis of Variance	A statistical technique which provides comparisons of means of several populations (e.g., corresponding to pilot/system responses to several levels or combinations of system variables) by comparing sampling error variances to variances resulting from differences between means.
Concomitant Task	A class of secondary task which is performed simultaneously with the primary task and is highly quantifiable in nature. In the study, the primary aircraft position control task was performed continuously and the pilot's formation flight display was intermittently blanked out. Then secondary task cues were provided, requiring that the pilot simultaneously perform the secondary task at a forced-pace (i.e., the frequency and time interval of the formation flight display interruption was controlled by the experimenter rather than left to pilot discretion). The levels of the secondary workload were defined in terms of percentage of time the pilot was required to perform the secondary task.
Data Rate (Update Rate)	The rate at which new information about the follower aircraft's position in space (with respect to the lead aircraft of the formation) is available for display.

Dependent Variables

Variables of an experiment which describe system performance. These performance measures are assumed to reflect changes in the levels of the independent variables of the experiment and are thus considered to be "dependent".

Independent Variables

Parameters of a system which are varied to investigate their effect on system performance.

Mean Position Error

$\left(\sum_{i=1}^{N} X_i \right) / N$, where X_i was the measured position in a specific axis during a specific maneuver and N was the total number of position measurements recorded during the maneuver.

Measurement Noise

Used to refer to the error in the measurement of the follower aircraft's position with respect to the leader. The sensor system was assumed to include noise with a normal (Gaussian) distribution described by the standard deviation. In the referenced studies these standard deviations were defined in terms of the bearing (σ_B), elevation (σ_E), and range (σ_R) measurements, or in terms of the longitudinal (σ_X), lateral (σ_Y), and vertical (σ_Z) position (in feet).

PFI Display

Plan Position Indicator - A display format configured for the formation flight mode which presented a horizontal view of all aircraft in the formation.

Quickening

A method of providing lead or anticipatory information regarding the system's response. As used in the referenced studies, it consisted of adding higher order derivatives (i.e., rate of change of position) of the system's response (change in aircraft position) to the actual position error. The resultant sum was used to drive one element on the display

RMS

Root-Mean-Square $\sqrt{\left(\sum_{i=1}^{N} X_i^2\right)/N}$, where X_i was the measured position in a specific axis during a specific maneuver and N was the total number of position measurements recorded during the maneuver. The RMS measure was also used to represent the levels of pilot and aircraft control activity during a given maneuver, in which case X_i represented respectively the rate of movement of the control stick or the aircraft's attitude.

Standard deviation

$\sqrt{\left(\sum_{i=1}^{N} (\bar{X} - X_i)^2\right)/N}$, where $\bar{X}$ is the mean value of the observations (X_i) and N is the total number of observations.

Statistical Significance

As used in this report, statistical significance signifies an acceptably low probability (< 0.10) that performance differences of the magnitude observed from the experimental test data could have occurred by chance -- thus a high probability (>0.90) that the experimental data reflect true differences between treatment effects.

Subsidiary Pilot Workload

The pilot's workload on tasks other than his primary task (aircraft position control in the referenced studies). See the description of "concomitant task" for more detail on how this subsidiary workload was simulated.

REFERENCES

1. Display Requirements Study for Helicopter IFR Formation Flight. JANAIR Technical Report No. NR 213-054, January 1968.

2. Experimental Evaluation of a Formation Flight System. JANAIR Technical Report No. 6804002, July, 1968.

3. Evaluation of Conventional Flight Instruments for Use in Helicopter IFR Formation Flight. JANAIR Technical Report No. 680204, February, 1968.

4. Effects of Variation in System Data Rate and Accuracies on Pilot Performance in the Helicopter IFR Formation Flight System. JANAIR Report 680408, April 1968.

5. Brown, I.D.: The Measurement of Perceptual Load and Reserve Capacity. Applied Psychology Unit, Cambridge, Report No. APU509, 1964.

6. Knowles, W.B.: Operator Loading Tasks. Human Factors, 1963, 5, pp. 155-161.

7. Army Advanced Automatic Flight Control System Study, Technical Report ECOM -1216-5, July 1966.

8. Formation Flight Display Requirements for Various Vehicles, Tactics, and System Considerations. Unsolicited Proposal to ONR, Honeywell Document No. 8B-M-1, March 1968.

APPENDIX A

ANALYSIS OF VARIANCE SUMMARY TABLES FOR EXPERIMENTS I AND II

Analysis of Variance For RMS_X - Experiment I, Phase 2

Source	Sum of Squares	D. F.	Mean Square	F-Ratios	Significance Level
S	4870.14	3	1623.38		
M	3949.56	2	789.91	1.39	
W	36464.41	2	18232.20	51.07	0.001
SM	8521.86	15	568.12		
SW	2144.06	6	357.34		
MW	5187.89	10	518.78	1.59	
SMW	9755.31	30	325.17		

Analysis of Variance For RMS_Y - Experiment I, Phase 2

S	937.43	3	312.47		
M	2320.14	5	464.02	0.72	
W	19801.26	2	9900.63	18.23	0.005
SM	9703.45	15	646.89		
SW	3260.34	6	543.39		
MW	7143.88	10	714.38	1.52	
SMW	14069.04	30	468.96		

Analysis of Variance For RMS_Z - Experiment I, Phase 2

Source	Sum of Squares	D.F.	Mean Square	F-Ratios	Significance Level
S	11347.33	3	3782.44		
M	39969.44	5	7993.88	6.11	0.05
W	28884.50	2	14442.25	12.61	0.005
SM	19620.83	15	1308.05		
SW	6871.49	6	1145.24		
MW	18066.88	10	1806.68	2.32	0.05
SMW	23323.82	30	777.46		

Analysis of Variance For Pitch Activity Index - Experiment I, Phase 2

S	127.14	3	42.38		
M	185.03	5	37.00	9.7	0.001
W	182.42	2	91.21	10.25	0.01
SM	57.15	15	3.81		
SW	53.80	6	8.96		
MW	55.55	10	5.55	0.82	
SMW	202.21	30	6.74		

Analysis of Variance Roll Activity Index - Experiment I, Phase 2

Source	Sum of Squares	D. F.	Mean Square	F-Ratios	Significance Level
S	1748.07	3	528.69		
M	9513.31	5	1902.66	1.55	
W	19827.93	2	9913.96	32.82	0.001
SM	18407.27	15	1227.15		
SW	1812.86	6	302.14		
MW	12657.72	10	1265.77	1.01	
SMW	37465.46	30	1248.84		

Analysis of Variance For RMS_X - Experiment I, Phase 3

S	18747.11	3	6249.03		
M	3641.63	3	1213.87	0.94	
W	91152.92	2	40576.46	35.31	0.001
SM	11576.96	9	1286.32		
SW	6898.62	6	1149.77		
MW	4101.13	6	683.52	0.78	
SMW	15675.26	18	870.84		

Analysis of Variance For RMS_Y - Experiment I, Phase 3

Source	Sum of Squares	D. F.	Mean Square	F-Ratios	Significance Level
S	745.38	3	248.46		
M	6247.74	3	2082.58	0.97	
W	65748.96	2	32874.48	33.47	0.001
SM	19375.84	9	2152.87		
SW	5892.52	6	982.08		
MW	14351.63	6	2391.93	1.76	
SMW	24493.26	18	1360.73		

Analysis of Variance For RMS_Z - Experiment I, Phase 3

S	4643.65	3	1547.88		
M	2207.34	3	735.78	1.26	
W	27630.90	2	13815.45	28.19	0.001
SM	5267.88	9	585.32		
SW	2942.69	6	490.44		
MW	2498.82	6	416.47	1.80	
SMW	4171.11	18	231.72		

Analysis of Variance For Pitch Activity Index - Experiment I, Phase 3

Source	Sum of Squares	D. F.	Mean Square	F-Ratios	Significance Level
S	25.82	3	8.60		
M	128.42	3	42.80	4.45	0.05
W	230.35	2	115.17	59.37	0.001
SM	86.10	9	9.56		
SW	11.63	6	1.93		
MW	12.79	6	2.13	0.47	
SMW	82.02	18	4.55		

Analysis of Variance for Roll Activity Index - Experiment I, Phase 3

S	28184.04	3	9394.68		
M	47992.42	3	15997.47	13.29	0.005
W	107600.35	2	53800.17	8.39	0.025
SM	10833.07	9	1203.67		
SW	38443.56	6	6407.26		
MW	31182.79	6	5197.13	3.44	0.025
SMW	27220.58	18	1512.25		

Analysis of Variance For RMS_X - Experiment I, Phase 4

Source	Sum of Squares	D. F.	Mean Square	F-Ratios	Significance Level
S	6637.26	3	2212.42		
M	2824.41	3	941.47	0.38	
W	48120.12	2	24060.06	15.68	0.005
SM	21799.91	9	2422.21		
SW	9209.73	6	1534.95		
MW	3735.61	6	622.60	0.33	
SMW	33478.72	18	1859.92		

Analysis of Variance for RMS_Y - Experiment I, Phase 4

S	6874.39	3	2291.46		
M	40.22	3	13.40	0.06	
W	81579.44	2	40789.72	23.21	0.005
SM	20827.22	9	2314.13		
SW	10547.36	6	1757.89		
MW	4934.45	6	822.40	0.30	
SMW	48932.54	18	2718.47		

Analysis of Variance For RMS_Z - Experiment I, Phase 4

Source	Sum of Squares	D.F.	Mean Square	F-Ratios	Significance Level
S	2745.72	3	915.24		
M	20698.28	3	6899.45	3.85	0.05
W	23497.63	2	11748.81	10.87	0.025
SM	16131.38	9	1792.37		
SW	6487.12	6	1081.18		
MW	7311.46	6	1218.57	1.02	
SMW	21500.09	18	1194.44		

Analysis of Variance For Pitch Activity Index - Experiment I, Phase 4

S	165.10	3	55.03		
M	327.16	3	109.05	9.0	0.005
W	123.89	2	61.94	2.48	
SM	105.38	9	11.70		
SW	150.33	6	25.05		
MW	9.55	6	1.59	0.38	
SMW	74.35	18	4.13		

Analysis of Variance For Roll Activity Index - Experiment I, Phase 4

Source	Sum of Squares	D. F.	Mean Square	F-Ratios	Significance Level
S	15852.17	3	5284.05		
M	24344.96	3	8114.98	1.45	0.01
W	148616.55	2	74308.27	12.86	
SM	50347.38	9	5594.15		
SW	34667.55	6	5777.92		
MW	26877.66	6	4479.62	0.66	
SMW	122680.68	18	6815.59		

Analysis of Variance for RMS_X - Experiment II, Phase 2

Source	Sum of Squares	D. F.	Mean Square	F-Ratios	Significance Level
S	49855.45	3	16618.48		
M	11846.18	5	2369.23	1.30	
W	66341.84	2	33170.92	10.77	0.025
SM	27437.34	15	1829.15		
SW	18484.36	6	3080.81		
MW	12535.93	10	1253.59	0.93	
SMW	40494.91	30	1349.83		
R(SMW)	149209.99	144	1029.23		

Analysis of Variance for RMS_Y - Experiment II, Phase 2

S	18912.08	3	6304.02		
M	30740.74	5	6148.14	3.83	0.025
W	17849.62	2	8924.81	4.32	0.10
SM	24088.93	15	1605.92		
SW	12409.56	6	2068.26		
MW	7000.43	10	700.04	0.89	
SMW	23587.49	30	786.24		
R(SMW)	151218.66	144	1050.12		

Analysis of Variance for RMS_Z - Experiment II, Phase 2

Source	Sum of Squares	D. F.	Mean Square	F-Ratios	Significance Level
S	6073.38	3	2024.46		
M	87077.44	5	17415.48	19.28	0.001
W	8133.36	2	4066.68	5.67	0.05
SM	13550.33	15	903.35		
SW	4307.30	6	717.88		
MW	8631.02	10	863.10	1.23	
SMW	21131.63	30	704.38		
R(SMW)	101427.33	144	704.35		

Analysis of Variance for Pitch Activity Index - Experiment II, Phase 2

S	30.75	3	10.25		
M	86.70	5	17.34	11.72	0.001
W	9.50	2	4.75	6.86	0.05
SM	22.07	15	1.47		
SW	4.15	6	0.69		
MW	9.93	10	0.99	1.43	
SMW	20.84	30	0.69		
R(SMW)	224.00	144	1.55		

Analysis of Variance for Roll Activity Index - Experiment II, Phase 2

Source	Sum of Squares	D.F.	Mean Square	F-Ratios	Significance Level
S	6204.90	3	2098.30		
M	12845.91	5	2569.18	2.15	
W	6393.92	2	3196.96	3.56	0.10
SM	17904.06	15	1193.60		
SW	5383.00	6	897.16		
MW	4845.24	10	484.52	0.96	
SMW	15172.27	30	505.74		
R(SMW)	91570.66	144	635.90		

Analysis of Variance for RMS_X - Experiment II, Phase 3

Source	Sum of Squares	D.F.	Mean Square	F-Ratios	Significance Level
S	31769.38	3	10589.79		
M	5785.27	3	1928.42	0.62	
W	49149.84	2	24624.92	28.54	0.001
SM	28204.88	9	3133.87		
SW	5176.48	6	862.74		
MW	5609.43	6	934.90	0.88	
SMW	19240.90	18	1068.93		
R(SMW)	141199.33	96	1470.82		

Analysis of Variance for RMS_Y - Experiment II, Phase 3

S	11864.57	3	3954.85		
M	666.85	3	222.28	0.19	
W	35004.66	2	17502.33	59.92	0.001
SM	10603.00	9	1178.11		
SW	1752.44	6	292.07		
MW	9395.33	6	1565.88	3.19	0.005
SMW	8844.22	18	491.34		
R(SMW)	60025.33	96	625.26		

Analysis of Variance for RMS_Z - Experiment II, Phase 3

Source	Sum of Squares	D. F.	Mean Square	F-Ratios	Significance Level
S	21014.18	3	7004.72		
M	10770.74	3	3590.24	2.53	
W	47811.26	2	23905.63	5.06	0.05
SM	12770.34	9	1418.92		
SW	23681.62	6	3946.93		
MW	9154.90	6	1525.81	1.12	
SMW	24460.43	18	1358.91		
R(SMW)	122897.33	96	1280.18		

Analysis of Variance for Pitch Activity Index - Experiment II, Phase 3

S	293.74	3	97.91		
M	172.24	3	57.41	3.31	0.10
W	227.54	2	113.77	4.17	0.10
SM	155.89	9	17.32		
SW	163.56	6	27.26		
MW	67.90	6	11.31	1.32	
SMW	153.87	18	8.54		
R(SMW)	1128.66	96	11.75		

Analysis of Variance for Roll Activity Index - Experiment II, Phase 3

Source	Sum of Squares	D. F.	Mean Square	F-Ratios	Significance Level
S	32485.11	3	10828.37		
M	63755.38	3	21251.79	7.52	0.01
W	81860.37	2	40930.18	5.91	0.05
SM	25440.27	9	2826.69		
SW	41583.01	6	6930.50		
MW	36563.56	6	6093.92	2.43	0.10
SMW	206041.33	18	2505.66		
R(SMW)	206041.33	96	2146.26		

Analysis of Variance for RMS_X - Experiment II, Phase 4

Source	Sum of Squares	D. F.	Mean Square	F-Ratios	Significance Level
S	15575.63	3	5191.87		
M	1032.40	3	344.13	0.04	
W	70289.26	2	35144.63	7.39	0.025
SM	77037.72	9	8559.74		
SW	28543.18	6	4757.19		
MW	44088.90	6	7348.15	1.71	
SMW	77559.54	18	4308.86		
R(SMW)	399800.66	96	4164.59		

Analysis of Variance for RMS_Y - Experiment II, Phase 4

S	42792.02	3	14264.00		
M	16832.46	3	5610.82	0.38	
W	126803.62	2	63401.81	14.23	0.01
SM	133147.00	9	14794.11		
SW	26730.37	6	4455.06		
MW	44989.09	6	7498.18	1.16	
SMW	116416.68	18	6467.59		
R(SMW)	443636.66	96	4621.21		

Analysis of Variance for RMS_Z - Experiment II, Phase 4

Source	Sum of Squares	D.F.	Mean Square	F-Ratios	Significance Level
S	11056.68	3	3685.56		
M	57953.07	3	19317.69	14.63	0.001
W	43979.18	2	21989.59	17.13	0.005
SM	11881.45	9	1320.16		
SW	7702.54	6	1283.75		
MW	26797.65	6	4466.27	3.87	0.025
SMW	21295.06	18	1183.05		
R(SMW)	69152.66	96	720.34		

Analysis of Variance for Pitch Activity Index - Experiment II, Phase 4

S	34.18	3	11.39		
M	365.52	3	121.84	18.27	0.001
W	215.05	2	107.52	17.52	0.005
SM	60.00	9	6.66		
SW	36.83	6	6.13		
MW	164.50	6	27.41	4.20	0.01
SMW	117.38	18	6.52		
R(SMW)	1038.66	96	10.81		

Analysis of Variance for Roll Activity Index - Experiment II, Phase 4

Source	Sum of Squares	D. F.	Mean Square	F-Ratios	Significance Level
S	19325.79	3	6441.93		
M	22825.29	3	7608.43	0.83	
W	82055.51	2	41027.75	10.71	0.025
SM	82551.11	9	9172.34		
SW	22988.76	6	3831.46		
MW	33882.26	6	5647.04	0.97	
SMW	104711.23	18	5817.29		
R(SMW)	417997.99	96	4354.14		

APPENDIX B
SIMULATION EQUIPMENT DESCRIPTION

APPENDIX B
SIMULATION EQUIPMENT DESCRIPTION

The hybrid computer used in this study is a combination of elements, each a specialized item which, when joined, provides a system capable of approaching the duplication of the real world in real time. The fidelity of the present simulation using the hybrid system is subject only to the limitation placed on it by the accuracy of information regarding the simulated UH-1 vehicle and the simplifications made to expedite programming of the computer.

In general, the analog portion of the hybrid computer is used to provide calculation of relatively low accuracy. The digital portion of the computer is used to provide the high-speed and accuracy calculations and in the case of this simulation, was used to control the simulation. This is common practice because of the extensive logic and decision making capabilities of the digital machine.

DIGITAL COMPUTER

The digital computer is a high-speed, medium-word-length machine specifically designed for hybrid simulations, real-time control and rapid computati The main characteristics of this machine are:

- 24-bit word
- 24-K core memory
- 1.75-microsecond fixed-point add
- Floating point hardware
- Real-time FORTRAN IV language
- 16 priority intercept channels
- 600-line-per-minute printer
- Card reader and card punch
- Three magnetic tape units
- Console input/output typewriter

CRT DISPLAY

The heart of the simulation for the SK/FF study is the 17-inch CRT display which was programmed and driven by the hybrid computer and the linkage system.

The scope was used to display the cockpit instruments and various formats tested. It has the ability to:

- Plot 120,000 points/sec
- Plot 80,000 characters/sec
- Plot 20,000 vectors/sec
- Generate all FORTRAN IV characters
- Generate all Greek letters

ANALOG COMPUTER

The analog portion of the hybrid problem is programmed on the 60-amplifier analog computers. Two analogs were joined together through a trunk system of interconnects and operated simultaneously to provide solutions to the simulated vehicle equations of motion and the control authority calculations.

The information flowing into and out of the analog portion of the system emanates from and enters the digital portion via a linkage system of digital-to-analog and analog-to-digital converters.

A/D LINKAGE

The link system with its small capacity analog computer provides the means of coupling the larger analog computers which supply the simulation information with the digital computer which does all the calculation for the display and associated information output.

The link has:

- 24 channels of A/D with simultaneous sample and hold
- 24 channels of A/D without sample and hold
- 20 channels of DA/
- 6 discrete input channels
- 6 discrete output channels
- 10-Kc real time interrupt clock

The analog computer was the natural choice for solving the high-frequency rotational equations of motion and computing the aerodynamic forces present on the vehicle as a result of its motion and the system inputs. The analog was also chosen to simulate the control system of the vehicle because inputs from the controls are voltages.

Because the coordinate transformation and integration of the force equations involves so many multiplications, the digital computer was chosen to solve them along with the display calculations. Performing all of the multiplications and resolution on the analog computer would be prohibitive in terms of accuracy and physical equipment required to do the operation.

Figure B1 shows the simulation of the UH-1 helicopter and the SK/FF problem.

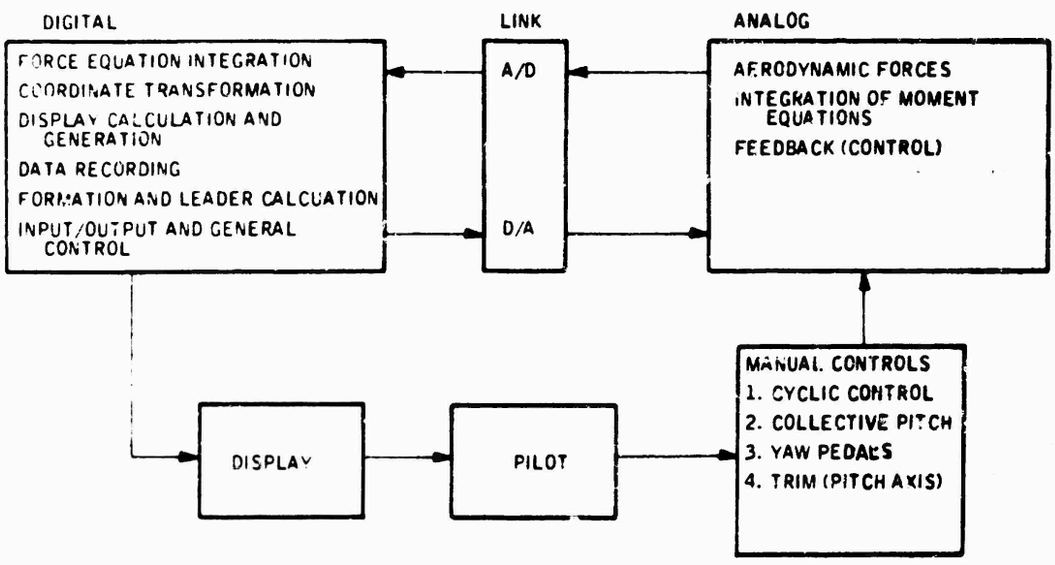

Figure B1. Simulation Setup

APPENDIX C
MATHEMATICAL MODEL - UH-1 ANALOG REPRESENTATION

APPENDIX C
MATHEMATICAL MODEL - UH-1 ANALOG REPRESENTATION

The equations of motion and the pertinent aerodynamic data were taken from abstracted reports received from Bell Helicopter, Fort Worth. The equations were simplified to "perturbation equations" and written in body axis coordinates with the vehicle's center of gravity as the reference. The simplified equations are linear and uncoupled as they depict the vehicle response to only perturbations from trimmed flight conditions.

The aerodynamic data is limited to specific flight conditions within the UH-1 speed regime, i.e., 0 mph, 50 mph, 100 mph, and 150 mph. The flight condition of 100 mph (88 knots) was chosen for the simulation as a realistic nominal airspeed for a formation flight situation. Commanded airspeeds for the simulated mission profile ranged from 70 knots for the deceleration phase to 100 knots for the left turn. It was felt that the errors introduced because of these deviations from the nominal airspeed of 88 knots are small when compared to the advantages gained in terms of simplicity and ease of mechanization when using the perturbation equations.

NOMENCLATURE

The following nomenclature is used in the equations of motion and data.

Symbol	Meaning	Units
u	X body axis perturbation velocity	(fps)
v	Y body axis perturbation velocity	(fps)
w	Z body axis perturbation velocity	(fps)
θ	pitch angle	(rad)

Symbol	Meaning	Units
ϕ	roll angle	(rad)
ψ	yaw angle	(rad)
X	X body axis force	(lb)
Y	Y body axis force	(lb)
Z	Z body axis force	(lb)
L	rolling moment	(ft-lb)
M	pitching moment	(ft-lb)
N	yawing moment	(ft-lb)
β	longitudinal blade flapping (pitch inclination of rotor)	(rad)
K	pitch inclination of stablizer bar	(rad)
λ	roll inclination of stablizer bar	(rad)
γ	lateral blade flapping (roll inclination of rotor)	(rad)
m	vehicle mass	(slugs)
I_{xx}, I_{yy}, I_{zz}	moments of inertia	(slugs/ft^2)
X_u, X_w, etc.	dimensionless aerodynamics coefficient $\left(\frac{\partial X}{\partial u}, \frac{\partial X}{\partial w}, \text{etc.}\right)$	
δ_θ	cyclic pitch control	(rad)
δ_ϕ	cyclic roll control	(rad)
δ_L	collective control	(rad)
δ_R	tail rotor control	(rad)

UH-1 EQUATIONS OF MOTION

The following equations of motion and subsequent data are generalized but with numbers corresponding to trimmed flight at 100 mph (U_o).

Longitudinal

X-axis $$\dot{u} - \frac{X_u}{m} u - \frac{X_w}{m} w - \frac{X_q}{m} \dot{\theta} + g\theta - \frac{X_{\dot{\beta}}}{m} \dot{\beta} - \frac{X_\beta}{m} \beta - \frac{X_K}{m} K = \frac{X_{\delta_\theta}}{m} \delta_\theta + \frac{X_{\delta_L}}{m} \delta_L$$

Z-axis $$\dot{w} - \frac{Z_w}{m} w - \frac{Z_u}{m} u - \left(U_o + \frac{Z_q}{m}\right) \dot{\theta} - \frac{Z_{\dot{\beta}}}{m} \dot{\beta} - \frac{Z_\beta}{m} \beta - \frac{Z_K}{m} K = \frac{Z_{\delta_\theta}}{m} \delta_\theta + \frac{Z_{\delta_L}}{m} \delta_L$$

Pitch $$\ddot{\theta} - \frac{M_q}{I_{yy}} \dot{\theta} - \frac{M_u}{I_{yy}} u - \frac{M_{\dot{w}}}{I_{yy}} \dot{w} - \frac{M_w}{I_{yy}} w - \frac{M_{\dot{\beta}}}{I_{yy}} \dot{\beta} - \frac{M_\beta}{I_{yy}} \beta - \frac{M_K}{I_{yy}} K =$$

$$\frac{M_{\delta_\theta}}{I_{yy}} \delta_\theta + \frac{M_{\delta_L}}{I_{yy}} \delta_L$$

Blade Flapping $$\dot{\beta} - \frac{1}{\beta_{\dot{\beta}}} \beta - \frac{\beta_w}{\beta_{\dot{\beta}}} u - \frac{\beta_w}{\beta_{\dot{\beta}}} w - \frac{\beta_q}{\beta_{\dot{\beta}}} \dot{\theta} - \frac{\beta_K}{\beta_{\dot{\beta}}} K = \frac{\beta_{\delta_\theta}}{\beta_{\dot{\beta}}} \delta_\theta + \frac{\beta_{\delta_L}}{\beta_{\dot{\beta}}} \delta_L$$

Stabilizer Bar $$\dot{K} + \dot{\theta} + 0.3K = 0$$

Lateral

Y-axis $$\dot{v} - \frac{Y_v}{m} v - \left(W_o + \frac{Y_p}{m}\right) \dot{\phi} - g \cos\theta_o \phi + \left(U_o - \frac{Y_R}{m}\right) \dot{\psi} - \frac{Y_\lambda}{m} \lambda - \frac{Y_\gamma}{m} \gamma =$$

$$\frac{Y_{\delta_\phi}}{m} \delta_\phi + \frac{Y_{\delta_R}}{m} \delta_R$$

Roll $$\ddot{\phi} - \frac{L_p}{I_{xx}} - \frac{L_v}{I_{xx}} - \frac{L_\gamma}{I_{xx}} \ddot{\psi} - \frac{L_\gamma}{I_{xx}} \gamma - \frac{L_\lambda}{I_{xx}} \lambda = \frac{L_{\delta_\phi}}{I_{xx}} \delta_\phi + \frac{L_{\delta_R}}{I_{xx}} \delta_R$$

Yaw $$\ddot{\psi} - \frac{N_R}{I_{zz}} \dot{\psi} - \frac{N_v}{I_{zz}} v - \frac{I_{xx}}{I_{zz}} \dot{\phi} \frac{N_p}{I_{zz}} \ddot{\phi} \frac{N_\gamma}{I_{zz}} \gamma - \frac{N_\lambda}{I_{zz}} \lambda = \frac{N_{\delta_\phi}}{I_{zz}} \delta_\phi + \frac{N_{\delta_R}}{I_{zz}} \delta_R$$

Blade Flapping (not included in simulation) $$\dot{\gamma} - \frac{1}{\gamma_{\dot{\gamma}}} \gamma - \frac{\gamma_p}{\gamma_{\dot{\gamma}}} \dot{\phi} - \frac{\gamma_R}{\gamma_{\dot{\gamma}}} \dot{\psi} \frac{\gamma_v}{\gamma_{\dot{\gamma}}} v - \frac{\gamma_\lambda}{\gamma_{\dot{\gamma}}} \lambda = \frac{\gamma_{\delta_\phi}}{\gamma_{\dot{\gamma}}} \delta_\phi$$

Stabilizer Bar $\dot{\lambda} + \phi + .3\lambda = 0$

UH-1 DATA (100 MPH)

Longitudinal

X_u/m	= -0.028	M_u/I_{yy}	= 0.00273
X_w/m	= 0.0015	M_w/I_{yy}	= -0.0167
X_q/m	= 9.16	$M_{\dot{w}}/I_{yy}$	= 0
$X_{\dot{\beta}}/m$	= 0	M_q/I_{yy}	= -0.495
X_k/m	= -0.895	$M_{\dot{\beta}}/I_{yy}$	= 0
X_{δ_θ}/m	= -5.6	M_β/I_{yy}	= 7.22
X_{δ_L}/m	= -3.0	M_k/I_{yy}	= 0.0046
X_β/m	= -59.0	M_{δ_θ}/I_{yy}	= 0.029
		M_{δ_L}/I_{yy}	= -2.005

Z_u/m	=	-0.0005	$\beta_u/\beta_{\dot{\beta}}$	=	0.00368
Z_w/m	=	-0.658	$\beta_w/\beta_{\dot{\beta}}$	=	0.0048
$(mU_o - Z_q)/m$	=	144.8	$\beta_q/\beta_{\dot{\beta}}$	=	-1.02
$Z_{\dot{\beta}}/m$	=	0	$1/\beta_{\dot{\beta}}$	=	-8.25
Z_β/m	=	-95.0	$\beta_k/\beta_{\dot{\beta}}$	=	1.52
Z_{δ_θ}/m	=	-95.0	$\beta_{\delta_\theta}/\beta_{\dot{\beta}}$	=	9.5
Z_{δ_L}/m	=	-316.0	$\beta_{\delta_L}/\beta_{\dot{\beta}}$	=	4.25

Lateral

$L_{\dot{\phi}}/I_{xx}$	=	-1.228	Y_v/m	=	-0.1467
L_R/I_{xx}	=	0	$(mU_o - Y_R)/m$	=	150.4
$L_{\dot{v}}/I_{xx}$	=	-0.00634	$(W_o + Y_p/m)$	=	-11.2
L_v/I_{xx}	=	-0.0376	$Y_{\dot{\lambda}}/m$	=	-0.308
$L_{\dot{\lambda}}/I_{xx}$	=	-0.019	Y_λ/m	=	5.15
L_λ/I_{xx}	=	0.32	Y_{δ_R}/m	=	23.0
L_{δ_R}/I_{xx}	=	13.58	Y_{δ_ϕ}/m	=	5.4
L_{δ_θ}/I_{xx}	=	34.0	Y_γ/m	=	not included
N_R/I_{zz}	=	0	N_{δ_ϕ}/I_{zz}	=	- 0.48

$N_{\dot{v}}/I_{zz}$	=	0.0098	I_{xz}/I_{zz}	=	0
N_v/I_{zz}	=	0.0386	N_p/I_{zz}	=	not included
N_{δ_R}/I_{zz}	=	-18.28	N_r/I_{zz}	=	not included
			N_λ/I_{zz}	=	not included

To prepare the equations for use on the analog, they must first be scaled. The following sensitivities and authorities assigned to the controls are those characteristics of the UH-1 vehicle.

		Sensitivity	Authority
Cyclic pitch	(δ_θ)	1.64 deg/in.	±6.5 in.
Cyclic roll	(δ_ϕ)	1.54 deg/in.	±6.5 in.
Collective	(δ_L)	1.33 deg/in.	+2 in. →-7in. (0≒ 100 mph)
Tail rotor	(δ_R)	2.0 deg/in.	± 3 in.
Pitch trim	0.46	0.46 deg/sec	

Scaling

$\dot{u}$ u	50 ft/sec = 100 v
$\dot{v}$, v, $\dot{w}$, w	20 ft/sec = 100 v
$\ddot{\phi}$, $\dot{\phi}$, ϕ, $\ddot{\theta}$, $\dot{\theta}$, θ	1 rad = 100 v
$\ddot{\psi}$, $\dot{\psi}$, ψ, $\dot{\lambda}$, λ	
δ_θ, δ_ϕ, δ_R, δ_L	
δ_{θ_c}	5.44 v/deg
δ_{ϕ_c}	6.5 v/deg
δ_{R_c}	5.0 v/deg
δ_{L_c}	7.5 v/deg

Placing the above sensitivities, authorities, and scaling into the equations of motion, the equations are ready for programming on the analog computer.

Scaled Equations

X $\quad [2\dot{u}] + 0.028\,[2u] - 0.0006\,[5w]^{*} + 0.183\,[100\dot{\theta}] + 1.18\,[100\beta]$

$+ 0.644\,[100\theta] + 0.018\,[100K] = -0.112\,[100\delta_\theta] - 0.06\,[100\delta_L]$

Z $\quad [5\dot{w}] + 0.658\,[5w] + 0.0013\,[2u]^{*} + 4.75\,[100\beta] - 7.24\,[100\dot{\theta}]$

$+ 76\,[100K] = -4.75\,[100\delta_\theta] - 15.8\,[100\,\delta_L]$

* Ignored in simulation because of negligible contribution

θ $\left[100\ddot{\theta}\right] + 0.495\left[100\dot{\theta}\right] - 0.137\left[2u\right] - 7.22\left[100\beta\right] + 0.334\left[5w\right]$
$- 0.0046\left[100K\right] = 0.029\left[100\delta_{\theta}\right] - 2.0\left[100\delta_{L}\right]$

K $\left[100\dot{K}\right] + \left[100\dot{\theta}\right] + 0.3\left[100K\right] = 0$

β $\left[100\dot{\beta}\right] + 8.25\left[100\beta\right] - 1.52\left[100K\right] + 1.02\left[100\dot{\theta}\right] - 0.096\left[5w\right]$
$- 0.184\left[2u\right] = 9.5\left[100\delta_{\theta}\right] + 4.25\left[100\delta_{L}\right]$

ϕ $\left[100\ddot{\phi}\right] + 1.228\left[100\dot{\phi}\right] + 0.75\left[5v\right] - 0.32\left[100\lambda\right] + 0.019\left[100\dot{\lambda}\right]$
$+ 0.12\left[5\dot{v}\right] = 34\left[100\delta_{\phi}\right] + 13.6\left[100\delta_{R}\right]$

ψ $\left[100\dot{\psi}\right] - 0.77\left[5v\right] - 0.2\left[5\dot{v}\right] = - 0.48\left[100\delta_{\phi}\right] - 18.3\left[100\delta_{R}\right]$

v $\left[5\dot{v}\right] + 0.147\left[5v\right] + 0.51\left[100\dot{\phi}\right] - 1.61\left[100\phi\right] + 7.52\left[100\dot{\psi}\right]$
$- 0.258\left[100\lambda\right] + 0.015\left[100\dot{\lambda}\right] = 0.27\left[100\delta_{\phi}\right] + 1.15\left[100\delta_{R}\right]$

λ $\left[100\dot{\lambda}\right] + \left[100\dot{\phi}\right] + 0.3\left[100\lambda\right] = 0$

CIRCUITRY

Figure C1 shows the analog simulation circuitry.

CONTROL FORCES

The following tabulation compares the forces for the various controls ;use in the simulation with the specified values supplied by Bell Helicopter, Fort Worth.

Forces and Displacements	Honeywell Simulator	Bell UH-1B
Collective stick vertical travel	7 in.	7 in.
Cyclic stick travel fore and aft	6.5 in.	6.3 in.
Cyclic stick travel lateral	6.5 in.	6.2 in.
Cyclic stick B/O fore and aft	2 lb	2 lb
Cyclic stick B/O lateral	1.2 lb	1 lb
Cyclic stick force gradient fore and aft	1.35 lb/in.	1.25 lb/in.
Cyclic stick force gradient lateral	0.85 lb/in.	0.79 lb/in.
Rudder Pedal travel	2.5 in.	3.25 in.
Rudder Pedal B/O	4 lb	1 lb
Rudder pedal force gradient	8 lb/in.	7.3 lb/in.

AUTOPILOT MECHANIZATION

Section IV is a detailed description of the operation of each autopilot mode. Figures C2 through C4 are the analog diagrams of the simulated AFCS.

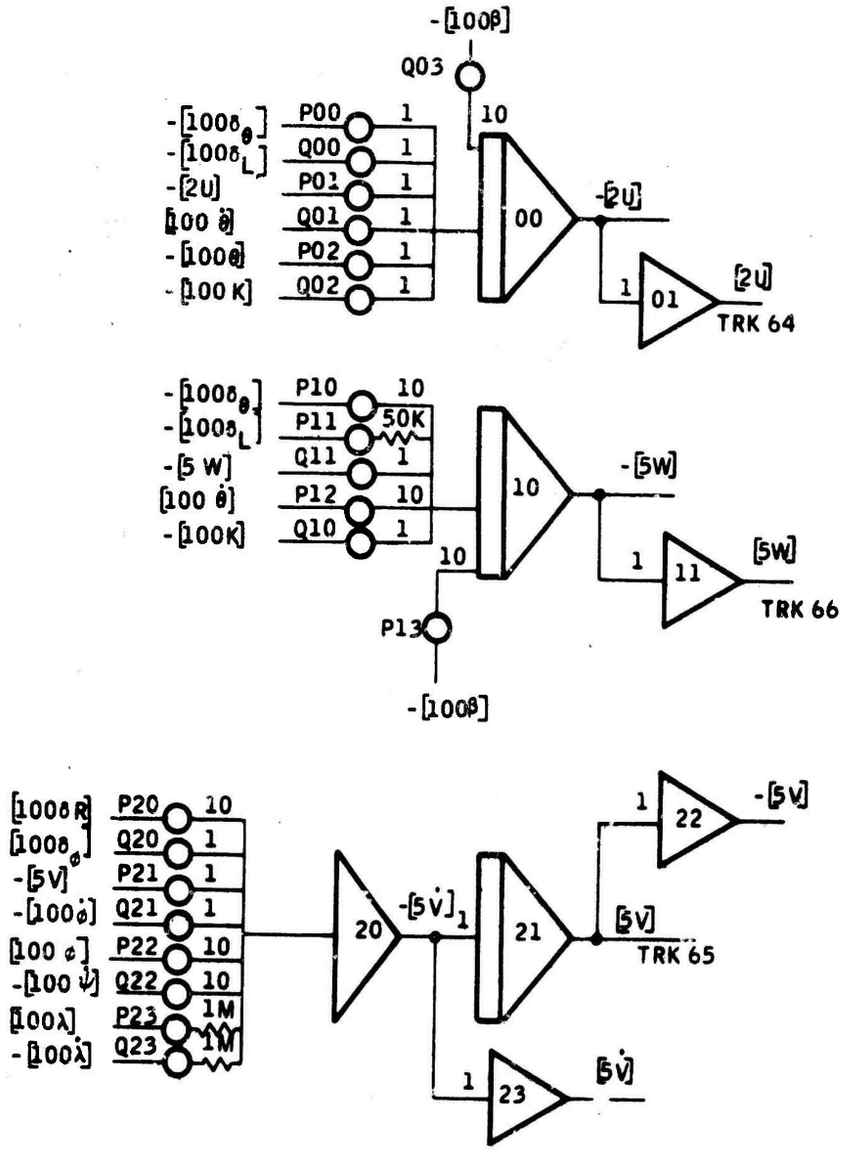

Figure C1. UH-1 Analog Simulation

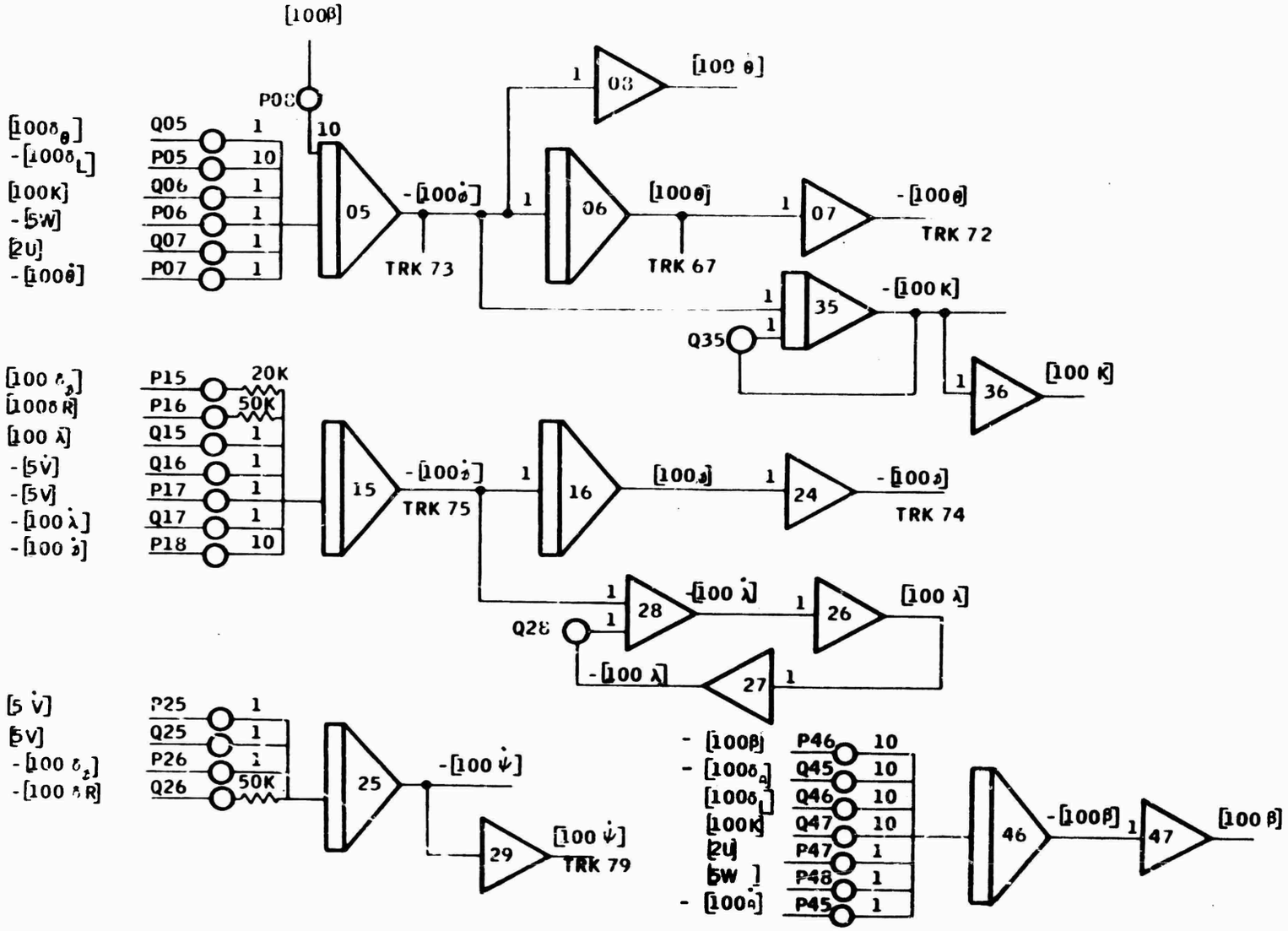

Figure C1. UH-1 Analog Simulation (Concluded)

$$\delta_R = \delta_{RC} + 0.075\left(\frac{3s}{1+3s}\right)\dot{\psi}$$

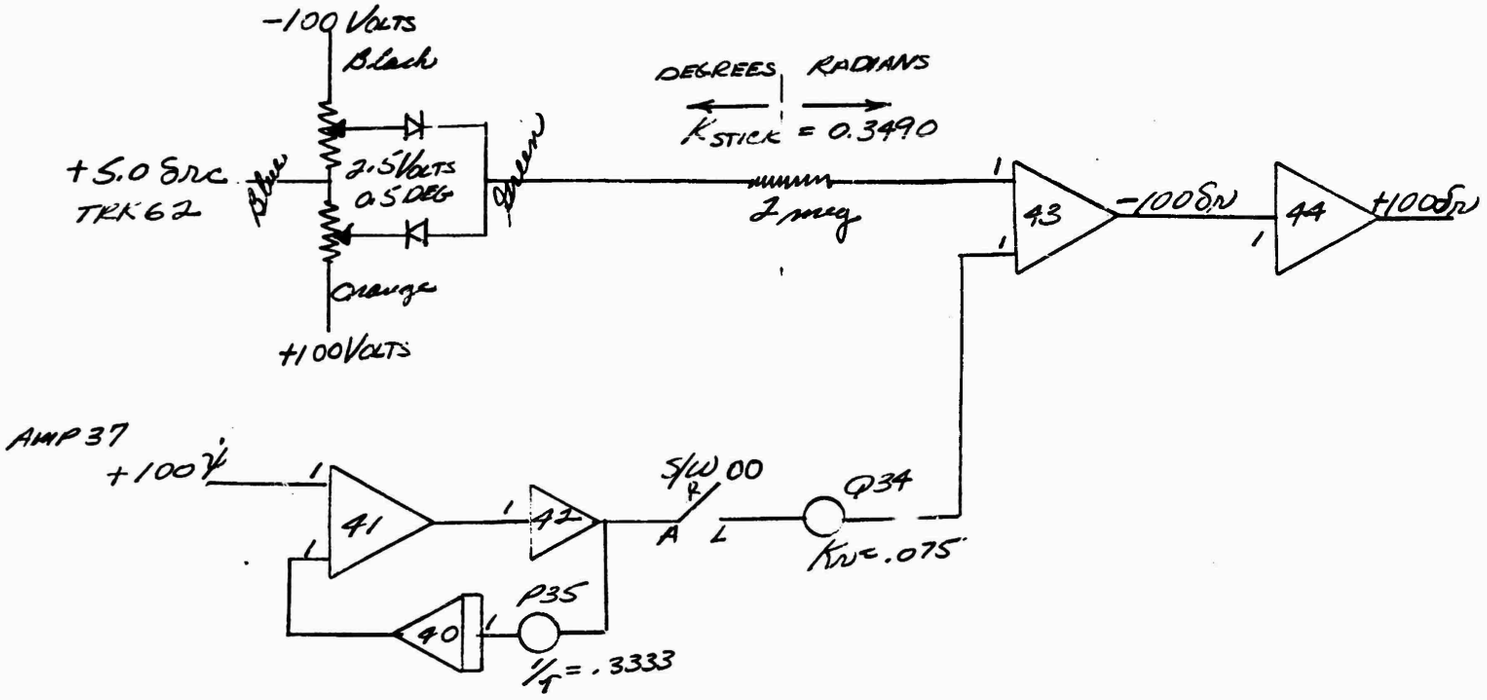

Figure C2. UH-1 Yaw Stability Augmentation

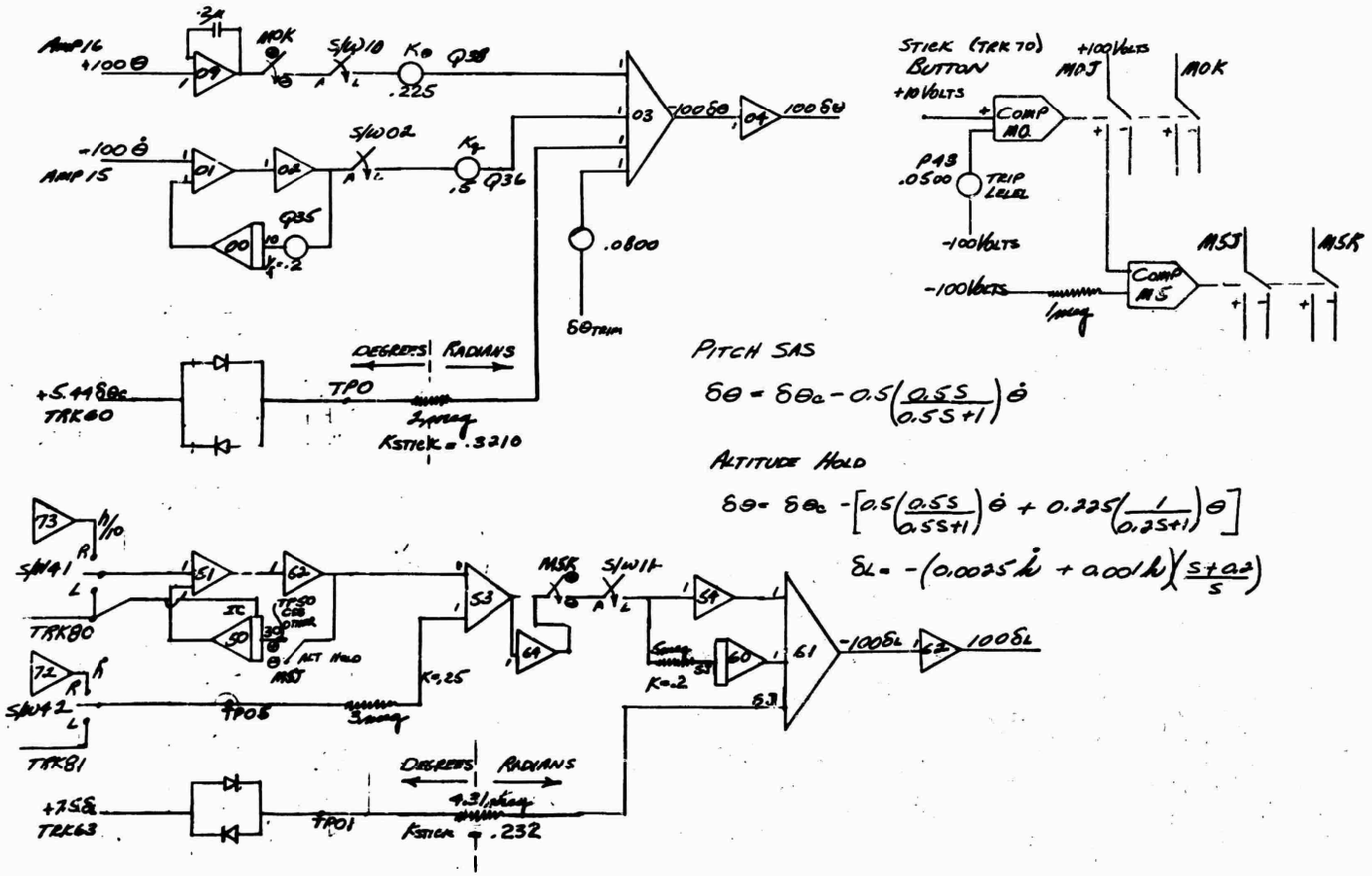

Figure C3. UH-1 Longitudinal Axis AFCS

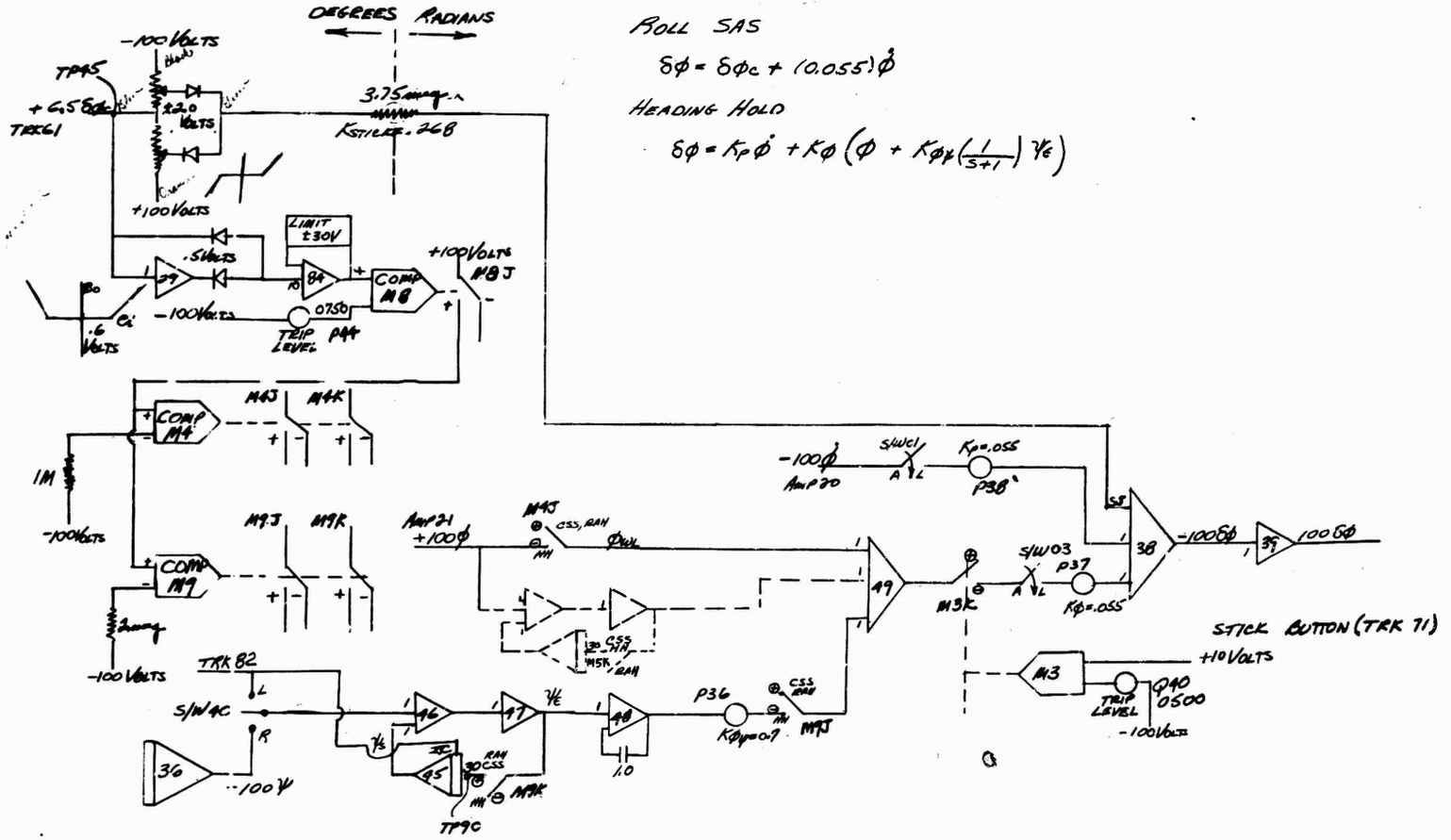

Figure C4. UH-1 Lateral Directional Axis AFCS

APPENDIX D

MATHEMATICAL MODEL - AH-56 ANALOG REPRESENTATION

APPENDIX D

MATHEMATICAL MODEL - AH-56 ANALOG REPRESENTATION

This appendix presents a description of the analog simulation of the AH-56A rigid rotor compound helicopter and autopilot for uses in the current JANAIR SK/FF study. This simulation is part of the hybrid simulation where the SDS 9300 digital computer generates cockpit instructions for display on the cathode ray tube.

FLIGHT ENVELOPE CONSIDERED

Figures 72 and 74 presented earlier in this report (Section VI) are functional block diagrams of the AFCS developed by Honeywell Inc. specifically for the AH-56A vehicle. These functional block diagrams represent the AFCS configured for the mid-range portion of the airspeed flight envelope (60 knots). This portion of the flight envelope was selected because it represents an autopilot of greater complexity than that developed for either high or low speeds. It represents the vehicle in its helicopter-to-fixed-wing aircraft transition region. Finally, the stability levels mechanized at this flight condition will give rise to study results demonstrating the pilot's ability to fly the station keeping problem, these results are directly applicable to both the high-and low-speed portions of the station-keeping operational flight envelope.

AH-56A MATHEMATICAL MODEL

The equations of motion used for the AH-56A vehicle simulation are linear perturbation equations for the vehicle in six degrees of freedom (roll, pitch, yaw, lateral, vertical, and horizontal) plus the equations for the rigid rotor blade and gyro control. These equations of motion, numerical data for the coefficients covering the speed range of interest, and flight condition data are detailed in Lockheed document FCS D11, dated 3 October, 1966, Model AH-56A, Title: Analytical Data for AH-56A Yaw SAS - AFCS System Supplier.

Figures D5 through D7 are the analog computer diagrams of the AH-56A equations of motion.

AH-56A FREE VEHICLE AND AUTOPILOT SIMULATION

Analog diagrams for the AH-56A autopilot's five control axes are shown in Figures D1 through D4. The control system characteristics are shown in Table D1. On all control axes, series servos were simulated instead of parallel servos as used in the actual vehicle. Simulating parallel servos

requires hydraulic and mechanical linkages and electrical pickoffs to the extent that a prototype of the actual vehicle to be simulated is the end result. Constructing such an "iron bird" is beyond the scope of this study. The effect of using simulated series servos is that servo outputs are not coupled as deriving functions to simulated control surfaces, and, of most importance, the control stick is not driven as a function of the servo position. Having a control stick that is not driven as a function of servo position requires that the subjects flying the simulated vehicle provide this function. An example of why this must be done follows: Assume that the pilot is commanding an altitude change through the collective axis. Upon reaching the desired altitude he engages altitude hold and the autopilot acts to maintain this altitude as a function of altitude error and his previously commanded collective pitch. Because the effects of atmospheric pressure do not enter into the problem to establish a new trim position on the collective axis, the collective command should be faded to zero upon reaching the desired altitude.

The functional representation of the collective axis altitude hold mode is shown in Figure 72, Section VI. As shown, vertical acceleration ($\ddot{h}$) and pitot static pressure are used in an electronic blending scheme to generate the rate of change of altitude (h_b) and altitude (h_b). Upon investigation of the equation programmed in the digital computer, it was found that altitude and altitude rate would be calculated as a function of the vehicle's current position. These parameters are exactly those needed to simulate the altitude hold mode. Therefore, the analog simulation of the altitude hold mode includes only those elements following the altitude rate and altitude points on the functional block diagram. Also, the altitude error as a function of bank angle was not simulated. The purpose of this loop is to prevent loss of altitude for large, steady-state bank angles. The steady-state bank angles achieved during this study are on the order of 7 deg. For bank angles of this magnitude altitude loss is small and may be neglected. The analog recording of the altitude hold mode (with these simplifications incorporated) were compared with analog recordings of the complete altitude hold mode simulation and no appreciable difference was detected.

The analog recording presented in Section VI of this report were compared with those analog time histories recorded during the autopilot development analysis. Results of this comparison disclosed that the analog simulation presented in Figures D1 through D4 is a good representation of the AH-56A helicopter and AFCS.

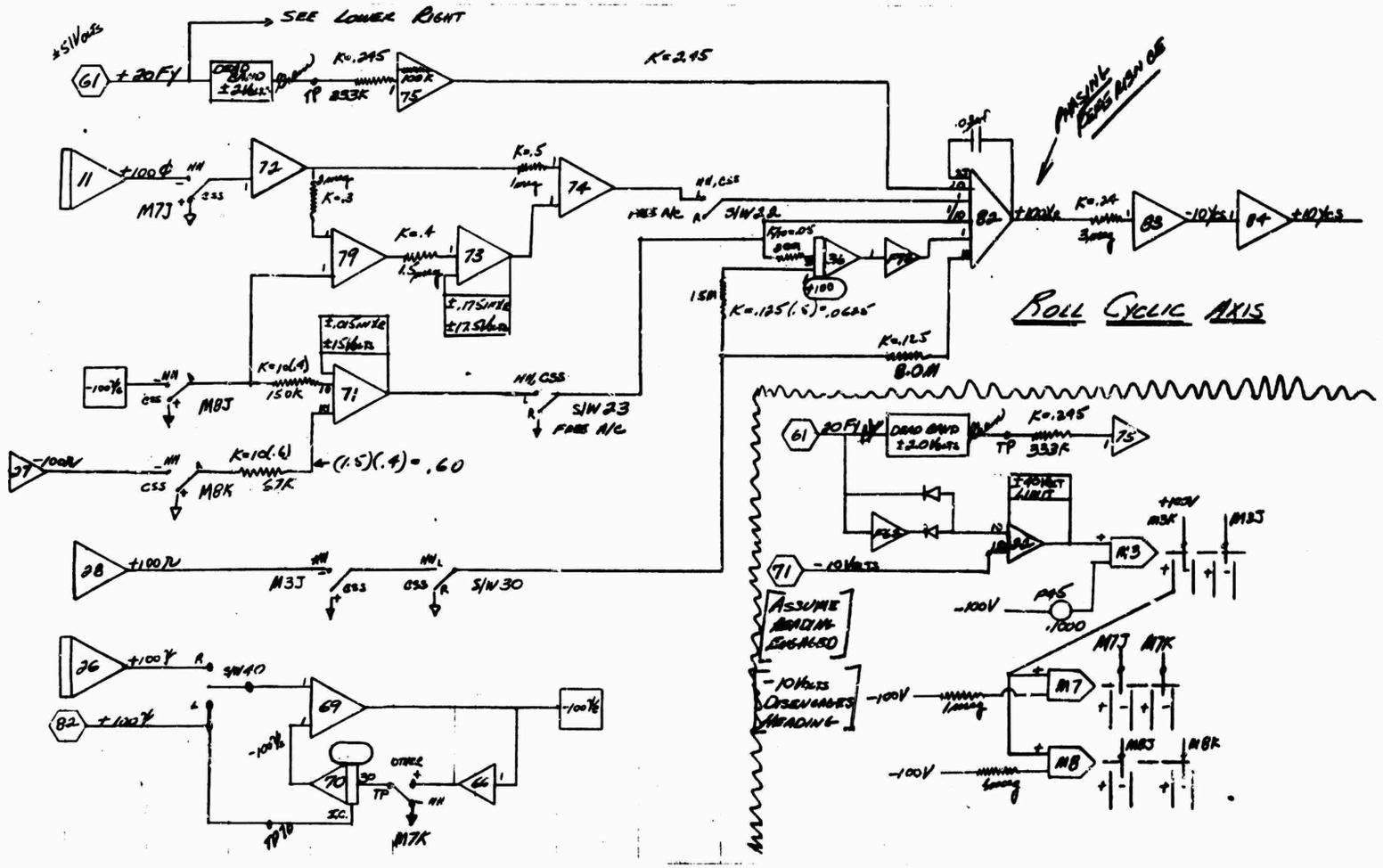

Figure D1. Analog Simulation

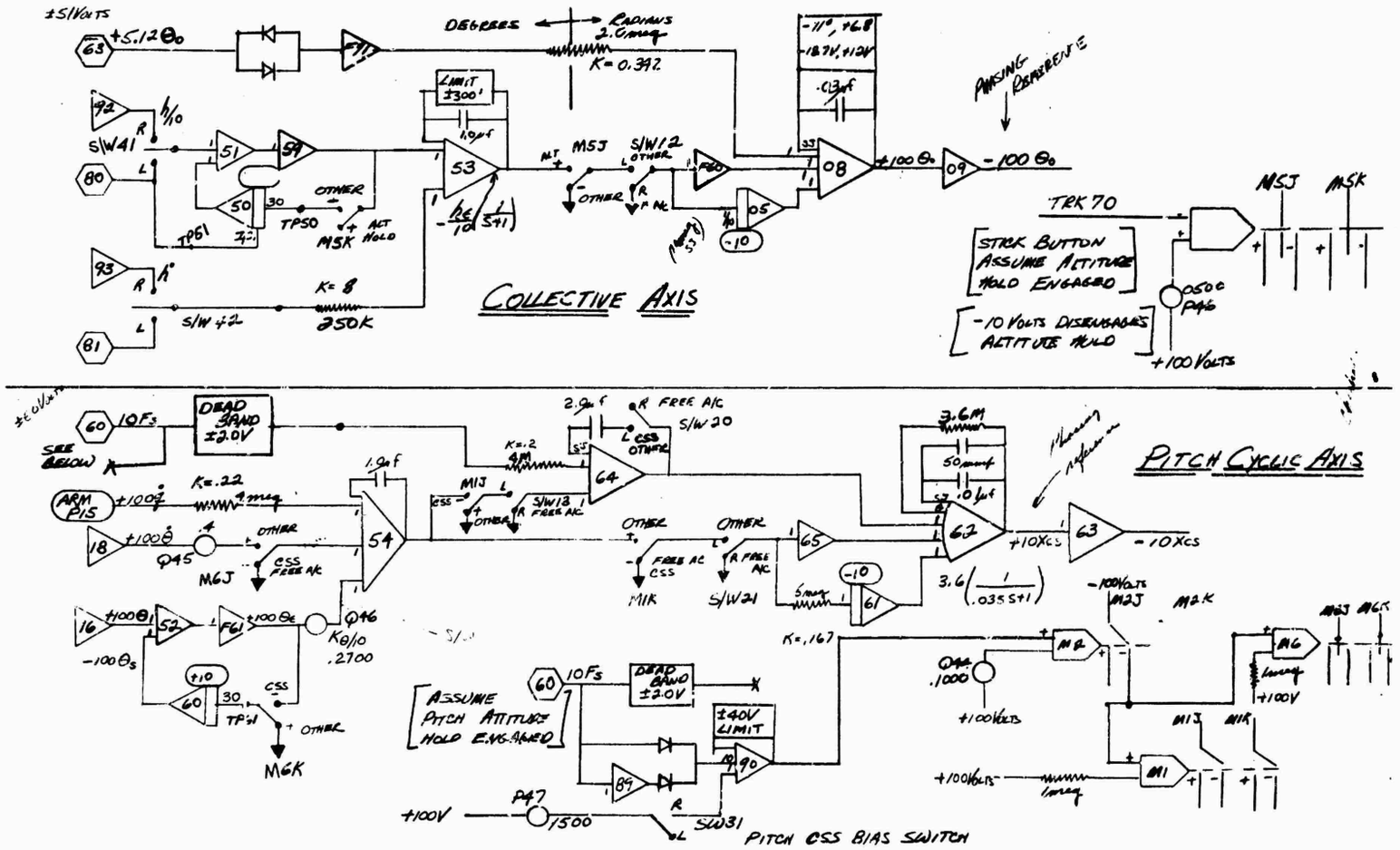

Figure D2. Analog Simulation

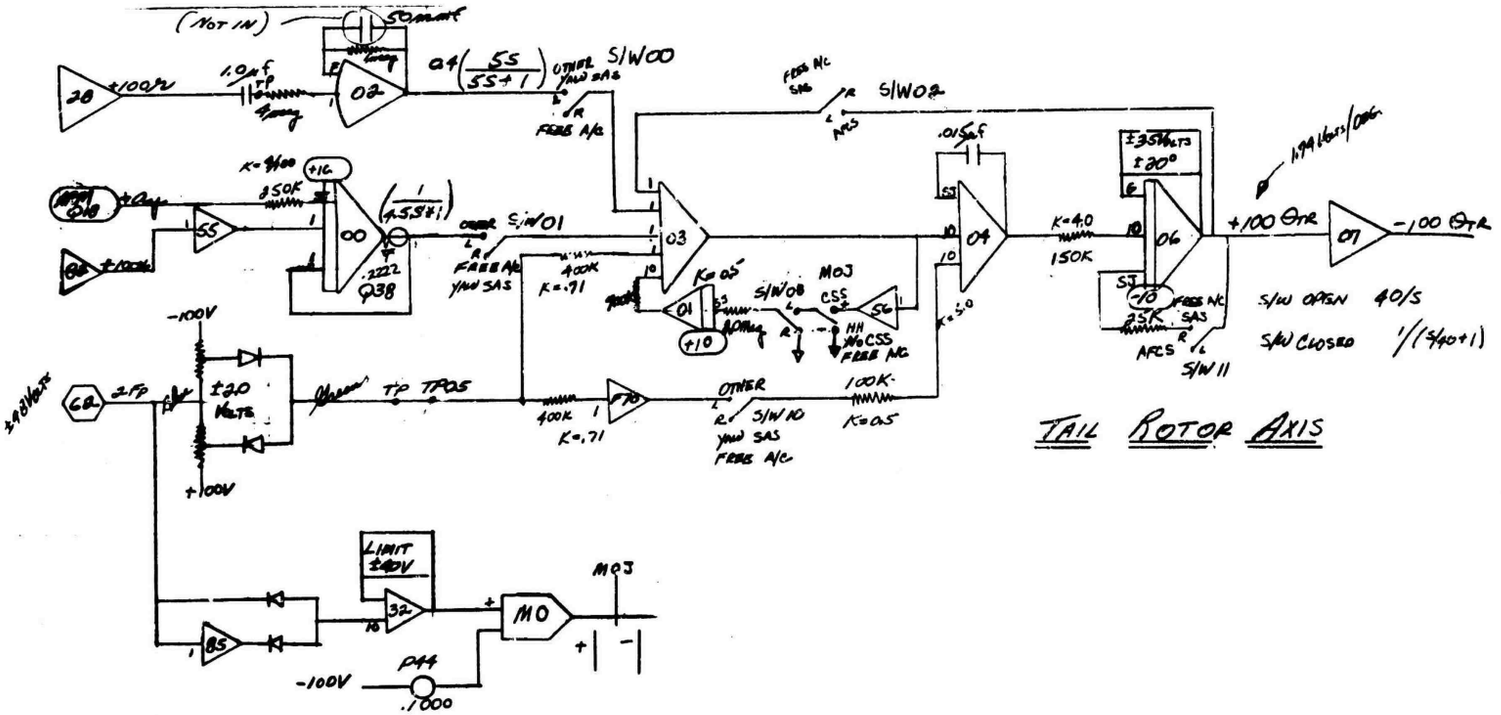

Figure D3. Analog Simulation

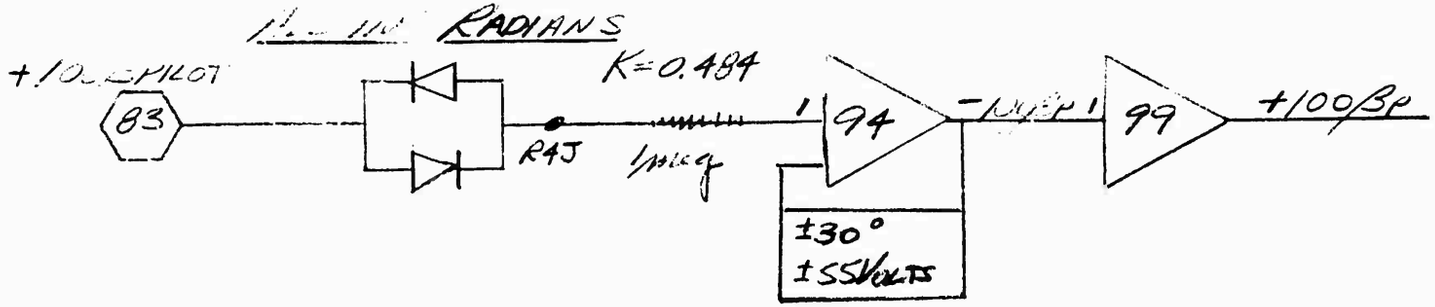

Figure D4. Analog Simulation

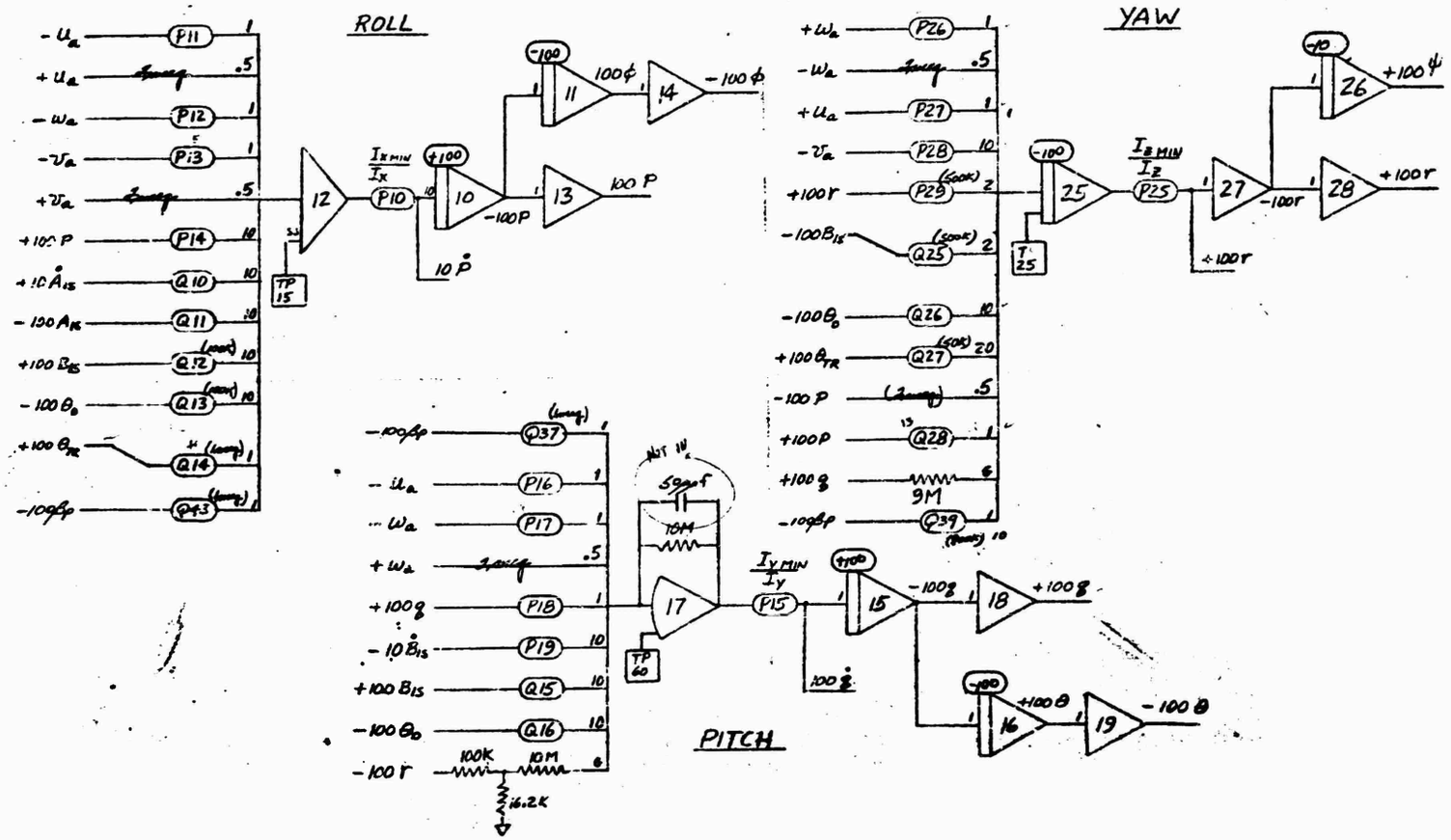

Figure D5. Airframe Rotational Degrees of Freedom

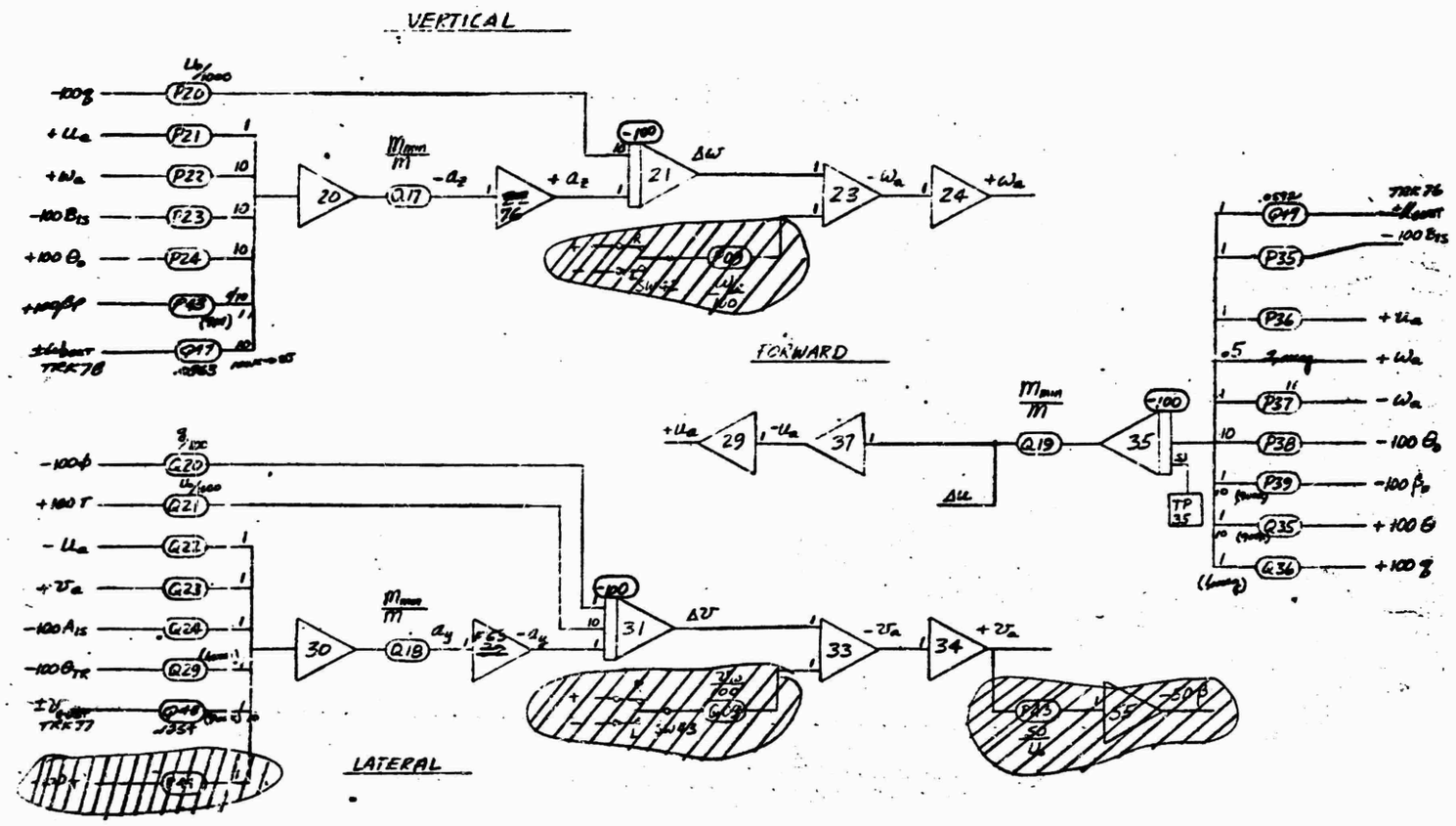

Figure D6. Airframe Translational Degrees of Freedom

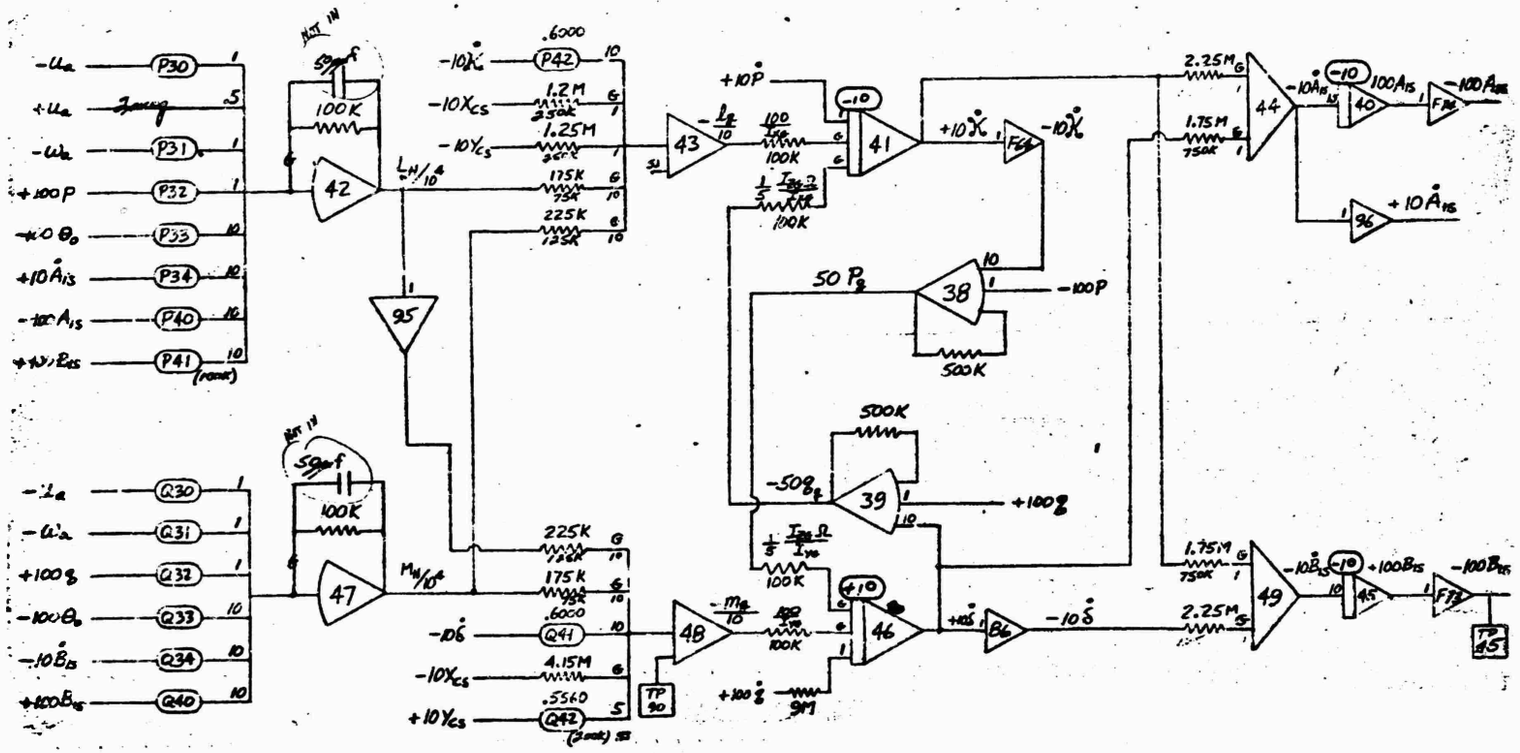

Figure D7. Cyclic Rotor Dynamics

UNCLASSIFIED
Security Classification

DOCUMENT CONTROL DATA - R & D
(Security classification of title, body of abstract and indexing annotation must be entered when the overall report is classified)

1 ORIGINATING ACTIVITY (Corporate author)
Honeywell Inc., Systems and Research Division, 2700 Ridgway Parkway, Minneapolis, Minnesota 55413

2a. REPORT SECURITY CLASSIFICATION
UNCLASSIFIED

2b. GROUP

3 REPORT TITLE
Effects of Varying Levels of Autopilot Assistance and Workload on Pilot Performance in the Helicopter Formation Flight Mode

4 DESCRIPTIVE NOTES (Type of report and inclusive dates)
Final Report, December 1967 through April 1968

5 AUTHOR(S) (First name, middle initial, last name)
Paul A. Anderson and Myrna L. Toivanen

6 REPORT DATE	7a. TOTAL NO. OF PAGES	7b. NO. OF REFS
March 1970	238	8

8a. CONTRACT OR GRANT NO.	9a. ORIGINATOR'S REPORT NUMBER(S)
N00014-66-C-0362	12543-FR4
b. PROJECT NO. NR 213-054	
c.	9b. OTHER REPORT NO(S) (Any other numbers that may be assigned this report)
d.	JANAIR Report 680610

10 DISTRIBUTION STATEMENT
This document has been approved for public release and sale; its distribution is unlimited.

11 SUPPLEMENTARY NOTES	12. SPONSORING MILITARY ACTIVITY
Joint Army-Navy Aircraft Instrumentation Research (JANAIR) Program	Office of Naval Research Air Programs, Code 461 Department of the Navy Washington, D.C. 20360

13 ABSTRACT

The objective of this study was to evaluate pilot performance in manual IFR formation flight with varying levels of autopilot assistance and pilot workload. The study was conducted for a conventional helicopter, i.e., the UH-1 Iroquois, and an advanced vehicle, the AH-56 Cheyenne. Man-in-the-loop simulations of these vehicles were conducted to evaluate pilot performance under six levels of autopilot assistance, ranging in sophistication from the free vehicle to outer loop hold modes in heading and altitude, and under three levels of pilot workload, consisting of a forced-pace, secondary concomitant task. Results of the study, within the constraints imposed by the simulation, indicated that increasing the level of autopilot assistance resulted in a less demanding task for the pilot and provided greater system stability. This was borne out in terms of both quantitative performance data and pilot opinion. However, position errors were not consistently reduced beyond the levels obtained during manual flight control modes where the highly quickened display was used. Only at the highest workload level tested did autopilot assistance serve to reduce the position errors from what was experienced under the manual control conditions.

DD FORM 1 NOV 68 1473 REPLACES DD FORM 1473, 1 JAN 64, WHICH IS OBSOLETE FOR ARMY USE.

UNCLASSIFIED
Security Classification

Security Classification

14 KEY WORDS	LINK A		LINK B		LINK C	
	ROLE	WT	ROLE	WT	ROLE	WT
IFR						
Formation Flight						
Autopilot						
UH-1						
AH-56						
Pilot Workload						
Helicopter						

Security Classification